Evolution of the northern KwaZulu-Natal coastal dune cordon; evidence from the fine-grained sediment fraction.

by

Christopher Ian Ware

Submitted in fulfilment of the requirements for the degree of Master of Science

in the

Faculty of Science

School of Geological and Computer Sciences

University of Natal,

Durban

JULY 2001

ABSTRACT

The geological evolution of the northern KwaZulu-Natal dune cordon includes a sequence of Quaternary dune building events driven by climatic oscillations. Interglacial times are characterised by high sea-levels, coastal erosion and relative inland dune stability. In contrast glacial times are characterised mass reworking and dune building phases due to increased wind velocities, sparse vegetation and a largely exposed, broad sediment-rich continental shelf.

Eight sedimentological units (K, A0, A2, A4, D1, D2, E and F) were identified in the central Zulti North lease area from diverse data gained from six boreholes and eight surface samples. Due to the difficulty in dealing with the fine-fraction (< 63 μm), a detailed laboratory procedure for extraction and analysis is presented. Analysis of the fine-fraction proved successful in separating all units with depositional interpretation being aided by bulk sample analysis. Lateral extensions of these units were determined from heavy mineral ratio data from a dense grid of borehole samples.

There is a general increase in fines down hole and from the coastal to the inland dunes which is correlated to an increase in degree of weathering with age. The degree of relative weathering is determined from the Chemical Index of Alteration as well as silt morphology and clay mineralogy, which was then correlated to absolute ages as determined from six luminescence dates. This revealed three generations of dune cordons; Unit K (Kosi Bay Formation), Units A0 and A2 (KwaMbonambi Formation) and Units A4, D1, D2, E and F (Sibayi Formation).

Unit K (*ca.* 250 - 350 ka; Dr N. Porat, Geological Survey of Israel, pers. comm, 1999 *In:* Maud & Botha, 2000) forms the core of the inland dune cordon and is correlated to the Kosi Bay Formation and probably overlies the consolidated Port Durnford Formation. It is a yellowish brown to light olive grey, poorly sorted, semi-consolidated upper fine aeolian sand. It is characterised by a high kaolinite abundance within the clay-fraction, low abundance of minerals containing high atomic elements (HAEM) within the silt-fraction, very high fines, negligible carbonate content and an extreme degree of grain weathering.

Unit A0 (*ca.* 190 - 250 ka) is correlated to the base of the KwaMbonambi Formation being deposited in a north/south aligned palaeo-valley as aeolian sands during the marine transgression prior to the penultimate interglacial highstand. It is a strong brown to yellowish brown, moderately sorted, semi-consolidated lower medium sand. It is characterised by goethite, interstratifications and kaolinite which dominate the clay-fraction, abundant HAEM within the silt-fraction, abundant fines, negligible bulk carbonate content and high to extreme degrees of grain weathering.

Unit A2 (*ca.* 130 - 190 ka) is correlated to the KwaMbonambi Formation being initially deposited during the highstand of the warm penultimate interglacial event and subsequently reworked during the regression brought on by the penultimate glacial maximum. It is a dark brown to yellowish brown, moderately well sorted, unconsolidated becoming semi-consolidated upper fine to lower medium aeolian (with minor fluvial inputs) sand. It is characterised by goethite, quartz, interstratifications and kaolinite dominating the clay-fraction, abundant minerals containing high atomic elements (HAEM) within the silt-fraction, intermediate to abundant fines, negligible bulk carbonate content and high to extreme degrees of grain weathering.

Unit A4 (19 - 29 ka) was derived from repetitive reworking of the older units during late Pleistocene sea-level and climatic oscillations. It is a dark yellowish brown to red, poorly to well sorted, unconsolidated

lower fine to lower medium aeolian (with local fluvial inputs) sand. It is characterised by quartz, goethite, interstratifications and kaolinite dominating the clay-fraction, intermediate to high HAEM within the silt-fraction, low to intermediate fines, negligible carbonate content and moderate to high degrees of grain weathering. Unit A4 has been correlated to the Sibayi Formation which implies an older Late Pleistocene depositional age than predicted from previous studies.

After the last glacial maximum sea-level rose rapidly from a level of about - 120 m amsl with the ameliorating climate, inundating the shelf while eroding, reworking and submerging dunes on the shelf. Extensive reworking of the coastal sediments during the transgression produced Unit D1 (11 - 19 ka) which is correlated to the Sibayi Formation. Unit D1 is a dark brown to dark yellowish brown, well sorted, calcareous unconsolidated lower medium aeolian sand. It is characterised by quartz, calcite and interstratifications within the clay-fraction, intermediate to high HAEM within the silt-fraction, low to intermediate fines, low to high carbonate content and a moderate degree of grain weathering.

The onset of the Holocene was dominated by a transgressive moist lacustrine period as sea-level stabilised to the present level resulting in the deposition (at *ca.* 11 - 5 ka) and later reworking (at *ca.* 2.1 ka) of Unit D2. Unit D2 (Sibayi Formation) is a dark yellowish brown, well sorted, unconsolidated calcareous upper fine to lower medium aeolian sand. It is characterised by quartz and calcite dominating the clay-fraction, intermediate to high HAEM within the silt-fraction, low fines, intermediate to high carbonate content and minor grain weathering.

The mid-Holocene highstand resulted in only minor reworking as the elevated temperatures promoted proliferation dense vegetation and dune stability. Sea-level briefly fell to - 2 m at *ca.* 3 ka whereupon Unit E was deposited initially as shallow marine sediments and consequently as transgressive dune sediments. This unit was consequently reworked less than 1.1 ka and is correlated to the Sibayi Formation. Unit E is a dark yellowish brown, well to moderately well sorted, unconsolidated calcareous lower medium sand. It is characterised by smectite, calcite, collophane and goethite dominating the clay-fraction, low to intermediate HAEM within the silt-fraction, low fines, low carbonate content and minor grain weathering.

Unit F (Sibayi Formation) represents the most coastal and recent proximal dune accretion within the study area being deposited at *ca.* 1.1 ka and reworked in modern times (150 BP). Unit F is a dark brown to dark yellowish brown, well sorted, unconsolidated calcareous lower medium sand. It is characterised by quartz, interstratifications, smectite, calcite and collophane dominating the clay-fraction, low to intermediate HAEM within the silt-fraction, low fines, low to intermediate bulk carbonate content and minor grain weathering.

PREFACE

The majority of research was carried out in the School of Geological and Computer Sciences and the Centre of Electron Microscopy at the University of Natal, Durban and Pietermaritzburg campuses respectfully, during the period February 1999 to June 2001.

I hereby declare that this is my own unaided work except where referenced or suitably acknowledged.

Signature 

Date signed 23-11-2001

ACKNOWLEDGEMENTS

The author would sincerely like to thank the following organisations and persons for their assistance, without which this dissertation could not have been written.

(1) Richards Bay Minerals for funding this project, with special thanks to Mr J. Selby, Mr K. Pietersen and Mrs A. Pietersen for their dedicated support, ideas and organising numerous site visits.

(2) Dr G. Whitmore and Dr R. Uken, as supervisors (University of Natal, Durban), for their tireless dedication to the project.

(3) Mr M. Seyambu of the University of Natal, Durban, for the arduous task of preparing numerous polished grain mounts.

(4) Mr R. Seyambu and Mr P. Suthan of the University of Natal, Durban, for their assistance with setting up the XRD machines and for XRF analyses.

(5) Mr V. Bandu and Mrs B. White of the Centre of Electron Microscopy, University of Natal, Pietermaritzburg, for their assistance in sample coating and in countless strippings of a very temperamental and stubborn "state-of-the-art" machine.

(6) Dr F. Graham of the Electron Microscope Unit, University of Natal, Durban, for her support and scientific assistance regarding Scanning Electron Microscopes as well as sample preparation techniques.

(7) Mr A. Bult of Innovative Metallurgy Products, for loaning the Crystalsizer for particle size analysis.

I am sincerely in debt to my family for their support, advice and encouragement whilst preparing this thesis.

TABLE OF CONTENTS

-Page-

1 INTRODUCTION

Southern Africa is at present the world's largest producer of titanium feedstock and zircon sand and looks set to continue this trend for some time. Despite this, relatively little is known regarding the stratigraphy, composition and evolution of these ores within the coastal dune systems. While several research projects have studied the dune sand and mineral separates (Pietersen, 1992; Hugo, 1993; Singh, 1995; Singh & Dunlevey, 1997; Sudan, 1999) there is a poor understanding of the fine-fraction (particles less than 63 μm) within the dunes. As these fine particles directly effect mining and beneficiation, this project has been sponsored by Richards Bay Minerals (RBM) to address this shortcoming. This thesis is currently focussed on coastal dunes north of Richards Bay, where the fine-fraction is less than 15 %. However, the results contained within are applicable to dunes containing higher abundances of fines (up to 30 %) as these are expected to be utilised during the next decade of mining operations.

1.1 RICHARDS BAY MINERALS

RBM have been extracting economic heavy minerals from unconsolidated coastal dune sands in northern KwaZulu-Natal for more than two and a half decades. Their operation utilises several dredge mining plants to produce a heavy mineral concentrate (ilmenite, leucoxene, rutile and zircon) and a purpose built smelter to produce titanium slag and pig-iron.

RBM is the trading name for Tisand (Pty) Limited and Richards Bay Iron and Titanium (Pty) Limited (RBIT), which are equally and jointly owned by the London-based RioTinto plc and Billiton plc. Tisand is responsible for dune mining and primary concentration of heavy minerals, and RBIT for smelting and beneficiation. Three ore bodies are currently being exploited, namely the Zulti South, Zulti North and Tisand lease areas (Figure 1.1).

Mining is in the form of a dredge operation whereby an artificial pond is created in the dunes, on which floats a suction-cutting dredger and gravity concentration plant. The base of the pond is a naturally occurring uneven hard silty-clay floor beneath the dunes (Port Durnford Formation). The dredger advances by undermining the mining face of the dune by means of a high intensity water jet causing it to collapse (Figure 1.2). The resultant slurry is sucked up to a floating concentrator. Here the heavy minerals (ilmenite, leucoxene, rutile, magnetite, zircon and non-economic gangue) are separated from lighter gangue minerals using spiral separators. Magnetite is removed from the heavy mineral fraction by low intensity wet magnets and combined with the tailings. The heavy mineral concentrate is then stockpiled for transportation to the

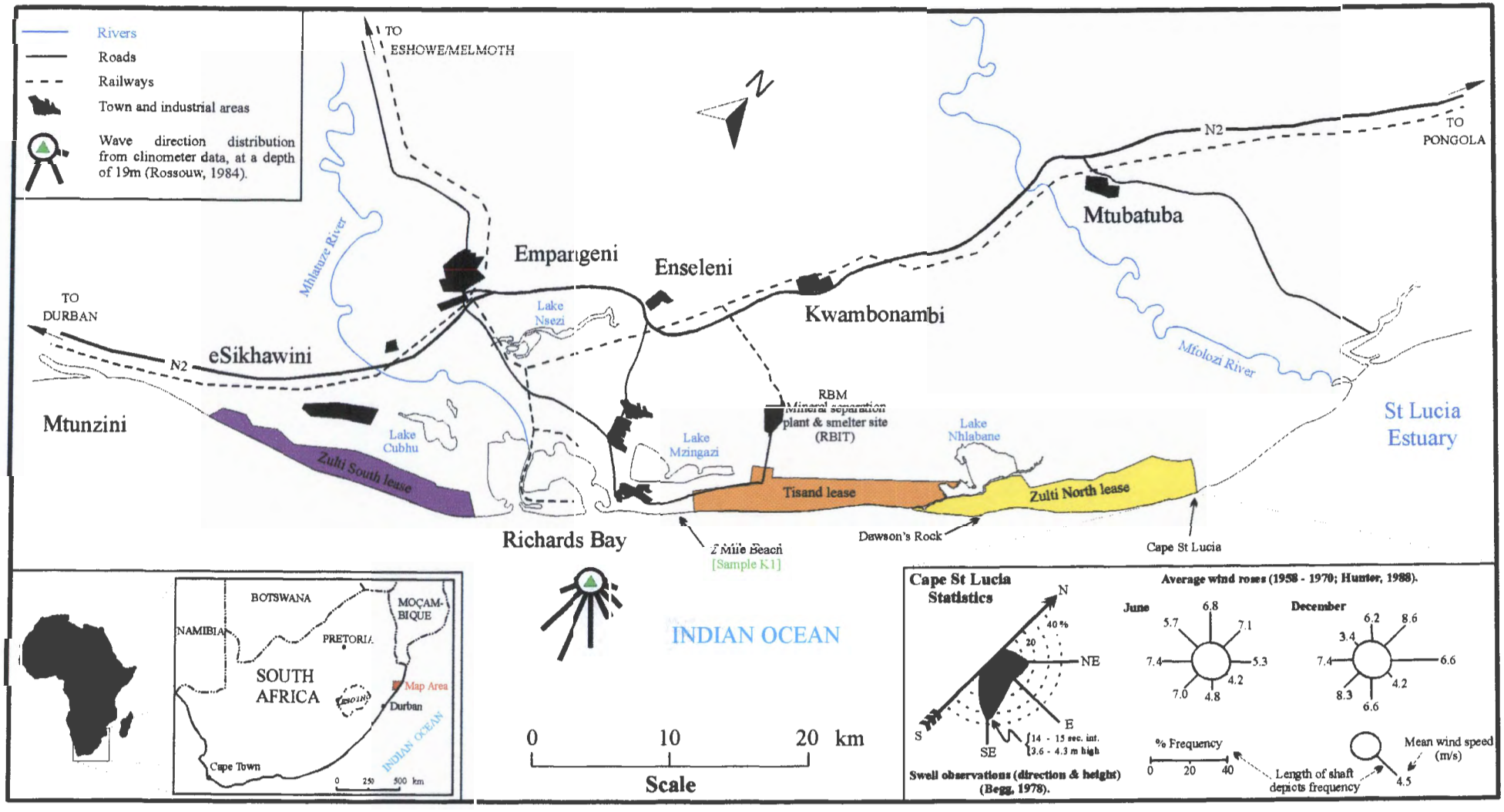

Figure 1.1 Locality of mineral lease areas operated by Richards Bay Minerals. The study area is within the Zulti North lease. Also shown are the wind and swell direction distributions recorded at Cape St Lucia and the wave direction distributions taken off Richards Bay Harbour, as well the position of sample K1 at 2 Mile Beach..

Figure 1.2 Suction dredge and water cannon at Mining Pond A, ZNL. Mining advances as the working face is undercut. Photo taken looking northeast, June 1999.

mineral extraction and smelting plant. Plant tailings from the mining operation are landscaped to approximately the original dune topography. These are then successively stabilised and vegetated.

1.2 LOCALITY

The study area represents a small portion of the northern KwaZulu-Natal coastal plain dune cordon, situated approximately 30 km north of Richards Bay (28°58″ S, 32°32″ E). This area is known as the Zulti North lease (ZNL; Figures 1.1, 1.3 & 1.4). It comprises a 2 km wide coastal strip extending approximately 20 km along the coast from Lake Nhlabane (28°37″ S, 32°16″ E) in the south, to Cape St Lucia (28°30″ S, 32°25″ E) in the north and has a relief of up to 180 m. The ZNL is currently being mined by four mining ponds, named Pond A, C, D and E (Figure 1.4).

1.3 SCOPE AND OBJECTIVES

This project is a continuation of the work carried out by Sudan (1999) who characterised the sand-sized fraction (particles greater than 63 μm) within the ZNL and proposed a geological history for dune formation. This study focuses on the fine-fraction (silt/clay) within the central ZNL, with special emphasis on the clay-fraction. It comprises detailed analytical data obtained from surface and borehole samples. Aspects covered include:

(1) Laboratory procedures to extract and analyse the fine-fraction.
(2) Characterising the mineralogical composition of the clay and silt within the fine-fraction.
(3) Documenting the abundance of silt and clay assemblages in order to delineate packages within the dune cordon and correlate these to dune units identified from the sand-fraction by Sudan (1999).
(4) Investigation of weathering and post-deposition alteration processes within the dune cordon.
(5) Collaborative analytical work to determine relative and absolute dune ages using luminescence dating within the ZNL area.
(6) To facilitate RBM in understanding the evolution of the dunes which they mine.

1.4 DEFINITIONS USED

Several key words used throughout this text can have various definitions and interpretations depending on

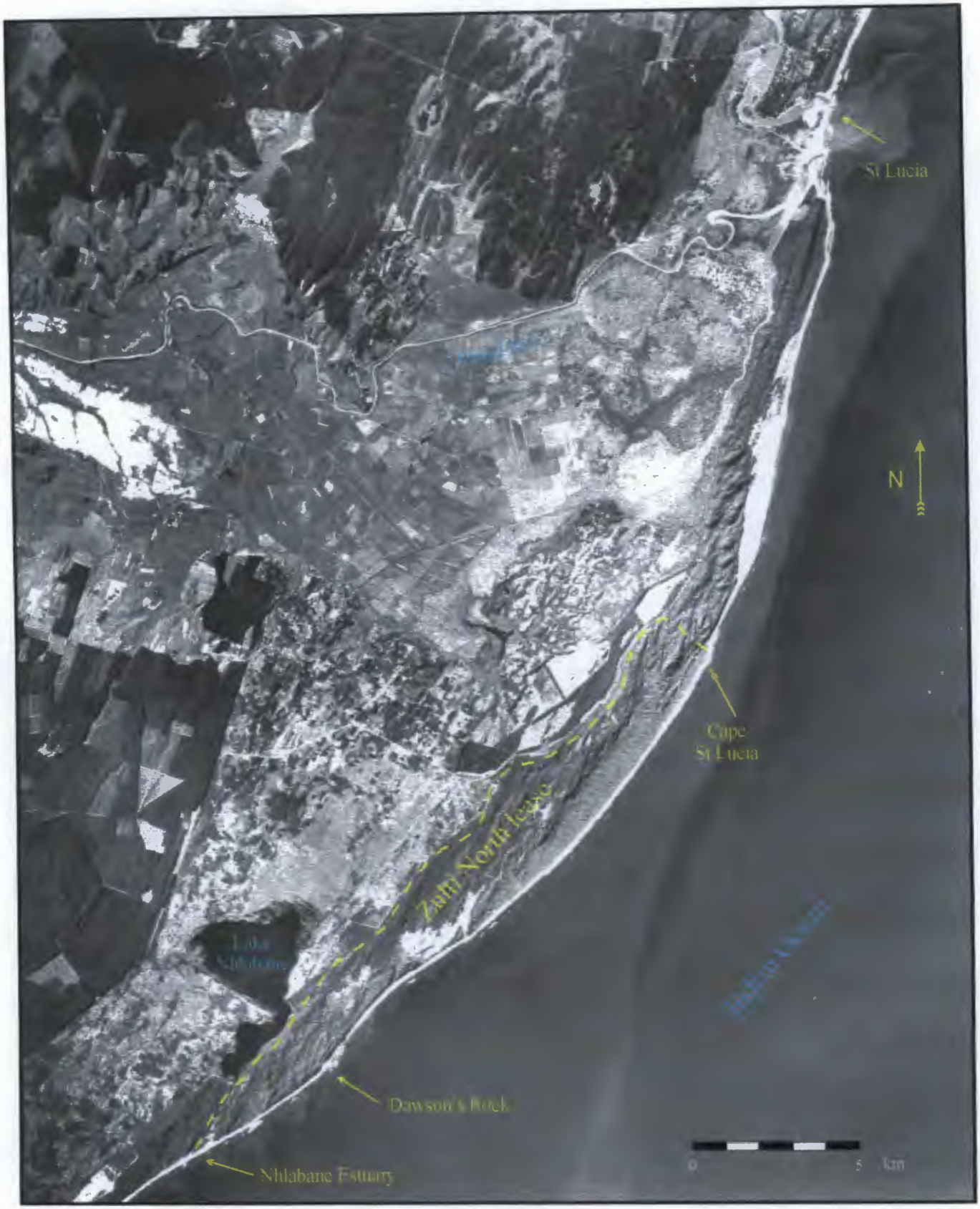

Figure 1.3 Aerial photograph of part of the northern KwaZulu-Natal coastal plain surrounding the Mfolozi River flood plain. The Zulti North lease is delineated by a dashed yellow line (The Air Survey Co., 1986).

the expression reviewed. To avoid ambiguity these are defined below.

(1) *Fines* will be used purely as a size distinction and will be considered as all particles less than 63 μm equivalent spherical diameter. It must be noted that RBM considers fines to be those particles less than 45 μm equivalent spherical diameter. These are unable to be extracted or smelted (blown out the furnace) and are thus included in the tailings; used purely as an extraction limit .

(2) The size fraction of particles between 2 μm and 63 μm equivalent spherical diameter will be referred to as *silt*. For a more detailed discussion on the choice of the silt size parameters and its formation, the reader is directed to Assallay *et al.* (1998).

(3) The size fraction of particles less than 2 μm equivalent spherical diameter will be referred to as *clay, clay particles* or *clay-fraction*.

(4) Hydrous layer silicates, in this study, being of the clay-fraction (< 2 μm equivalent spherical diameter) are referred to as *clay minerals* or by their appropriate group, sub-group or species names.

(5) Minerals (oxides, silicates, phosphates and carbonates) other than the hydrous layer silicates found within the clay-fraction, will be referred to as *other clays* or *other clay minerals*.

1.5 METHODOLOGY

1.5.1 SAMPLE LOCALITIES

RBM has drilled approximately 7000 boreholes on a 100 m × 50 m grid spacing in order to assess ore reserves within the ZNL. The company uses a unique grid as a reference system for the location of boreholes which does not use longitude or latitude (Figure 1.4). Instead, two parameters are utilised which correspond to the local coastline. "Eastings" are roughly perpendicular to the coast and "Northings" parallel to it. While the Northing axis is a metric scale, the Eastings axis is characterised by a numerical and alphabetical scale. Each successive alphabetical letter represents a 100 m Easting distance. This alphabetical scale is also referenced to point AA (numerical value 0) with double letters representing boreholes west and single letters to the east of AA. A numeric "/1" annotated to the borehole label, represents a fill in borehole that is intermediate to the 100 m spaced holes. According to this reference system, a borehole located at Northing 1200 and Easting 500 is denominated 1200/E (Figure 1.7). A borehole denominated 1200/BB/1 would be located at Northing 1200 and Easting -50. Due to possible confusion that "I" and "II" may cause with the numeric system they have been omitted, thus giving K and KK Easting values of 1000 and -1000 respectively.

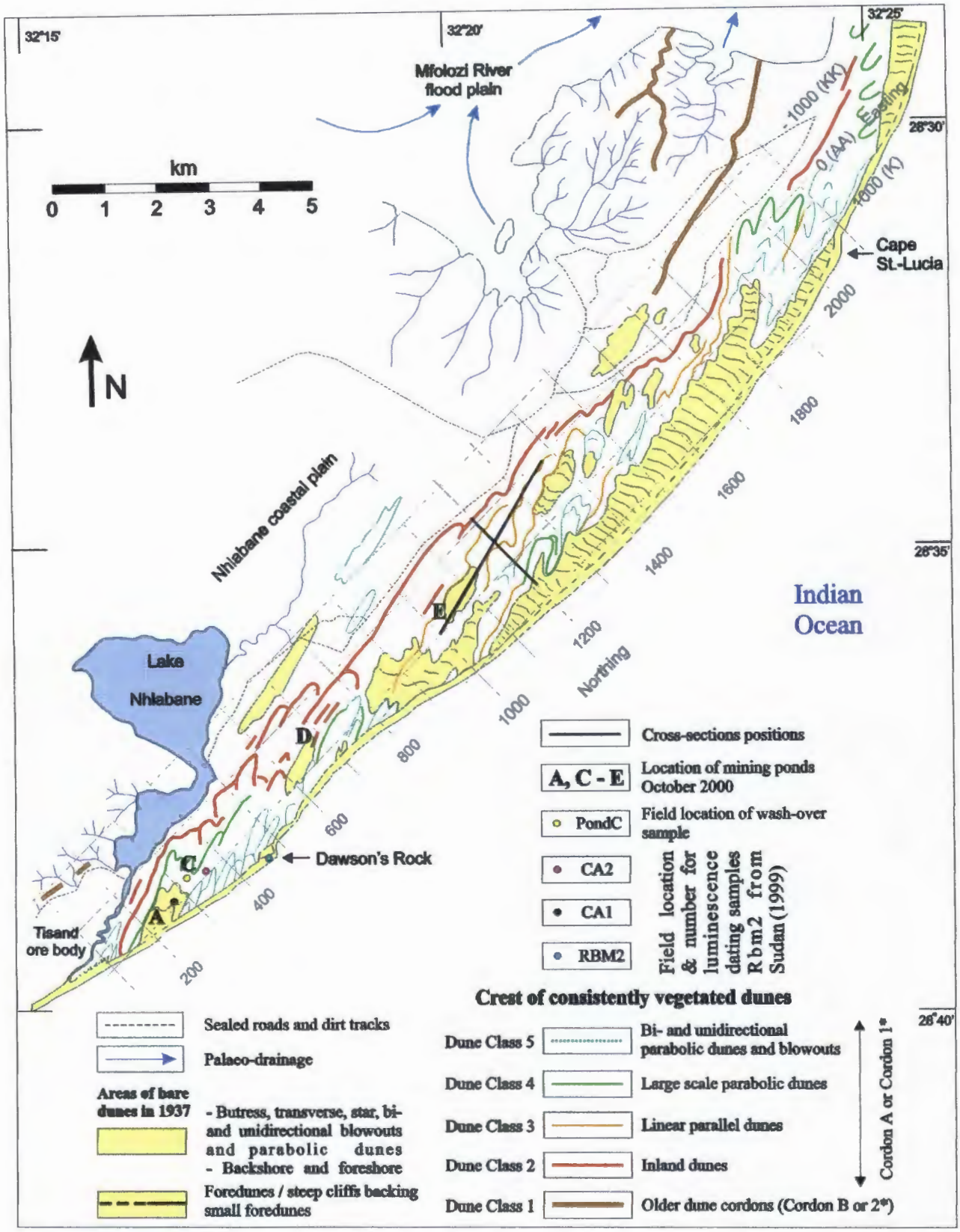

Figure 1.4 Geomorphological map for the Zulti North lease area, showing positions of cross-sections, luminescence dating samples CA1 and CA2, mining ponds and recognised dune classes. This map also shows the local coordinate system used by RBM as a stippled grid and grey line numbers. *Cordon A and B of Davies (1975), Cordon 1 and 2 of Wright (1999)(adapted from Sudan, 1999).

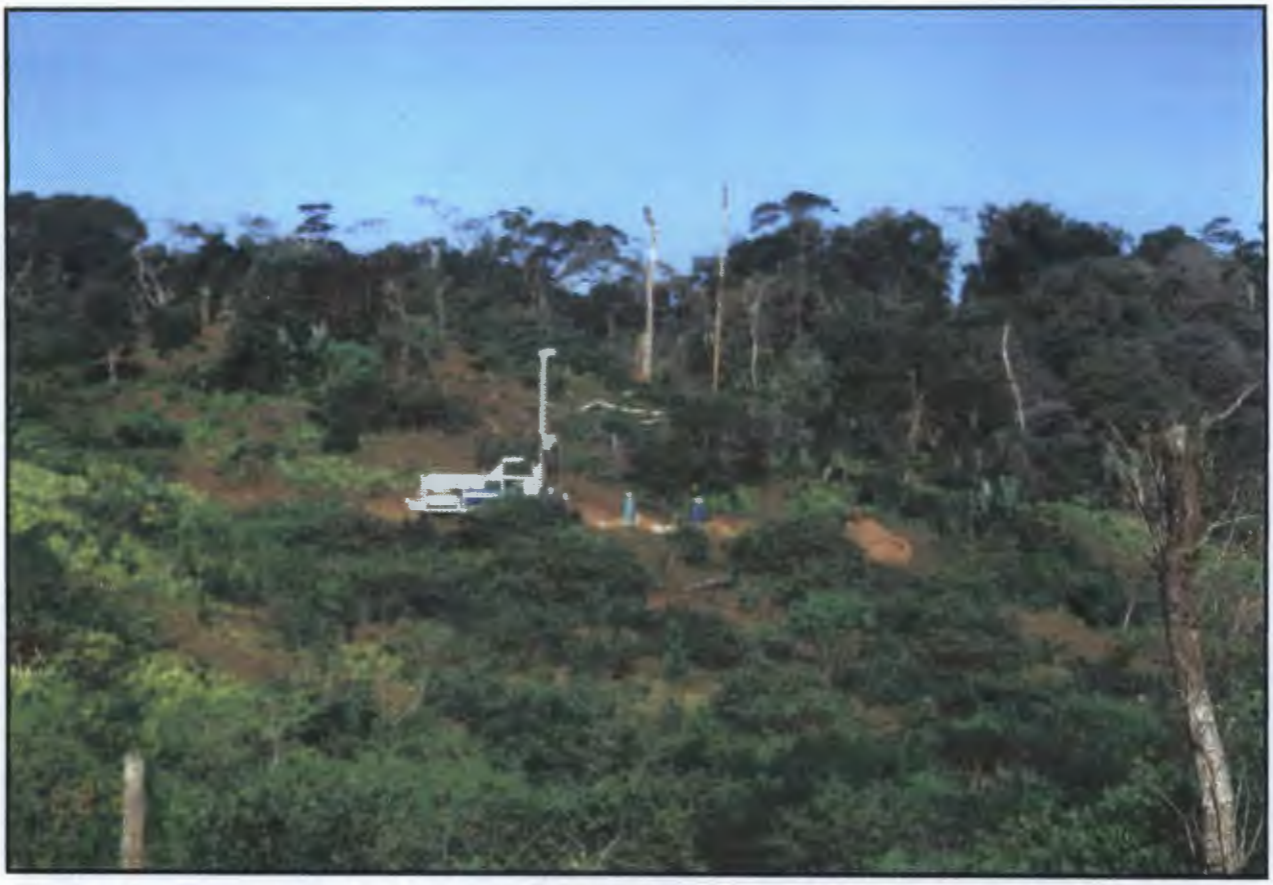

Figure 1.5 Reverse circulation drill rig, drilling borehole L1, June 1999. Photo taken looking east. Refer to figure 1.7 for location.

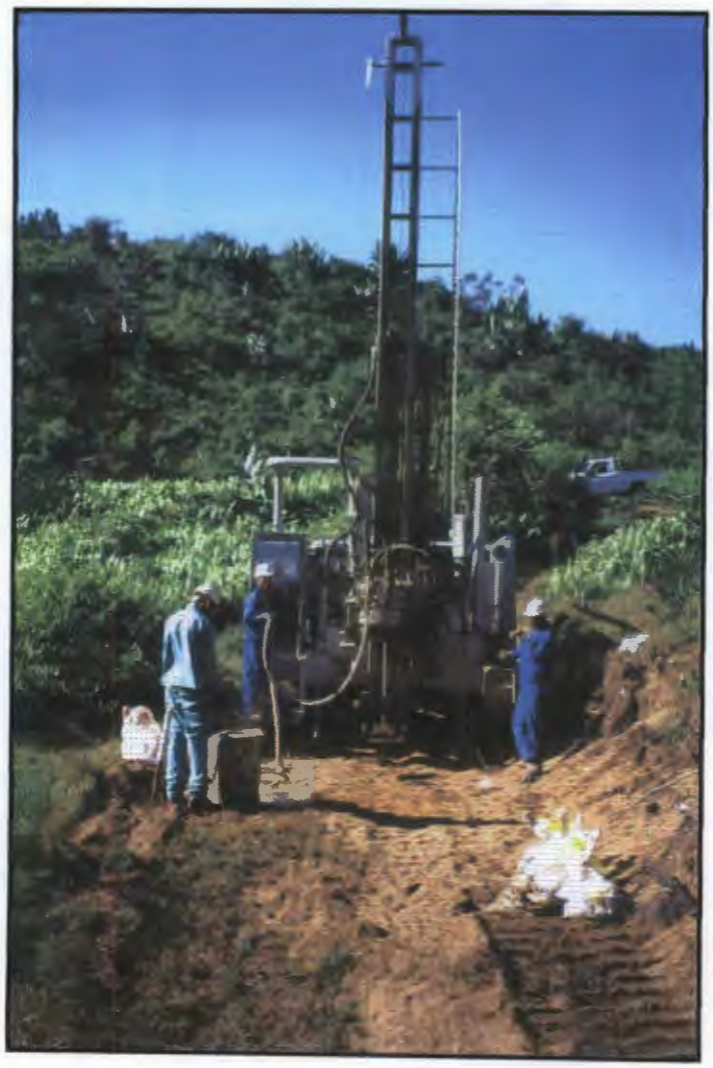

Figure 1.6 Close up of Figure 1.5 showing bulk samples in the foreground.

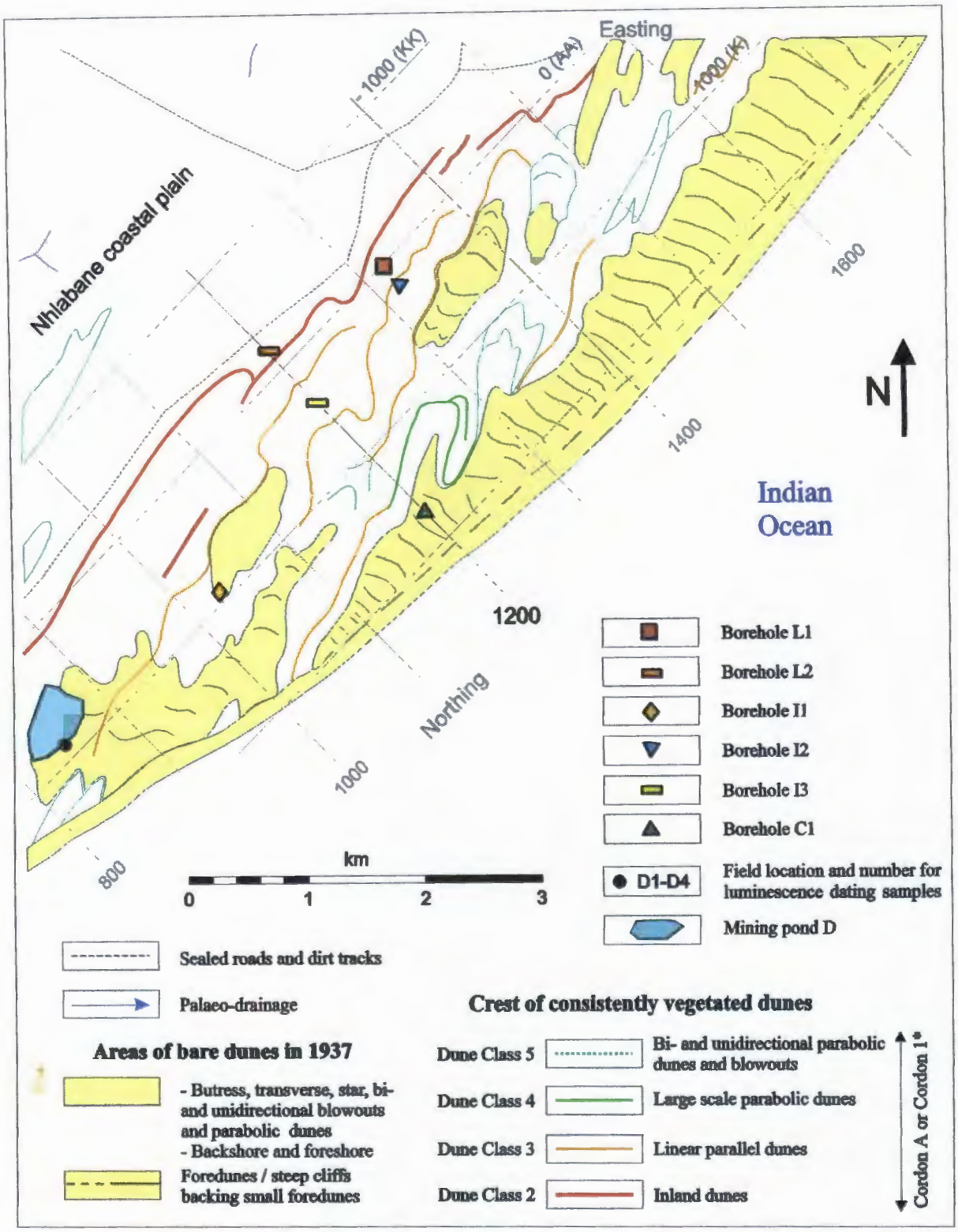

Figure 1.7 Geomorphological map of the central Zulti North lease area (adapted from Sudan, 1999), showing the location of all boreholes, which intercept Dune Classes 2, 3 and 4. Also shown are the field location of the luminescence dating samples D1-D4. *Cordon A of Davies (1975), Cordon 1 of Wright (1999).

Each of the 7000 boreholes have been logged and bulk samples, representing a 6 m down-hole interval, split, analysed and archived. These samples have been utilised for past research (Sudan, 1999) but could not be used in this study as the RBM sample preparation techniques result in loss of fines and destruction of clays during aggressive oven drying. As this study is dependent on the preservation of the fine-fraction, six boreholes were drilled adjacent to old boreholes under the supervision of the author.

A custom built track mounted reverse-circulation drill rig was used with a 44 mm diameter core so that an *ca.* 20 kg sample was obtained for each 6 m down hole interval (Figure 1.5 & 1.6). Three boreholes were drilled in June 1999 to quantify and identify the minerals within the fine-fraction and a further three in March and June 2000 to intersect all central dune units identified by Sudan (1999).

A northwest/southeast cross-section (Figure 1.8) was constructed perpendicular to the coast intersecting dune units identified by Sudan (1999) using the sand-fraction from Northings line 1200 (Figure 1.4). A second cross-section (Figure 1.9) was constructed parallel to the coast in a northeast/southwest direction (Figure 1.4).

To clarify the dune stratigraphy, six near surface samples (D1 - D4, CA1 & CA2) were taken from mining faces (Figures 1.4, 1.7 & 6.1) for luminescence dating and one basal, semi-consolidated, clay-rich sample (K1) from 2 mile beach (Figures 1.1 & 6.1). To characterise fines within an active mining pond, sample PondC was collected from the spill over area of mining Pond C (Figures 1.4).

Table 1.1 Borehole locations; above mean sea-level is annotated amsl; Figure 1.7. Boreholes are abbreviated relative to the coast as follows: L = inland, I = intermediate, & C = coastal.

Borehole	RBM nomenclature	Date drilled	Location	Collar elevation amsl (m)	Bottom elevation amsl (m)	No. of samples
L1	1310/A/1	6/1999	N1310, E 150	62.0	-6.5	12
L2	1200/BB/1	3/2000	N1200, E -50	62.0	17.0	8
I1	1030/J/1	6/1999	N1030, E 950	40.0	-3.0	8
I2	1310/B/1	6/1999	N1310, E 250	66.0	-3.4	12
I3	1200/E/1	3/2000	N1200, E 600	88.0	-23.4	19
C1	1200/R	6/2000	N 1200, E 1800	22.0	-31.0	9

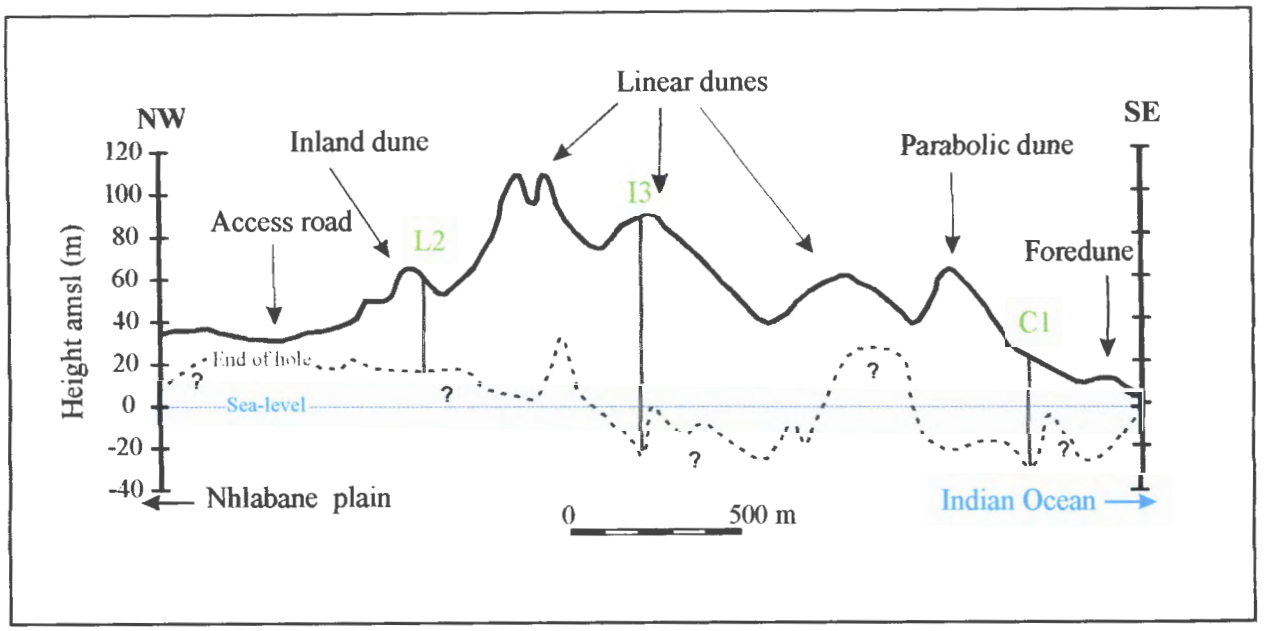

Figure 1.8 Topographic coast normal (northwest/southeast) cross-section through the central part of the ZNL area. Three boreholes (L2, I3 & C1) were studied in detail. The dashed line represents the end of hole. Boreholes are spaced every 50 m and most often terminated at consolidated material referred to here as basement.

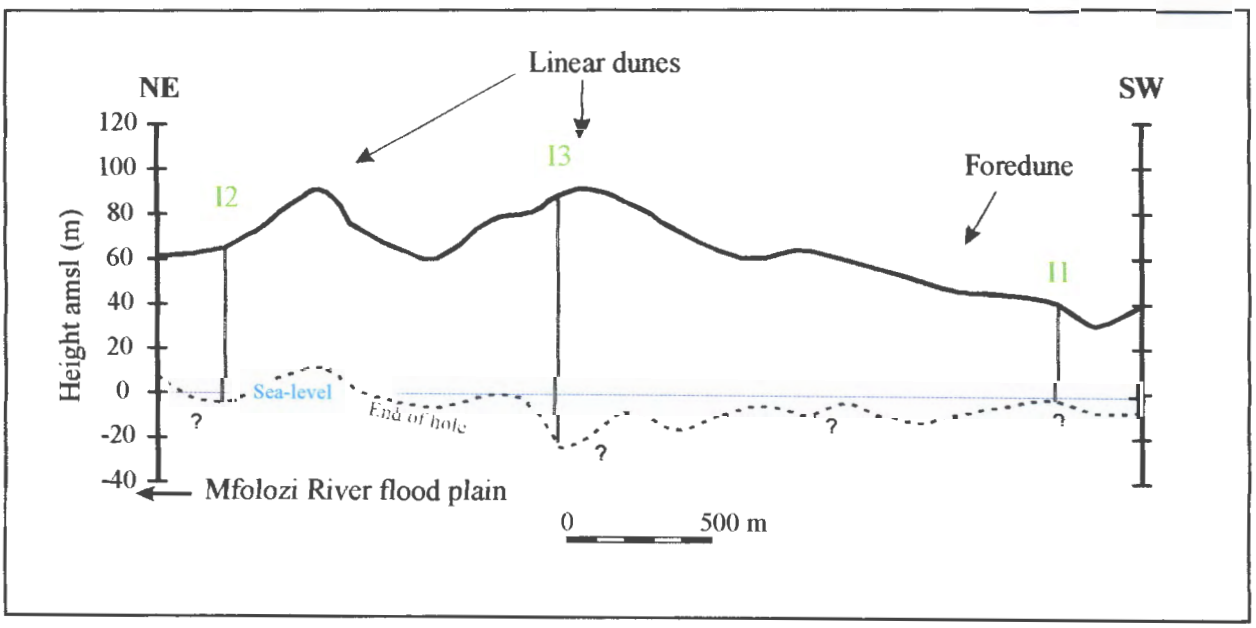

Figure 1.9 Topographic coast parallel (northeast/southwest) cross-section through the central part of the ZNL area. Three boreholes (I2, I3 & I1) were studied in detail. The dashed line represents the end of hole. Boreholes are spaced every 50 m and most often terminated at consolidated material referred to here as basement.

1.5.2 SAMPLE PREPARATION

Sample preparation took place at the University of Natal, School of Geological and Computer Sciences. Each of the 68 bulk borehole samples, 6 luminescence dating samples and the 2 mile beach sample were classified according to colour and then split into three representative sub-samples of 5 kg, 1 kg and 0.25 kg (Figure 1.10). These sub-samples were for silt, clay and bulk studies respectively. The spill over sample from mining Pond C was only used for the clay study.

The 5 kg sub-sample was wet sieved using a custom made sieve table (Figure 1.10) to obtain a 63 μm particle separation. The greater than 63 μm portion was oven dried at 60 °C and dry sieved on a 63 μm aperture sieve to ensure that all the fines were retained (some fines are held by surface tension of water on the sieve mesh and/or grain surfaces). The greater than 63 μm particles were stored and the dry sieved fines (generally less than 0.5 % of the total test sample) were added to the wet sieved fines. This fine-fraction was further split (when necessary) to obtain a representative 100 g oven dried (at 60 °C) sample. Silt was extracted by gravity settling in accordance to the procedure set out in Appendix A1. The 1 kg sub-sample was processed in the same manner and the fine-fraction split to extract clay using gravity settling (Appendix A2).

The 0.25 kg sub-sample was oven dried at 105 °C and split into two equal portions. One half was used for particle size analysis and the other was milled in a tungsten-carbide mill for 45 seconds. This sample was again split into two equal portions. One of these sub-samples was used for bulk chemistry determination (XRF) and the other for carbonate content determination.

1.5.3 METHODS OF SAMPLE ANALYSIS

1.5.3.1 X-ray diffraction analysis

Clays were identified using a Philips PW 1710 diffractometer (XRD) with CoKα radiation source (together with a graphite monochromator; long line focus) with the generator's voltage and current set at 40 kV and 30 mA respectively. A scan speed of 0.020 °2θ/s was used together with 1 second time interval per step. Samples with preferred mineral orientation were prepared on a glass slide using the smear technique (Moore & Reynolds, 1989). Patterns were recorded from 2 - 45 °2θ. Samples containing diverse/complex clay groups were subjected to a combination of six possible treatments on orientated specimens (Gibbs, 1965; Moore & Reynolds, 1989; Novich & Martin, 1983) to aid in sub-group and species identification

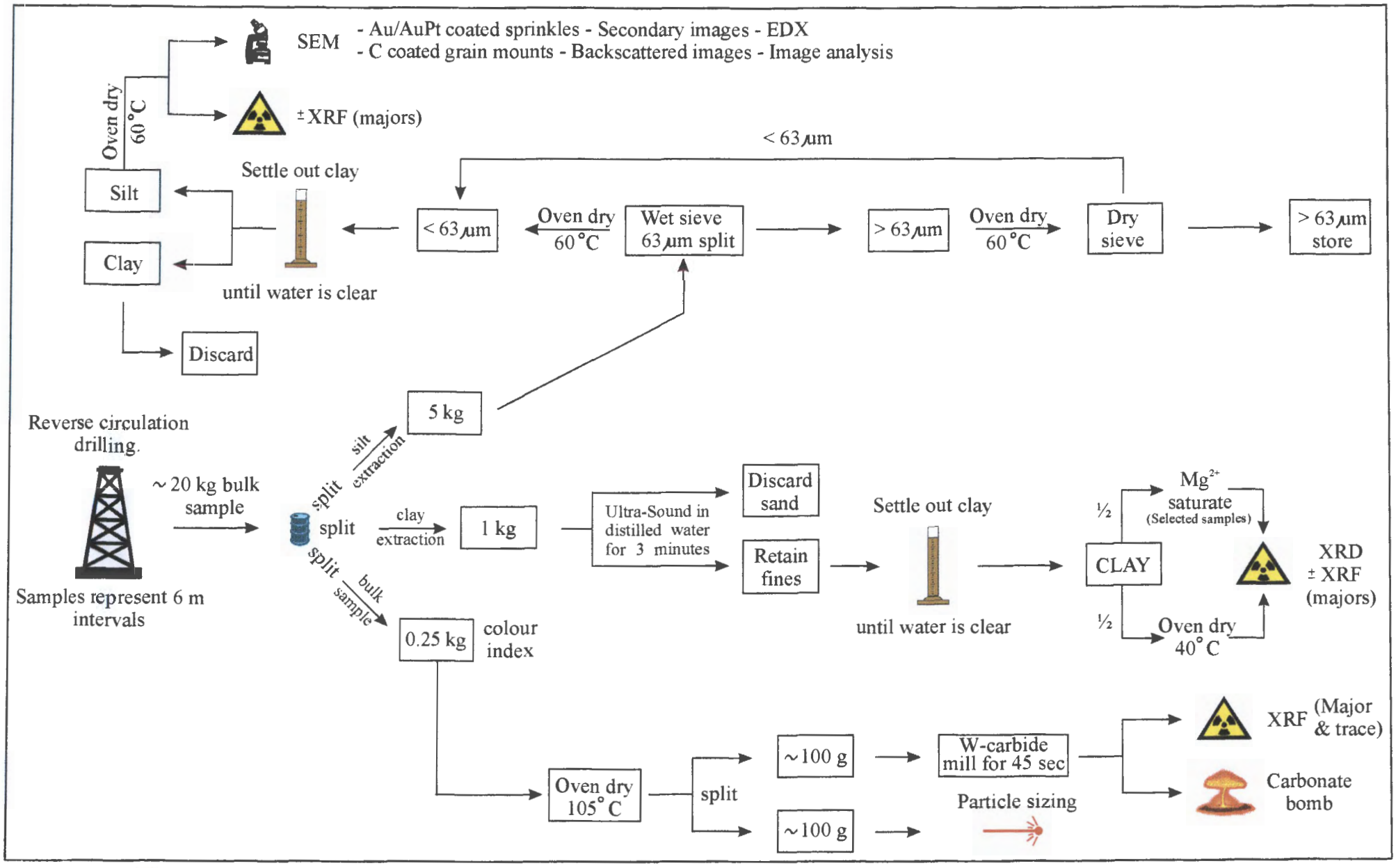

Figure 1.10 Sample preparation flow chart for the extraction and analysis of: bulk samples, the silt-fraction, and the clay-fraction.

(Chapter 3). These included:

(1) Heat treatment (4 hours at 550 °C) to collapse swelling clay minerals by dehydrating the interlayer and converting kaolin to an amorphous state. Chlorite's first order peak intensity increases and shifts to about 14 Å. Smectites show dehydration and the first order peaks shifts from about 15 Å to 10 Å. Goethite also shows dehydration with the disappearance of the 4.18 Å peak and the appearance of strong 2.69 Å and 2.51 Å peaks which resembles hematite. Serpentine is not affected by such treatment.

(2) Formamide (1 drop of solution on the orientated sample, left to react for 10 minutes and analysed immediately) treatment to differentiate kaolinite from halloysite. In this time, the first order peak of halloysite will expand from 7.2 Å to 10.4 Å after such treatment, were as kaolin would be unaffected by such treatment.

(3) Hydrazine intercalation (vapour at 60 °C for 7 days) treatment to determine the crystallinity of kaolinite and to further differentiate kaolinite from serpentine and chlorite. Well ordered kaolinites (and halloysites) first order peak shifts to 10.4 Å whereas disordered kaolinites do not show this shift. Serpentine and chlorite are unaffected by such treatment.

(4) Ethylene glycol (vapour at 60 °C for 12 hours) treatment to differentiate smectites, vermiculites and interstratifications. After such treatment, smectites produce a strong first order peak at 17 Å and a subordinate peak at 8.5 Å. Vermiculites produce a strong first order peak at 17 Å while the peak at 8.5 Å is absent. Interstratifications show a shift in the d(003) peak to higher diffraction angles with the remaining interstratification peaks not obeying Méring's principles (Méring, 1949).

(5) Mg^{2+} saturation (equilibrated with 1 M $MgCl_2$ solution for 24 hours and then washed several times in a centrifuge with distilled water and finally with water/ethanol mix to remove Cl^-) to differentiate Mg-saturated vermiculites from smectites (see point 6 below).

(6) Glycerol (vapour at 80 °C for 12 hours) treatment to aid in the differentiation of smectites from vermiculites. Mg-vermiculite retain a first order peak of 14.5 Å after glycerol solvation whereas smectites expand to about 18 Å after such treatment.

A back-packed, air-dried (AD) at ambient humidity (clays can expand or contract in higher or lower humidity respectfully by the intake of water into their interlayers) powder technique was used. By back-packing the aluminium sample holder, which are placed face down on filter paper, a near-random orientation of minerals are achieved. This is necessary for dioctahedral and trioctahedral mineral identification with the aid of peaks corresponding to the 060 crystal indices and for quantitative analyses. Patterns were recorded from 2 - 90 °2 θ.

The modal percentage of clay obtained from the air-dried analyses were calculated using the integrated intensity of the strongest peak (Moore & Reynolds, 1989; Appendix B). This is achieved by calculating the area under each of the strongest peaks for each clay identified. The area was approximated by multiplying the peak-height, minus the background intensity, by the peak width at half-height. Each clay's integrated intensity is them summed and dived by the summation to give a relative modal percentage for each clay. Inaccuracies of estimated clay abundances are possible as a result of the difficulty in differentiating between overlapping peaks. However, when known overlapping peaks were encountered on the strongest peak for a certain clay, the theoretical intensities (at that specific overlapping peak) of the "offending" peak was subtracted. Although this method is inaccurate due to the many variables involved (especially the presence of gels), it was considered adequate as relative variation in clay abundances was the aim of this exercise. Errors for major constituents are in the order of 10 % and 20 % for minerals whose concentrations are less than 20 % (Griffith, 1967; Moore & Reynolds, 1989). Internal standards and mineral mixtures were used to try and quantify percentage clay composition. However, this proved unsuccessful due to the polyminerallic nature of the specimens under investigation. A further attempt to quantify clay abundances was made on selected XRD samples using major element abundances; method discussed in section 1.5.3.2. Use of slightly larger sample holders towards the end of this study caused aluminium peaks at 52 and 61 °2 θ (2.0 Å & 1.8 Å) which were consequently ignored.

1.5.3.2 X-ray fluorescence analysis

X-ray Fluorescence (XRF) analyses on the milled sample were conducted using a Philips X'Unique 11. Major elements determinations were performed on fused disks (0.35 g of sample mixed with 2 g of Spectroflux in a Pt/Au crucible for 2 hours at 1000 °C) and trace element determinations from pressed powder pellets (8 g of sample mixed with 0.6 ml Mowiol glue and compressed by 8 tonnes). Analytical accuracy is within 0.2 to 0.5 % of the abundance for major elements, and 5 to 10 % for trace elements.

1.5.3.3 Scanning electron microscopy

The silt-fraction was analysed using a Philips XL 30 environmental scanning electron microscope (SEM; LaB_6 cathode) with an energy dispersive X-ray (EDX) attachment to aid in mineral identification. The SEM is housed at the University of Natal, Pietermaritzburg campus, Centre for Electron Microscopy. Due to continuos down-time on the latest Philips XL 30, selected grain morphology samples (Table 4.1) were analysed on a Hitachi 520 fitted with a W-cathode together with EDX for mineral identification.

Samples were prepared using two methods. First, grain morphology and identification studies were conducted using secondary images obtained by sprinkling *ca.* 0.5 g of silt sample onto carbon tape secured to a 1.5 cm diameter copper stub. These stubs were coated with Au or Au/Pd to create a conductive surface and the minerals were analysed semi-quantitatively using EDX. The second method involved impregnating *ca.* 5 g of silt sample with clear resin in 25 ml plastic vials. After hardening these were cut in half perpendicular to the settling direction to avoid errors caused by particle segregation. These "silt blocks" were then polished, coated in carbon and viewed as backscattered images. A total of ten images were obtained per silt block, giving a total of 750 images. These images were analysed using a software package called ImageJ, version 1.16f; Rasband, 2000, to determine the modal abundances of high atomic element minerals (ilmenite, rutile, zircon, monazite etc) relative to low atomic element minerals (quartz, feldspars etc.). A detailed method of the image analysis technique is given in Section 4.2.1.1.

1.5.3.4 Particle size analysis

Particle size analysis was conducted on bulk samples at the University of Natal, School of Geological and Computer Sciences using a loaned Crystalsizer (Retsch Technology, 2000) which uses incoherent light diffraction to measure particles of between 2.5 mm and 0.7 µm. Due to its high clay content, sample PondC was analysed using a laser-based SediGraph 5100 (v. 3.07) at the Council for Geoscience, Marine Section, Bellview.

1.5.3.5 Carbonate analysis

The milled sample was also analysed for calcium carbonate content (carbonate bomb; Schink *et al.*, 1979). This was used to assess the quantity of CaO (determined by XRF) within calcite versus Ca-bearing silicate minerals.

1.5.3.6 Colour index

A Munsell Soil Colour Chart (Munsell, 2000) was used to classify the bulk sample's colour in a moist state. There are three dimensions that combine to describe all colours in the Munsell system; Hue (relation to Red, Yellow, Green, Blue, and Purple), Value (lightness; black 0 - white 10) and Chroma (strength; departure from a neutral of the same lightness). The Hues "R", "YR" and "Y" correspond to the redness to yellowness with a prefix number 0 to 10 reflecting an increasing yellowness. Colours are then given an appropriate name, such as a 10YR 4/4 would be a dark yellowish brown.

1.5.3.7 Luminescence dating

Luminescence dating samples (D1-D4, CA1 & CA2) were collected from various mine faces (Figures 1.4, 1.8 & 6.1) under the supervision of Dr Woodborne of the Quaternary Dating Research Unit, Environmentek, Council for Scientific and Industrial Research (CSIR), Pretoria. All samples were collected in PVC pipes (5 cm diameter and 30 cm in length) which were forced into the exposed *in situ* dune sands. The tubes were carefully extracted and the ends sealed off from sunlight. The ends were subsequently excluded from analysis. Details of the luminescence dating procedures are given in Appendix G.

2 REGIONAL SETTING

2.1 REGIONAL GEOLOGY

A knowledge of the geological and geomorphological setting of southern Africa, especially KwaZulu-Natal (KZN), is important if variations in the mineralogy, distribution and alteration states of the coastal dune cordons under study are to be understood. The catchment geology (Figure 2.1 a & b) of rivers draining KZN comprise basement rocks of the Archaean Kaapvaal Craton and the Proterozoic Namaqua-Natal Metamorphic Province. These are overlain by a generally flat-lying Phanerozoic cover succession with Cretaceous to Recent deposits along the coast. These rock types are discussed below, as broad stratigraphic units, with emphasis on those that have contributed significant amounts of sediment to the northern KZN coastal dune cordons.

2.1.1 ARCHAEAN

Kaapvaal Craton

The Kaapvaal Craton is located north of the Tugela Fault (Figure 2.1 a) and is exposed inland of Richards Bay. Current exposure of the Kaapvaal Craton is drained by both the White and Black Mfolozi Rivers (Figure 2.1 a & b). The rocks of the Kaapvaal Craton comprise Archaean granitoids and gneisses which have intruded deformed greenstone relicts. These in turn have been intruded by granodiorite and tonalite, now deformed to gneiss (Matthews, 1959; Charlesworth, 1981).

Pongola Supergroup

The Pongola Supergroup formed within a basin developed on the Kaapvaal Craton and is exposed inland of Richards Bay where it forms part of the catchment geology of the White and Black Mfolozi Rivers. It comprises a supracrustal succession that accumulated during cratonisation in the late Archaean (Linström, 1987). It obtains a maximum thickness of 10.6 km and is subdivided into the lower Nsuze Group and the upper unconformable Mozaan Group (SACS, 1980).

The basal Nsuze Group comprises a succession of quartzites and lavas (basalt, andesite and rhyolite) with subordinate shale, dolomite, conglomerate and tuff (SACS, 1980). The group obtains a maximum thickness of 8.8 km (SACS, 1980), with the felsic volcanic rocks having a mean radiometric age of 2 984 ± 2.6 Ma

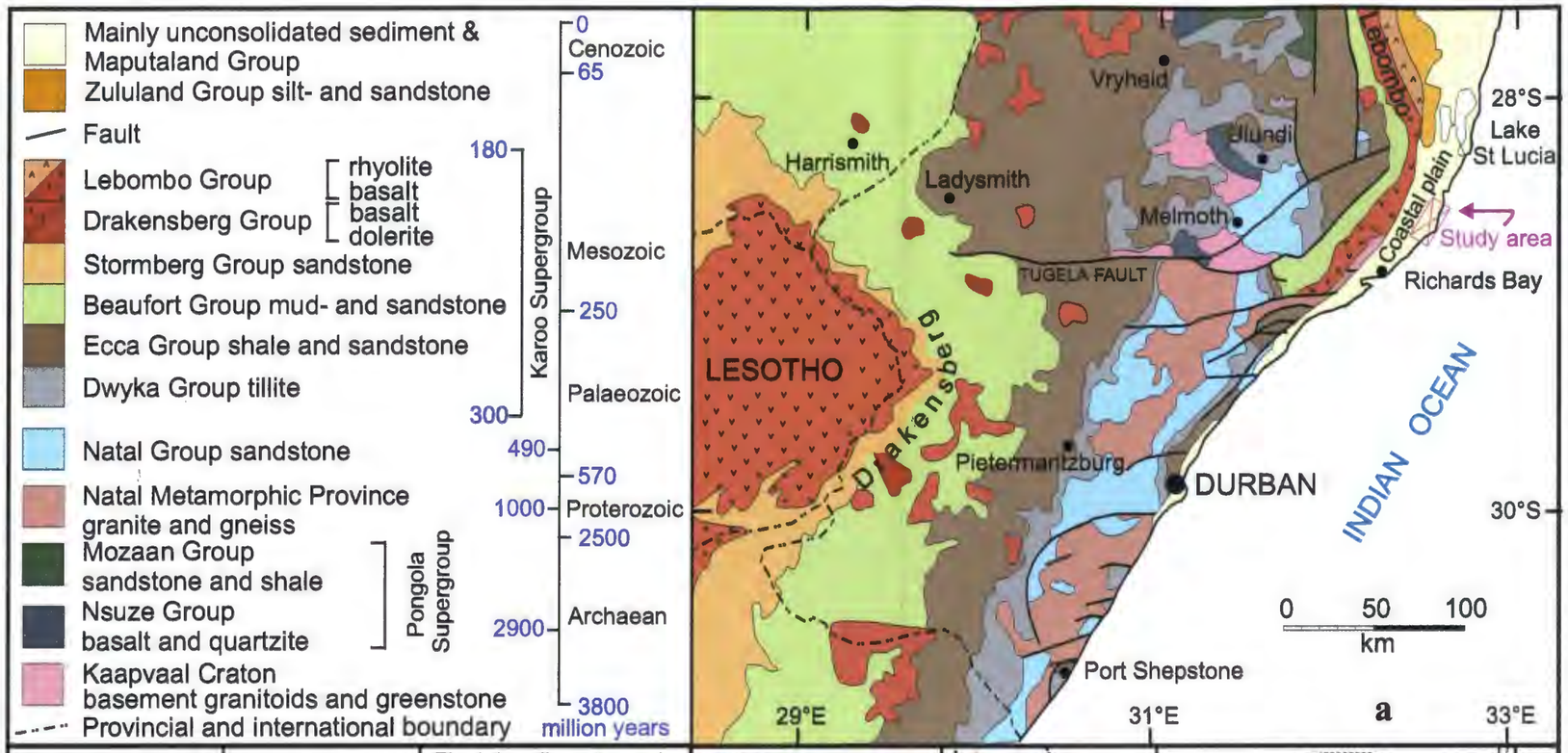

Major KZN Rivers	Catchment (km²)	Fluvial sediment supply (10^6t/yr)
Tugela	29 101[1]	8.8[3]
Mfolozi	10 075[1]	2.4[1]
St Lucia system	~ 9 000[2]	2.3[5]
Mzimkulu	6 745[1]	2.2[1]
Mgeni	4 432[1]	1.7[3]
Mkomazi	4 310[1]	1.6[3]
Mvoti	2 829[1]	0.8[3]
KZN TOTAL	~81 000	30[4]

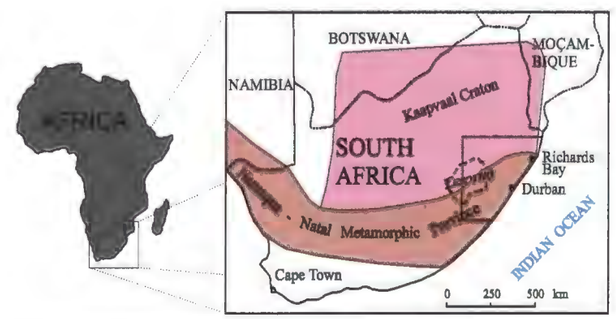

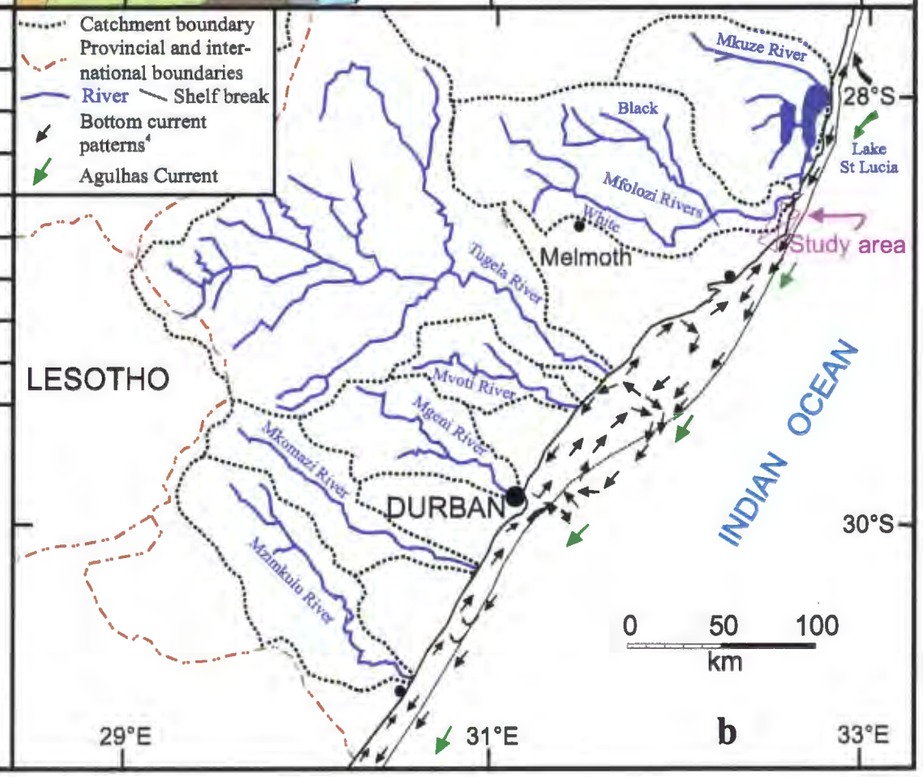

Figure 2.1 (a) Simplified geology of KwaZulu-Natal (adapted from Whitmore *et al.*, 1999). **(b)** Drainage patterns of the major rivers in KwaZulu-Natal. The St Lucia system includes the Mkuze River and smaller fluvial inputs from the Mzinene, Hluhluwe, Nyalazi & Mpate Rivers. References shown with superscripts are as follows: [1] McCormick *et al.* (1992), [2] Wright *et al.* (1990), [3] Cooper (1991), [4] Flemming & Hay (1988) and [5] Average of the Mfolozi & Mzimkulu Rivers, however the fluvial sediment is greatly retained in the lake system.

(Hegner *et al.*, 1993). According to Linström and Marshall (1982) the overlying Mozaan Group consists essentially of a lower arenaceous and an upper argillaceous sequence with subordinate acid lava. It obtains a maximum thickness of 6.8 km.

2.1.2 PROTEROZOIC

Natal Metamorphic Province

The late Proterozoic Natal Metamorphic Province crops out south of the Tugela Fault (Figure 2.1 a) in a series of poorly exposed basement inliers, which cover some 10 000 km^2 of central to southern KZN (Thomas *et al.*, 1990). These rocks have radiometric ages varying between ~1 200 and ~900 Ma (Eglington *et al.*, 1989; Thomas & Eglington, 1990) and a general east to east-north-east structural trend. Metamorphic grade increases progressively from north to south (Matthews, 1981). Greenschist facies rocks, dominated by mafic lithologies are exposed in the Tugela Valley. These have been interpreted by Matthews (1959, 1981) as a mafic/ultramafic ophiolite suite obducted onto the southern flank of the Kaapvaal Craton as a series of nappes. These are in turn overlain by metasediments and metalavas. Amphibolite facies rocks comprising mafic and felsic gneisses form the central portion of the exposed basement which pass into granulite facies rocks in the Port Shepstone area (Thomas *et al.*, 1990).

2.1.3 PALAEOZOIC

Natal Group

Ordovician rocks ($^{40}Ar/^{39}Ar$ age of 490 Ma; Marshall & von Brunn, 1999) belonging to the fluvial Natal Group were deposited on the Archaean and Proterozoic basement rocks in an elongate basin, the axis of which was more or less parallel to the present KZN coastline (Visser, 1974; Thomas *et al.*, 1992). They consist essentially of medium-grained quartz-feldspathic sandstones and siltstones with occasional conglomerates. The group varies considerably in thickness from a few 10's of metres to approximately 600 m (Roberts, 1981; Linström, 1987) with an estimated minimum thickness of 1.3 to 2.6 km at the time of deposition (Marshall & von Brunn, 1999). According to Marshall and von Brunn (1999) the provenance for the major portion of the Natal Group sediments was probably a Pan-African orogenic belt situated in southern Moçambique. Although the Natal Group is generally resistant to erosion, it is deeply weathered and carries an early Cenozoic laterite capping on remnants of the African erosion surface developed thereon (Partridge & Maud, 1987).

Karoo Supergroup

The Karoo Supergroup ranges in age from Carboniferous to Jurassic, outcrops extensively throughout KZN and is a major source of sediment to the south east coast (Figure 2.1 a & b). The Supergroup was deposited in a vast intracratonic basin formed on Gondwana, which obtained its maximum depth in the south with its basal group deposited unconformably on various older rocks including those of the Kaapvaal Craton, Pongola Supergroup and the Natal Group (Visser, 1989). It is subdivided into the following units.

Dwyka Group

The Dwyka Group forms the base of the Karoo Supergroup and was deposited during the Permo-Carboniferous glaciation. It consists of massive tillite and mudstones that reach a maximum thicknesses of 370 m in the Durban area (King & Maud, 1964). However, the uneven erosional surface on which the tillite is deposited results in a highly variable thickness for this group.

Ecca Group

Rocks belonging to the Ecca Group are Permian in age and crop out predominantly in the marginal areas of the main Karoo basin, with the northern facies represented in KZN (Visser, 1989). The rocks were deposited in a large sea as Gondwana drifted north into warmer climates. The group comprises a basal fissile shale and siltstone unit (Pietermaritzburg Formation) overlain conformably by an alternating sequence of sandstones and micaceous shales with subordinate coal seams (Vryheid Formation). This is inturn overlain by a further shale and mudstone sequence (Volksrust Formation). The entire group obtains a maximum thickness of 1.2 km and can also be found cropping out west of Richards Bay due to block faulting (SACS, 1980).

Beaufort Group

The Beaufort Group covers approximately 200 000 km^2, in the Karoo basin and reaches a maximum thickness of ~6 km in the Eastern Cape Province (Johnson, 1976). It consists of alternating immature sandstones and mudstones. This group transgresses the Palaeozoic/Mesozoic boundary and was deposited in an enclosed foreland basin during a transition from marine to terrestrial environments (Visser, 1989).

2.1.4 MESOZOIC

Stormberg Group

The mid-to-late Triassic Stormberg Group comprises the Molteno, Elliot, and Clarens Formations. The Molteno Formation consists of up to 450 m of alternating mudstones and subordinate medium-grained sandstone consisting of fining-upward cycles deposited in a fluvial environment (Johnson, 1984). Occasional coal seams and conglomerate units are developed locally. The Elliot Formation was deposited conformably on the Molteno Formation and is composed of mudstone, siltstone, and shale, alternating with sandstone deposited on an extensive flood plain (Visser, 1989). The formation reaches a maximum thickness of 500 m and thins to the north where it is only 100 m thick in the vicinity of Harrismith (Figure 2.1 a). Fossils are common and include silicified wood, vertebrates, and fish (Du Toit, 1954). The Clarens Formation consists of very variable thicknesses of fine-grained aeolian sandstone, deposited as large dunes in a desert environment, which contains scarce fossils of silicified wood, reptilian remains, crustaceans and fish imprints (Du Toit, 1954; Johnson, 1984).

Drakensberg Group

The early Jurassic Drakensberg Group forms the extensive Drakensberg Plateau which covers practically the entire Kingdom of Lesotho, with an estimated outcrop area of 140 000 km^2 (Tankard *et al.*, 1982). This plateau is considered to be a remnant of once extensive lava flows thought to have covered much of Gondwana. It comprises 1.4 km of basaltic lava (with thin subordinate sandstone) which was poured out in great regularity and in rapidly succeeding flows (Visser, 1989). The main peak of volcanic activity was *ca.* 180 Ma and is probably coincident with the initial stage of Gondwana breakup when Antarctica separated from southern Africa to form the Indian Ocean (Eales *et al.*, 1984).

Lebombo Group

The middle Jurassic to early Cretaceous Lebombo Group embraces the entire succession of basic and acid lavas occurring along the eastern margin of southern Africa and forms the Lebombo Range. The basal unit (Letaba Formation) is predominately basalt with subordinate andesite, rhyolite, and tuff, totalling at least 3.6 km in thickness. This is overlain conformably by the Jozini Formation which is a thick unit of rhyolitic lava totalling more than 8 km in the north, but thins to the south and wedges out in the environs of the St. Lucia Lake (Visser, 1989). The rhyolite, which has been dated at 179 ± 4 Ma (Allsopp *et al.*, 1984), dips

at approximately 10° to 20° towards the east and gives rise to the prominent Lebombo Range. This is inturn overlain unconformably by the Cretaceous Movene and Mpilo Formations which comprises a thickness of up to 2 km of basaltic to andesitic lava, with individual beds dipping at *ca.* 8° towards the east (Visser, 1989). These are further overlain and intruded by syenites and rhyolites representing the felsic phases of the 133 ± 4 Ma Bumbeni Complex (Allsopp *et al.*, 1984).

Karoo Igneous Province

The Karoo Igneous Province refers to the vast intrusion of dolerite into rocks of the Karoo Supergroup during the Jurassic Period. It has been estimated that in South Africa the outcrop of dolerite intrusions covers an area of about 570 000 km^2, with an original area of ~900 000 km^2, if erosion is taken into account (Du Toit, 1921; Visser, 1989). Intrusion is preferential into the soft, argillaceous rocks of the Karoo Supergroup especially those of the Ecca Group. The numerous intrusions take the form of horizontal and inclined sills and narrow near vertical dykes; preferentially striking north-west or west-north-west (Du Toit, 1954). The intrusions appear to form the feeder system of the Drakensberg Group and have thus been included with the latter in Figure 2.1 a. Encarnación *et al.* (1996) obtained a U-Pb age of 183.7 ± 0.6 Ma for one such intrusion. Another swarm of Jurassic dolerite dykes were emplaced sub-parallel to the western side of the Lebombo Range extending northwards from the southern Lebombo region into Swaziland to the northwest of the study area. Known as the Rooi Rand dyke swarm these multiple dykes span more than 200 km in a north-south orientation and are between 10 - 22 km in lateral extent (Saggerson *et al.*, 1983). The dyke swarm is believed to mark the initial stage of Gondwana breakup in the Lebombo region and represents a failed rift system (Saggerson *et al.*, 1983; Meth, 1996) .

Zululand Group

Rocks belonging to the Zululand Group were deposited on the eastward tilted Lebombo Group during a marine transgression from the north due to fragmentation of Gondwana (Visser, 1989). They are Cretaceous to early Tertiary in age and consist of the Makatini, Mzinene and St Lucia Formations. They unconformably overlie the Lebombo Group volcanics and are all stratigraphically conformable with general easterly dips of 1° to 5°. These formations underlie most of the northern KZN coastal plain, yet are only exposed as thin units along inland areas and isolated patches surrounded by younger sediments. The lower two formations narrow and disappear at depth around Richards Bay (Wolmarans & Du Preez, 1986).

The Makatini Formation forms the base of the Zululand Group and comprises non-marine conglomerate,

with pebbles of volcanic (mainly dolerite) and quartzitic rocks, that are often interbedded with shallow-water marine siltstones and are finally overlain by fully marine, fossiliferous sandstone (Wolmarans and Du Preez, 1986). Tankard *et al.* (1982) regard this formation as a prograding succession of braided, fluvial deposits, laid down in a shallow sea, from *ca.* 120 Ma to about 114 Ma ago (Watkeys *et al.*, 1993). The overlying Mzinene Formation, deposited between 112 Ma to 91 Ma ago, comprises shallow marine siltstones and sandstones, which are glauconitic and locally pebbly, with sandy and shelly concretions (Watkeys *et al.*, 1993).

The overlying marine St Lucia Formation transgresses the Cretaceous-Tertiary boundary and extends into the Palaeocene (Danian; approximately 60 Ma), however it is only documented in boreholes within the Richards Bay area (Maud & Orr, 1975). It consists of a basal conglomerate overlain by cross-bedded siltstones and fine-grained sandstones, which are in turn overlain by glauconitic siltstones and fine-grained sandstones with interbedded calcareous concretions. This formation is rich in Mollusca, Echinoidea, and Foraminifera (Kennedy & Klinger, 1975; Dingle, 1981; Cooper, 1988; Klinger & Kennedy, 1990).

2.1.5 CENOZOIC

The Cenozoic Era rocks comprise a thin veneer of superficial deposits of sand, gravel, semi-consolidated sandstone and limestone and have been estimated to cover 40 % of the pre-Cenozoic geology in KZN (SACS, 1980). Marine deposits of middle Eocene age have only been encountered in boreholes near Kosi Bay where they are seen to be unconformable with overlying early Miocene rocks (Botha, 1997 a). There are no rocks of Oligocene age exposed on land, probably due to marine regression during these epochs. However early Oligocene calcarenites and limestones were encountered in boreholes drilled during hydrocarbon exploration on the northern KZN coastal plain and offshore Borehole JC1 (McMillan, 1997).

Maputaland Group

Recent advances in understanding sea-level changes along the south-east margin of southern Africa has led the SACS Cenozoic Task Group (Botha, 1997 a) to provisionally redefine the Cenozoic stratigraphy (Figure 2.2). The Maputaland Group is exposed along the beaches and composite dune systems on the northern KZN coastal plain (Botha, 1997 a). It represents deposits which accumulated in response to eustatic sea-level changes and epeirogenic-isostatic uplift during the Neogene and Quaternary periods, and will be discussed under the following formations.

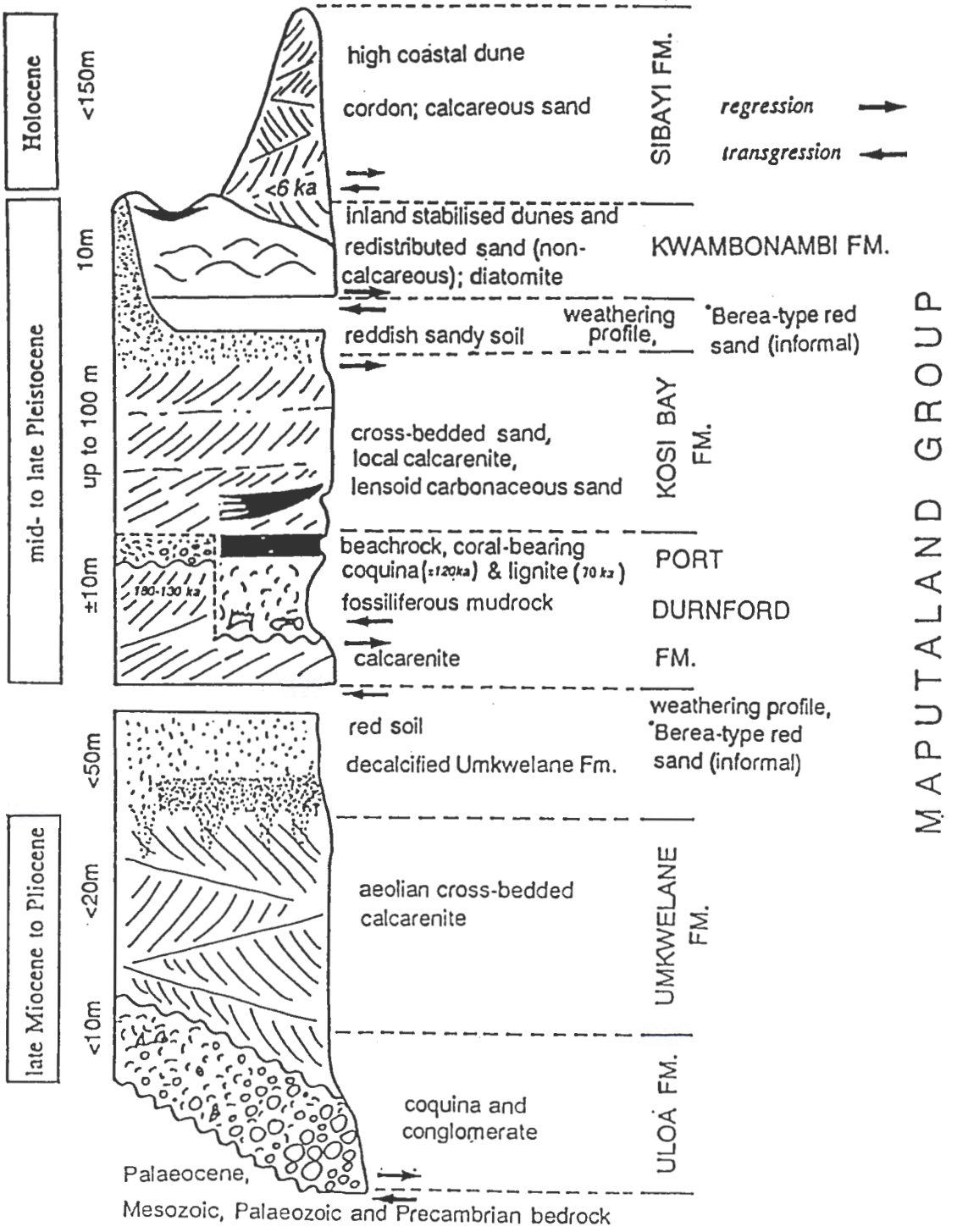

Figure 2.2 A schematic, composite section through the Maputaland Group* showing the regressive marine couplets of littoral and dune sediments deposited primarily during the Mio-Pliocene marine regression and Mid-to Late Pleistocene sea-level changes (Botha, 1997a). * Not formally recognised by the South African Committee for Stratigraphy (SACS).

Uloa Formation

Several studies have indicated that the Uloa Formation formed during the late Miocene (Liu, 1995; Maud & Orr, 1975). In contradiction to this McMillan (1997) suggests a Pleistocene age based on microfossil evidence. However, Stewart (1998) considers the Pleistocene age to be unlikely as key microfossil evidence identified by McMillan (1997) has not been identified by subsequent studies. According to Liu (1995) the Uloa Formation rests disconformably, as a veneer, on siltstones of the St Lucia Formation. It consists of a lower yellowish-brown hard coarse coquina of shell fragments (mainly mollusc; *Aequipecten uloa*) and an upper sandy calcarenite member revealing karst weathering (Maud & Orr, 1975). The maximum total thickness of the lower and upper units is about 15 m (Wolmarans & Du Preez, 1986).

Umkwelane Formation

The Umkwelane Formation (early Pliocene) rests on the karst-weathered surface of the Uloa Formation, and in places, directly on underlying Cretaceous sedimentary rocks (Maud & Botha, 2000). It comprises a lower marine stratified calcarenite and an upper cross-bedded aeolianite, which was deposited during a marine regression along the Lebombo foothills and towards the coast (Botha, 1997 a). According to Botha (1997a) a series of sea-level stillstands during this regression are marked by remnants of dune cordons which are now deeply weathered and decalcified to form Berea-type red (rubified) clayey sand. The greatest thickness of the lower littoral marine portion is about 5 to 8 m, whereas the aeolian upper part is up to 25 m thick on the bank of the Pongola River, approximately 30 km south of the Moçambique border (Maud & Botha, 2000).

Port Durnford Formation

The mid-to-late Pleistocene, Port Durnford Formation underlies the seaward portion of the Maputaland coastal plain, where it rests unconformably on either the Uloa, Umkwelane Formations or on Cretaceous sediments (Maud & Botha, 2000). The formation comprises a fossiliferous basal argillite member ($\leq$ 10 m) and an upper (~15 m) arenaceous member separated by a discontinuous lignite bed. The lignite was deposited at the beginning of the Last Glacial (Isotope Stage 4). The underlying aeolian, marine and lagoonal deposits are therefore ascribed to the Last Interglacial (Oschadleus & Vogel, 1996; Maud, 1993). The basal shelly mudrock has yielded early- to middle- Pleistocene mammalian fossils whereas the lignite has been radiometrically dated using $^{230}Th/^{234}U$ at *ca.* 70 000 ± 5 000 yrs BP (Oschadleus & Vogel, 1996). According to Maud & Botha (2000) the aeolian sediments lying above the basal argillites, including the

lignite deposit, should be included in the younger Kosi Bay Formation due the marked unconformity which separates these members.

Kosi Bay Formation

The Kosi Bay Formation is up to 50 m thick and rests unconformably on the underlying Port Durnford Formation. Past workers assigned the core of the coastal dune cordon, as well as the lower parts of the inland dune cordons to the Kosi Bay Formation. However Sudan (1999) only identified the Kosi Bay Formation towards the north of the ZNL (Figure 1.1). The basal lignite bed averages 1.3 m in thickness, with its base occurring at an elevation varying from approximately 1 to 3 m amsl (Scott *et al.*, 1992). The single $^{230}Th/^{234}U$ lignite date of 70 000 ± 5 000 yrs BP (Oschadleus & Vogel, 1996) is considered too young as recent luminescence dates of the sand above and below the lignite near Port Durnford lighthouse, and the lowermost white clayey sand overlying the basal mud at 5-Mile beach north of Richards Bay are between *ca.* 350 - 250 Ka (Dr. N. Porat, Geological Survey of Israel, pers. comm, 1999 *In:* Maud & Botha, 2000). The lignite is overlain by about 15 m of orange or grey weathered semi-consolidated dune sands and finally by white to light grey semi-consolidated clayey sands (Botha, 1997a). The colour of these sands is attributed to a high kaolinite content (~ 10%) and a low heavy mineral abundance of < 3 - 4 % (Singh & Dunlevey, 1997). This colour grades upwards into a yellow to red-brown with abundant mottles and concretions (Singh & Dunlevey, 1997). The top of the formation is locally characterised by the presence of ferricrete (Maud, 1968; Johnson, 1986; Singh & Dunlevey, 1997).

Kwambonambi Formation

During the subsequent marine regression (Isotope Stages 4 to 2) aeolian deposition and reworking of the older dune sands (especially the Kosi Bay Formation), as well as interdune wetland deposits formed the Kwambonambi Formation (Botha, 1997 a). According to Botha (1997 a) and Sudan (1999) the lower sea level exposed much of the continental shelf and caused rivers to incise during the peak of the Last Glacial Maximum (~ 17 ka; Figure 2.4). The Kwambonambi Formation comprises 5 to 15 m of redistributed yellowish red, grey and white unconsolidated dune sands and is extensive over much of the Maputaland coastal plain and northwards into southern Moçambique. The sands are yellowish red, grey and white and contain less abundant fine-fraction and more abundant heavy minerals than the underlying Kosi Bay Formation (Fockema, 1986; Singh, 1995).

Sibayi Formation

According to Botha (1997 a) and Sudan (1999) the subsequent Holocene marine transgression (Figure 2.4) flooded coastal valleys and lakes, with alluvial sedimentation infilling many bedrock valleys close to the coast. The mid-Holocene high sea-level at +3.5 m amsl (4 480 years BP; Ramsay, 1995) is recorded by beachrock along the coastal lake systems, which achieved their current form after accretion of the coastal dune cordon (Sibayi Formation) blocked former links with the sea (Botha, 1997 a). They thus represent the youngest phase of sand accreted immediately inland from the shoreline and consist of brown to grey unconsolidated calcareous sands, which have locally been rubified and decalcified to depths of several metres. The sands also contain abundant heavy minerals in economic concentrations.

2.2 PHYSIOGRAPHY AND EAST COAST DYNAMICS

In order to understand the transport and weathering of minerals along and within the northern KZN dune cordon, a summary of the physiography is presented below.

2.2.1 CLIMATE

According to the Okolowicz Classification (Martyn, 1992), southern Africa lies in zone 2 of tropical climates, with KZN having a humid subtropical to intermediate climate with mountain variants. The atmospheric circulation over southern Africa is controlled by the permanent anticyclonic South Atlantic and South Indian Ocean Highs stationed at latitude 30°South (Martyn, 1992). Their positions vary by only *ca.* 4° latitudinally from season to season and are commonly referred to as the southern sub-tropical high-pressure belt (Hunter, 1988). They lie farthest north in mid-winter (July-August) and are in their southernmost situation in mid-summer (February).

The weather stations of Cape St Lucia (28°30′S; lighthouse keeper's records) and Richards Bay are the closest weather stations to the ZNL; therefore these climatic data, where available, will be used in preference to regional weather stations.

2.2.1.1 Rainfall, temperature and humidity

Rainfall is highly seasonal over most of southern Africa and is almost entirely a summer phenomenon, except for the southwest coast where winter rainfall dominates. The summer rainfall region receives 80%

of the annual rainfall between October and March (Tyson, 1986). Rainfall along the northern KZN coast averages 1000 - 1100 mm annually, but this declines progressively inland or westward to approximately 600 mm at the base of the Lebombo Range (Maud, 1980). On the crest of the Lebombo Range the annual rainfall increases to approximately 800 mm (Maud, 1980). The annual average coastal temperature increases slightly towards the north and averages 20 °C to 26 °C. The air temperatures are characterised by a relatively low seasonal range which is due to the cooling effect of land and sea breezes, increased cloud cover, high atmospheric humidity, and the moderating effects of the adjacent ocean as the warm Agulhas Current gives a positive anomaly of 2 °C (Tinley, 1986; Hunter, 1988; Martyn, 1992). The hinterland is characterised by a larger seasonal range and lower annual average air temperatures. The winter months, especially June and July, are the coldest where air temperatures of below zero are commonly recorded in the Drakensberg Mountains, together with frost and snow-falls.

The weather station at Richards Bay recorded a mean annual rainfall of 1102 mm with highest and lowest monthly rainfall of 144 and 31 mm respectively for January and June (South African Weather Bureau, 1986). The annual air temperature at 14H00 is 25.5 °C, varying from 22.7 °C in June to 28.2 °C in January, with a mean annual relative humidity of 83 % at 08H00 which decreases to 68 % by 14H00 (South African Weather Bureau, 1986). According to Martonne's Index of Aridity, Cape St Lucia is the wettest area on the coast of southern Africa (Tinley, 1985).

The occurrence of tropical cyclones over northern KZN are rare, although when they do occur, (1984, 1987 and 1988), extensive wave and flood damage ensues (Hunter, 1988). Most tropical cyclones develop northeast of Madagascar between November and April, with an average of less than one each year affecting KZN (Hunter, 1988). Heavy, wide-spread rainfall may also occur during "cut-off lows" (1971 and 1974; Hunter, 1988).

2.2.1.2 Wind

A striking feature of average, seasonal wind roses for Cape St Lucia (Hunter, 1988; Figure 1.1) is the high frequency of strong winds blowing parallel to the northeast/southwest trending coastline, especially in summer. North to northeasterly winds dominate the December wind rose, whereas the June wind rose shows a significant increase in offshore flow; this being related to nocturnal land breezes (Hunter, 1988). Data from Voluntary Observing Ships (VOS) show that southwesterly through to southerly winds generally have the highest velocities although wind conditions vary greatly (Hunter, 1988). The warm Agulhas Current gives the region an enhanced land breeze circulation offshore and there may be a link between this

circulation and the initiation of convection both over the Agulhas Current and, at times, over the coast (Hunter, 1988).

The importance of aeolian coastal sediment transport, especially by coastal winds, in the ZNL is evident by the partially vegetated coastal barrier dune complex that dominates the northern KZN coastline (Wright, 1999). In the Durban region it has been calculated by Swart (1987) that the potential sand transport direction by wind is equally divided between northeast and southwest. For the St Lucia estuary it has been estimated by Van Heerden and Swart (1986) that the resultant drift potential is 20×10^3 m^3/km/year in a northerly direction, however Wright and Mason (1993) calculate a figure of 13×10^3 m^3/km/year, for the same area. In general a northerly movement of aeolian sands for the northern KZN coastline can be noted which corresponds to the general wind directions.

2.2.2 COASTAL HYDRODYNAMICS

2.2.2.1 Tidal range

Tides on the KZN coast are semi-diurnal, with a tidal range averaging 2 m (Schumann & Orren, 1980). The coast can therefore be described as high microtidal (Davies, 1964) or lower mesotidal (Hayes, 1979).

Table 2.1. Predicted tidal elevations for Durban and Richards Bay (from South African Tide Tables, 1997), with respect to chart datum (-0.99 m relative to land leveling datum or mean sea level). LAT = Lowest astronomical tide; MLWS = mean low water springs; MLWN = mean low water neaps, ML = mean level; MHWN = mean high water neaps; MHWS = mean high water springs; HAT = highest astronomical tide.

	LAT	MLWS	MLWN	ML	MHWN	MHWS	HAT
Durban	0	0.24	0.85	1.1	1.35	1.96	2.3
Richards Bay	-0.11	0.19	0.83	1.1	1.35	1.99	2.37

2.2.2.2 Swell regime

The northern KZN coast receives persistent high-energy waves and prevailing large-amplitude swells from the southeast for ~35 % of the year with northeasterly to easterly onshore swells prevailing another 40 %

of the time (Begg, 1978; Swart & Serdyn, 1981; Rossouw, 1984; Van Heerden & Swart, 1986; Figure 1.1). When northeasterly winds prevail, subordinate low-amplitude, short period northeasterly swells are generated which become superimposed on the dominate southeasterly swell (Ramsay *et al.*, 1989). Ramsay *et al.* (1989) further explain that when the northeasterly winds are persistent for a considerable period it becomes the dominate swell direction. The seasonal and annual wave-height percentage for Richards Bay is given in Table 2.2 and shows only a slight difference between the wave-height and the season. Approximately 70 % of the wave-heights are between 1.0 and 1.99 m (Rossouw, 1984).

The tidal and swell regimes result in a wave-dominated coastal sedimentary environment characterised by a single beach berm (Tinley, 1986). Due to the waves striking the coast obliquely from a southeast direction, there is a dominate longshore drift towards the north. The calculated mean northward sediment flux at Richards Bay is 0.8×10^6 m^3/year (Swart, 1980), 1×10^6 m^3/year just south of St Lucia (Van Heerden & Swart, 1986), and 1×10^6 m^3/year at the Tugela River-mouth (Nicholson, 1983). However Cooper (1991) regards these as over-estimates as the rates are calculated from refraction diagrams and take no account of sediment availability or grain-size.

Table 2.2. Percentage occurrence at Richards Bay of significant wave-height per season and per year (Rossouw, 1984).

Wave-height (m)	Autumn	Winter	Spring	Summer	Year Ave. of seasons	Year All data
0.0 - 0.49	0.08	0.14	0.19	0.00	0.10	0.11
0.5 - 0.99	17.00	17.57	11.10	11.49	14.29	14.13
1.0 - 1.49	43.00	43.43	45.50	50.57	45.63	45.64
1.5 - 1.99	24.08	24.93	29.04	25.70	25.94	26.10
2.0 - 2.49	10.50	8.86	8.81	7.79	8.99	8.94
2.5 - 2.99	3.50	3.07	3.45	3.17	3.30	3.30
3.0 -3.49	1.58	1.57	1.53	0.68	1.34	1.35
3.5 - 3.99	0.17	0.21	0.19	0.45	0.26	0.26
4.0 - 4.49	0.08	0.07	0.13	0.08	0.09	0.09
4.5 - 4.99	0.00	0.14	0.06	0.08	0.07	0.07
> 5.00	0.00	0.00	0.00	0.00	0.00	0.00
No. of records	1 200	1 400	1 567	1 323	-	5 490

2.2.3 OCEANOGRAPHY

The most important off-shore large-scale oceanographic feature is the Agulhas Current which is recognised as one of the world's major geostrophic currents (Schumann, 1988). According to Schumann (1988) it sweeps polewards with the core generally just offshore of the shelf break (Figure 2.1 b) and thus markedly affects the waters on the shelf. Offshore Richards Bay, there is a temperature decline of 4°C from summer to winter, with a maximum temperature of *ca.* 25 to 26°C in February for the upper 50 m of the water column (Schumann, 1988). North of Cape St Lucia maximum speeds of the current have been measured at *ca.* 1.5 m/s (Schumann, 1988), inducing a southward bed load transport (Flemming & Hay, 1988; Ramsay, 1994). According to Flemming (1981) the changes in the morphology of the KZN coastline together with atmospheric forcing in the wake of coastal low-pressure fronts causes multiple cyclonic eddies to occur inducing small northward flowing nearshore currents (Figure 2.1 b). This results in bedload parting zones where sediment transport occurs in a northerly direction (Ramsay, 1994; Flemming, 1981; Flemming & Hay, 1988).

The shelf off KZN is extremely narrow, compared to the global average of 75 km, and is characterised by submarine canyons, coral reefs and steep gradients (1° to 2.5°; world average is 0.116°) on the continental slope (Maud, 1968; Flemming, 1981; Ramsay, 1996). The shelf break which occurs at a depth of 60 - 100 m, is at its widest off the Tugela River where it is found at 45 km offshore but is only 3 km wide north of St Lucia (Flemming, 1981; Ramsay, 1996). For further readings on the shelf morphology and sediment dispersion, the reader is directed to Flemming (1981), Schumann (1988), Flemming & Hay (1988) and Ramsay (1996).

2.2.4 TOPOGRAPHY AND DRAINAGE

KZN is located on the eastern side of the Great Escarpment of southern Africa. The escarpment rises to over 3 300 m above sea-level in Lesotho with the port city of Durban situated only 230 km away (Figure 2.1 a). This results in a steep coastal hinterland which impacts on the drainage patterns causing high flow velocities (Cooper, 1991). In addition, rivers have little opportunity to coalesce and consequently most drain small, laterally restricted catchments, separated by marked divides in the deeply dissected hinterland (Cooper, 1991). River courses of the eastern Escarpment are narrow and have poorly developed flood plains which offer little storage capacity for alluvium (Le Roux, 1990).

To the northeast of KZN a striking feature is the Lebombo Range which forms a high lying ridge up to 700

m above sea-level and striking almost north-south. To the east lies the low, flat to undulating topography of the northern KZN (historically referred to Zululand, Maputaland and Tongaland) coastal plain which extends from Mtunzini (28°57' S) in the south through Moçambique, Tanzania, Kenya and into Somalia to the north. At the KZN and Moçambique border (27°51′ S) it is approximately 80 km wide whereupon it broadens appreciably as it extends into Moçambique. The South African section of the coastal plain has an area of some 5 700 km^2. Due to the shallow gradient and the presence of coastal dunes, rivers such as the Mkuzi River are unable to carry their sediment load resulting in the deposition of sediments onto the plain (Wright, 1999). As a result these rivers often drain into large coastal lagoons rather than directly into the sea.

Palaeodune cordons provide topographic highs on the coastal plain with numerous small pans occurring in the associated topographic lows between the dune palaeotopography. A high coastal dune barrier occurs adjacent to the coast, and reaches a maximum height of 182 m at Cape St Lucia. To the north of the study area, three large coastal water bodies dominate the coastal plain morphology. These are the Kosi lake and estuary system (26°50′S to 27°11′S and 32°38′E to 32°53′E), the St Lucia lagoonal system (27°52′S to 28°24′S and 32°21′E to 32°34′E) and the fresh water Lake Sibaya (27°15′S to 27°25′S and 32°33′E to 32°43′E).

The major river draining KZN is the Tugela River which has a catchment of approximately 29 101 km^2 (McCormick *et al.*, 1992) and accounts for 36 % of the total catchment area of the province and 30 % of the annual fluvial sediment supply (Figure 2.1 b). The other major rivers include the Mfolozi, St Lucia, Mzimkulu, Mgeni, Mkomazi and Mvoti respectively. It has been estimated by Flemming & Hay (1988) that the total fluvial sediment supply for KZN is approximately 20×10^6 m^3/year or 30×10^6 t/year. These total sediment volumes are small compared with the estimated annual yield of 65.1×10^6 m^3 (Goodlad, 1986) or 33×10^6 t (Milliman & Meade, 1983) for the 410 000 km^2 Limpopo River catchment which dominates Moçambique to the north of the study area, but indicate much higher sediment yields per km^2 (Cooper, 1991).

2.2.5 VEGETATION

Vegetation on the KZN coastal plain is directly correlated to climate and thus is an important indicator of past climatic conditions and soil formation. Also, erosion and sediment input into rivers is ultimately controlled by vegetation binding the soil.

Climatic conditions of KZN have led to a rich biodiversity with various vegetational types recognised with their associated endemic species. The vegetational types include swamp forests, dune forests, sand forests, mistbelt forests, montane forests, savanna, grasslands and wetlands. A brief overview of the three main vegetation types will be discussed and the reader is directed to Pooley (1994 & 1998) for further clarification and information. The latter vegetation types discussed are dune forests, savanna and grasslands.

The dune forests are confined to a very narrow strip spanning almost the entire KZN coast but have been severely disturbed by urbanization south of Mtunzini. Within the study area the dunes are among the highest forested dunes in the world (Pooley, 1994). Generally the dune forest flora are tolerant to sea-spray and high humidity. The dominate forest species include trees *Mimusops caffra*, *Sideroxylon inerme* and *Diospyros rotundifolia* with common plant species *Acokanthera oblongifolia*, *Aloe thraskii* and *Allophylus natalensis* to name but a few (Pooley, 1994). Further inland to the drier central and northern KZN, savanna vegetation (also referred to as bushveld or woodland) dominates and includes spreading trees belonging to the acacia family, various aloe species and grasses dominated by the subfamily Panicoideae. Grasslands are found in western KZN in generally higher rainfall areas than the savanna vegetation but tolerate the lower winter temperatures of the higher altitudes. The vegetation is dominated by various grasses of the subfamilies Pooideae and Panicoideae as well as small shrubs.

Within the last 75 years or so there has been a marked increase in cultivated crops, especially within the coastal areas where sugar cane and *Casuarina equisetifolia*, used for dune stabilisation initially and subsequently charcoal production, have been favored. Further inland Eucalyptus and Pine tree plantations together with an assortment of grazing lands are the norm.

2.2.6 SOIL

The soils of northern KZN coastal plain are strongly associated with the underlying geology and topography and vary from base rich clays to base poor sands and shallow rocky soils (Goodman, 1990). According to Goodman (1990) the nature of the parent material has the overriding influence over the other soil forming processes with topography having a strong influence on the soil texture. This is especially true for the volcanic rocks and dune cordon sands.

On the Lebombo Range the combination of relatively steep slopes and the erosion resistant rhyolites have given rise to lithosols of various depths (Goodman, 1990). Within the incised valley floors the soils are

predominantly shallow gritty clays, generally kaolinite. The early Cretaceous siltstones and sandstones have resulted in soils of varying depths, texture and mineralogical composition (Goodman, 1990). Elevated soils are generally more leached lithic or ferruginous containing kaolinite, while valley bottom soils are characteristically unleached calcimorphic soils and vertisols containing non-expansive 2:1 lattice clay minerals (Goodman, 1990). Late Cretaceous deposits have resulted in a relatively uniformly deep soil mantle comprising calcimorphic clay to sandy clay loam soils with the clay mineralogy dominated by kaolinite and non-expansive 2:1 lattice clay minerals (Goodman, 1990). Vertisols are also common with hydromophic gley soils restricted to shallow, pan forming depressions.

Tertiary and Quaternary sand deposits generally give rise to infertile sandy soils. According to Goodman (1990) the older inland dunes are dominated by deep soil profiles which are rubified and display an advanced mineral diagenesis and can be classified as ferruginous arenosols. The more coastal younger dunes show poorly developed soil profiles and consist of yellow to orange arenosols. The coastal dunes are generally dystrophic pallid sands (95 - 99 % quartz sand with subordinate clay, feldspar and heavy minerals) with high relief and steep slopes that have been stabilized by dune forest and scrub (Watkeys *et al.*, 1993). Leaching of the sands have lead to the development of impermeable horizons and the formation of rhizocretions. Between the irregularly spaced dune ridges, the remainder of the coastal plain is flat to gently undulating and is covered by dystrophic loose sand (Watkeys *et al.*, 1993).

Large river systems have lead to a variety of alluvial soils ranging from bouldery sands to eutrophic silty clays. The clay mineralogy of the alluvium is sparse in the literature but Ware (1997) identified smectite and illite/smectite interstratification as the dominate clay species for Holocene dark grey lagoonal silty clays found in a tributary of the Mgeni River. The provenance of these clays are the Ecca Group shales and the Karoo volcanics. Similar clays are found on the floodplain just east of Richards Bay (Ware, 1997).

2.2.7 MIDDLE TO LATE PLEISTOCENE AND HOLOCENE SEA LEVEL CHANGES

During the Quaternary, climatic variations have been correlated to variations in ice volumes which are considered an important control on coastal dune cordon formation and reworking.

The record of sea-level change during the mid-Pleistocene through to the Holocene can be determined from two principal sources; namely from beachrocks associated with ancient shorelines and from oxygen isotope records recovered from deep sea drilling projects. Along the KZN coastline there are few dateable outcrops making it difficult to determine sea-level fluctuations especially during the early to mid-Pleistocene. This

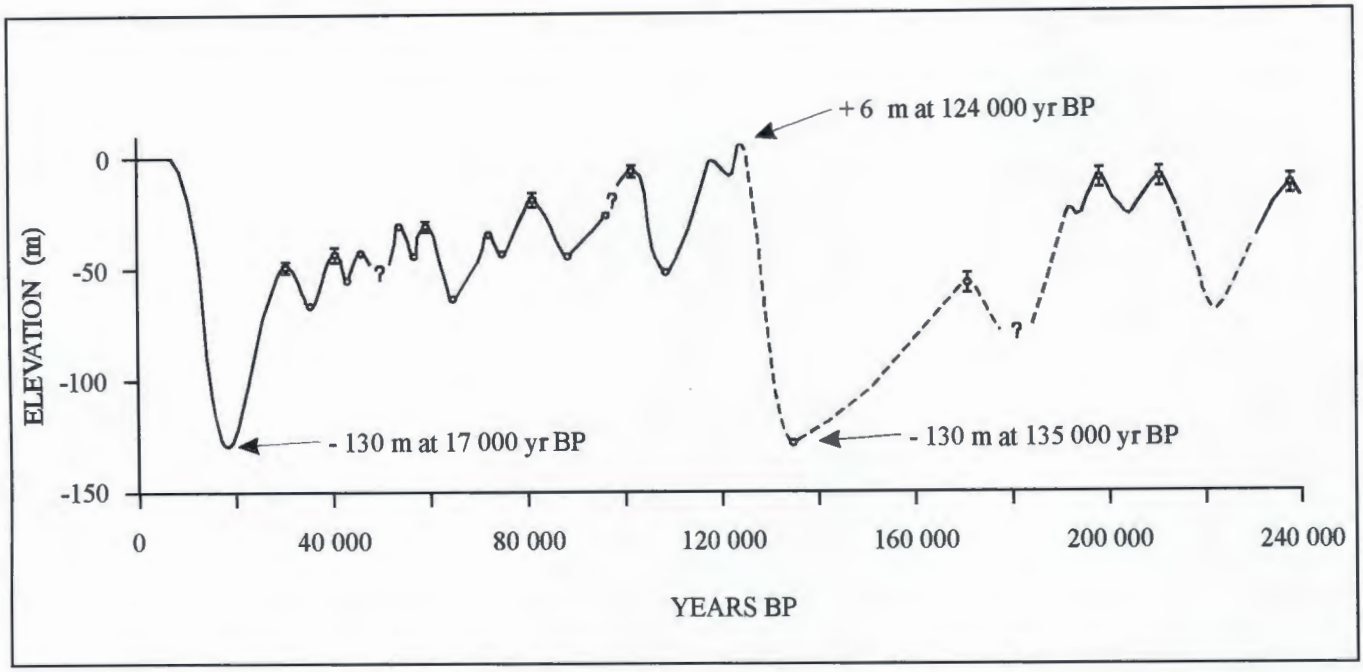

Figure 2.3 Detailed corrected sea-level curve for Huon Peninsula, Papua New Guinea; site HP 2 (Chappell & Shackleton, 1986).

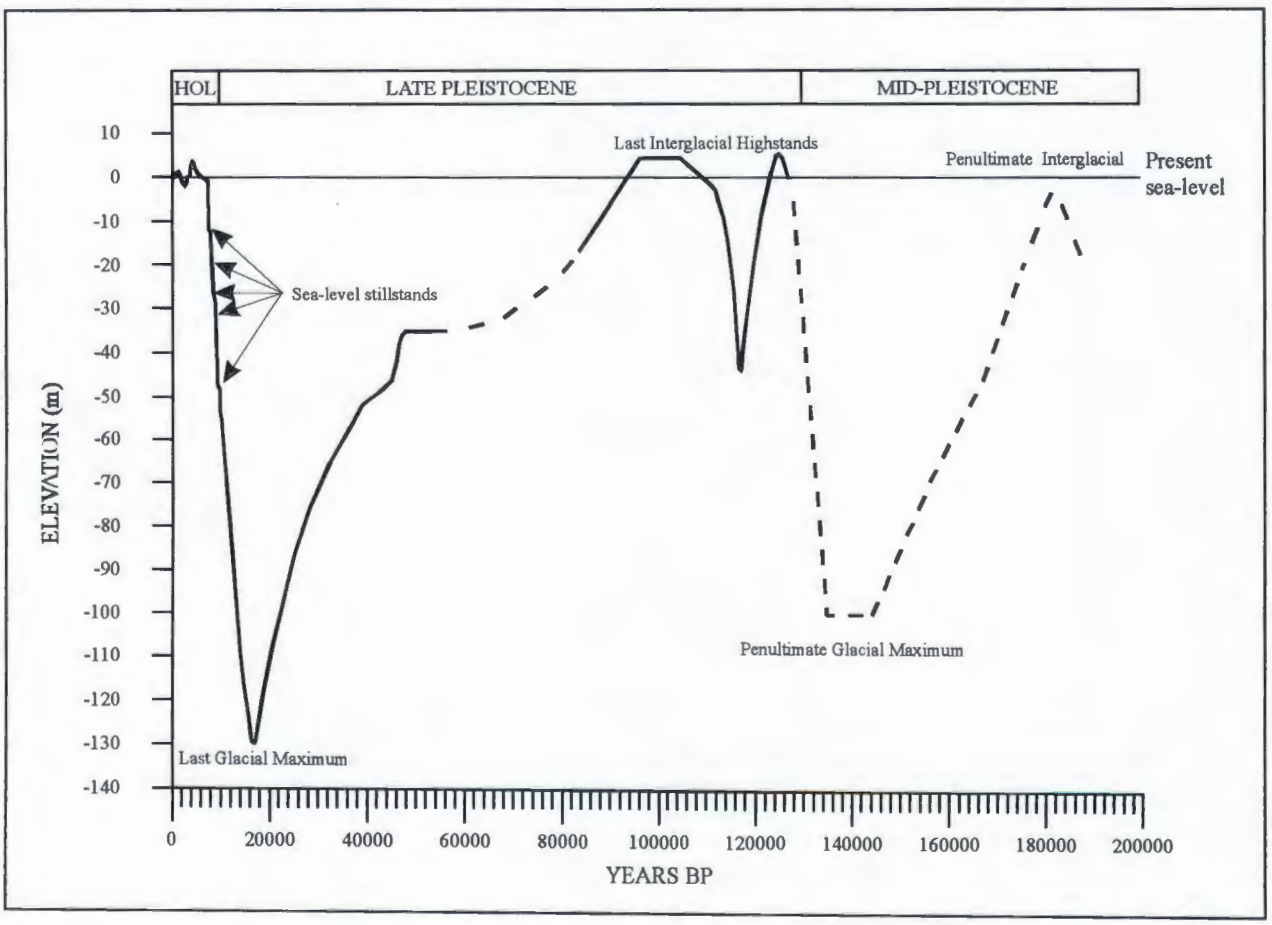

Figure 2.4 Quaternary sea-level curve for southern Africa based on beachrock dating (Ramsay, 1999).

is probably due to the fact that most early and mid-Pleistocene outcrops, that would have formed on the shelf during previous regressions, have been eroded by the late Pleistocene regression-transgression cycle (Ramsay, 1996). Sea-level changes derived from detailed oxygen isotope records from elsewhere can be interpellated, bearing in mind that variations around the globe are to be expected as a result of adjustments to glacial/interglacial changes of ice and ocean volumes (Chappell & Shackleton, 1986).

Glacial advances over the last 500 000 years have exhibited regular pulses of 100 000 years duration with intervening short warm interglacial periods lasting for 10 000 years (Nicholson & Flohn, 1980). The mid-Pleistocene (Figure 2.3) was dominated by three main highstands at approximately - 10 m at *ca.* 240 000, *ca.* 213 000 and 200 000 BP respectively with a eustatic glacial low at 135 000 BP of - 130 m (Chappell & Shackleton, 1986). During glacial periods the lowered sea-level promotes reworking of the shelf sediments and river incision. Conversely during interglacial periods incised valleys become drowned sites of sediment deposition.

According to Ramsay (1997) there were two sea-level highstands during the late Pleistocene along the KZN coastline (Figure 2.4). The first at about 126 000 BP at an elevation of + 5 m and another at about 100 000 BP at an elevation of + 4 m, separated by a eustatic low of - 40 m around 117 000 BP. The sea-level curves of Chappell and Shackleton (1986) correlate well with the curve proposed by Ramsay (1997) but show greater oscillations during the late Pleistocene. These oscillations however could be due to Chappell and Shackleton's (1986) assumption of uniform uplift of the Huon Peninsula. On the other hand, outcrop dated by Ramsay (1997) could have been amongst a select few which survived the numerous regression/transgression cycles at this time. Sea-level was at its lowest during the Last Glacial Maximum about 17 000 BP occurring at -130 m below present after which it rose rapidly with deglaciation at a rate of 167 cm/100 years (Tankard, 1976; Cooper, 1991; Chappell & Shackleton, 1986; Ramsay, 1997).

The Holocene sea-level history in southern Africa has been documented by Ramsay (1995) using beachrocks and planation episodes (Figure 2.5) and corresponds to work by Tankard (1976), Milliman and Emery (1968) and Williams *et al.* (1981). According to Ramsay (1995) sea-level rose at an average of 8 mm/year between 9 000 BP and 8 000 BP, reaching its present level along the South African coastline at *ca.* 6 500 BP. It then rose depositing a series of beachrocks at an elevation of + 2.75 m. This sea-level highstand persisted for a period of 2 500 years with the highest recorded Holocene stillstand at + 3.5 m dated at 4 480 BP (Ramsay, 1995), the Climatic Optimum or Hypithermal according to Tyson (1986). This was followed by a regression with sea-level reaching its present level at 3 880 BP where it remained for the next *ca.* 500 years (Ramsay, 1995). This was followed by a lowering in sea-level to - 2 m

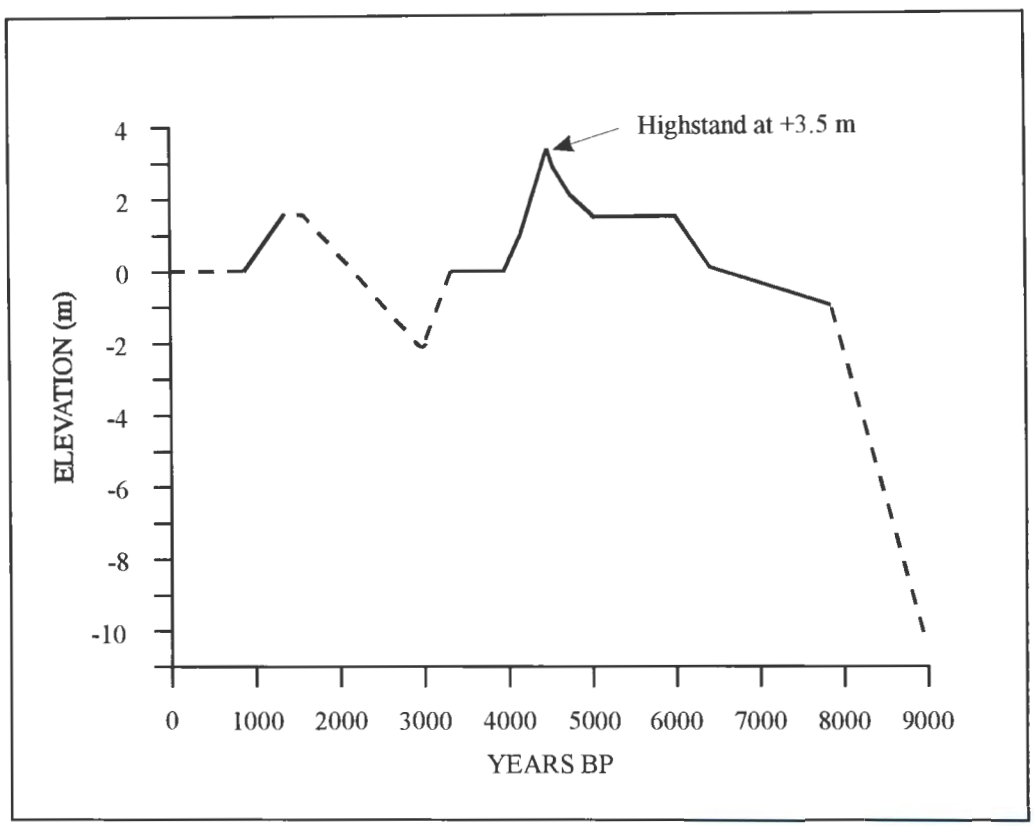

Figure 2.5 Holocene sea-level changes in southern Africa based on beachrock dating (Ramsay, 1995). Detail from Figure 2.4.

approximately 3 000 BP whereupon it rose to + 1.5 m at 1 610 BP and obtained its present level at *ca.* 900 BP (Ramsay, 1995).

2.2.8 LATE QUATERNARY PALAEOENVIRONMENTS

There has been little work carried out on the Quaternary palaeoenvironments of KZN, however southern Africa has received considerable attention due to anthropological interests. Palaeoenvironments are generally discussed in terms of glacial advances and retreats with the climate changes being attributed to the equatorward shift (3 ° to 5 ° North/South) of circulation belts during glacial advances. Southern Africa was not glaciated *per se* during the Quaternary, but did experience long periods of cooler temperatures (5 °C to 9 °C cooler than at present) when ice caps expanded at high latitudes and at high altitudes resulting in some periglacial landforms (Deacon & Lancaster, 1988; Grab, 2000). It must be stressed that sea-level change has a close correlation with palaeoenvironmental change as high stands generally follow warm interglacial periods and eustatic lows occur during cold glacial periods.

Three different palaeoenvironmental models for southern Africa have been proposed for the Last Glacial period (Nicholson & Flohn, 1980; Butzer *et al.*, 1978; Tyson, 1986). All agree that the climates were probably wetter, windier, and cooler in the winter rainfall region (southwest Africa) which extended further north and east than at present, and the summer rainfall region (which includes the study area) was cooler and probably drier. The drier conditions can be attributed to the cooler oceans (and weaker Agulhas Current) supplying less moisture for precipitation. Where mid-Holocene climates are discussed, the situation is reversed. An amelioration of climate followed the Last Glacial and a moist, lacustrine period *ca.* 10 000 - 8 000 BP ensued (Scholtz, 1986; Deacon & Lancaster, 1988).

The closest cave to the study area where detailed palaeoenvironmental studies have been recorded is the Border Cave (Deacon & Lancaster, 1988). It is situated at an elevation of 600 m in the Lebombo Range (27°14′S, 31°58′E) and provides a record of the palaeoenvironment of the last 100 000 BP. In general the micromammalian data reveal that grassland predominates during glacial periods and woodland during interglacial periods (Table 2.3; Avery, 1982 a).

The northern KZN dune cordons would have formed during glacial times when high wind velocities blew across large expanses of exposed shelf sediments (Tinley, 1986). Subsequently, these would have been largely reworked or destroyed by rising sea-level with only cemented dune cores remaining submerged as sublittoral ridges (Tinley, 1986).

Howard (1985) studied the oxygen isotope record from foraminifera tests just off the south east coast of Africa. His studies indicate that the interglacial climate was similar to that of today with the glacial-to-interglacial sea-surface temperature changes of some 5 °C. This is in agreement with global depressed temperatures during glacial periods of 5 °C to 15 °C given by Allen (1997). The Palaeoclimate Model Intercomparison Project (PMIP), reveals that the lowering of temperature over southern Africa at 21 000 BP was 2 - 5 °C over much of the subcontinent, except in the southwestern parts (Joussaume & Taylor, 1995). Current thinking suggests that vegetation has a very rapid response to climatic change, with estimated tree advance rates following the last glaciation of 200 km/1 000 years (Allen, 1997).

During the Holocene fluctuations in both temperature and humidity occurred, but the scale of change was considerably lower than that observed during the late Pleistocene (Deacon & Lancaster, 1988). Terms such as "wetter", "drier", "warmer" and "cooler" should therefore be viewed as relative estimates in the Holocene. Maximum temperatures during the Holocene were reached about 4000 to 6000 BP, since then the temperature has fluctuated about a general cooling trend (Tyson, 1986). This was also a moist lacustrine period experienced throughout Africa (Nicholson & Flohn, 1980) and corresponds to a highstand at + 3.5 m proposed by Ramsay (1995). Scholtz (1986) studying charcoal assemblages and pollen records in caves in the southern Cape, recognised three climatic phases over the last 4 000 BP. Between 4 000 and 2 500 BP the climate was equatable, relatively moist and conducive to the spread of forest vegetation which resulted in slope and dune stability. From 2 500 to 1 800 BP the climate is interpreted to have been cooler therefore, drier and less favorable to forestation resulting in remobilization of the dunes. The climate then ameliorated and since 1 800 BP has been similar to present.

Table 2.3. Border Cave palaeoenvironmental inferences based on micromammalian data (Avery, 1982 b).

Excavation units	Approximate age (years BP)	Vegetation	General climatic conditions
1a	present to 700	Fairly open savannah woodland; some ranker vegetation	Very mild, dry
Hiatus	700 - 13 000		
1b	13 000 - 29 000	Open grassland on flats and slopes	Mild (late glacial), cool, dry
Hiatus	29 000 - 33 000		
2-3	33 000 - 38 000		Moderate to cool
4	40 000 - 60 000		Mild, dry
5	60 000 - 70 000	Thick dense grass probably fairly damp; more extensive forest or thick bush; scrub on slopes	Moderate
6-7a			Cool
7b-8	80 000 - 100 000		Mild, relatively dry
9-10	> 100 000		Cool, wet
11		Fairly open dry savannah woodland; some ranker vegetation	Mild, dry

2.3 PROVENANCE OF COASTAL HEAVY MINERALS

The provenance of heavy minerals in coastal sediments on the east coast of southern Africa have been studied by Hammerbeck (1976), Fockema (1986), Hugo (1990 & 1993), and Sudan (1999). Fundamental to the abundance and distribution of heavy minerals is the geology, physiography and coastal dynamics of the region. These factors have resulted in the detritus from the various rock types being transported by rivers, dispersed along the coast by currents and concentrated on beaches and dunes by wave action and aeolian processes respectively.

The primary source of ilmenite and magnetite are rocks belonging to the basement rocks of the Kaapvaal Craton and the Natal Metamorphic Province, as well as Karoo and post-Karoo volcanics. Zircon and garnets have been primarily derived from the Kaapvaal Craton and the Natal Metamorphic Province with

rutile solely being derived from the latter. Reworking of these heavy minerals from Phanerozoic sedimentary rocks has also occurred, resulting in the Natal Group and Karoo Supergroup sediments being intermediate sources of heavy minerals.

Ocean currents of the southeast African coast have resulted in sediment compartments (Figure 2.1 b; Flemming & Hay, 1988) with a compartmental convergence occurring at the Tugela River. Thus at present, it seems unlikely that rivers south of the Tugela would provide significant sediment to the study area as ocean currents and eddies flow south. Longshore drift may result in some sediment migration north but these are unlikely to proceed past the Tugela River mouth and Tugela Cone. At the Tugela River, eddies flow north and coupled with the south flowing Agulhas Current just off the continental shelf, as well as longshore drift, the Tugela River, Mfolozi Rivers and St Lucia system seem probably sources of sediment.

Past climates may have caused the present sediment compartments to shift thereby allowing rivers south of the Tugela River to contribute sediment to the study area. If rutile is derived solely from the Natal Metamorphic Province, the provenance south of the Tugela River is essential. Detailed sediment studies of these rivers are required to provide conclusive proof of mineral provenance from these differing drainage basin lithologies (Figure 2.1).

2.4 GEOMORPHOLOGY AND DUNE CLASSIFICATION WITHIN THE ZULTI NORTH LEASE

The northern KZN coast is backed by an almost continuous dune cordon designated as Cordon A and B by Davies (1975) and Cordon 1 and 2 by Wright (1999). These were further subdivided into five classes by Sudan (1999) within the ZNL (Figure 1.4). Dune Class 1 comprises the older dune cordons which are red and contain abundant clays. Dune Class 2 represents the low lying inland dunes and are a mixture of parabolic, hairpin parabolic and wind-rift dune types. Light orange linear parallel dunes comprise Dune Class 3 with large scale light orange parabolic dunes representing Dune Class 4. The youngest dunes (Dune Class 5) comprise small scale parabolic dunes which are pale yellow to light grey and are noted to contain abundant heavy minerals. However, Sudan (1999) noted that these dune classes were merely superficial units that have been built upon older units and thus proposed an alphabetical classification based on borehole data.

Ten sedimentological units were identified; Units K, A1, A2, A3, A4, B, C, D1, D2 and E (Figures 1.4 & 2.6; Sudan, 1999). Unit K (no surface expression) was interpreted as the Kosi Bay Formation and is

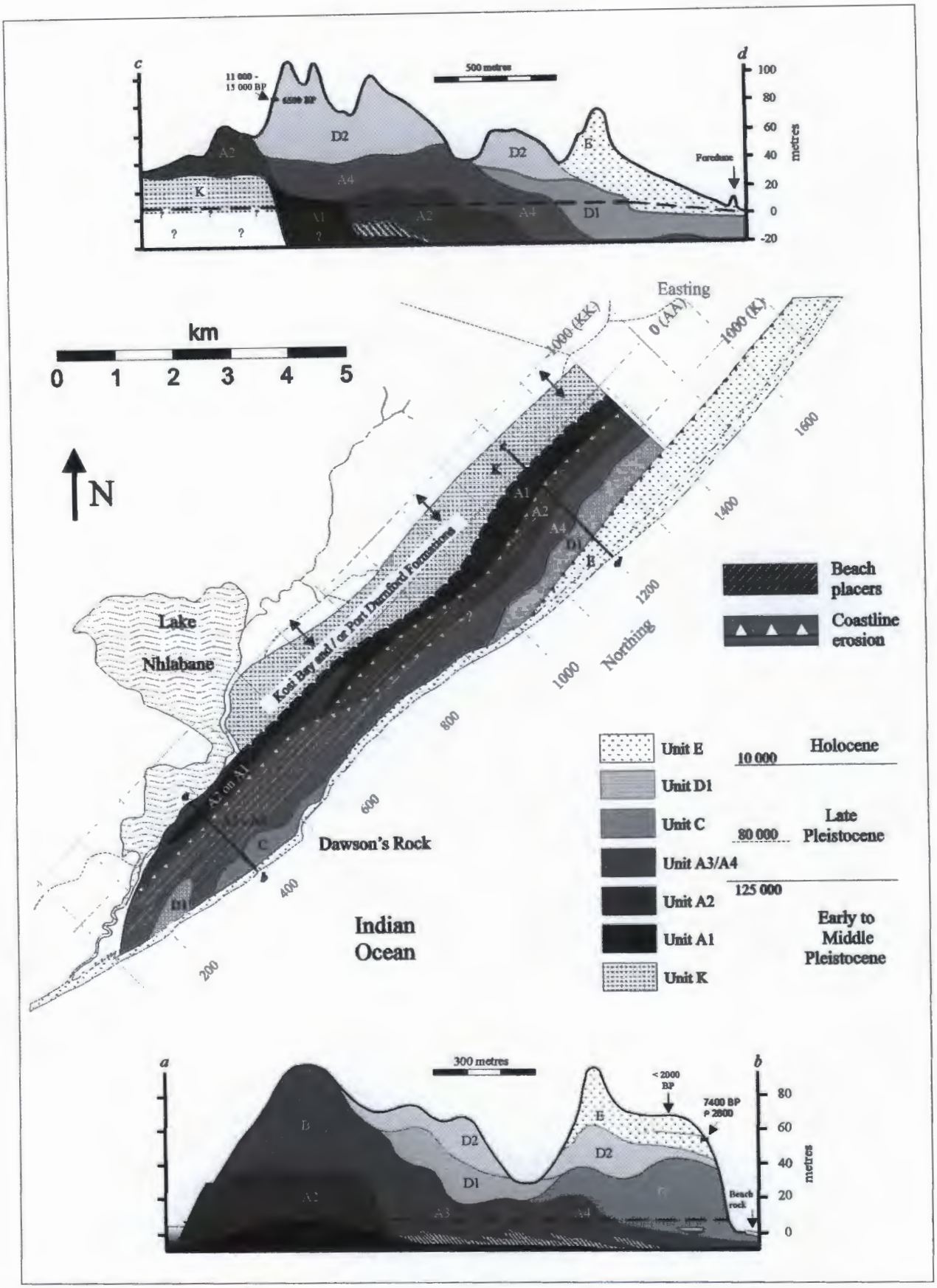

Figure 2.6 Interpretation of dune units within the ZNL area (after Sudan, 1999). The plan map represents a horizontal cross-section at *ca.* 5 - 10 m amsl. The two vertical cross-sections a - b and c - d characterise the northern and southern sections of the deposit.

characterised by aeolian with minor marine, beach or fluvial inputs. It is characterised by a light olive to white (dry state), medium-fine grained, non calcareous, moderate titanium (TiO_2 within various minerals) bearing sand. Unit A1 (Dune Class 1) was interpreted as the KwaMbonambi Formation being of transgressive aeolian, with minor marine or fluvial inputs, origin. It is characterised by a dark orange-brown, medium-fine grained, non calcareous, low to moderate titanium bearing sand. Unit A2 (Dune Class 2) was interpreted as the KwaMbonambi Formation and comprises transgressive aeolian and beach sediments. It is characterised by a dark orange-brown, medium-very fine grained, non calcareous, high to very high titanium bearing sand. Units A3 and A4 (no surface expression) was interpreted as the KwaMbonambi Formation and consists of transgressive aeolian and beach sediments. They are characterised by a dark orange-brown, medium-very fine grained, slightly calcareous, moderate to high titanium bearing sand. Unit B (Dune Class 2) was interpreted as the KwaMbonambi Formation being derived from the reworking of older aeolian sediments. It is characterised by a dark orange-brown, medium grained, slightly to moderately calcareous, moderate to high titanium bearing sand. Unit C was interpreted as the KwaMbonambi Formation and comprises the coastal cliffs near Dawsons Rock (Figure 1.1). It is characterised by a orange, coarse-medium grained, slightly calcareous, very low titanium bearing sand. Unit D1 (no surface expression) was interpreted as the Sibayi Formation and comprises transgressive aeolian sediments. It is characterised by a light orange, medium-fine grained, highly calcareous, low titanium bearing sand. Unit D2 (Dune Class 4/3) was interpreted as the Sibayi Formation and consists of transgressive aeolian sediments. It is characterised by a light orange, medium-fine grained, extremely calcareous, low titanium bearing sand. Unit E (Dune Class 4/5) was interpreted as the Sibayi Formation being of transgressive aeolian origin. It is characterised by a light grey to pale yellow, medium-fine grained, extremely calcareous, high titanium bearing sand. A comprehensive study of the geomorphology and dune classification in the ZNL is given by Sudan (1999) and the reader is referred to this work for further information.

3 CLAY-FRACTION

The clay-sized fraction of sediments contain clay minerals, which by their nature give plastic properties, and other "non-phyllosilicate minerals", referred to here as "other clays", which can greatly impact on the behaviour of clays. These other clays are predominantly rock forming minerals (quartz, feldspars etc.), carbonates, phosphates and weathering products (goethite, hematite, gibbsite etc.).

Clay minerals are found in virtually all types of sedimentary rocks, sediments, soils and in igneous and metamorphic rocks that have been subjected to physical, chemical and/or biological weathering. The process of rock weathering results in primary minerals being altered to secondary minerals, of which clay minerals form a significant portion. Due to their small particle sizes and variable degrees of crystallinity, it is often difficult to identify clay species. However, advances in analytical techniques, such as XRD and electron microscopy allow most clay species to be unambiguously identified. Other techniques used in clay studies include infrared, differential thermal analysis, differential thermo-gravimetry, Mössbauer spectrometer and characteristic isotopes, however XRD remains the most commonly utilised tool of the argillogist. As clay minerals are often poorly understood, especially in terms of their nomenclature, a brief overview is presented below.

3.1 CLAY MINERALS OVERVIEW

For more information on clay structure and classification the reader is referred to books written in the last two decades by Bailey (1980 a & b and 1988), Brindley & Brown (1980), Nemecz (1981), Velde (1985), Wilson (1987), Chamley (1989), Weaver (1989) and Moore & Reynolds (1989) as well as specialised journals dedicated to the study of clays. Weaver & Pollard (1973) provide details on the chemistry of various clay minerals. A summary on the structure of clays from the before mentioned texts is given below.

3.1.1 STRUCTURE OF PHYLLOSILICATES AND CLAY MINERALS

Clay minerals are crystalline hydrous layer silicates which constitute a large part of the family of phyllosilicates. Their structure is based upon infinite two-dimensional sheets of silicate tetrahedra with their bases in one plane. Each tetrahedron shares the three basal corners (the basal oxygen atoms) with adjacent tetrahedra, and with their apices all pointing in the same direction forming a hexagonal mesh pattern. Clay minerals typically contain silicon (Si), aluminium (Al) or magnesium (Mg), oxygen (O), and hydroxyl (OH), with various cations according to their species.

Two types of sheets can be identified, namely tetrahedral and octahedral sheets (Figure 3.1). Tetrahedral sheets have a general composition of T_2O_5 (T = tetrahedral cation; mainly Si, with varying amounts of Al^{3+} or Fe^{3+}, and rarely Be^{2+} or Be^{3+}). The silicon cation (Si^{4+}) is located in the centre of the tetrahedra with four oxygen anions (O^{2-}) forming the corners. The fourth tetrahedral corner points in a direction normal to the sheet. Its oxygen (the apical oxygen) is integrated into the octahedral sheet due to its spare negative charge together with unshared hydroxyls, groups or ions. The hydroxyls are located at the centre of each tetrahedral sixfold ring, at the same level as the apical oxygens.

Octahedra comprise cations at their centre (usually Al^{3+}, Mg^{2+}, Fe^{2+}, or Fe^{3+}) and oxygen anions at the six corners. Individual octahedra are linked laterally with adjacent octahedra, and vertically with tetrahedra by sharing oxygen anions forming sheets. The smallest structural units within an octahedral sheet contain three octahedra. Octahedral sheets can further be characterised as trioctahedral (sometimes called a Brucite sheet; $Mg(OH)_2$) or dioctahedral (sometimes called a Gibbsite sheet; $Al(OH)_3$) sheets depending on the predominate cation. Trioctahedral sheets generally contain three divalent cations at their centre (usually Mg^{2+}, Fe^{2+}) while dioctahedral sheets contain two trivalent cations (usually Al^{3+}, Fe^{3+}) and one cation site is vacant.

Stacked tetrahedral and octahedral sheets comprise clay minerals which are defined by their layer and interlayer composition (Figure 3.2). Two main layer types can be identified according to their tetrahedral to octahedral sheet ratios. The 1:1 layer clays (diphormic) consists of one tetrahedral sheet and one octahedral sheet and an interlayer forming a structural unit. The structural unit of the 2:1 layer clays (triphormic) contain one octahedral sheet sandwiched between two tetrahedral sheets and an interlayer. The two tetrahedral sheets are inverted with respect to each other, hence both sets of apical oxygen are shared by the octahedral sheet. When hydroxide interlayer groups join laterally, the result can give rise to an additional octahedral sheet bonding to give a 2:1:1 configuration (tetraphormic). The pilling up of many structural units constitute a clay mineral.

When the layers are electrostatically neutral, the interlayers are generally devoid of ions, however many clay minerals (especially 2:1 clays) have a negative layer charge which is neutralised by cations. Due to differences in the lateral dimension of tetrahedral and octahedral sheets and in cation dimensions, strained planes often result within clay crystals. These strained lattice planes result in crystals which appear "corrugated" or "rolled-up" sheets with a fibrous appearance. The ionic bonding between the interlayers also allows for the presence of water molecules giving clays, especially smectites, their characteristic swelling properties.

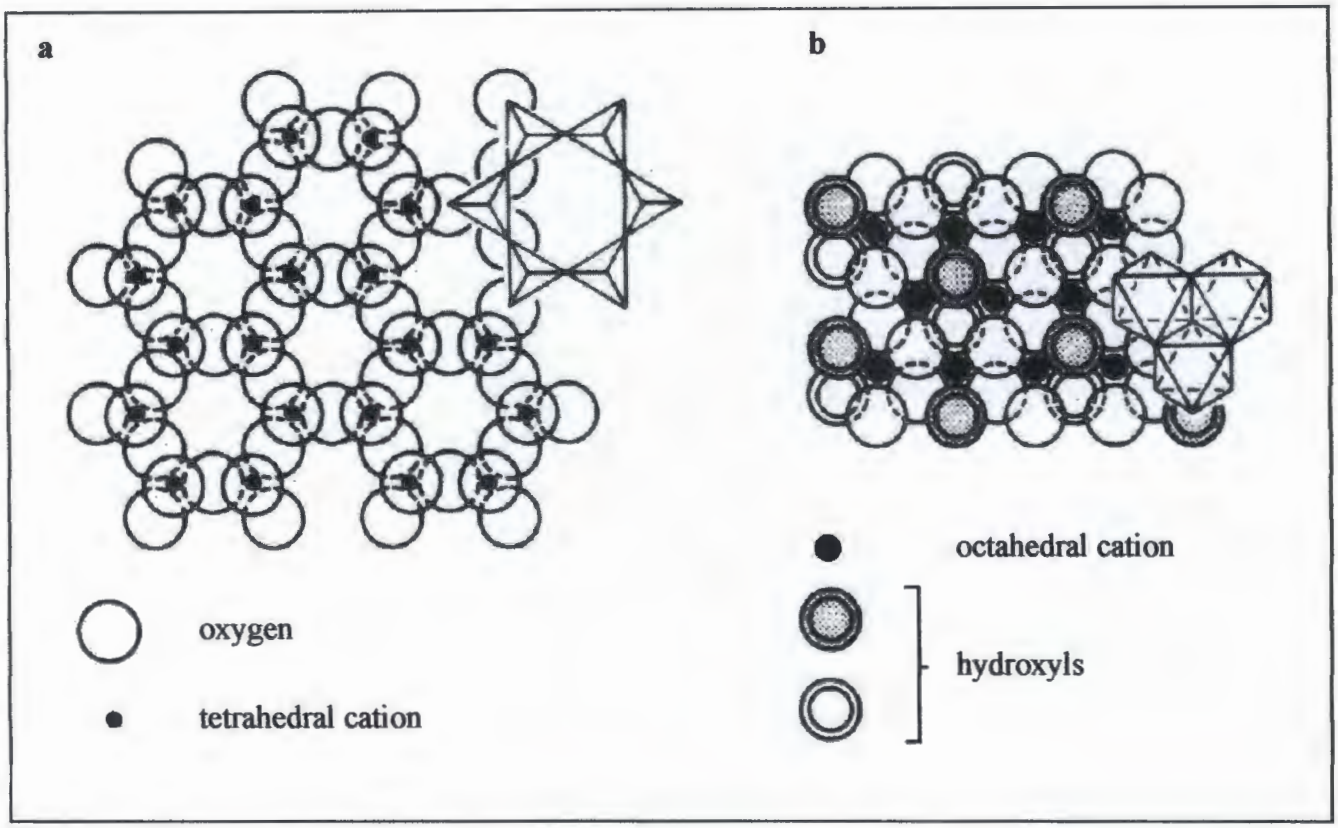

Figure 3.1 Structure of hydrous layer silicates **(a)** Plan view of an ideally hexagonal tetrahedral sheet. **(b)** Plan view of an octahedral sheet with inner hydroxyl groups of 2:1 layers (Chamley, 1989 modified from Bailey, 1980a).

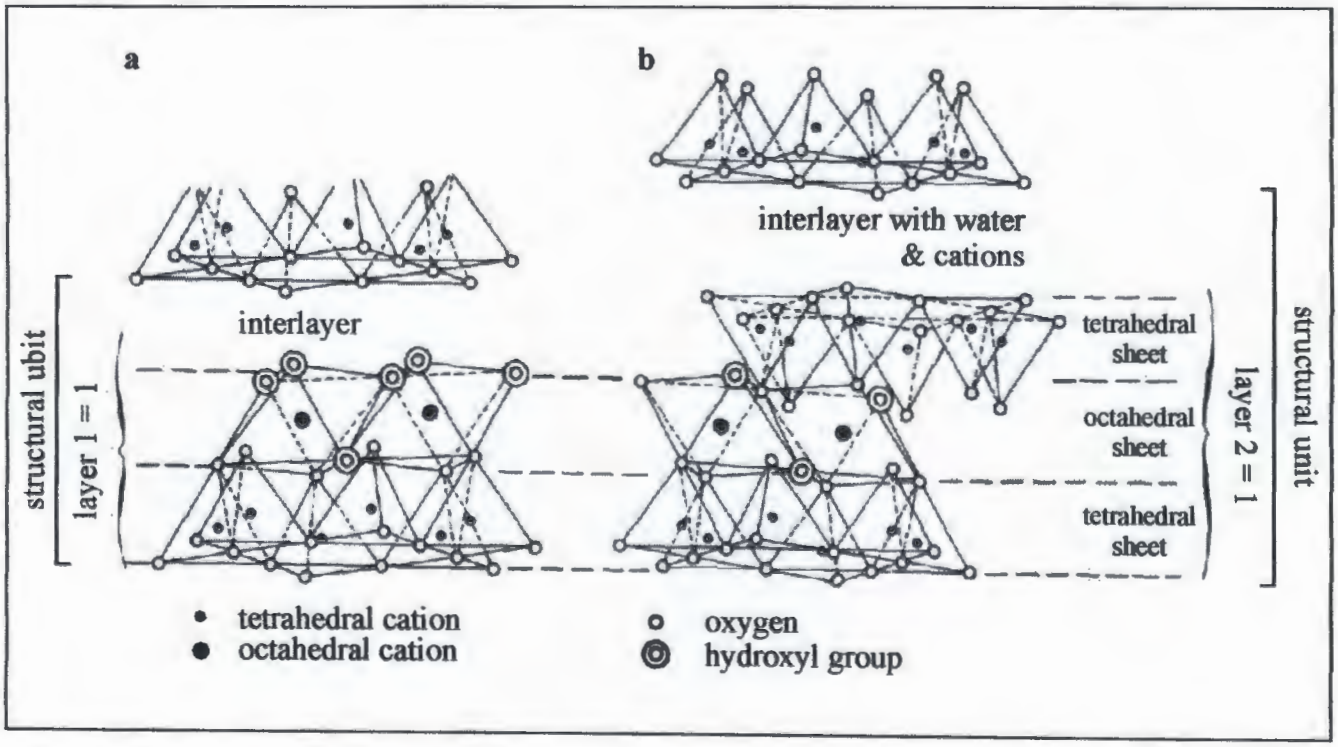

Figure 3.2 Three-dimensional sketch of the structure of **(a)** kaolinite and **(b)** smectite (Grim, 1968).

3.1.2 CLAY MINERAL NOMENCLATURE

The number and type of ions in octahedral and tetrahedral sheets and interlayer spaces is used to define seven broad clay mineral groups (Table 3.1). Each group contains associated subgroups and species. The names used for groups, subgroups, and species are those approved by the AIPEA (Association Internationale Pour l'Étude des Argiles) Nomenclature Committee or by the IMA (International Mineralogical Association) Commission on New Minerals and Mineral Names (Bailey, 1988).

The kaolin-serpentine group are 1:1 layer clays, which can be identified by a general 7 Å basal spacing (distance between the basal planes of atoms which correspond to the structural units; known as the d-value) and an overall near neutral layer charge. Five groups of 2:1 layer clays have been identified with a general 10 Å basal spacings. These comprise pyrophyllite-talc, smectite, vermiculite, true mica and brittle mica with an increasing negative layer charge per formula unit respectively. The 2:1:1 layer clays belong to the chlorite group and have a general 14 Å basal spacing with a variable negative layer charge.

Mixed layered clays or interstratified clays are characterised by a vertical stacking sequence of two or more types of single layers; be it 1:1, 2:1 and/or 2:1:1 types and are not included in Table 3.1. Interstratification results from the weak chemical and structural linkage existing between the successive layers in a given clay particle with these layers still keeping mobile interfaces. Mixed layered clays exhibit properties intermediate between two single clay minerals. Three main types of interstratification are recognised (Reynolds, 1980):

(1) Regular or ordered mixed-layers have a periodic alternation of layers of two types A and B. These are arranged as ABABAB... (1:1 interstratification) or AABAABAAB... (2:1 interstratification) and have a well defined X-ray diffraction pattern. These are generally named by the single layer names separated by a hyphen (e.g., regular chlorite - smectite), however there are five named types: aliettite (talc - saponite), corrensite (tri- smectite or tri- vermiculite -.tri-chlorite), kulkeite (talc - chlorite), rectorite (di- smectite - illite) and tosudite (di- smectite - di -, tri- chlorite).

(2) Irregular and randomly mixed-layered clays have a random alternation of each type of single layer, for example, AABABBBAAABAABA. This often results in a poorly defined XRD pattern with dome-, plateau- or wedge-like shapes. They are also named by the single layer names separated by a hyphen (e.g., irregular illite - smectite or irregular illite - chlorite -smectite). One named type has been specifically named, that is tarasovite which is a 3:1 alternation of mica and smectite layers.

Table 3.1 General classification of clay minerals; ē = layer charge: net negative per formula unit (after Bailey, 1980 a&b and 1988).

Layer type	Interlayer	Group	Subgroup	Species (Not all examples are given)
1:1	None or H_2O only	Kaolin-serpentine (ē~0)	Serpentines (Trioctahedral) Kaolins (Dioctahedral)	Chrysotile, lizardite, amesite, berthierine, cronstedtite, etc Kaolinite, dickite, nacrite, halloysite
2:1	None	Pyrophyllite-talc (ē~0)	Talcs (Trioctahedral) Pyrophyllites (Dioctahedral)	Talc, willemseite Pyrophyllite, ferripyrophyllite
	Hydrated exchangeable cations	Smectite (ē~0.2-0.6)	Montmorillonites (Dioctahedral smectite) Saponites (Trioctahedral smectite)	Montmorillonite, beidellite, nontronite, volkonskoite, etc Saponite, hectorite, sauconite, stevensite, etc
	Hydrated exchangeable cations	Vermiculite (ē~0.6-0.9)	Dioctahedral vermiculites Trioctahedral vermiculites	Dioctahedral vermiculite Triotahedral vermiculite
	Non-hydrated cations	True Mica (ē~0.5 - 1.0)	Dioctahedral true micas Trioctahedral true micas	Muscovite, paragonite, illite, glauconite, tobelite, celadonite etc Phlogopite, biotite, lepidolite, zinnwaldite, annite, etc
	Non-hydrated cations	Brittle mica (ē~2.0)	Dioctahedral brittle micas Trioctahedral brittle micas	Margarite Clintonite, anadite, kinoshitalite, bityitite
2:1:1	Hydroxide sheet	Chlorite (ē variable)	Dioctahedral chlorites Trioctahedral chlorites Di, trioctahedral chlorites	Donbassite Clinochlore, chamosite, nimite, pennantite, baileychlore Cookeite, sudoite

(3) Partially ordered structures are an intermediate between regular and irregular types, however little is known about their structure and they are not specifically labelled.

3.2 DUNE MINERALOGY

Both clay minerals and other clays (silicates, oxides, phosphates and carbonates) were identified. These two mineral groups will be dealt with in the respective sections below. All smoothed (smooth factor 2) random air-dried XRD traces are presented on CD-ROM; Appendix H1. Crystallographic Miller indices d(*hkl*) have been included for diagnostic reflections/peaks in Figures 3.3 - 3.7.

3.2.1 CLAY MINERALS

Three clay mineral groups were identified by XRD; kaolin-serpentine, smectite and true mica, as well as an irregular interstratification of a combination of these minerals and/or other clay minerals.

3.2.1.1 Kaolin-Serpentine Groups

The presence of kaolin-serpentine group minerals were determined by strong 7 Å (15 °2 θ) reflections in the AD state (Figure 3.3a). In order to determine the species present, orientated samples were subjected to three possible treatments; heat, hydrazine and formamide (Figure 3.3 b). The 550 °C heat treatment for 4 hours distinguishes the subgroups kaolins from serpentines. Heat treatment results in kaolin becoming amorphous to X-rays causing a collapse of the respective reflections, whereas the serpentine structures are not affected. All samples showed complete destructions of the kaolin reflections and thus no serpentine minerals are present. The chlorite group minerals' d(002) basal spacing correspond to the d(001) basal spacing of kaolin-serpentine group minerals, however the 14.2 Å (7.2 °2 θ) reflection would remain after heat treatment if there were any chlorites present. In order to differentiate halloysite from kaolinite, the samples were intercalated with formamide for 10 minutes at room temperature and humidity. Halloysites would expand from 7.2 (14.3 °2 θ) to 10.4 Å (9.9 °2 θ), however there was no change in the reflections and kaolin is therefore present. Kaolin species were further distinguished by the presence of a 2.34 Å (45.0 °2 θ) peak identifying kaolinite (polytype 1T) rather than the polymorph dickite or nacrite (Figure 3.3a). In order to determine the crystallinity of the kaolinite, samples were intercalated with hydrazine for 7 days in an oven set at 60 °C. Well ordered kaolinites (and halloysites) expand to 10.4 Å whereas disordered kaolinites do not show this expansion. Both ordered and disordered kaolinites are present as seen in Figure 3.3 b (and in all other kaolinitic samples).

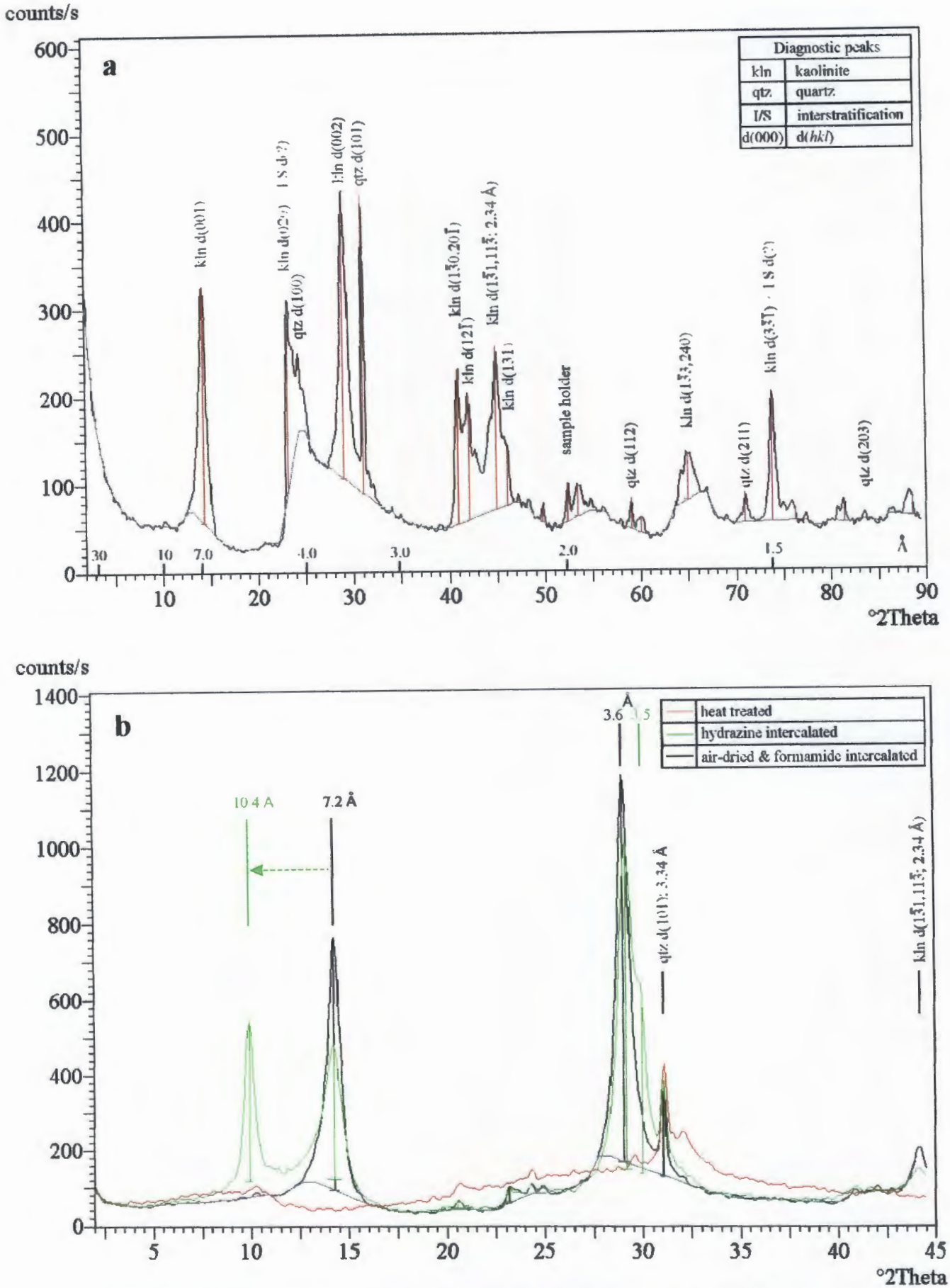

Figure 3.3 Characteristic X-ray diffraction traces for borehole L2, 18.5 m amsl. (a) Typical random air-dried X-ray diffraction trace for samples dominated by kaolinite (*ca.* 74 %) with minor irregular interstratified clays (*ca.* 4 %). Also shown is other clay; quartz (*ca.* 22 %). The peak at 52 °2 Theta corresponds to the aluminium sample holder. (b) Typical orientated air-dried and diagnostic kaolinite treatments. Preparation procedure is presented in section 1.5.3.1. Note that the formamide treated sample showed no change from the air-dried sample and was thus not included.

3.2.1.2 Mica Group

The presence of true mica minerals was determined by the basal reflection at 10 Å (10 °2 θ). However, due to the minor amounts present and interfering reflections of other minerals, it was not possible to confidently determine species. Phlogopite-biotite minerals are rarely encountered in the clay-fraction (Moore & Reynolds, 1989) and together with orientated samples showing a weak 5.0 Å (20.6 °2 θ) reflection, which glauconite does not, the probable species name would be illite. It must be noted that illite is considered by Moore & Reynolds (1989) to be an end member of a series, with muscovite on the one extreme and smectite (discussed later) on the other. Thus illite will hence forth be used as the species name of the 10 Å reflection belonging to the true mica group.

3.2.1.3 Smectite and Vermiculite Groups

The smectite and vermiculite groups have very similar X-ray characteristics and thus require a number of tests to distinguish them. Samples were saturated in a divalent cation (Mg^{2+}) as Mg-vermiculite will retain a d(001) after glycerol solvation whereas smectite produces a d(001) at 17 Å (6.0 °2 θ) to18 Å (5.7 °2 θ), after such treatment. Figures 3.4 a & b show this shift to 17 Å and thus the presence of the smectite group. This was confirmed by ethylene glycol-solvated samples which showed a d(001) peak shift from 15 Å (6.8 °2 θ) in the AD state to 17 Å together with a subordinate peak at 8.5 Å. After heat treatment, this d(001) reflection collapsed to 10 Å, resembling illite. These tests unequivocally show the presence of a 15 Å smectite group with vermiculite not being detected in any of the samples. The subgroup determination was inconclusive, as was the species name. This was due to the d(060) reflections, which separate montmorillonites (1.49 to 1.51 Å) from the saponites (1.51 to 1.56 Å), had a 1.51 ± 0.01 Å d(060) reflection. But in saying this, the d(060) reflection tended to be more commonly nearer 1.52 Å and thus saponites are suspected (also see Section 3.4). The only conclusive method of telling these subgroups apart is by the modified Greene-Kelly test (Byström-Brusewitz, 1975), however this treatment was not conducted due to time constraints.

3.2.1.4 Interstratified Clays

The identification of irregular interstratified (I/S) clay minerals was problematic and a difficult to quantify, which is typical of these minerals (Moore & Reynolds, 1989). Duplicate samples were sent to the Council for Geoscience, Pretoria (Appendix H1) which confirmed preliminary findings. I/S manifests itself as a series of erratic peaks which did not obey Méring's principles. According to this concept, the observed

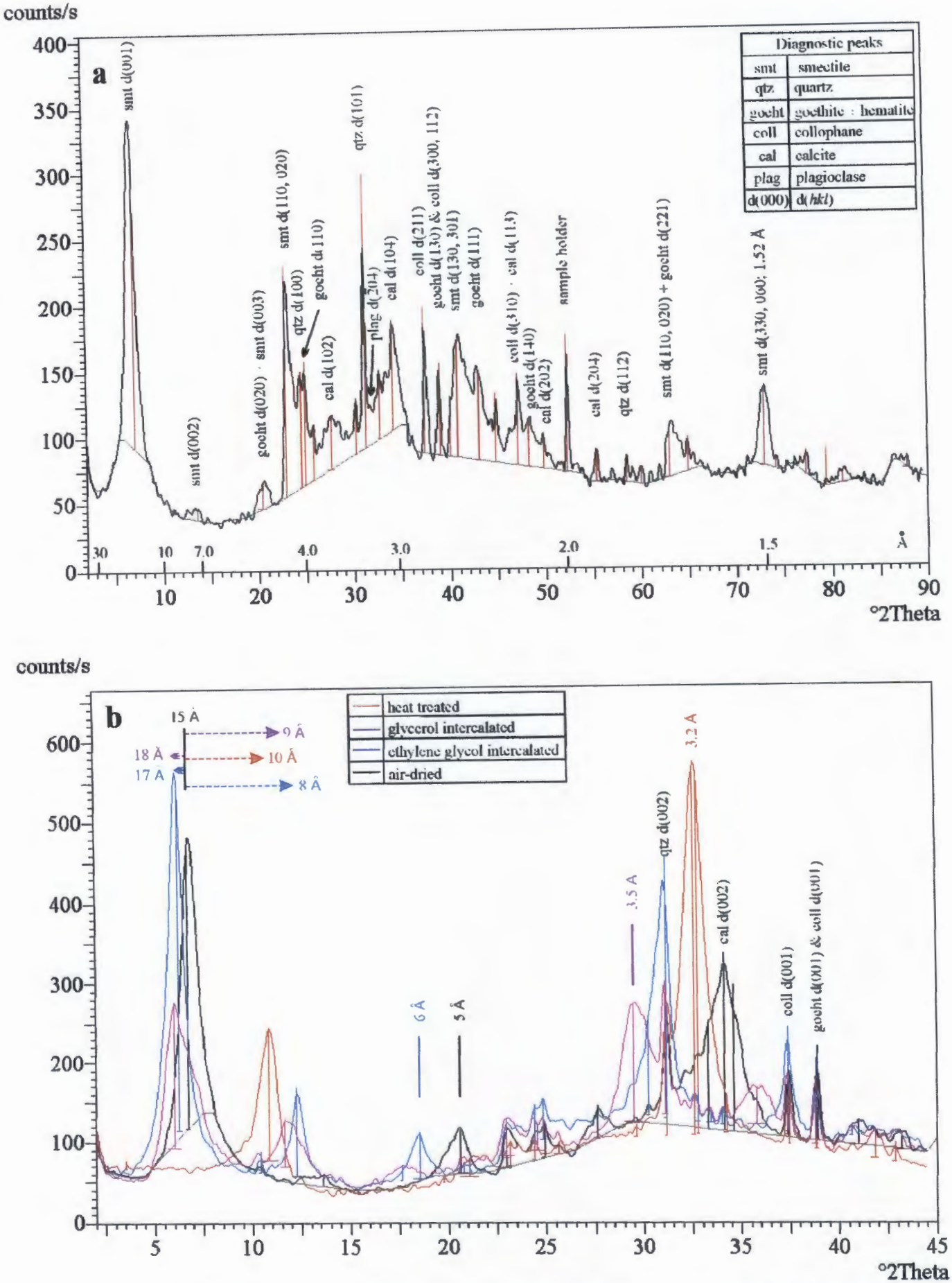

Figure 3.4 Characteristic X-ray diffraction traces for borehole C1, -11 m amsl. (a) Typical random air-dried X-ray diffraction trace for samples dominated by smectite (*ca.* 60 %). Also shown are the other clays; quartz (*ca.* 10 %), goethite ± hematite (*ca.* 15 %), collophane (*ca.* 9 %), calcite (*ca.* 5 %) and plagioclase (*ca.* 2 %). The peak at 52 °2 Theta corresponds to the aluminium sample holder. (b) Typical orientated air-dried and diagnostic smectite treatments. Preparation procedure is presented in section 1.5.3.1.

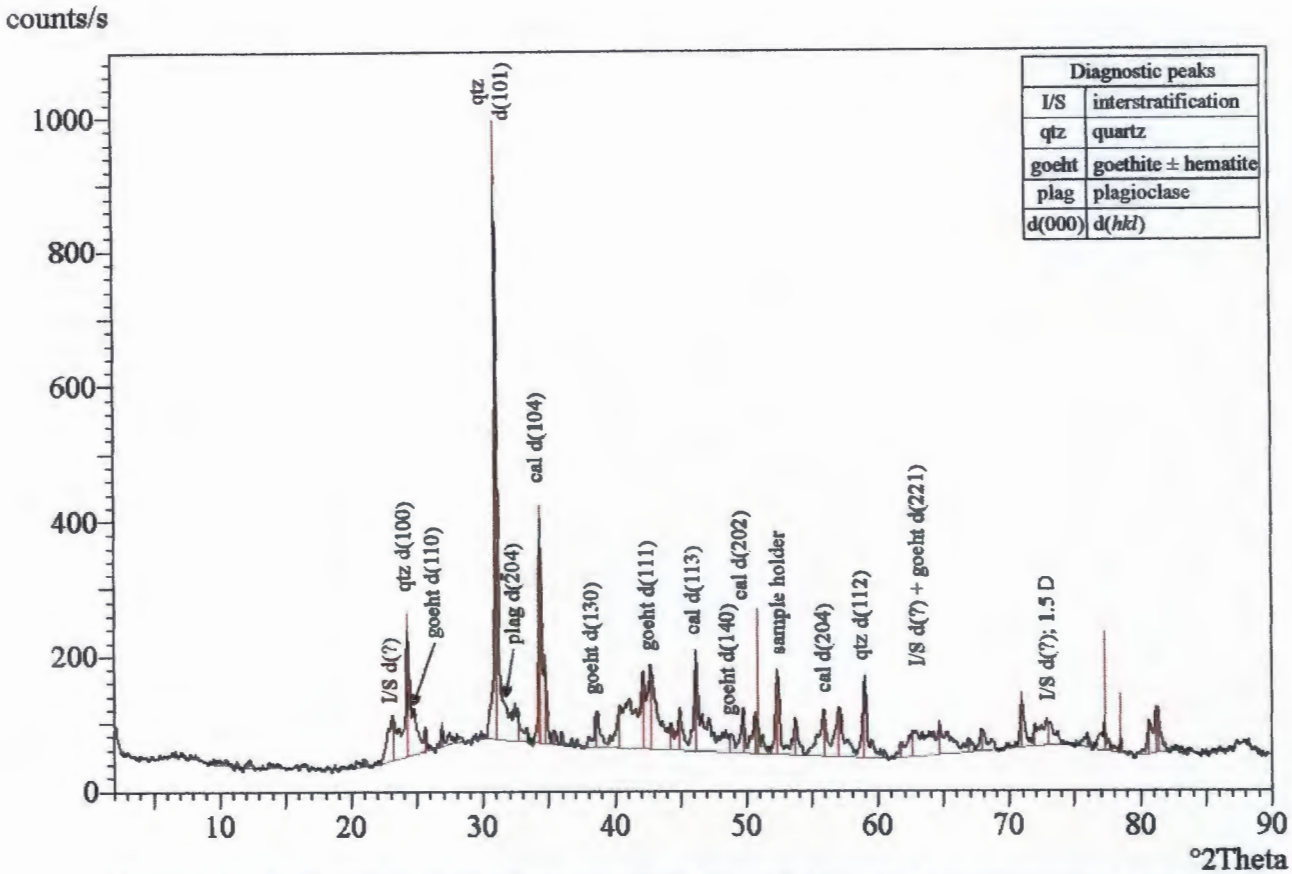

Figure 3.5 Typical random air-dried X-ray diffraction trace showing for samples containing irregular interstratified (*ca.* 16 %) clays in the absence of other clay minerals. Also shown are other clays; quartz (*ca.* 50 %), calcite (*ca.* 21 %), goethite ± hematite (*ca.* 9 %) and plagioclase (*ca.* 3 %); borehole I3, 55 m amsl. The peak at 52 °2 Theta corresponds to the aluminium sample holder.

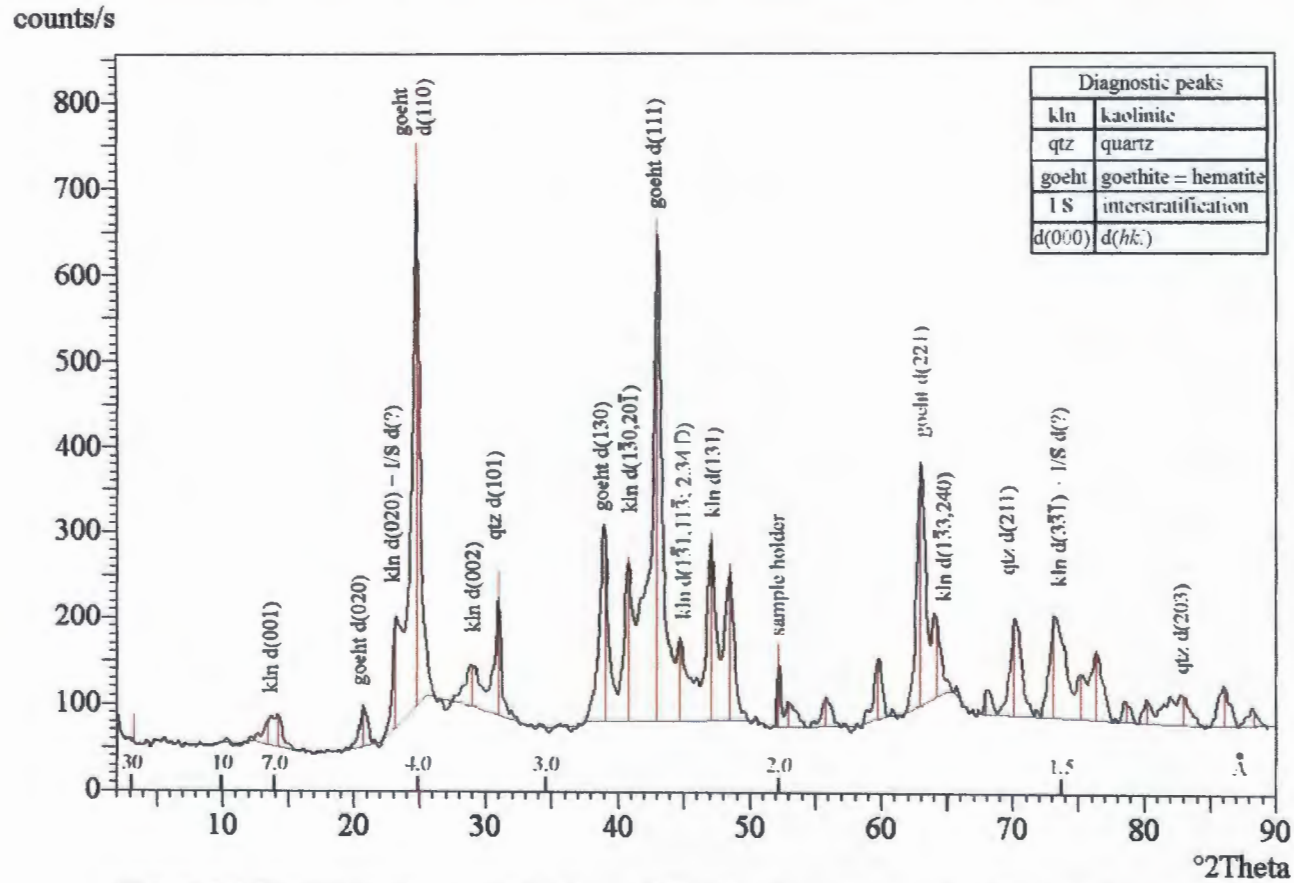

Figure 3.6 Typical random air-dried X-ray diffraction trace for samples dominated by goethite ± hematite (*ca.* 67 %). Also shown are the interstratified (*ca.* 18 %) and kaolinite (*ca.* 9 %) clays, as well as quartz (*ca.* 6 %); borehole I3, -19.2 m amsl. The peak at 52 °2 Theta corresponds to the aluminium sample holder.

regular I/S reflections should be composites, or compromises, of the two clay mineral end-member reflections, yet this was not observed. Thus I/S were identified by the presence of broad low intensity peaks at 4.5 Å (22.9 °2 θ) together with one at 1.5 Å (73.2 °2 θ) (Figure 3.5), even though in many cases there were no consistent peaks > 20 Å (< 5 °2 θ). These reflections also overlap with kaolinite and smectite reflections. When these two minerals were present in the sample their theoretical peak intensity at 4.5 Å (relative to their d(001) reflections) was subtracted to calculate the relative abundance of interstratified clay minerals. Although this method has its shortcomings, it did prove successful in quantifying the existence of an irregular I/S.

3.2.2 OTHER CLAYS

Clay minerals are rarely found as monomineralic materials, and commonly have other minerals associated with them. These other clay minerals were easily identified by their relatively sharp narrow peaks (Figures 3.3 - 3.7). At least three diagnostic peaks were used as conformation of the existence of these minerals paying careful attention to the possibility of overlapping peaks of other minerals. Despite this, errors in identifying minor constituents are possible and as such, their presence is tentative.

By far the most common other clay mineral identified in all samples was quartz, followed by goethite ± hematite, calcite, and subordinate feldspars including both microcline and plagioclase. Hematite has been included with goethite as their peaks interfere, but it is subordinate to goethite and may, or may not, be present in goethite containing samples. Upon heat treatment goethite dehydrated to hematite. Ilmenite was also present in minor amounts. Apatite was also found in substantial amounts in samples from the coastal borehole only. The species of apatite was difficult to determine, with two possibilities having similar XRD characteristics; fluorapatite and hydroxyl-apatite. The sack term "collophane" will hence forth be used to describe this cryptocrystalline apatite (Battey, 1981). Pyriboles, although not detected in XRD, must be present (trace) in the clay-fraction as they were identified in the silt-fraction (Chapter 4).

Selected quantitative XRD results were checked by XRF major element analysis (Appendix C2). However, complexities within the mineral species identified (eg. I/S representing an unknown mixture of elements), the diverse mineral suite and errors calculating modal percentage did produce anomalies. Goethite is known to have certain amounts of SiO_2, H_2O, as well as Al^{3+} and Mn^{3+} substituting in the crystal lattice (Deer *et al.*, 1992; discussed in section 4.3). The chemical composition of kaolinite is subject to little variation, however Fe_2O_3, TiO_2, MgO, and CaO are nearly always present and K_2O and Na_2O usually present (Weaver & Pollard, 1973). Smectites and illites are more susceptible to chemical variations (Weaver &

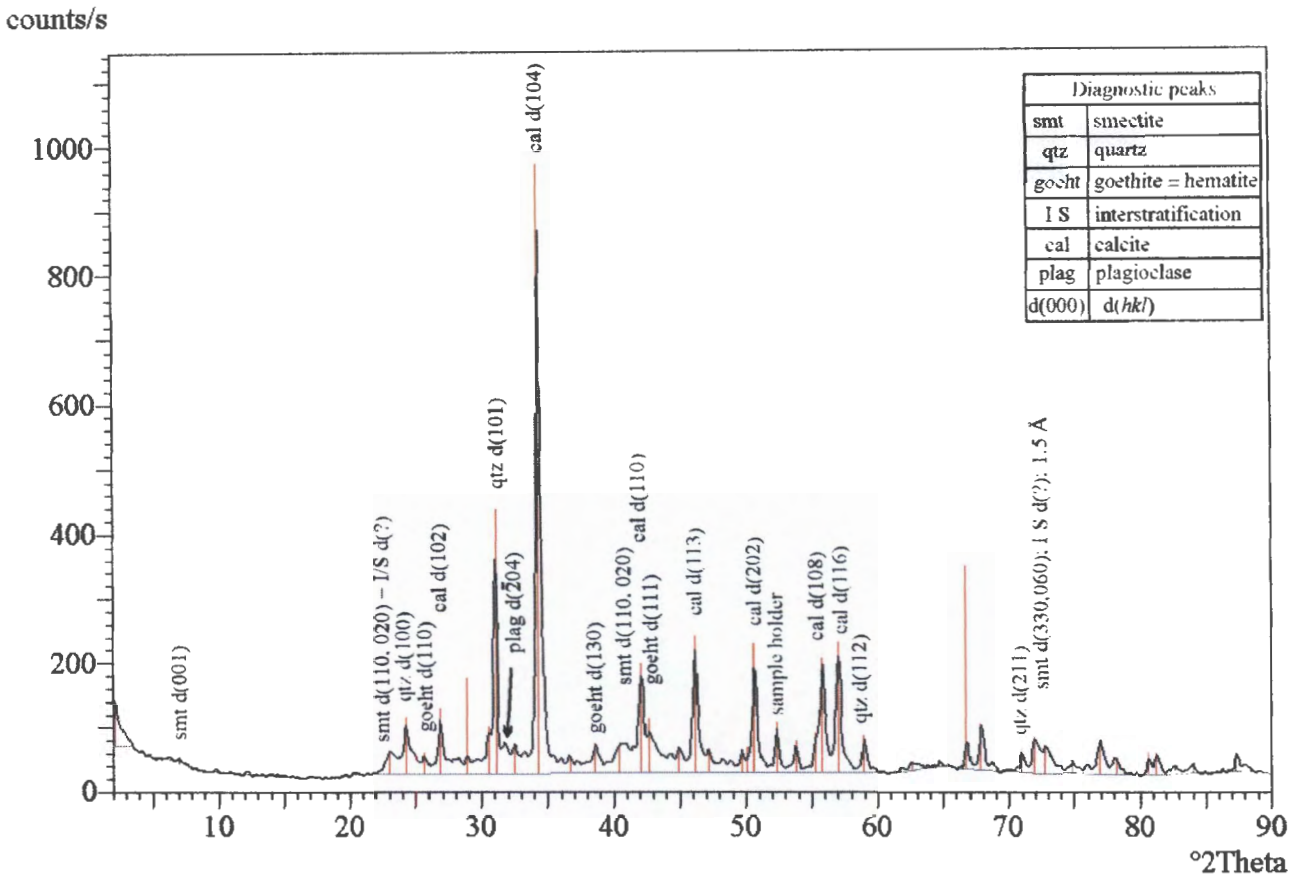

Figure 3.7 Typical random air-dried X-ray diffraction trace for samples dominated by other clay minerals; calcite (*ca.* 63 %) and quartz (*ca.* 23 %). Also shown are irregular interstratified (*ca.* 6 %) and smectite (*ca.* 1 %) clays minerals, as well as minor plagioclase (*ca.* 4 %) and goethite ± hematite (*ca.* 3 %); borehole I3, 57 m amsl. The peak at 52 °2 Theta corresponds to the aluminium sample holder.

Pollard, 1973) creating even greater difficulties in using XRF analyses as a check on XRD mineral abundances.

There is a general positive correlation between the relative modal percentage of mineral species identified from XRD and the expected abundance of their constituent elements determined by XRF. The most reliable mineral which could be used to recalculate XRD mineral abundances from XRF analyses was calcite. This is due to its simple mineralogical composition with CaO only found in trace amounts of plagioclase and other clays. The abundance of calcite tended to be higher when calculated from the XRD traces compared to calcite recalculated from CaO from the XRF analyses (Appendix C2). The calculated calcite results were generally underestimated by *ca.* 20 % (for major abundances of calcite: < 15 %) and unreliable for minor calcite abundances. The relative abundances of other dominant clay-sized minerals from quantitative XRD analyses is thus considered fairly reliable (within XRD quantitative errors). A possible source of error in the calcite abundance was in an underestimate in the quantity of irregular I/S due to its poor crystallinity, or because of an amorphous phase present (allophane/ferrihydrite?). This amorphous phase was identified by Dunlevey (1997) working on similar red Pleistocene aeolian dune sands. If I/S was underestimated or an amorphous phase present it would effectively result in a relative dilution of calcite as calculated from the XRD traces.

The dominant source of K_2O should be microcline and illite, however their relationship in the XRF major element analyses (Appendix C2) suggests other sources of K_2O. The highest K_2O content in Borehole 11 is 1.49 weight % (sample 37 m amsl), however there wasn't any microcline detected and only trace illite. This suggests that the K_2O must be in the I/S. Yet sample 19 m amsl of the same borehole contains marginally less K_2O (1.35 weight %) but has a microcline content of *ca.* 7 %, similar I/S content (*ca.* 17 %) and trace illite. This observation suggests two possibilities; either there is another host for K_2O (gels?) or it demonstrates the limiting use of the XRD quantitative analysis method. However in saying this, the highest concentration of K_2O (1.55 weight %) did correlate to the highest microcline content of *ca.* 8 %, together with *ca.* 13 % I/S and trace illite and smectite.

TiO_2 accounted for up to 3 weight % of the XRF major element analyses (Appendix C2) but was not observed in the same samples in the form of ilmenite or other Ti-bearing minerals within the respective XRD traces. The XRD samples that did contain detectable ilmenite were unfortunately not analysed by XRF. These samples are thus expected to contain much higher quantities of TiO_2 than predicted by XRD. The amount of TiO_2 present, as determined by the XRF analyses, could be the result of titanium substitution within clays (Weaver & Pollard, 1973), however one would expect there to be micron-sized

ilmenite and rutile. The absence of detectable Ti-bearing minerals in samples containing 3 weight % TiO_2 is thought to reflect inaccuracies when determining the XRD relative modal percentages of minor mineral abundances.

3.3 DOWN HOLE VARIATIONS

Clay-fraction relative modal percentage results are tabulated in Appendix C1 and summarised graphically in Figures 3.8 to 3.10. Stratigraphic dune units are delineated from their clay abundances and occurrences. These units are further constrained with the addition of data from the silt-fraction and bulk samples (Chapters 4 & 5). Unit names have been chosen to correlate with the work of Sudan (1999) with the exception of Unit A1 (not identified) and the addition of Unit F.

3.3.1 QUARTZ

Quartz is the most abundant mineral in the upper sections of all boreholes where it generally accounts for *ca.* 50 % of the clay-fraction. The abundance gradually lessens with depth with the lowest abundances of *ca.* 6 % found at the bottom of borehole I3. Samples Pond C, D2, D3 and D4 also contain abundant quartz.

3.3.2 KAOLINITE

There is a general increase in kaolinite down hole with the inland boreholes (L1 & L2) terminating within a kaolinitic rich unit. The highest percentage of kaolinite was found at the base of borehole L2 consisting of *ca.* 74 % of the clay-fraction. This high kaolinite abundance was also observed in sample K1 (*ca.* 67 %). XRF analyses show increasing Al_2O_3 corresponding to increasing kaolinite with a > 30 weight % Al_2O_3 abundance generally correlating to > 30 % kaolinite.

3.3.3 GOETHITE

Variations in goethite generally show a positive correlation to kaolinite and gradually increases down hole. It is however, dramatically depleted when kaolinite increases to over *ca.* 40 % of the clay-fraction (borehole I1 & L2). Goethite dominates the clays towards the bottom of the boreholes I3 and C1 where it obtains a maximum abundance of *ca.* 67 %.

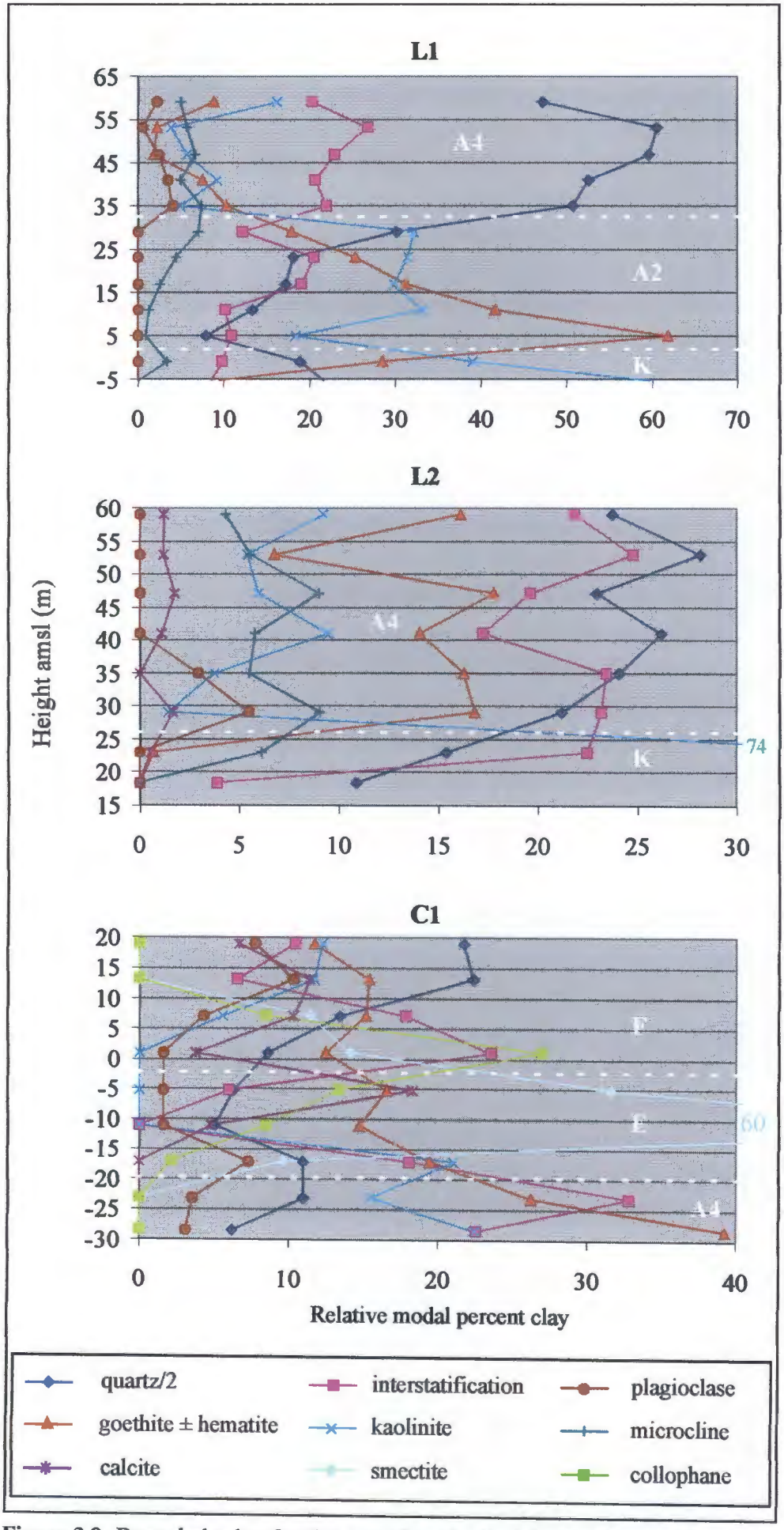

Figure 3.8 Down hole clay-fraction variations for the inland and coastal boreholes L1, L2 and C1 respectively. NB: quartz abundance is divided by 2 except for borehole L1 for which absolute values are plotted. White dashed lines and corresponding letter and numerical value delineate dune units according to the clay-fraction.

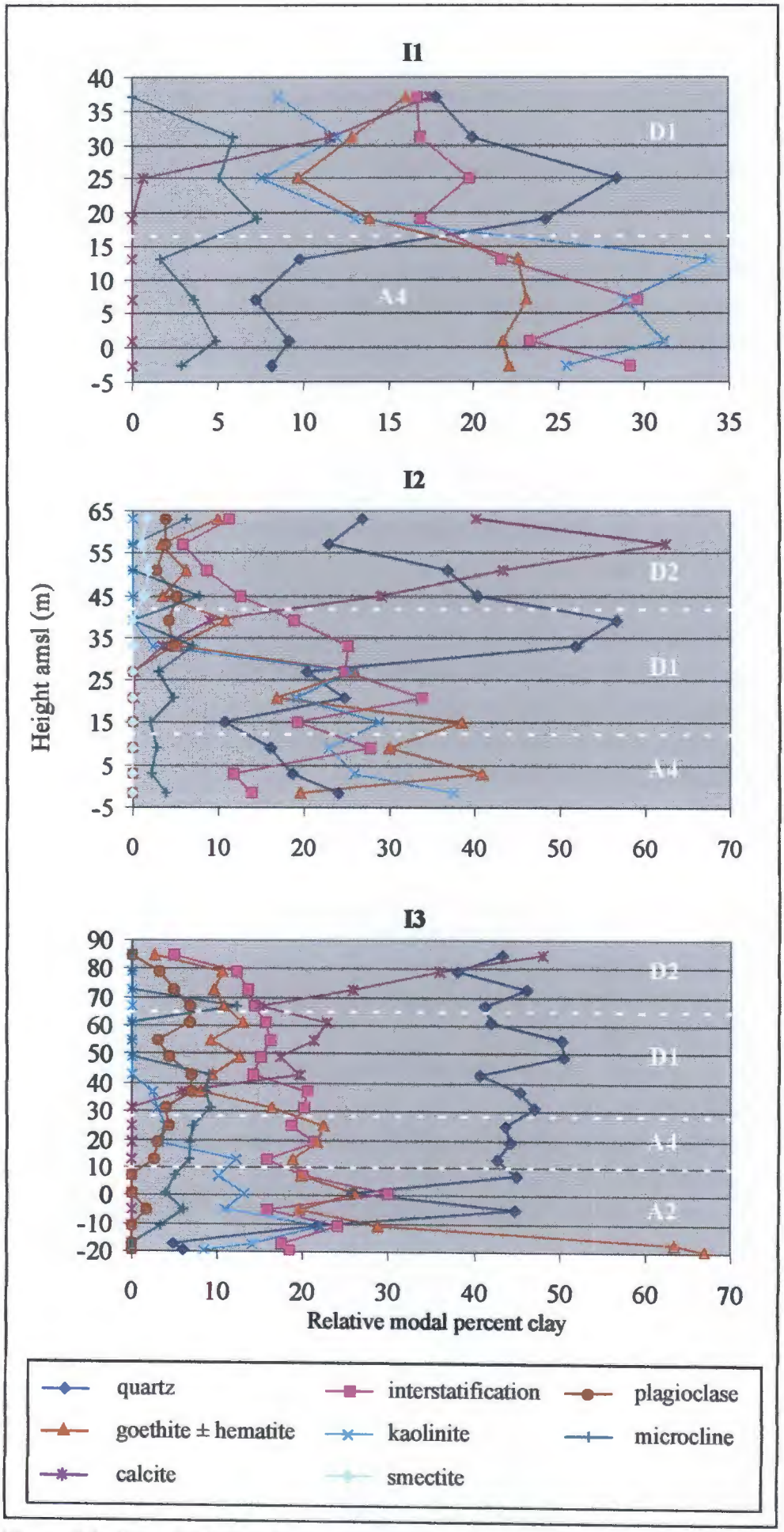

Figure 3.9 Down hole clay-fraction variations for the intermediate boreholes I1, I2 and I3 respectively. NB: quartz abundance is divided by 2 for borehole I1. White dashed lines and corresponding letter and numerical value delineate dune units according to the clay-fraction.

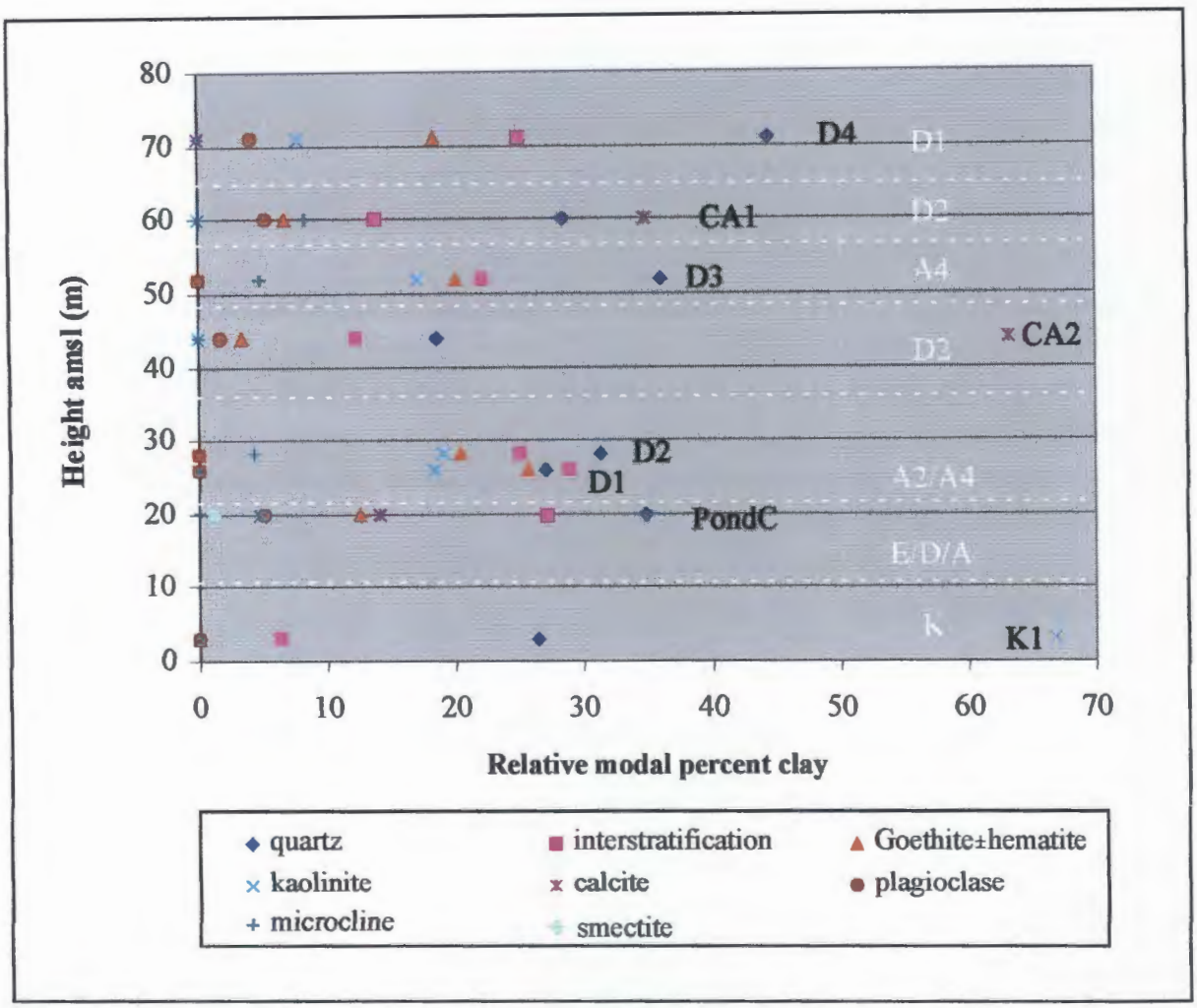

Figure 3.10 Clay-fraction variations for the surface samples. Samples are labelled in black. White dashed lines and corresponding letter and numerical value delineate dune units according to the clay-fraction.

3.3.4 SMECTITE

Smectite is only found in the upper 18 m of the intermediate boreholes I2 & I3, generally in minor amounts of less than *ca.* 2 %. In borehole C1 smectite dominates the clays from - 2 to - 14 m amsl, peaking at *ca.* 60 % at - 11 m amsl.

3.3.5 INTERSTRATIFIED CLAYS

I/S abundances show relative decreases in the inland boreholes and increases in the intermediate and coastal boreholes. I/S is the dominate clay mineral only when kaolinite and smectite have low abundances. This antipathetic relationship with kaolinite and smectite is typically observed at the bottom of the inland boreholes where kaolinite dominates and at - 11 m amsl within the coastal borehole where smectite is dominant.

3.3.6 CALCITE

Calcite is restricted to the intermediate and coastal boreholes where it shows a rapid down hole depletion rarely surviving below 22 m amsl, except in borehole C1 where it is precent to - 17 m amsl. Samples CA1, CA2 also contain abundant calcite with sample PondC containing a minor abundance. Clay XRF analyses also show this rapid depletion of CaO with depth, the relationship being a positive correlation to calcite abundance from XRD analysis. This tentatively indicates that most of the CaO is found in calcite rather than Ca-bearing silicate minerals.

3.3.7 FELDSPAR

Plagioclase concentration gradually decreases with depth and is present to greater depths in the intermediate and coastal boreholes than in the inland boreholes. Microcline shows a similar trend, however it is found to greater depths and in greater abundances than plagioclase. Microcline is absent from borehole C1, except for the first six metres where it is found in minor abundance.

3.3.8 COLLOPHANE

Collophane is restricted to borehole C1. It is not present in the upper 12 m of the borehole but increases rapidly in abundance to *ca.* 27 % at 1 m amsl. The concentration subsequently decreases and is not found below - 17 m amsl.

3.3.9 ILLITE

Illite is found only in minor relative abundance. It is absent in borehole L2 and in the surface samples except K1 which contains *ca.* 1 % illite. Borehole I2 shows an increasing illite abundance down hole with the basal sample containing *ca.* 1 %.

3.3.10 ILMENITE

Ilmenite occurs in very minor amounts, rarely exceeding *ca.* 1 %. It is generally restricted to borehole L2 where it shows an abundance decrease down hole. Boreholes I1, I2 and C1 as well as samples D1 - D2, D3, D4, K1 and Pond C do not contain ilmenite. Sample CA1 is enriched with ilmenite (*ca.* 3 %) compared to the other samples studied.

3.3.11 STRATIGRAPHY BASED ON CLAY-FRACTION ABUNDANCES

Stratigraphic units can be characterised from the clay-fraction as follows (Figure 3.8 - 3.10):

3.3.11.1 Unit K

Unit K is confined to the base of the inland boreholes and is differentiated primarily by a very high kaolinite abundance, especially towards the bottom where it comprises greater than *ca.* 60 % of the sample. Goethite and I/S show a rapid decrease in abundance towards the bottom of this unit. Plagioclase is absent as is ilmenite, calcite, smectite and collophane. Microcline is present in minor amounts but is absent at the base of the unit. Illite generally makes up 0.5 % of clays. Sample K1 correlates well with Unit K having a kaolinite content of *ca.* 67 %.

3.3.11.2 Unit A2

Unit A2 is found towards the bottom of borehole I3 and overlying Unit K in borehole L1. It is defined by a rapid increase (*ca.* > 60 %) of goethite towards its base with a sympathetic decrease in the other clay minerals. Microcline shows a gradual decrease towards the base of the unit. Plagioclase is generally absent as is ilmenite and illite. Calcite, smectite and collophane are absent. Samples D1 and D2 show fair correlation to the top of this unit.

3.3.11.3 Unit A4

Unit A4 overlies Unit A2 and is defined by the absence of calcite, smectite and collophane and intermediate abundances of other clays. Quartz is the dominate clay mineral. Kaolinite and goethite show a gradual increase in abundance towards the base of the unit. Samples D2 and D3 correlate well with this unit, all having quartz as the dominant clay sized mineral.

3.3.11.4 Unit D1

Unit D1 overlies Unit A4 and is restricted to the intermediate boreholes. It is defined by the dominance of quartz and a low calcite abundance (*ca.* < 20 %). Subordinate I/S, kaolinite, goethite and feldspars show gradual increase towards the base of this unit. Smectite and collophane are absent. Sample D4 correlates well with this unit.

3.3.11.5 Unit D2

Unit D2 overlies Unit D1 and is restricted to the intermediate boreholes I2 and I3 where it forms the uppermost unit. It is defined by a high calcite (*ca.* 20 - 60 %) and quartz (*ca.* 25 - 55 %) abundance with minor smectite found in the uppermost samples (*ca.* < 2 %). Calcite rapidly decreases in abundance towards the bottom of this unit with a sympathetic increase in quartz. Other clay minerals are subordinate with collophane being absent. Samples CA1 and CA2 correlates well to this unit, both containing *ca.* > 30 % calcite and no smectite.

3.3.11.6 Unit E

Unit E is restricted to the coastal borehole where it overlies Unit A4. It is defined by a high smectite abundance (*ca.* 10 - 60 %), a low calcite and kaolinite abundance as well as a rapid decrease in collophane. Kaolinite does, however, increase towards the base of this unit, as does goethite and plagioclase.

3.3.11.7 Unit F

Unit F is also restricted to the coastal borehole where it forms the uppermost unit. It is defined by the presence of intermediate abundances of all clays. Collophane is diagnostic showing a rapid increase to *ca.* 25 %.

3.3.11.8 Undifferentiated sample

Sample PondC does not correlate well with any units as it contains low abundances of calcite and smectite with intermediate to high abundances of quartz and interstratifications. The other clay minerals are subordinate, with collophane being absent. The sample probably represents a mixing of units which is to be expected as it is a wash-over sample from the mining process.

3.4 DISCUSSION

Clays are a function of climate, both past and present, with warmer climates being attributed to increased weathering conditions and thus clay formation. Due to density sorting (winnowing), only minor amounts of clay (< 2 %) would have been deposited with the aeolian dune sands. The weathering of these dunes can therefore be considered as *in situ* and post-depositional.

Northern KZN currently has a hot-humid subtropical climate (Section 2.2.1) where hydrolysis is the dominate weathering agent. Under these climatic conditions, strong hydrolysis leads to the neoformation of kaolinite (monosialitisation), often with associated goethite, independent of the source material weathered (Chamley, 1989). Nahon (1986) further identified that goethite generally becomes depleted with depth whereas kaolinite becomes enriched and more crystalline such as observed in Unit K.

Kaolin and goethite are ubiquitous in the samples studied, with kaolinite increasing with depth at the expense of goethite, except in boreholes I3 and C1 where goethite is enriched at depth, perhaps indicating a less mature weathering profile (Unit A). Goethite forms as the weathering product of iron-bearing minerals under well drained oxidising conditions. Upon dehydration, via the amorphous phase ferrihydrite, goethite converts to hematite and vice versa upon hydration (Schwertmann & Taylor, 1977). The presence of magnetite, other FeTi-oxides and Fe-silicates create obvious weathering sources of goethite and hematite. Ferrihydrite would be the obvious choice of the suspected amorphous phase present. Goodman (1990) identified similar kaolinite and ferruginous mineral dominated soils developing inland on the northern KZN coastal plain.

If extreme hydrolysis prevailed, gibbsite followed by boehmite, would form (Chamley, 1989), however these minerals were not observed in any of the samples. Other clays also develop in the early stages of weathering, especially I/S and smectite (Chamley, 1989; Jackson, 1959).

The pH of the dunes is also important in weathering. The presence of calcite in the upper reaches of the intermediate and coastal dunes results in them being slightly alkaline (pH *ca.* 8; Tinley, 1986) with calcite acting as a pH buffer. Kaolinite is noted by Birkeland (1984) to be stable under these pH conditions. The dunes have a high permeability and are freely draining resulting in leaching of calcite. This calcite-rich leachate is consequently lost from the dune system (to inland lakes/marine ?) manifesting as calcite depletion with depth. The presence of calcite also retards downward clay migration as it causes flocculation (Birkeland, 1984). Moderate alkalinity also favours the formation of smectite (commonly saponites), especially in peri-marine environments (Chamley, 1989; Birkeland, 1984). The presence of smectite in the upper 18 m of the boreholes is interpreted to reflect modern soil horizons which would be expected to contain smectite under humid climatic conditions (Birkeland,1984; Chamley, 1989). Upon further leaching smectite would alter to kaolinite by the stripping of silicon sheets from smectite. These relationships suggest that the younger dune sands will be characterised by smectite and calcite (Units F, E and D respectively).

Apatite is a common accessory mineral in many rock types, with fluorapatite dominant in igneous rocks (Deer *et al.*, 1992). Apatite is also the principal material of bones (hydroxyl-apatite) and teeth (fluorapatite) with fluorapatite having a greater resistance to decay than the other apatites (Battey, 1981). This also reinforces the relatively younger age of Unit F as none of the other units contain collophane, presumably lost due to leaching. The source of the collophane can possibly be attributed to the abundance of sharks teeth or to numerous bone-rich middens present on the dunes and therefore could be an isolated occurrence. Analyses of more coastal boreholes would confirm this.

Illite, although in minor amounts, is generally considered to form in a terrestrial environment from the weathering of K-feldspar (Equation 3.1; Weaver & Pollard, 1973; Birkeland, 1984). Feldspars, under moderate pH conditions (as observed in the dunes), weather to kaolinite and smectite (Equation 3.2 - 3.4; Birkeland, 1984). Microcline is also more resistant to leaching than plagioclase and is found to greater depths in the intermediate and inland boreholes. It is however, absent from the coastal borehole, possibly indicating a different source material. Plagioclase is present throughout the coastal borehole but shows an increasing relative depletion down hole. Mechanical weathering due to abrasion, is considered to be the main origin of quartz within the clay-fraction (Krinsley & Smalley, 1973).

K-feldspar (Microcline) illite

$$3KAlSi_3O_8 + 2H^+_{(aq)} + 12H_2O \rightarrow KAl_3Si_3O_{10}(OH)_2 + 6H_4SiO_{4(aq)} + 2K^+_{(aq)} \qquad [3.1]$$

K-feldspar (Microcline) kaolinite

$$2KAlSi_3O_8 + 2H^+_{(aq)} + 9H_2O \rightarrow Al_2Si_2O_5(OH)_4 + 4H_4SiO_{4(aq)} + 2K^+_{(aq)} \quad [3.2]$$

Plagioclase (Albite) kaolinite

$$2NaAlSi_3O_8 + 2H^+_{(aq)} + 9H_2O \rightarrow Al_2Si_2O_5(OH)_4 + 4H_4SiO_{4(aq)} + 2Na^+_{(aq)} \quad [3.3]$$

Plagioclase (Albite) smectite

$$8NaAlSi_3O_8 + 6H^+_{(aq)} + 28H_2O \rightarrow 3Na_{0.66}Al_{2.66}Si_{3.33}O_{10}(OH)_2 + 14H_4SiO_{4(aq)} + 6Na^+_{(aq)} \quad [3.4]$$

4 SILT-FRACTION

Silt-sized particles between 2 and 63 μm form a significant portion of the fine-fraction within the ZNL. The origin of silt has traditionally been considered to lack specific geological control, however its origin and formation has been studied by Kuenen (1969), Pye (1983), Blatt (1987) and Assallay *et al.* (1998) to name a select few. The silt-fraction generally represents fine material derived by mechanical and/or chemical breakdown of sand-sized particles. Variations in silt should therefore reflect variations in the sand-sized fraction, however aeolian sorting processes and the inherent larger surface area of silt also influences its nature and distribution. Unlike clays, most silt particles are active in aeolian processes and thus both depositional (mechanical) and post-depositional (chemical) processes will govern its composition.

Silt minerals were studied on selected samples using SEM secondary images and identified semi-quantitatively using EDX spectroscopy (n = 501; Table 4.1). Relative abundances were obtained empirically from secondary images, together with grain morphology. As traditional optical microscopy point counting techniques can not be used for silt, an image analysis technique has been developed. This involved using software to calculate the abundance of minerals using backscattered images. This chapter documents the mineralogical composition, distribution and weathering within the silt-fraction of the central ZNL.

4.1 MINERALS PRESENT

Mineral groups identified included: silicates, oxides, carbonates, phosphates, and organics. As no attempt was made to quantify mineral abundances using secondary images, these will be described empirically in terms of being common or rare.

Silicates are very common within the silt-fraction. They are dominated by quartz with subordinate amphiboles, pyroxenes, feldspars (alkaline & plagioclase), and occasional zircons, very rare garnet and aluminosilicate. Oxides were common and dominated by spinels (magnetite & very rare chromite), goethite, ilmenite, altered ilmenite, leucoxene, rutile and unidentified Mn-oxides. Carbonates were common in the upper parts of the coastal and intermediate boreholes and consisted of calcite and occasional bioclasts. Monazite, the only phosphate present, was relatively rare. Very rare organic particles were identified as fungal spores and mycelium.

Magnetite and hematite are chemically the same when identified via EDX. As magnetite has been identified

by Hugo (1993) as more common (4 % of the heavy mineral suite) than hematite (which also occurs as exsolution lamellae within ilmenite), magnetite will hence forth be used as a generic name for iron oxide. Goethite generally contains appreciable amounts of Al_2O_3 and SiO_2 (Deer *et al.*, 1992), and together with its morphology, can easily be distinguished from "magnetite". Similarity pyroxenes and amphiboles have been included in the generic term pyriboles (Hugo, 1993) as they have similar chemistry and generally could not be separated by morphology due to weathering and size.

Thin iron-aluminium grain coatings are relatively rare which is contrary to sand-fraction analysis by Sudan (1999) and Singh & Dunlevey (1997) who documented grain coatings on most grains from the same area. It is suspected that ultrasonic dispersion during sample preparation for this study resulted in the removal of grain coatings.

Table 4.1 Selected samples for the silt mineral morphology study using a Philips XL 30 scanning electron microscope (SEM) secondary images. * denotes samples studied using a Hitachi 520 SEM. See Figures 1.1, 1.4 & 1.7 for the location of boreholes and samples.

Borehole	Sample position studied: Height amsl (m)
L1	59, 53, 47, 41, 35, 23, 11, 5, - 1 & - 5.3
L2	59, 53, 35, 29, 23 & 18.5
I1	37, 31, 25, 19, 13, 7, 1 & - 2.5
I2	63, 45, 39, 21, 15, 9 & - 1.7
I3	85*, 67, 43*, 19, 7*, -5 & - 19.2
C1	19*, 13, 1*, - 17, - 23* & - 28.5
Samples	D1, D2, D3*, CA1 & K1

4.2 DOWN HOLE VARIATION

It is apparent that each mineral species responds to chemical and physical processes differently depending on the crystallography such as cleavage, chemical stability, hardness, fracture and a combination of these features will determine the mineral's micro-texture and relative abundance. The large surface areas of the grains also makes them more susceptible to weathering than their sand-sized counterparts.

4.2.1 EMPIRICAL ABUNDANCES AND GRAIN MORPHOLOGY

There is an overall increasing trend in grain weathering down hole and from the coastal to the inland boreholes. This allowed relative ages to be determined based on the relative extent of weathering. The silicate silt-sized grains are predominantly angular which is contrary to the sand-sized particles of aeolian origin which show a high degree of rounding (Sudan, 1999). The more resistant non-silicates grains are generally more rounded and of low to moderate sphericity. Highly weathered grains were occasionally found with non-weathered to sightly weathered grains of the same species, especially in the younger dune units (Units F, E, D2 & D1). This evidence for sediment reworking has also been documented by Hugo (1993) and Sudan (1999).

Only the more common minerals within the boreholes and surface samples could be used for morphological comparison to determine relative weathering states. These included quartz, feldspars, pyriboles and ilmenite, and to a lesser extent rutile, magnetite, goethite, calcite, monazite and zircon. Rare minerals and organics are mentioned for completeness, but have not been studied in detail. Weathering states will be described as slightly, moderately, highly or extremely weathered. Textural descriptions have been taken from a selection of SEM texts (Krinsley & Doornkamp, 1973; Krinsley & McCoy, 1978; Setlow, 1978; Berner & Holdren, 1979; Nixon, 1979; Smart & Tovey, 1981; Berner & Schott, 1982; Lee & Parsons, 1995; Lee *et al.*, 1998). Samples have been characterised into units according to the revised units identified in section 4.2.2.2.

4.2.1.1 Quartz

Quartz has a high stability with the crystallographic cleavage probably being dominate in determining the morphology in the silt-fraction (Krinsley & Smalley, 1973; Smalley & Krinsley, 1974). Quartz occurs in all samples generally as very angular to rounded (rare) anhedral primary grains with a low relief and occasionally as euhedral secondary overgrowth crystals (normally less than 2 μm in size). Generally the more coastal grains show a slight degree of weathering whereas the base of the inland boreholes are extremely weathered (Figure 4.1).

Slightly weathered quartz grains mainly exhibit mechanical features due to aeolian abrasion. This is most evident in Units, F, E, and D2. Mechanical features are typified by conchoidal breakage patterns, arc steps, blocky fractures and a series of parallel ridges or plates (upturned plates) on some grain surfaces. The grains exhibit a low relief with surfaces being generally free of precipitates. Grains in borehole C1 (Unit

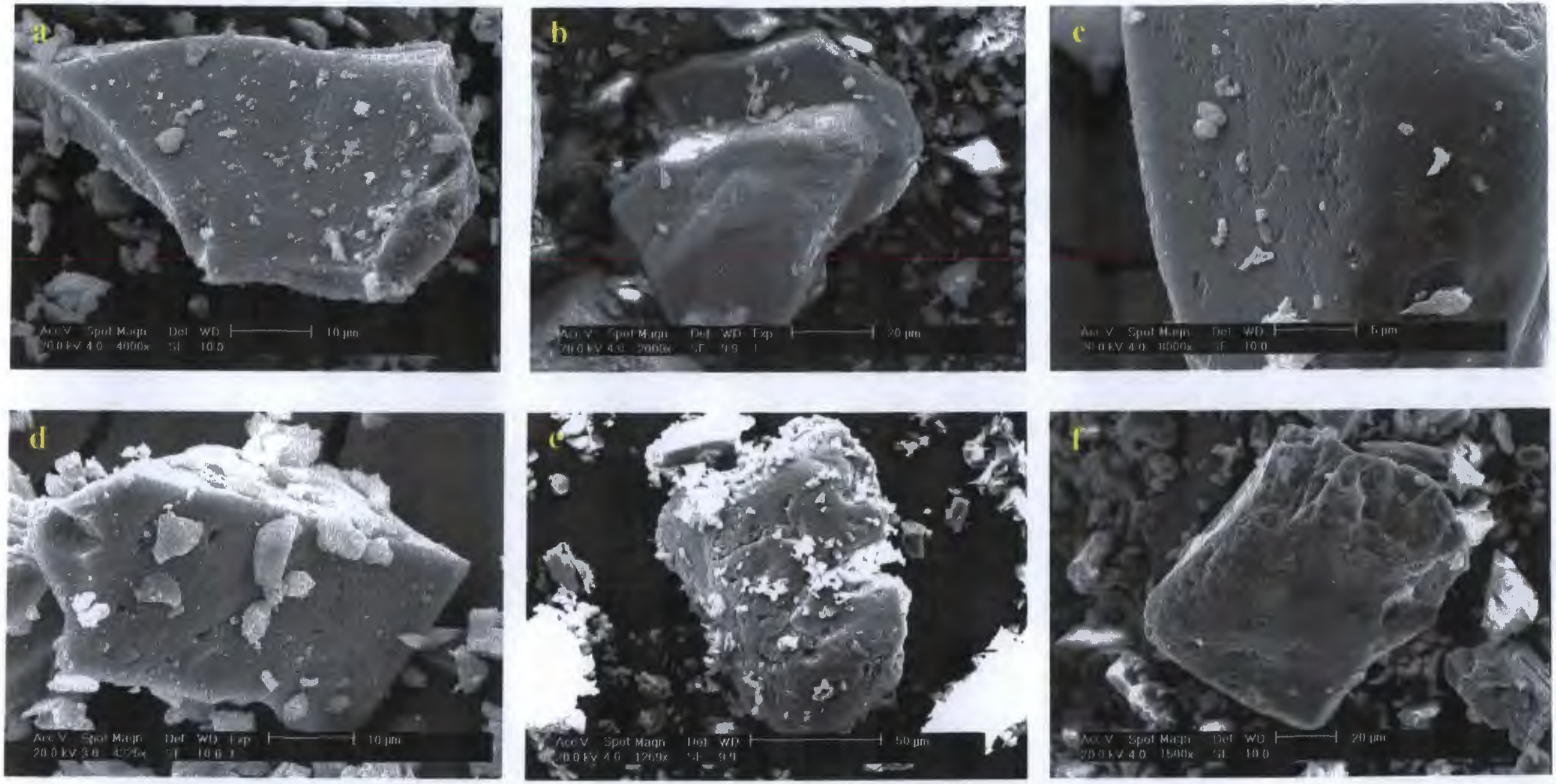

Figure 4.1 Scanning electron microscope secondary images of quartz showing progressive weathering states from the coastal to inland boreholes. (a) Slightly weathered angular quartz shard exhibiting typical mechanical aeolian features such as conchoidal breakage patterns, arc steps, blocky fractures and upturned plates grain edges; borehole C1, 13 m amsl, Unit F. (b) Slightly weathered grain showing upturned plates (centre) as well as minor solution etching (top left); sample CA1, Unit D2, (c) Slightly altered well rounded grain with mechanical V's typical of a littoral environment. Upturned plates are also present (top);borehole C1, - 11 m amsl, Unit E.(d) Moderately weathered grain with numerous irregular solution etch pits and blocky fractures; borehole I1, 25 m amsl, Unit D1. (e) Moderately weathered rounded grain with enlarged etch pits, solution grooves and striations (centre). Modified upturned plates are present throughout the grain. Silica precipitation has formed smooth surfaces (centre); borehole I2, 45 m amsl, Unit D2. (f) Grain showing similar characteristics as (e); borehole I2, 15 m amsl, Unit D1.

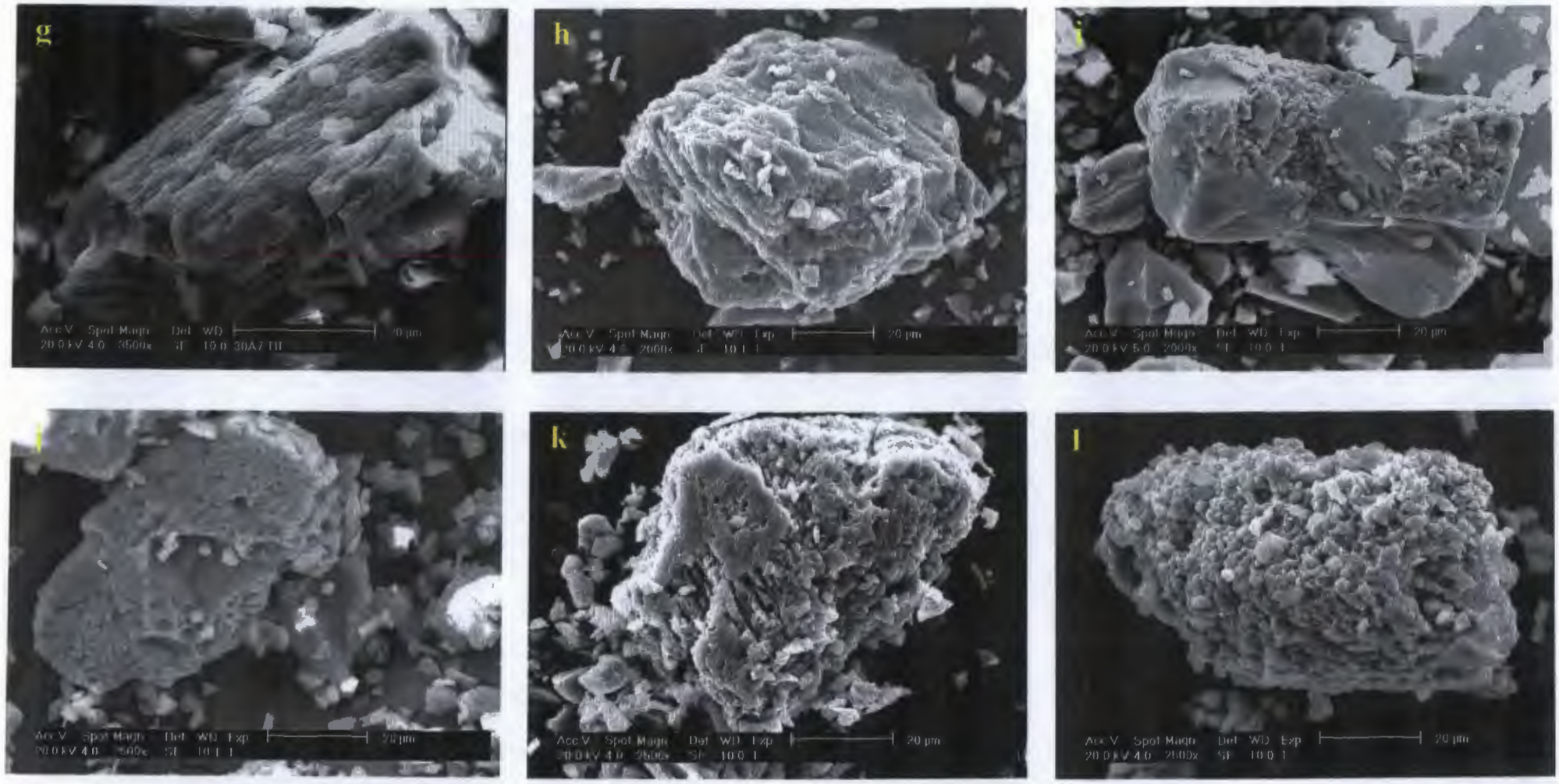

Figure 4.1 (continued). (g) Highly weathered quartz grain showing enlargement and modification of upturned plates resulting in parallel solution grooves; borehole I2, 9 m amsl, Unit A4. (h) Highly weathered quartz gain showing similar characteristics to (g); borehole L1, 59 m, Unit A4. (i) Highly weathered quartz grain with silica precipitation resulting in smoothed surfaces; borehole L1, 23 m amsl, Unit A2. (j) Extremely weathered quartz grain exhibiting deep solution etching(bottom centre) and precipitated upturned silica plates (top and bottom); borehole L1, - 1 m, Unit K. (k) Extremely weathered quartz grain with deep interconnecting etch pits. Silica precipitation in visible on the top right of the grain; borehole L2, 29 m amsl, Unit A2 (l) Extremely weathered quartz grain showing intense chemical weathering resulting in a "sieve" texture. Silica precipitation is also visible (bottom right); borehole L2, 18.5 m amsl, Unit K.

E, -11 m) show V-shaped indentations (mechanical "V's") which is typical of a littoral environment due to high energy inter-granular collision (Krinsley & Donahue, 1968; Nordstrom & Margolis, 1972; Krinsley & Doornkamp, 1973; Lin *et al.*, 1974; Le Ribault, 1978; Kaldi *et al.*, 1978).

As the degree of grain weathering progresses to moderate (Units D2 & D1) there is a combination of mechanical and chemical features. The grains have a low to moderate relief with surfaces occasionally veneered with iron-aluminium-silicate precipitates. Mechanical features are common and similar to the slightly weathered grains however grain cracking is also observed. Upturned plates (characteristic of non-desert aeolian environment) become common in Unit D1. Chemical features include irregular solution etch pits which progressively enlarge and combine to form linear solution grooves and striations. The etch pits probably start at crystal dislocations or in voids of exposed fluid inclusions.

Highly weathered grains are typical of Units A4 and A2 where upturned plates occur on more than 80 % of the grains. The upturned plates have been subsequently modified by solution of silica (presumable due to the alkaline conditions; section 3.4) resulting in deep grooves. Silica precipitation has resulted in the smoothing of some surfaces, confining upturned plates to the edge of the grains. The grains have a moderate to high relief.

Extremely weathered grains are only found at the base of the inland and intermediate boreholes and are typical of the basal portions of Units A4, A2 and especially K. Mechanical features have been masked by silica solution and precipitation. Precipitated upturned silica plates are common. The etch pits have enlarged and interconnected to such a degree that the original grain morphology has been totally masked resulting in a "sieve" texture. The grains have a high to extreme relief.

4.2.1.2 Feldspars

Feldspars have been grouped into the broad sub-groups of plagioclase and alkali feldspars, discussed below. Figures 4.2 & 4.3 show the progressive weathering of plagioclase and alkali feldspars respectively.

Plagioclase

Plagioclase feldspars were generally associated with Unit A4 but showed progressive weathering down hole and from the coastal to the inland boreholes. In the upper reaches of Unit A4 the grains are slightly weathered, sub-angular and have a low relief. Mechanical features include blocky fractures, steps and

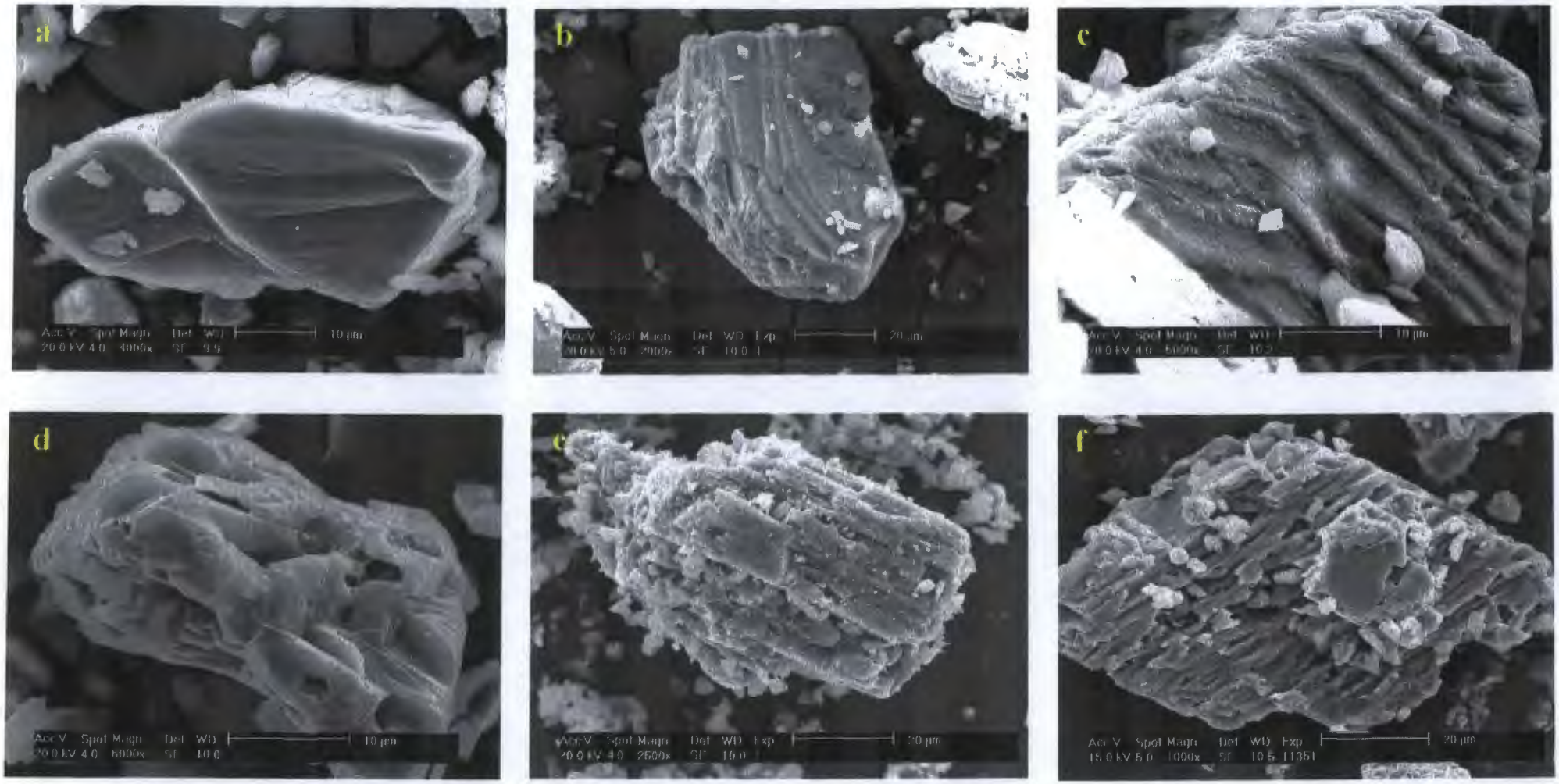

Figure 4.2 Scanning electron microscope secondary images of plagioclase feldspar showing progressive degrees of weathering mainly within Unit A4. (a) Slightly weathered sub-angular grain showing blocky fractures and steps; borehole C1, - 28.5 m, Unit A4. (b) Slightly weathered sub-rounded grain showing breakage along cleavage planes as well as slightly modified upturned plates (bottom); borehole L1, 35 m amsl, Unit A4. (c) Probable reworked grain showing a moderate degree of weathering in the form of deep parallel solution channels and silica precipitation (left). Grain cracking is also visible (top); borehole I2, 45 m amsl, Unit D2. (d) Highly weathered grain showing deep prismatic etch pits; borehole C1, - 28.5 m amsl. Unit A4. (e) Extremely weathered grain exhibiting end-to-end coalescence of etch pits forming solution channels; borehole L2, 35 m amsl, Unit A2 (f) Fragile honeycomb-like shell representing the finale stages of dissolution; borehole I1, - 2.5 m amsl, Unit A4 (basal).

upturned plates are common on grain edges. Chemical weathering has subsequently modified the upturned plates, especially towards the centre of Unit A4.

Moderately weathered grains exhibit chemical weathering which masks most of the mechanical features. The grains are sub-rounded with moderate relief. Features observed associated with chemical weathering include preferentially aligned prismatic (square-shaped) etch pits orientated along the principal (001) cleavage surface with their long axes approximately parallel to the c-axis (Berner & Holdren, 1979), shallow solution channels and siliceous precipitates. Grain cracking is commonly observed.

As weathering proceeds, highly weathered grains are characteristically sub-rounded with a high relief. The prismatic etch pits have coalesced and enlarged to mask any mechanical features. Iron-aluminium-silica precipitates are common, especially within the etch pits.

The base of Unit A4 is characterised by extremely weathered grains where an almost complete coalescence of etch pits has occurred resulting in deep solution channels forming a fragile honeycomb-like structure. The etch pits also penetrate deep into the grains and commonly contain iron-aluminium-silica precipitates. Plagioclase grains were not observed in Units K nor A2.

Alkali Feldspar

Alkali feldspars show similar degrees of weathering as plagioclase feldspars however they are comparatively more resistant to weathering and are consequently found in Unit K. Slightly weathered grains are dominated by mechanical block fractures, arc steps and upturned plates on grain boundaries. These have subsequently been modified by chemical weathering features. The grains are angular and of low relief. These features are typical of grains from Units F, E, D2 and D1.

Moderately weathered grains are associated with the upper portions of Unit A4. Grains are characteristically sub-angular to rounded and have a low relief. Mechanical features are still visible, especially upturned plates, but chemical features are common throughout the grains. Small shallow prismatic (< 0.5 μm) etch pits are always aligned parallel to each other corresponding almost exclusively to preferentially leached albite exsolution lamellae (Lee & Parsons, 1995; Lee *et al.*, 1998). Siliceous precipitates are common.

Highly weathered grains are characteristically angular to rounded with a high relief and are associated with

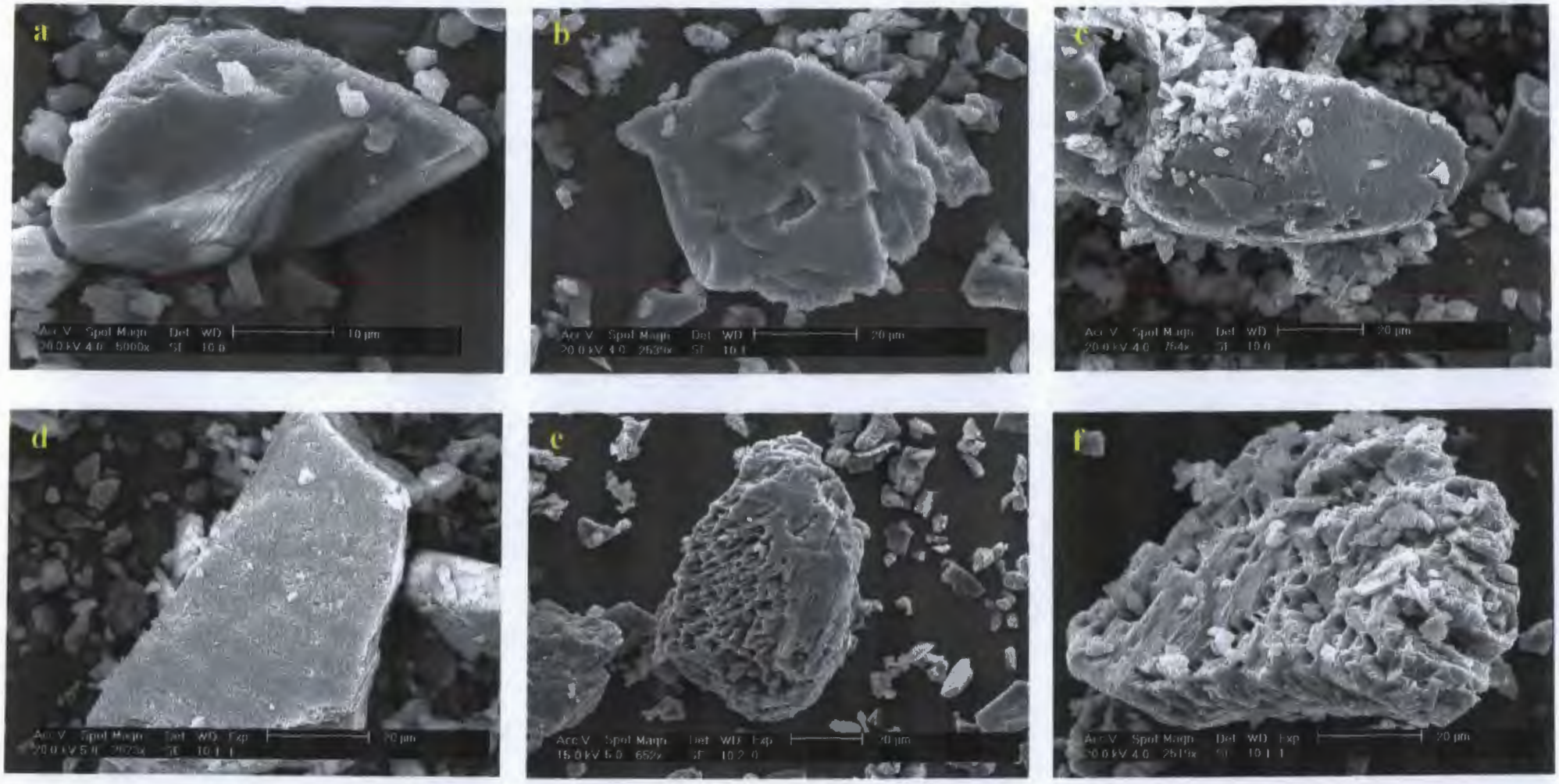

Figure 4.3 Scanning electron microscope secondary images of alkali feldspar showing progressive weathering from the intermediate to the inland boreholes. (a) Slightly weathered, sub-angular grain showing blocky fractures, upturned plates (top) and arc steps (bottom); borehole I2, 39 m, Unit D2. (b) Slightly weathered, sub-rounded grain showing upturned plates on the grain edges which have been modified by chemical action; borehole I2, 21 m amsl, Unit D1. (c) Moderately weathered, rounded grain with modified upturned plates and shallow etching. A relic of clay coating is still visible on the bottom left of the grain; borehole I1, 13 m amsl, Unit A4. (d) Moderately weathered, sub-angular grain showing shallow parallel aligned prismatic etch pits. This alignment corresponds almost exclusively to preferentially leached albite exsolution lamellae (Lee & Parsons, 1995; Lee *et al.*, 1998). Some pits show end-to-end coalescence to form solution channels; borehole L1, 59 m amsl, Unit A4. (e) Highly weathered grain showing deep solution channels and silica precipitation; borehole I1, 7 m amsl, Unit A4 (f) Fragile honeycomb-like shell representing the finale stages of dissolution. Note the deep penetrating prismatic etch pits; borehole L2, 18.5 m amsl, Unit K.

the basal portions of Unit A4 and Unit A2. Deep solution channels (0.5 - 2 μm) caused by the coalescence of etch pits cover more than 50 % of the grains. No mechanical features are preserved and siliceous precipitates are very common both within the etch pits and on clean grain surfaces resulting in smooth surfaces.

Unit K contains extremely weathered alkali feldspar grains resulting in a very high grain relief. More than 95 % of the grain comprises deep solution channels (> 2 μm) and individual etch pits have coalesced to such an extent that they have formed etch holes that penetrate the grain resulting in a honeycomb-like structure. Siliceous precipitates are common throughout the grains.

4.2.1.3 Pyriboles

Slightly weathered pyribole grains are generally elongate, have a low relief and are typical of Units F, E, D2 and D1 (Figure 4.4). Mechanical features are primarily controlled by breakages along cleavage planes resulting in elongate grains. Chemical weathering is manifested by shallow lens-shaped etch pits developed mainly on dislocation outcrops and are always aligned with their long axes parallel to the c-axis of the crystal (Berner & Schott, 1982). Pyribole teeth are also common on the basal sections of crystals. Siliceous precipitates are common in all weathering states.

An increase in weathering from medium to extreme states is manifested by means of the enlargement and coalescence of the lens-shaped etch pits. Their side-by-side coalescence results in the formation of *en-echelon* "cracks" or wider compound pits whereas end-to-end coalescence results in a grooved and striated surfaces. Upturned plates have been chemically modified and are commonly associated with siliceous precipitates. Grains relief increases with increasing degrees of weathering. A moderate degree of weathering is typical of the upper section of Unit A4 and a high degree of weathering of the central section. Extreme degrees of weathering are found in the basal sections of Unit A4 (especially in the inland boreholes), Unit A2, and Unit K resulting in fragile honeycomb-like shells.

4.2.1.4 Ilmenite

Ilmenite grains are generally well rounded, of moderate to high sphericity and of low relief (Figure 4.5). Slightly weathered grains show cracking, blocky fracture patterns and upturned plates on the edge of the grains. These have subsequently been chemically weathered. Siliceous precipitates on grain surfaces are common. This is typified by grains found in Units F, E, D2 and D1. It must be stressed again that these

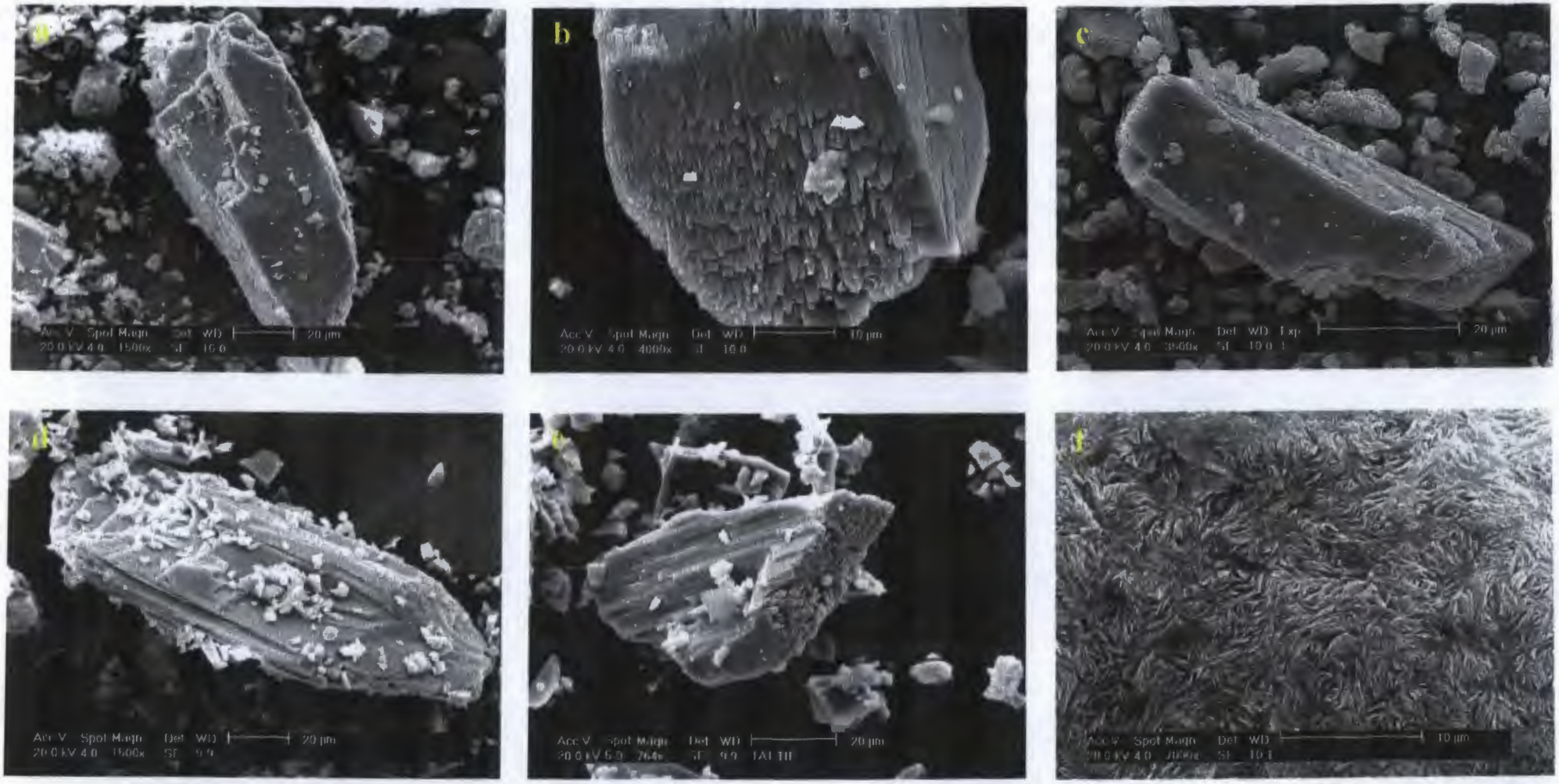

Figure 4.4 Scanning electron microscope secondary images of pyriboles showing progressive degrees of weathering from the coastal to the inland boreholes. (a) Slightly weathered grain showing breakage along cleavage planes resulting in an elongate sub-rounded morphology; borehole C1, 13 m, Unit F. (b) Basal section of a slightly weathered grain showing typical teeth structures. Also note the elongate etches aligned parallel to the c-axis of the crystal (right); borehole C1, - 11 m amsl, Unit E. (c) Slightly weathered elongate sub-rounded grain showing typical parallel orientated lens-shaped etch pits; sample CA1, Unit D2. (d) Slightly weathered grain showing the end-to-end coalescence of etch pits resulting in solution channels and striations; borehole I2, 45 m amsl, Unit D2. (e) Moderately weathered grain exhibiting extensive end-to-end coalescence of etch pits forming solution channels. Teeth are also present on the basal section of the crystal; borehole I1, 31 m amsl, Unit D1 (f) Close up view of modified upturned plates resulting in randomly orientated blades. Note iron-aluminium-silica precipitation (top left); borehole I2, 21 m amsl, Unit D1.

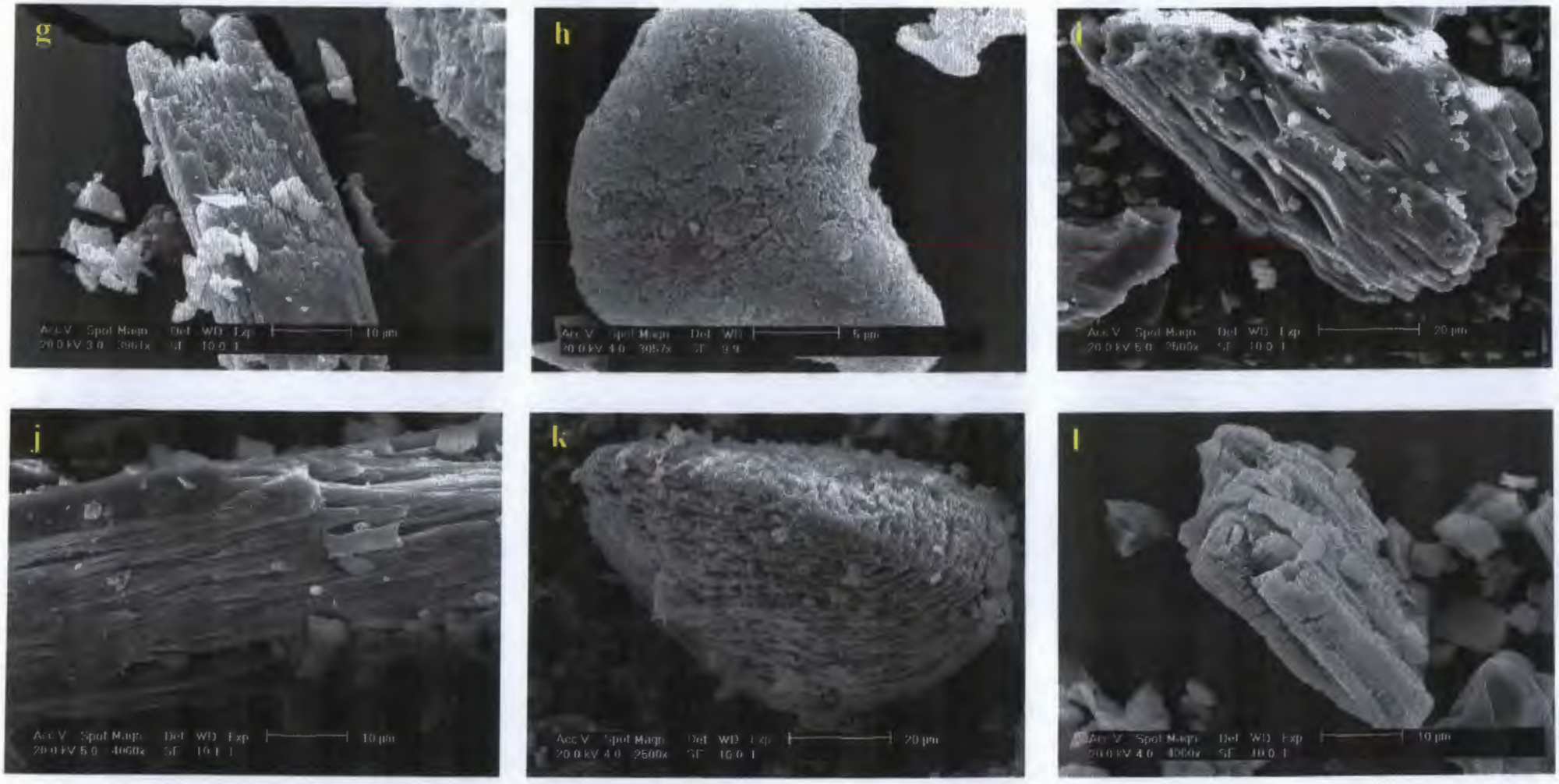

Figure 4.4 (continued). (g) Moderately weathered grain showing enlargement and enlargement of etch pits parallel to the c-axis of the crystal deep solution grooves as well as teeth; borehole I1, 25 m amsl, Unit D1. (h) Highly weathered, rounded gain showing chemical enlargement of upturned plates together with extensive precipitation of silica; borehole I1, 1 m, Unit A4. (i) Highly weathered grain exhibiting side-by-side and end-to-end coalescence of lens-shaped etch pits; borehole L1, 35 m amsl, Unit A4. (j) Highly weathered grain exhibiting deep solution channels and micro-cavities; borehole L1, 35 m, Unit A4. (k) Extremely weathered grain with deep interconnecting etch pits resulting in a fragile platey morphology; borehole L2, 35 m amsl, Unit A2 (l) Extremely weathered grain showing intense chemical weathering resulting in a fragile "cracked" shell; borehole L2, 18.5 m amsl, Unit K.

units contain grains which show all degrees of weathering. This is clearly the result of reworking of the dunes and blending of weathering products (Hugo, 1993).

Moderately weathered grains have greater number of cracks with mechanical features (upturned plates) being masked and deepened by chemical weathering. Chemical weathering features are found on some grain surfaces as well as on grain boundaries. Altered ilmenite is a common weathering product which seems to protect the original grain from further weathering (Figure 4.5 f). Other siliceous precipitates are common. The grains have a moderate relief. These weathering features are common within the upper portions of Unit A4.

Upturned plates on highly weathered grains have been extensively weathered by chemical processes resulting in a moderate relief and a rolling topography. Solution etches are found throughout the grains in the form of lenticular elongate pits (often bridged by fine needles) which enlargement and coalesce as weathering increases. Their side-by-side coalescence results in the formation of circular micro-throughs whereas end-to-end coalescence results in a grooved and striated surfaces. Etching is probably controlled by the preferentially leaching of lenticular exsolved hematite (Hugo, 1993). This is confirmed by a relative increase in TiO_2 compared to FeO within these grains. These features are common in the lower section of Unit A4 and Unit A2.

Extremely weathered grains are generally confined to Unit K and have a high relief. The etch pits have coalesced to such an extent that the grains appear to be platey and contain micro-cavities. TiO_2 is generally enriched with respect to FeO, also noted by Hugo (1993), resulting in most of the grains being altered ilmenites or leucoxenes. Secondary iron-silica-aluminium precipitates are commonly observed on grain surfaces as well as within voids.

4.2.1.5 Rutile

Rutile has a high degree of resistance to weathering, however ilmenite-hematite intergrowths show preferential leaching forming lenticular voids (Hugo, 1993). Rutile is relatively rare and only observed in Units A4, A2 and Unit K (Figure 4.6). Slightly weathered grains (upper Unit A4) have blocky fracture patterns, arc steps, of low relief and are irregular in outline. Upturned plates are commonly observed on the edge of the grains. Moderately to highly weathered grains are more rounded and of moderate relief and are found in the lower sections of Unit A4 and Unit A2. They contain parallel aligned lenticular voids and most surfaces contain upturned plates which have been smoothed and elongated by chemical weathering.

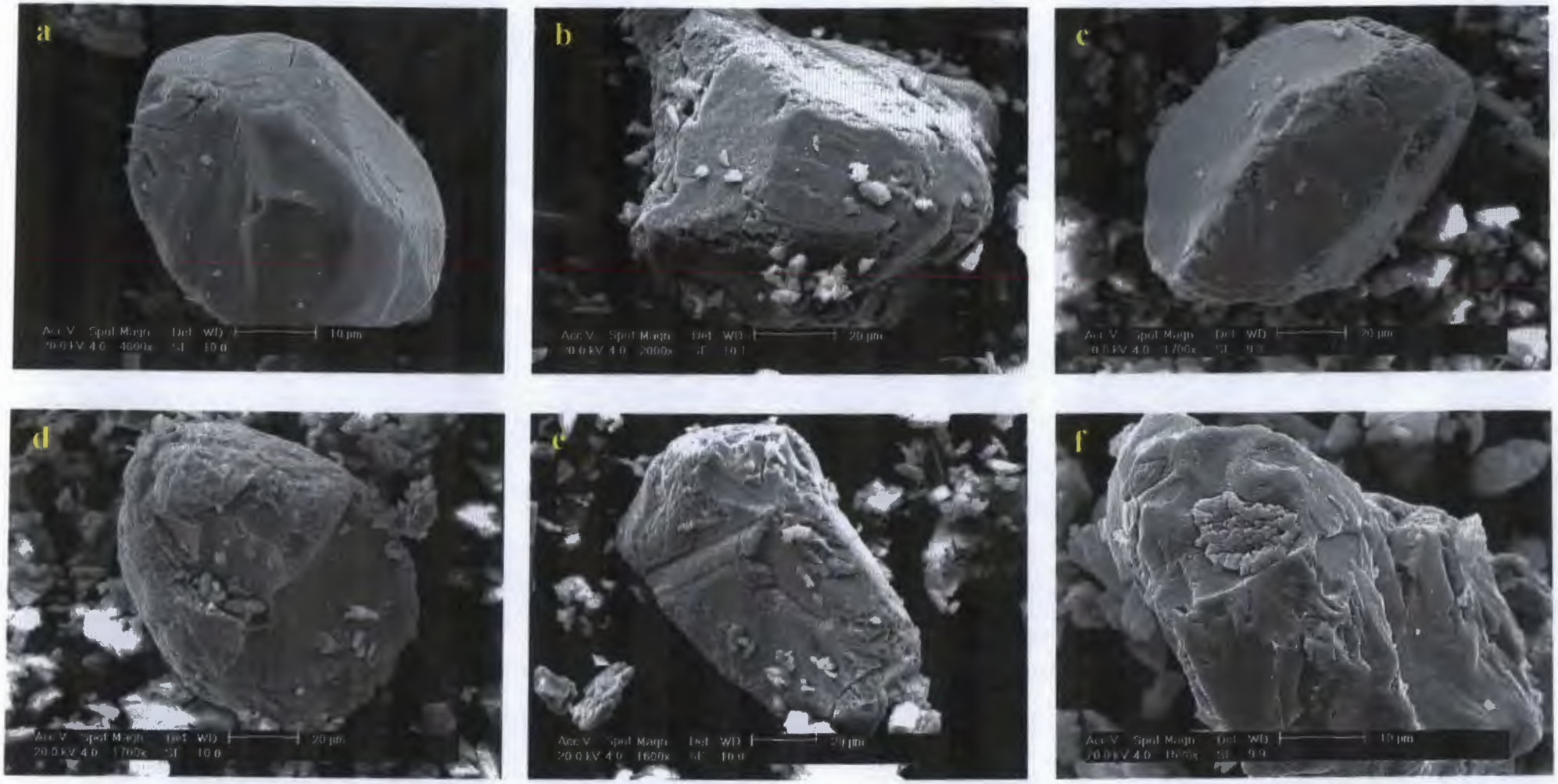

Figure 4.5 Scanning electron microscope secondary images of ilmenite showing progressive degrees of weathering from the coastal to the inland boreholes. (a) Slightly weathered, well rounded grain showing blocky fractures (top left), striations and widened cracks; borehole C1, - 11 m, Unit E. (b) Slightly weathered, sub-rounded grain showing upturned plates on grain edges which have been subsequently modified. Note grain cracking (centre); borehole C1, - 11 m amsl, Unit E. (c) Slightly weathered, sub-rounded grain showing similar features as (b; borehole I2, 45 m amsl, Unit D2. (d) Moderately weathered, rounded grain showing modified upturned plates and silica precipitation (top); borehole I2, 15 m amsl, Unit D1. (e) Moderately weathered, rounded grain exhibiting grain cracking, modified upturned plates, solution channels and silica precipitation (top left); borehole I2, - 1.7 m amsl. Unit A4 (f) Angular grain with remnant altered ilmenite cryptocrystals (top centre) which would have presumable covered the original grain protecting the grain from further alteration. Also shown are blocky fractures and prismatic etch pits; borehole I1, 1 m amsl, Unit A4.

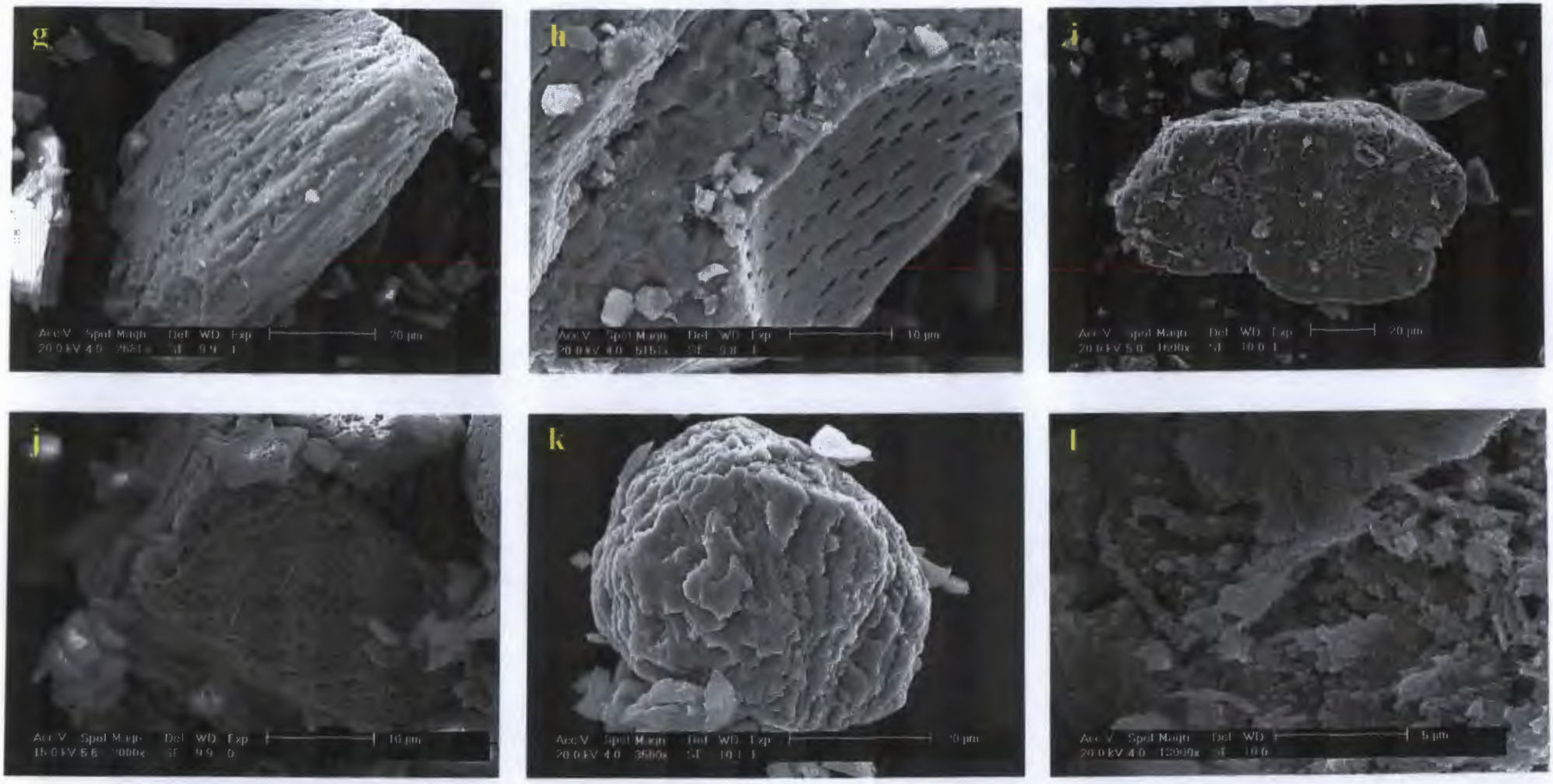

Figure 4.5 (continued). (g) Highly weathered grain showing enlargement and alteration of parallel etch pits presumably by the leaching of exsolved hematite; borehole L1, 41 m amsl, Unit A4. (h) Highly weathered grain showing the cross-sectional and surface expression of lens-shaped etch pits with some showing end-to-end coalescence. Etch pits are also bridged by needles. Modified upturned plates are also visible but masked by etching (top); borehole L1, 41 m amsl, Unit A4. (i) Highly weathered grain exhibiting side-by-side and end-to-end coalescence of prismatic etch pits; borehole L1, 35 m amsl, Unit A4. (j) Highly weathered grain exhibiting a box-work texture, presumably along hematite exsolution lamellae; borehole L1, 11 m amsl, Unit A2. (k) Extremely weathered grain resulting in a platey morphology; borehole L2, 18.5 m amsl, Unit K. (l) Extremely weathered leucoxene grain showing intense chemical alteration resulting in plates and blades. Iron-aluminium-silica precipitates are visible forming flat areas (top centre); sample K1, Unit K.

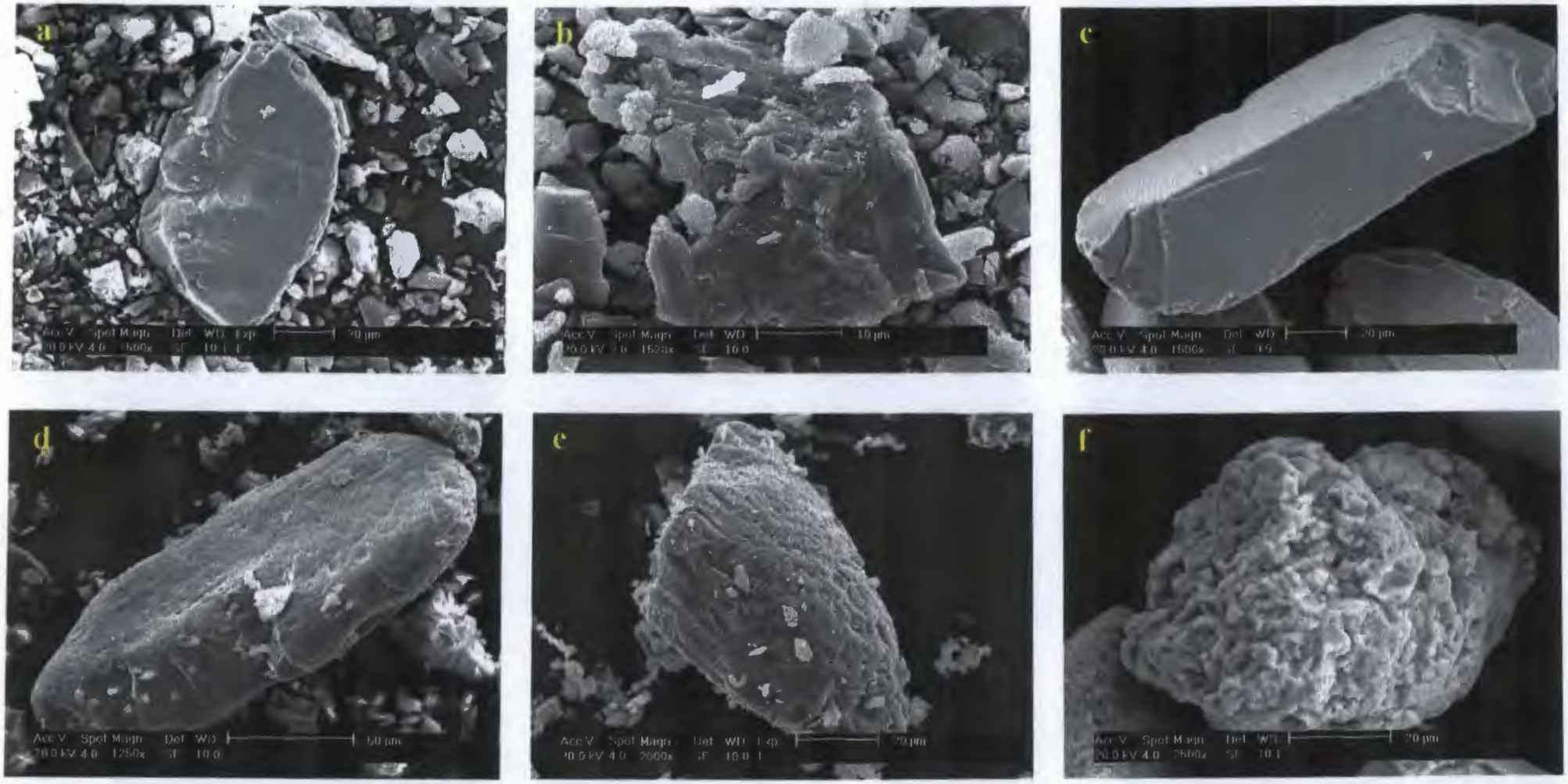

Figure 4.6 Scanning electron microscope secondary images of rutile showing progressive degrees of weathering within Units A4 and A2. Note images (c) and (d) are taken using the Hitachi 520 SEM. (a) Slightly weathered grain showing arc steps and blocky fractures. Very shallow etch pits are also visible (centre); borehole L1, 59 m amsl, Unit A4. (b) Slightly weathered, irregular grain with upturned plates (top). Twinning is probably responsible for this morphology; borehole I1, 13 m amsl, Unit A4. (c) Slightly weathered crystal with small etch pits visible. This crystal has probably been recently liberated; borehole L2, 23 m amsl, Unit K. (d) Moderately weathered, rounded grain exhibiting extensively modified upturned plates and blocky fractures resulting in a rolling topography; borehole I2, - 1.7 m amsl, Unit A4 (e) Highly weathered grain showing extensively modified upturned plates, striations and solution channels; borehole L2, 35 m amsl, Unit A2. (f) Extremely weathered grain showing extensively modified upturned plates and deep coalesced etch pits resulting in a blocky morphology; borehole L1, -5.25 m amsl, Unit K.

This results in a smooth topography. Micro-cracks within grains are common and have been chemically widened. Extremely weathered grains of high relief are observed in Unit K. The etch pits have coalesced resulting in a blocky grain morphology.

4.2.1.6 Magnetite

Magnetite is highly susceptible to weathering, and only moderately to extremely weathered grains were observed in the samples studied (Figure 4.7). Magnetite grains are generally rounded, of low sphericity and become more irregular with increasing degrees of weathering. Goethite is commonly found on the surface of magnetite grains.

Magnetite grains with less than 30 % of the surfaces not affected by chemical weathering are generally confined to Units F, E, D2 and D1 (moderately weathered). The only mechanical features present are upturned plates, however these have been widened and smoothed by chemical action. Weathering results in deep irregular voids or micro-cavities (0.1 - 3 μm) often bridged by iron "needles".

Highly weathered grains are abundant in the upper sections of Unit A4 with less than 10 % of the surfaces not affected by chemical weathering. Theses grains typically have a sponge- or coral-like texture due to the widening and coalescence of voids. Iron-silica-aluminium precipitates are common on grain surfaces and within voids.

As weathering progresses, extremely weathered magnetite grains show intense chemical weathering. Iron needles are less abundant and randomly orientated, while radiating single blades of goethite are common. These grains are relatively abundant within the lower portion of Units A4 and A2, however they were not observed in Unit K. This suggests that either Unit K was devoid of magnetite or more likely that the grains have been completely leached. Goethite precipitates are common, especially at grain boundaries.

4.2.1.7 Goethite

Goethite is a secondary mineral formed by the alteration of Fe-bearing minerals, notably magnetite. Goethite is abundant in Units D1, A4 and A2, which corresponds to high goethite abundances within the clay-fraction (Figure 4.8). The most common occurrence of goethite is as clustered botryoidal or globular growths and single blades on magnetite grain surfaces. Iron needles, blades and spheres (*ca.* 4 μm in diameter) are commonly found as "grains". Chemical analysis revealed appreciable quantities of SiO_2 (<

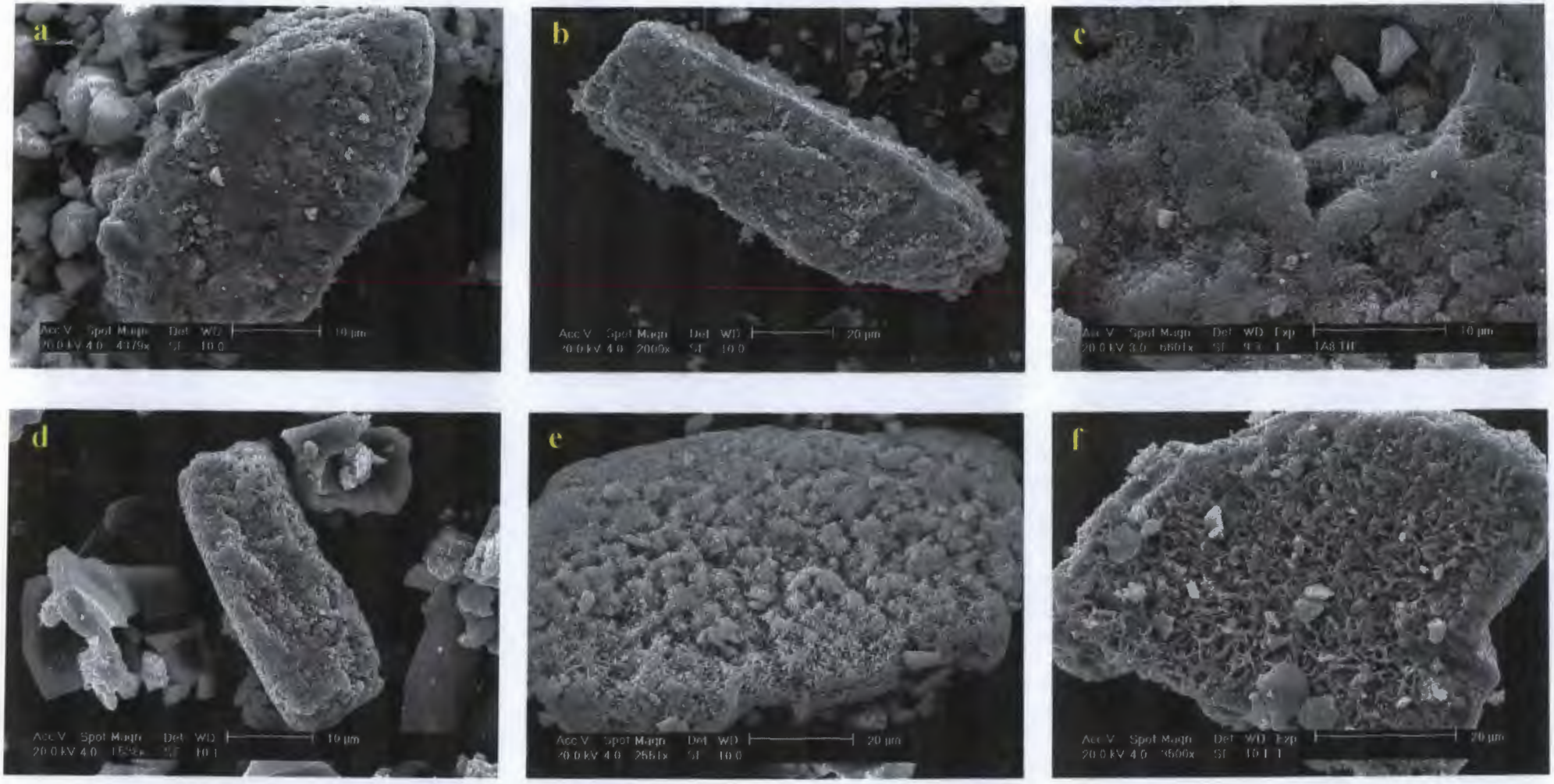

Figure 4.7 Scanning electron microscope secondary images of magnetite showing progressive degrees of weathering from the coastal to the inland boreholes. (a) Moderately weathered grain showing upturned plates that have been modified into deep irregular etch pits or micro-cavities together with silica precipitation (smooth areas); borehole C1, 13 m amsl, Unit F. (b) An elongate moderately weathered grain with similar features as (a); borehole I3, 73 m amsl, Unit D2. (c) Close up view of a highly weathered grain showing micro-cavities, iron-needles and blades; borehole I1, 31 m amsl, Unit D1. (d) Highly weathered grain showing extensive weathering in the form of deep etch pits and micro-cavities resulting in a sponge/coral morphology. Goethite often fills the voids; borehole I1, 7 m amsl, Unit A4. (e) Extremely weathered grain exhibiting extensive dissolution with goethite precipitating in the form of radiating needles and blades giving a sponge/coral morphology; borehole I3, 19 m amsl, Unit A4 (f) Extremely weathered grain with radial and random single blades of goethite masking the original grain morphology; borehole L2, 35 m amsl, Unit A2.

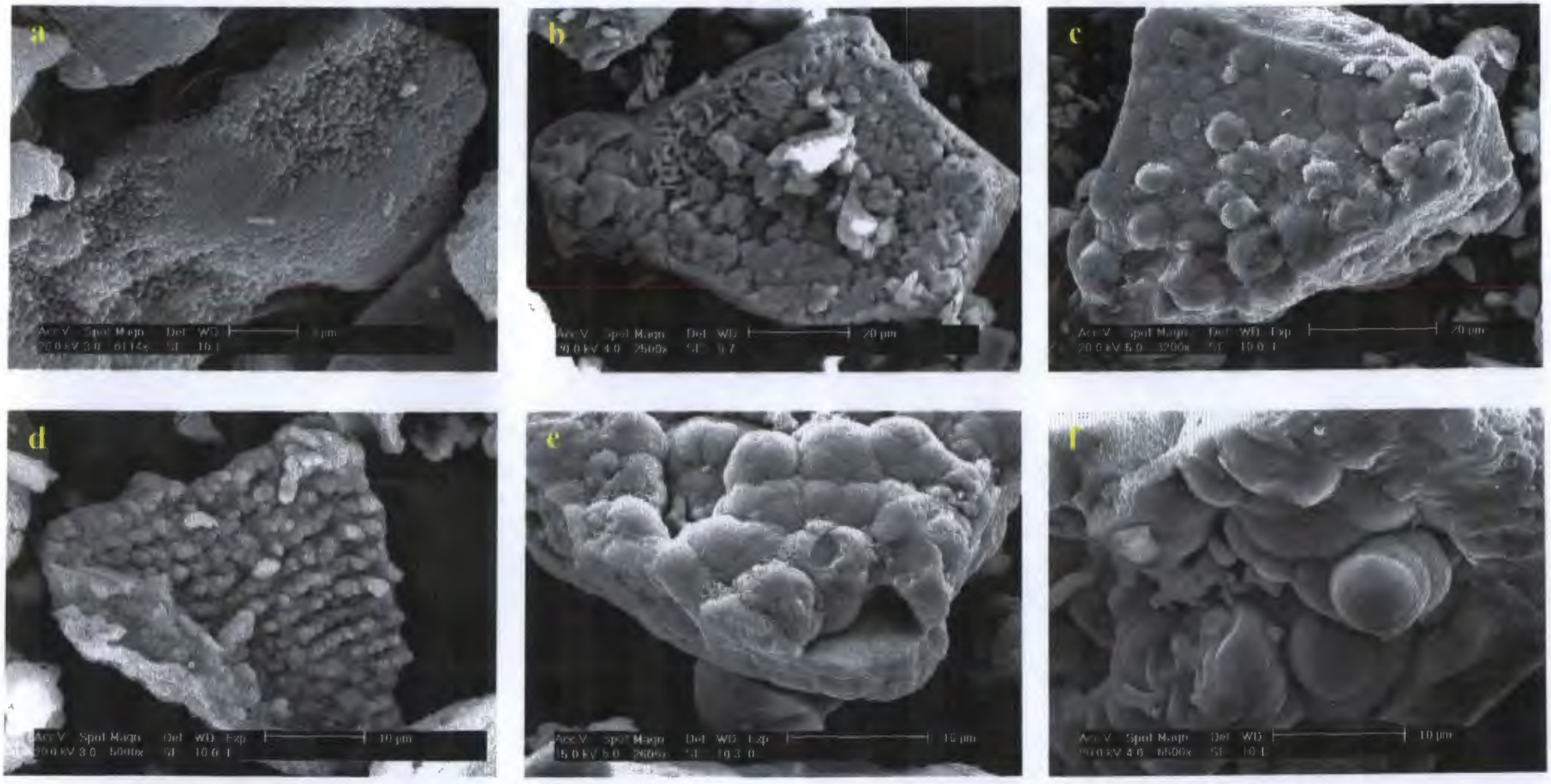

Figure 4.8 Scanning electron microscope secondary images of goethite showing contrasting morphologies. (a) Goethite spheres precipitating directly on a magnetite grain; borehole I1, 13 m amsl, Unit A4. (b) Botryoidal precipitates and single blades adhering to a magnetite grain; borehole I2, 15 m amsl, Unit D1. (c) Botryoidal growths with associated radiating needles on a goethite substrate; borehole L1, 35 m amsl, Unit A4. (d) Clustered spheres intimately connected by fibrous needles; sample D1, Unit A4/A2. (e) Botryoidal growths interconnected by needles on a massive (goethite) substrate; borehole I1, 7 m amsl, Unit A4 (f) Globular growths on a massive (goethite) substrate; borehole I3, - 19.2 m amsl, Unit A0.

20 %) and Al_2O_3 (< 20 %) within all goethite "grains". This aluminium-silica contamination is typical of these minerals (Deer *et al.*, 1992).

4.2.1.8 Calcite

As in the clay-fraction, calcite grains were only observed in the upper reaches of the coastal and intermediate boreholes corresponding to Units F, E, D2 and D1. Calcite is found in two forms; primary highly altered sub-rounded bioclasts and as secondary precipitated grains (Figure 4.9). The former were very rare and only observed at the very top of boreholes I1 and C1. These shell fragments were unable to be identified. Secondary anhedral calcite grains were typically irregular in shape with a high relief. Numerous phases of carbonate growth and solution were noted on most of the grains. Grains in Unit D1 showed the highest degrees of dissolution.

4.2.1.9 Monazite

Monazite grains were only observed in Units D2, D1, A4 and A2 and do not show progressive degrees of weathering from the top of the coastal to the base of the inland boreholes. Instead the monazite grains show a range of weathering states even when intimately associated with each other. This finding supports the idea that highly resistant minerals are concentrated by successive reworking. The majority of grains are rounded and of low to moderate relief (Figure 4.10). Mechanical features were observed on most grains in the form of conchoidal fractures, blocky fractures, steps and upturned plates. Chemical etching tends to concentrate on grain boundaries causing uneven grain edges. The weathering of upturned plates has resulted in parallel solution grooves. Precipitated upturned silica plates were noted on the more weathered grains.

4.2.1.10 Zircon

Zircon showed similar characteristics to monazite with no clear weathering trends. This is probably due to the extreme resistance to these minerals allowing grains to survive multiple reworking events (Pietersen, 1992). Zircon was found in three basic forms all of low relief; as euhedral crystals, anhedral shards and as well to very well "rounded" grains (Figure 4.11). The very well "rounded" grain (Figure 4.11 c) is probably a result of only slight abrasion of a multifaceted, probably euhedral zircon crystal. Other well rounded grains exhibited fresh clean rounded surfaces as well as upturned plates. These grains have an onion-skin appearance, probably due to mineral zoning. This is further evidence of multiple reworking of these grains. The upturned plates are similar to those obtained experimentally by Pietersen (1992) using

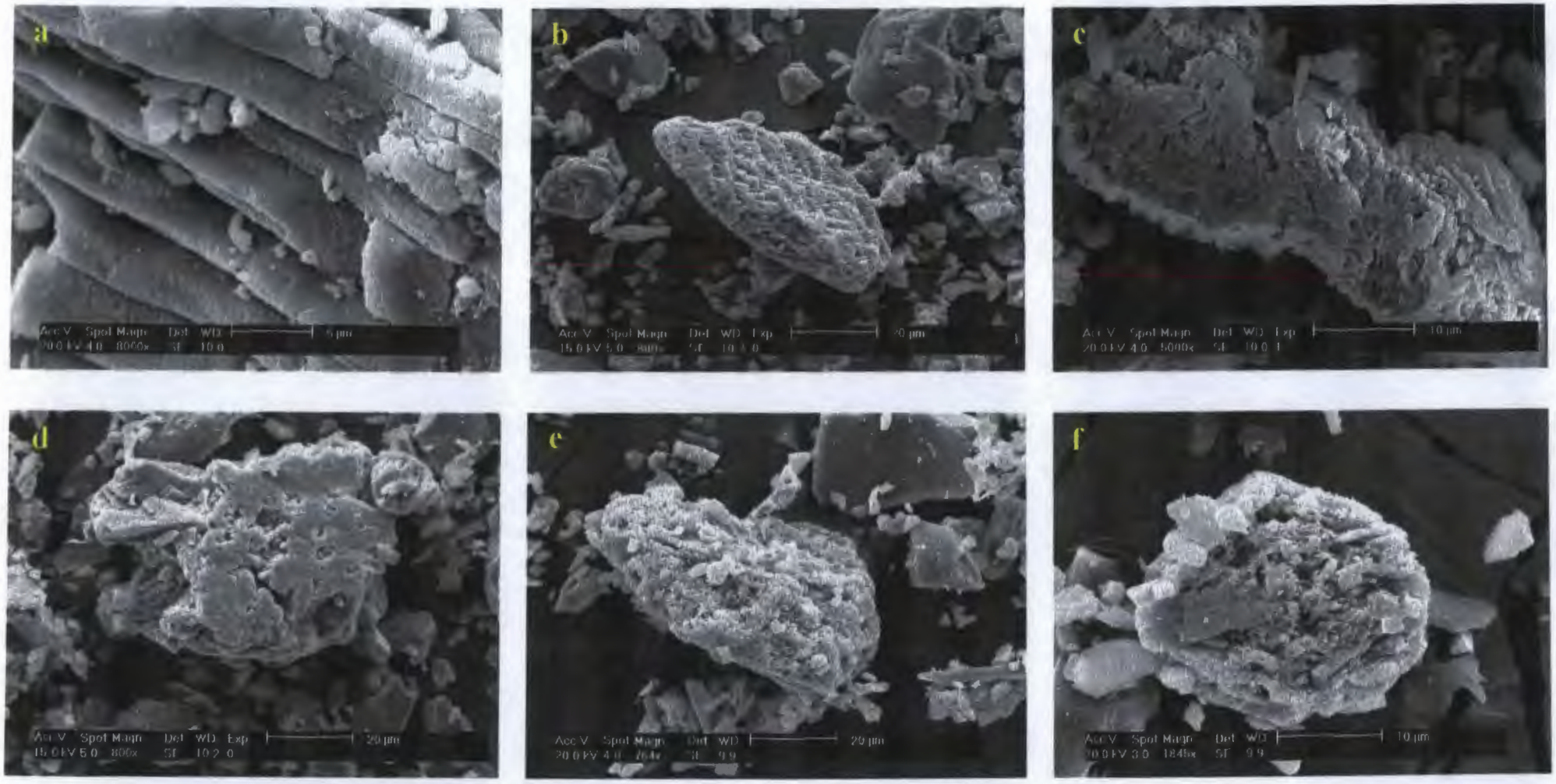

Figure 4.9 Scanning electron microscope secondary images of calcite grains. (a) Unidentified shell fragment showing a platey morphology. Fine pitting and cracking is also visible on most of the plates; borehole C1, 13 m amsl, Unit F. (b) A sub-rounded unidentified shell fragment; borehole I1, 37 m amsl, Unit D1. (c) Elongate grain showing irregular micro-cavities (secondary?); sample CA1, Unit D2. (d) Secondary grain showing two phases of carbonate growth (top left and centre); borehole I1, 37 m amsl, Unit D1. (e) Extremely weathered secondary grain exhibiting extensive dissolution; borehole I1, 31 m amsl, Unit D1 (f) Extremely weathered secondary grain with deep irregular solution micro-cavities; borehole I1, 19 m amsl, Unit D1.

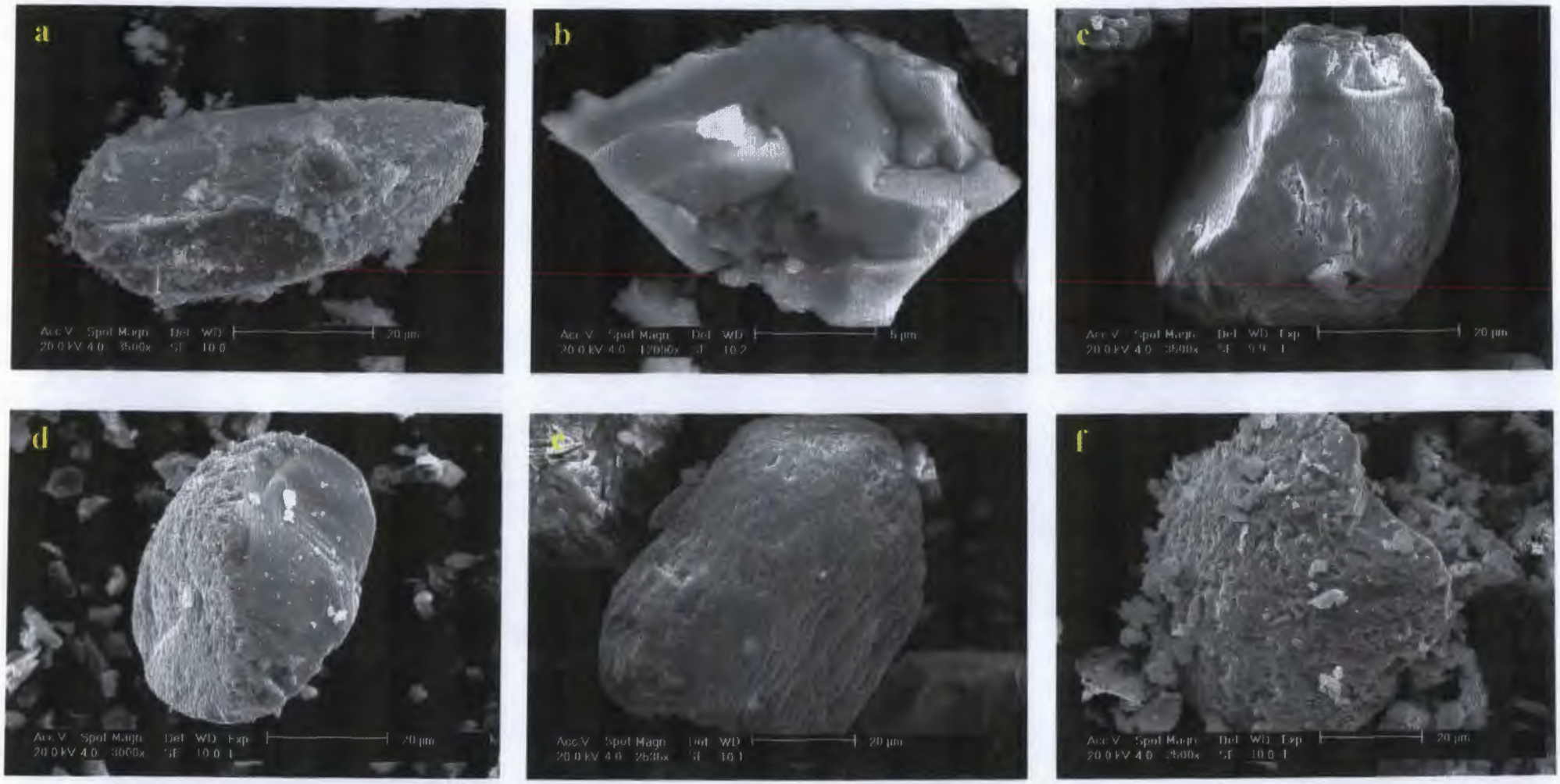

Figure 4.10 Scanning electron microscope secondary images of monazite grains. (a) Sub-rounded slightly weathered grain with silica precipitation (bottom centre) and upturned plates on the grain edges; borehole I3, 73 m amsl. Unit D2. (b) Slightly weathered, angular grain showing upturned plates (bottom) and grain cracking (top left); borehole I3, - 19.2 m amsl, Unit A0. (c) Moderately weathered sub-rounded grain showing enlargement of upturned plates by etching; borehole L1, 5 m amsl, Unit A2. (d) Moderately weathered, rounded grain showing extensive etching of upturned plates (left) together with a smooth surface exhibiting arc steps (right); borehole L2, 59 m amsl, Unit A4. (e) Highly weathered, rounded grain exhibiting extensive etching resulting in parallel aligned shallow solution channels; borehole I2, 21 m amsl, Unit D1 (f) Extremely weathered grain with deep irregular etch pits and micro-cavities; borehole L2, 53 m amsl, Unit A4.

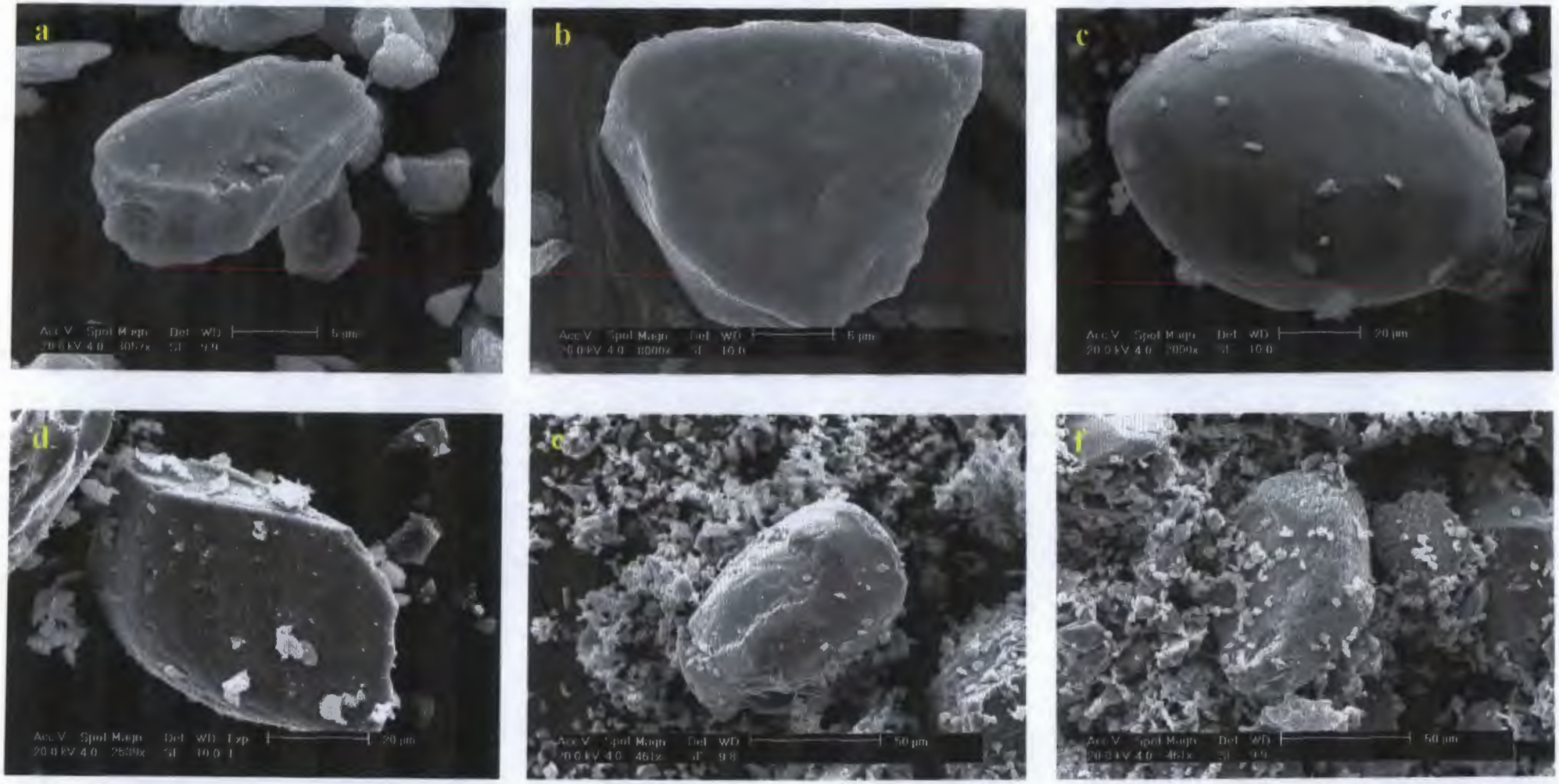

Figure 4.11 Scanning electron microscope secondary images of zircon grains. (a) Slightly weathered, euhedral zircon crystal with blocky fractures (centre) and etching along grain edges. Upturned plates are also visible (bottom centre); borehole I1, sample at 31 m, Unit D1. (b) Slightly weathered, angular grain showing upturned plates and a relatively low relief; borehole C1, - 28.5 m amsl, Unit A4. (c) A multifaceted grain showing rounding and slight weathering by means of shallow circular etch pits; borehole I2, - 1.7 m amsl, Unit A4. (d) Moderately weathered grain showing the rounding (right) of the otherwise euhedral crystal. Upturned plates are visible on all surfaces; borehole L2, 35 m amsl, Unit A2 (e) Highly weathered, rounded grain exhibiting fresh clean surfaces as well as upturned plates resulting in a onion-skin morphology (presumably due to zoning); borehole I1, 19 m amsl, Unit D1 (f) Highly weathered, rounded grain with extensive upturned plates on grain edges; borehole I1, 19 m amsl, Unit D1.

wind abrasion techniques.

4.2.1.11 Rare minerals and organics

Rare minerals included garnet, aluminosilicate, chromite, unidentified manganese oxides, fungal spores and mycelium (Figure 4.12). However, the isolated occurrences of these minerals/organisms does not indicate any systematic variation or distribution.

The only garnet? grain identified (Figure 4.12 a) is extremely weathered with deep solution etches and micro-cavities which penetrate the grain giving it a porous morphology. The unusually high amount of MnO (*ca.* 50 weight %) within the grain inconclusively identifies it as a garnet (maximum 43 weight % MnO). This grain maybe enriched in manganese due to a manganese-rich surface coating This grain could also be secondary with high concentrations of manganese.

A single smooth unweathered aluminium-silicate needle (Figure 4.12 b) was observed which has been tentatively identified as kyanite as it has been described in the sand-sized fraction by Fockema (1996) and Hugo (1990 & 1993). Goethite has adhered to the top left of what is likely to be a freshly liberated needle.

The chromite grain is extremely weathered resulting in a very high relief (Figure 4.12 c). Etching has probably preferentially removed iron resulting in a series of interconnecting irregular blades. This grain has probably been reworked as it is found at the very top of borehole I1 (Unit D1).

A few grains of unidentified manganese oxides (restricted to Unit A4) were noted and can be described as a globular cluster with radial plates (Figure 4.12 d). These grains could possibly be clays minerals such as a Mn-rich smectite (Smart & Tovey, 1981). However, smectite was not found in the clay fraction of these samples which may suggest it is a Mn-rich interstratified clay?

Fungal spores (species ?) were the most common of the rare "minerals" with six being observed (Figure 4.12 e) in various units and depths. They were generally highly spherical, smooth and *ca.* 5 μm in diameter. They are probably contamination from the atmosphere during the silt extraction procedure, however this needs to be confirmed.

An interesting find in the silt-fraction was that of a microbe (Figure 4.12 f). It was identified by it's organic composition, morphology and by the presence of FeO fixing to the fungal mycelium. It probably belongs

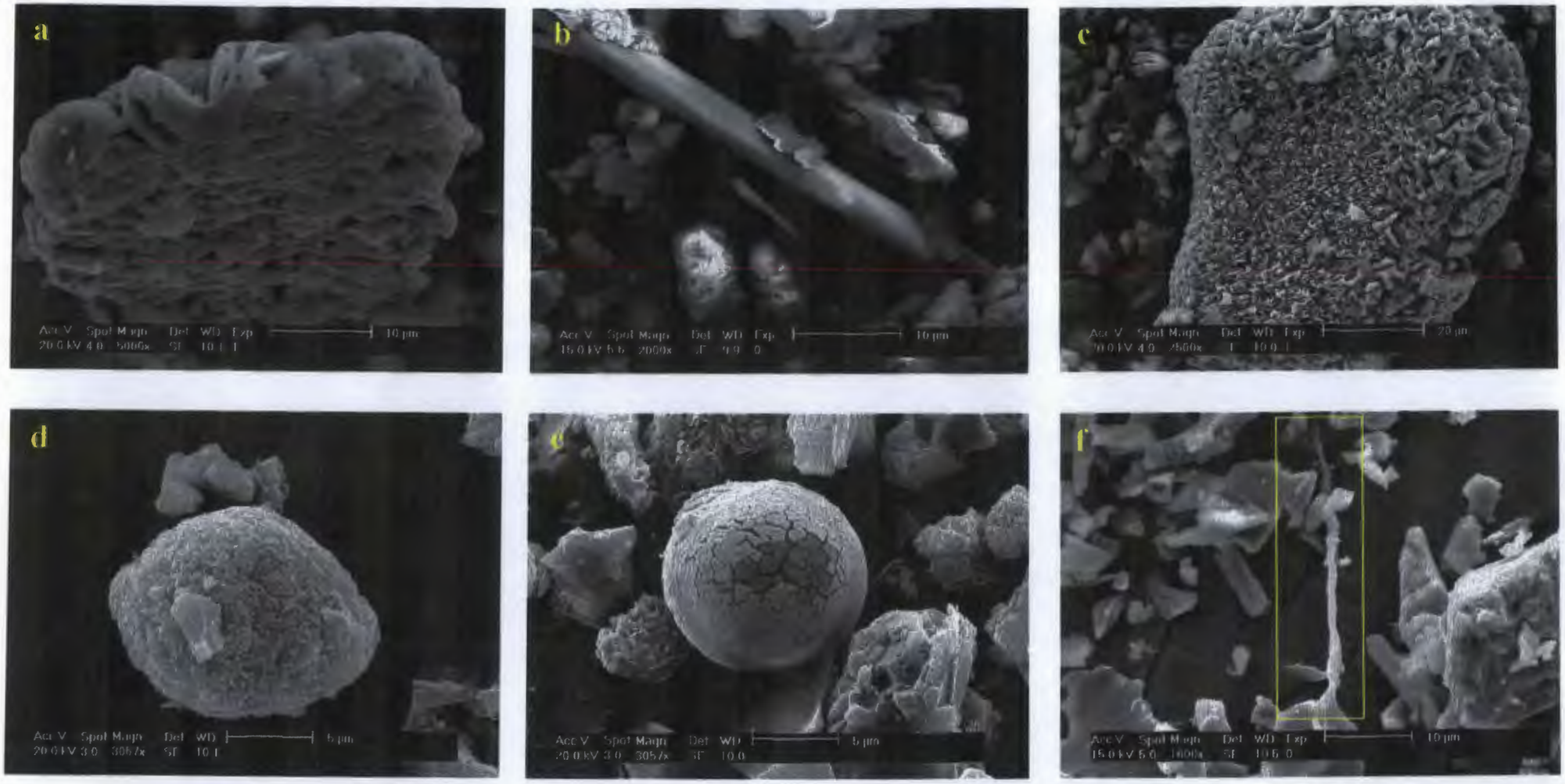

Figure 4.12 Scanning electron microscope secondary images of rare minerals and organics. (a) An extremely weathered garnet grain with deep solution etches and micro-cavities resulting in a porous morphology; sample D2, Unit A4. (b) A freshly liberated, smooth aluminasilicate needle with adhered goethite (top left); borehole L1, 11 m amsl, Unit A2. (c) Extremely weathered chromite grain with deep etching forming micro-cavities and interconnecting irregular blades; borehole I1, 37 m amsl, Unit D1. (d) Unidentified manganese oxide forming a globular cluster with radial plates. This mineral may be a Mn-rich clay (smectite/ interstratified?); borehole I1, 13 m amsl, Unit A4. (e) Fungal spore (species ?) showing rupturing caused by the X-ray beam during analysis; borehole I1, 7 m amsl, Unit A4 (f) Fungal mycelium (*Metallogenium*?); borehole I1, 37 m amsl, Unit D1.

to the budding bacteria *Metallogenium* which is part of the microbial iron cycle (Nealson, 1983). With the abundance of iron within the dunes it is probable that many different microbes species are present, each playing an unique role in mineral weathering. Although more examples need to be examined and positively identified it does lead the way to exciting research into how these microbes interact in grain degradation. The types, associations, and depths of existence of these microbes may be important if weathering is to be holistically understood.

4.2.2 IMAGE ANALYSIS

Although individual mineral types were unable to be separated, variations in broad mineral groups were obtained by measuring the area of grains (volume percent) in a silt grain mount containing dominantly "high" atomic elements (atomic number > 20) and those containing dominantly "low" atomic elements (atomic number < 20). Minerals dominated by high atomic elements (HAE) included metallic oxides, zircon, monazite, carbonates, pyriboles, whereas minerals dominated by low atomic elements (LAE) included quartz, feldspars and organics.

4.2.2.1 Method

No references have been found in the literature on the use of this unique "point counting" technique, so a detailed method is presented below (Figure 4.13):

- Samples were prepared as described in section 1.5.3.3 and viewed as backscattered images at a magnification of 119 x (image size: 560 × 740 μm or 484 × 712 pixels) so as not to exclude fine silt particles.
- HAE minerals appeared light grey becoming white with increasing atomic numbers whereas LAE appeared as mid- to dark greys (Figure 4.13 a).
- The grey-scale of the image was then inverted so that the resin in which the silt was impregnated was effectively removed from analysis (Figure 4.13 b). This also caused HAE to appear mid- to dark greys whereas the LAE appeared light grey.
- Although all attempts were made to keep the contrast and brightness of the images constant, variations were unavoidable due to SEM operating conditions. Thus thresholds were chosen visually (Figures 4.13 c & d) with the choice of the HAE/LAE mineral partition being aided by EDX analysis of individual grains. Not all of the images showed good contrasts as in Figure 4.13 and thus individual minerals groups could not be separated.

Figure 4.13 (over leaf) Example of the image analysis method used for "point counting" silt. The relative abundances (volume %) calculated using ImageJ computer software allowed discrimination of units. (a) A typical backscattered image obtained from the scanning electron microscope; accelerating voltage = 20 kV, spot size = 5.0, working distance = 10.0 cm. (b) The image's grey-scale is inverted making dark grains appear light and visa versa. (c) The threshold is chosen to extract minerals containing high atomic elements (HAE). (d) The threshold is chosen to extract minerals containing low atomic elements (LAE). (e) HAE minerals are extracted. (f) LAE minerals are extracted. (g) HAE particle's areas are calculated and summed with edge particles and those larger than 3500 pixels excluded (n=446). Grains are sequentially numbered as they are counted so that individual grain areas can be viewed.(h) LAE particle's areas are calculated and summed with edge particles and those larger than 3500 pixels excluded (n=1311). Typical mineral grey-scales are as follows: 1 = monazite/zircon, 2 & 3 = Fe-Ti oxides, 4 & 5 = carbonates, pyroxenes & amphiboles, 6 = quartz, feldspars and organics. HAE = 35vol %, LAE = 65 vol %.

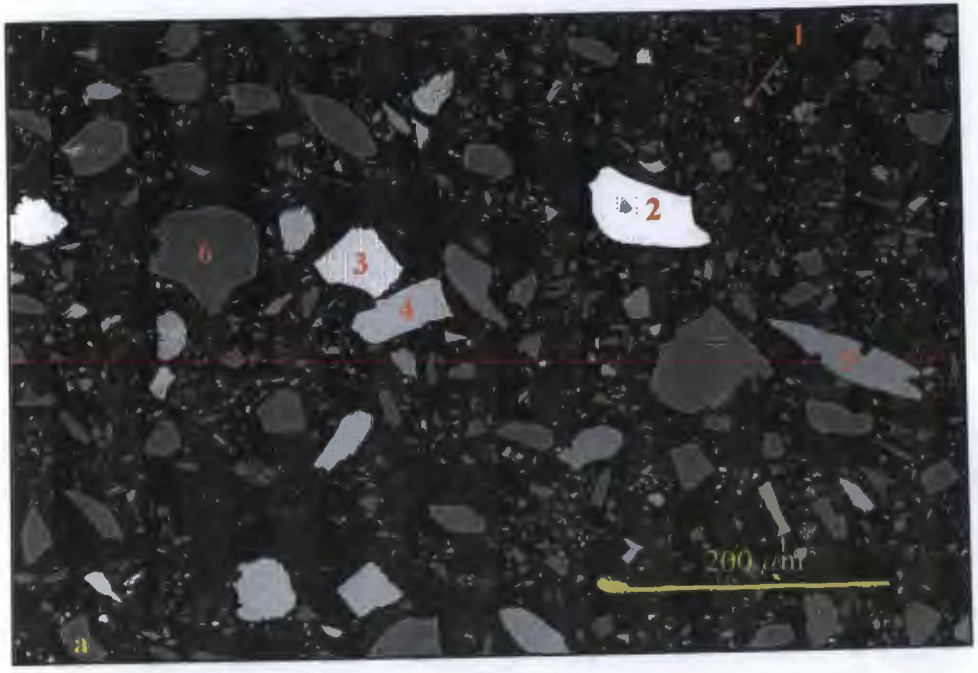
1
2
3
4
5
6
200 µm
a

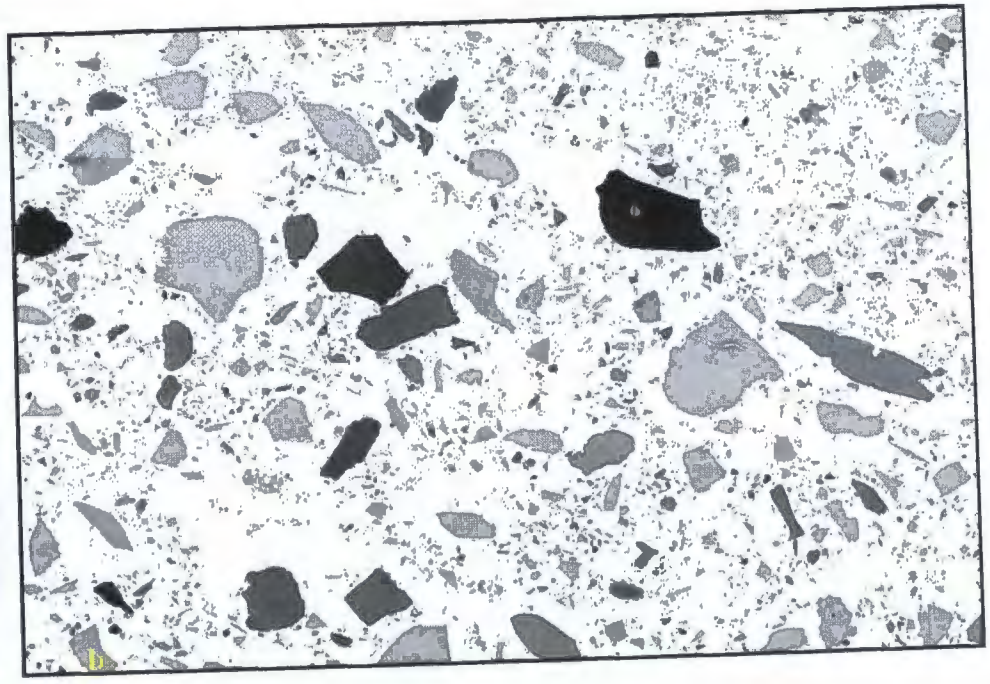
b

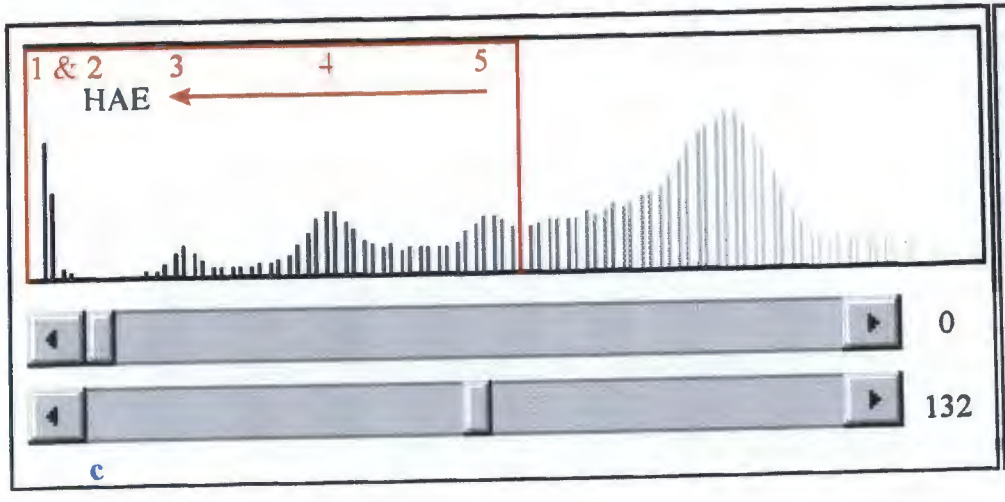
1 & 2
3
4
5
HAE
0
132
c

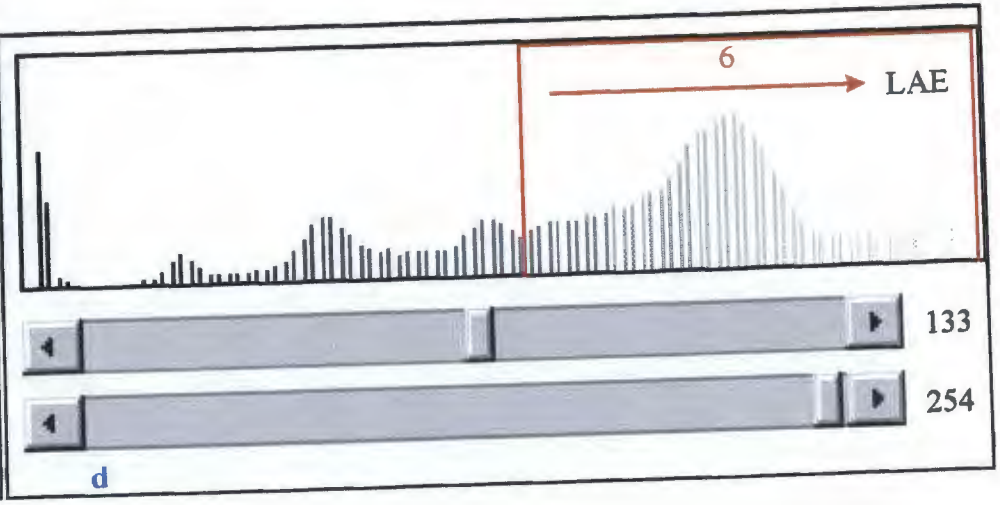
6
LAE
133
254
d

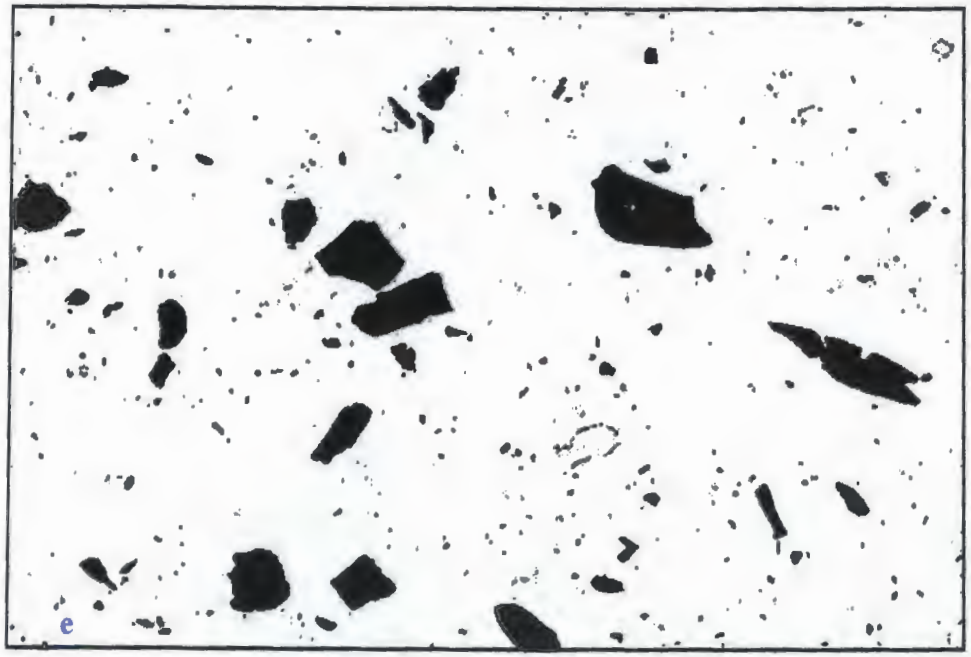
e

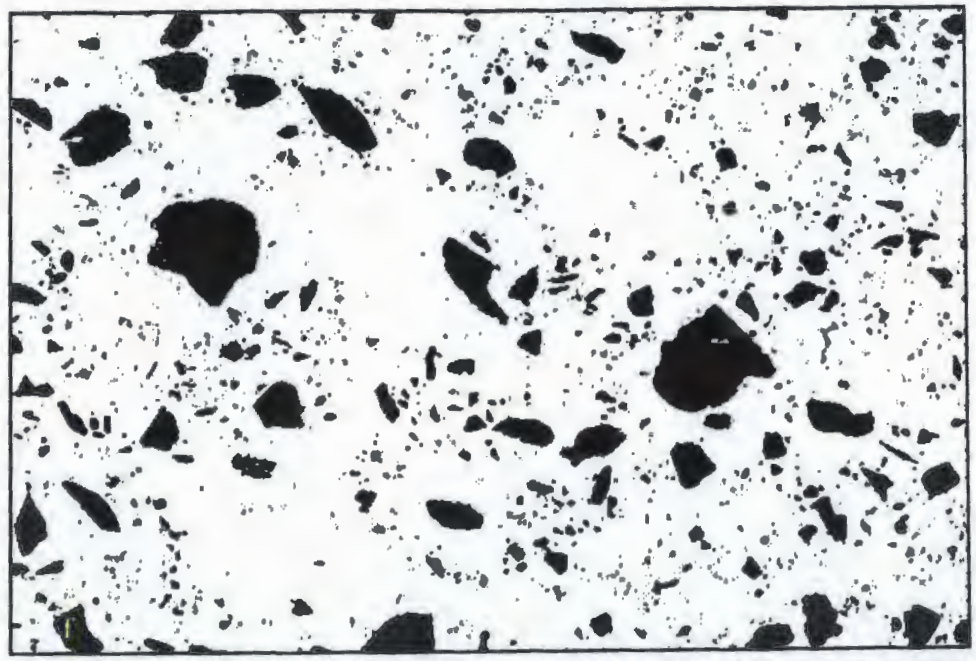

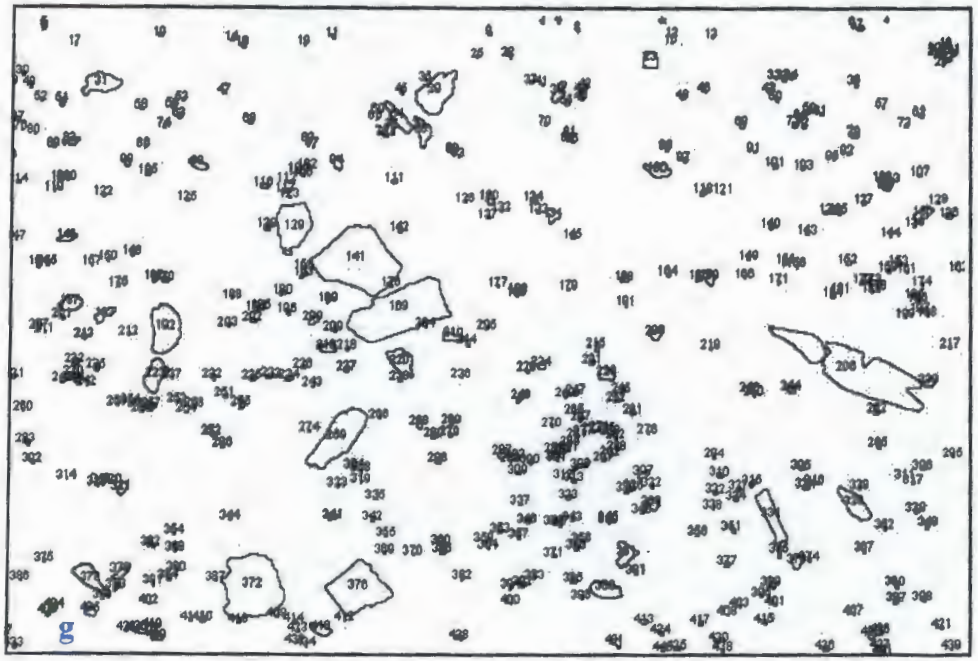
g

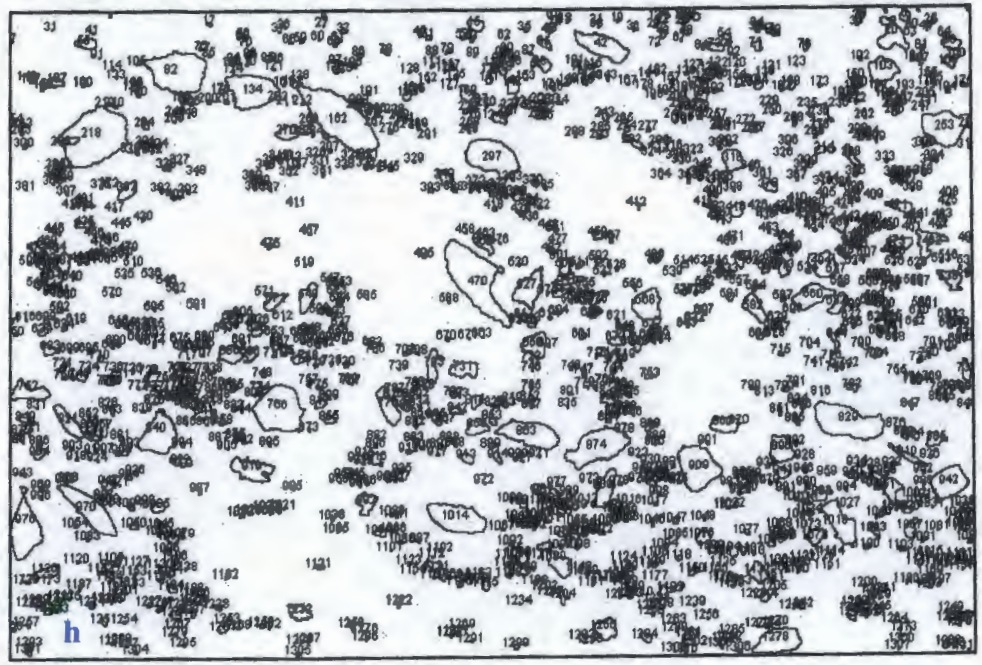
h

- Areas of the image corresponding to HAE minerals were separated from the LAE minerals (Figures 4.13 e & f). These images were then were "despeckled" to remove noise.
- Mineral areas were then calculated (volume percent) for the HAE and LAE mineral separates respectively with particles touching the edge of the image being excluded from the analysis. Particles greater than 3500 pixels (if present) were also excluded as these were generally contamination by fine sand-sized grains.
- Problems encountered not mentioned above included:
  (1) Some samples exhibited bright grain boundaries caused by polishing. These bright grain boundaries were therefore removed manually using the eraser tool.
  (2) Fine particle agglomerates occurred due to inadequate mixing of silt and liquid resin. These were manually excluded from the analysis using the eraser tool.
  (3) Particle segregation due to density settling was common. To avoid possible bias sections were cut perpendicular to the settling direction and 10 images per sample were analysed. Segregation was also minimised by adding 3 extra drops of hardener per 50 ml resin to decreased the setting time. However, if too much hardener was added the resin blocks cracked and could not be used.

4.2.2.2 Results

Image analysis results (Appendix D1) will be discussed in terms of volume percent HAE mineral abundances as LAE mineral abundances are relative to the latter. As a check on image analysis as a point counting technique, the silt-fraction of borehole I2 was also analysed using XRF for major element abundances (Appendix D2).

There is a strong positive correlation between the weight percent XRF metallic elements + zirconium versus the relative abundance (volume percent) of HAE minerals (Figure 4.14). There has been no attempt to mathematically relate weight percent oxides to volume percent minerals due to the diverse mineral suite present. Nevertheless, the HAE abundances are an overestimate compared to the weight percentage of equivalent minerals by a factor of approximately two. Deviations in HAE minerals from the positive relative trends compared to XRF results, as seen in samples at - 2 and 51 m amsl, could be due to a greater or lesser abundance of pyriboles respectively. The image analysis results are thus comparable showing similar trends to the results obtained from XRF major element analyses and hence is a useful tool for silt point counting. Similar HAE/XRF correlations are therefore expected for the other samples. Further XRF analyses on the silt-fraction is recommended if this technique is to be widely used.

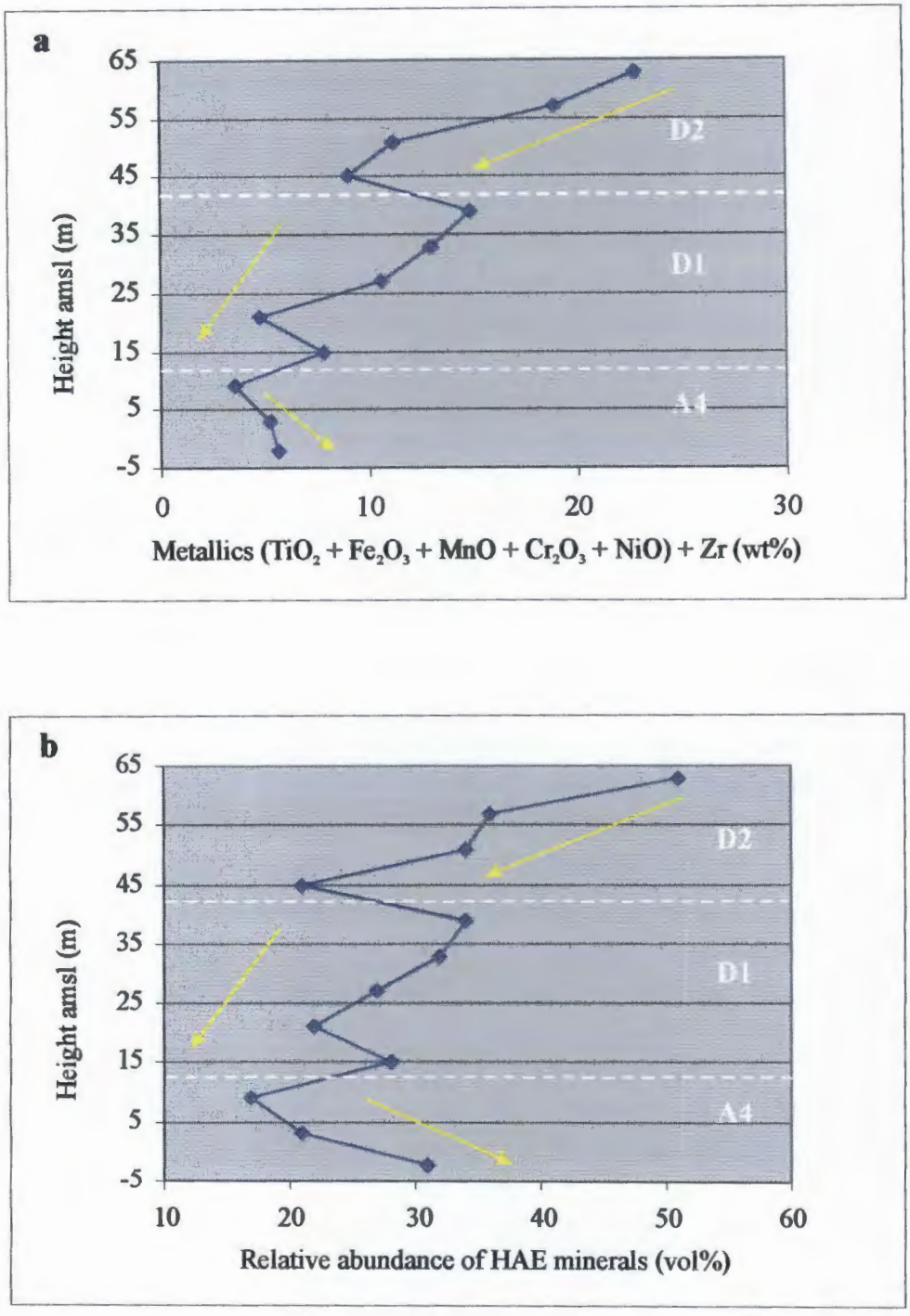

Figure 4.14 Comparison of XRF and image analysis of the silt-fraction; borehole I2 (a) XRF abundance of metallic elements + zirconium. (b) Image analysis results showing the relative abundance of minerals containing high atomic elements (HAE). Yellow arrows indicate general trends. White dashed lines and corresponding letter and numerical value delineate dune units according to the silt-fraction.

All boreholes show distinct alternating down hole increasing and decreasing trends in HAE mineral abundances. Sedimentological units have thus been separated by abrupt changes in these trends. These trends also correspond closely with clay variations, allowing some units to be redefined such as the addition of Unit A2 to further partition Unit A4 (boreholes L2 & I1) and Unit A0 to further partition Unit A2 (borehole I3; Figures 4.14 - 4.16). Image analysis data is tabulated in Appendix D1.

Borehole L1

Borehole L1 shows a slight decrease of HAE minerals from the top of the borehole to *ca.* 33 % at 35 m amsl, corresponding to Unit A4 (Figure 4.15). Thereafter a rapid increase is observed to *ca.* 48 % immediately followed by a steady decrease to *ca.* 21 % at 5 m amsl. This HAE mineral distribution corresponds to Unit A2. The HAE mineral abundance then stabilises at *ca.* 23 % corresponding to Unit K.

Borehole L2

Borehole L2 shows similar trends with a general decrease from *ca.* 35 % at the top of the borehole to *ca.* 22 % at 29 m amsl (Unit A4), punctuated only by a relative higher value of *ca.* 30 % at 35 m amsl (Figure 4.15). This reset in the decreasing trend has led to the further subdivision of this unit into Unit A2, at 38 m amsl. The relative abundance of HAE minerals then stabilises towards the bottom of the borehole at *ca.* 23 %, corresponding with Unit K.

Borehole I1

Borehole I1 shows a relative increase from the top of the borehole (*ca.* 37 %) to *ca.* 39 % at 19 m amsl, corresponding to Unit D1. A rapid relative increase follows (*ca.* 47 % at 13 m amsl), upon which a steady depletion to 35 % at 1 m amsl occurs (Figure 4.16). This depletion in HAE minerals corresponds to Unit A4. The basal sample shows a relative increase to *ca.* 39 % which may be a localised basal variation in Unit A4, but this is not conclusive.

Borehole I2

Borehole I2 contains *ca.* 51 % at the top of the borehole which rapidly decreases to *ca.* 21 % at 44 m amsl

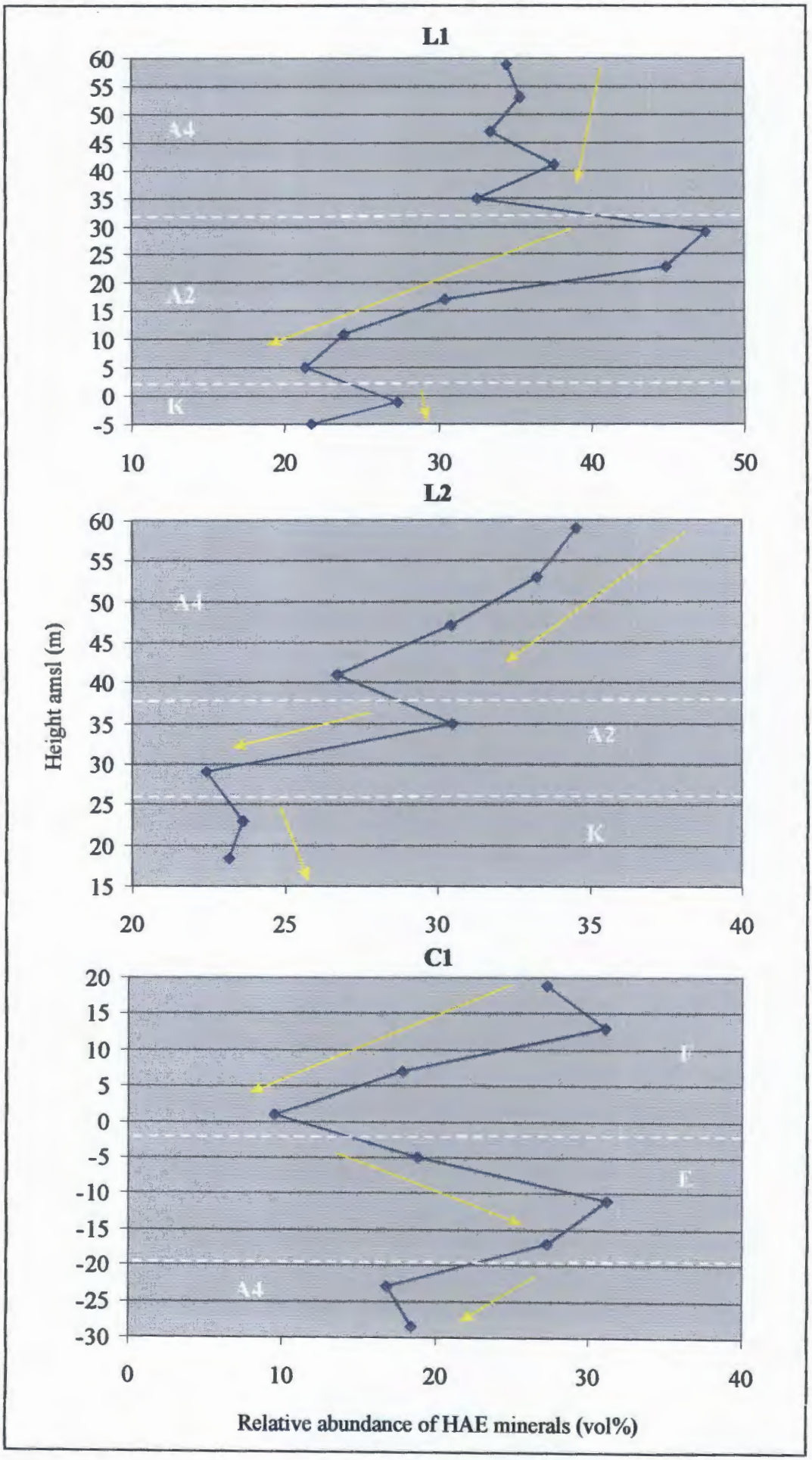

Figure 4.15 Down hole silt-fraction image analysis results showing the relative abundance of HAE minerals; boreholes L1, L2 and C1 respectively. Yellow arrows indicate general trends. White dashed lines and corresponding letter and numerical value delineates dune units according to the silt-fraction.

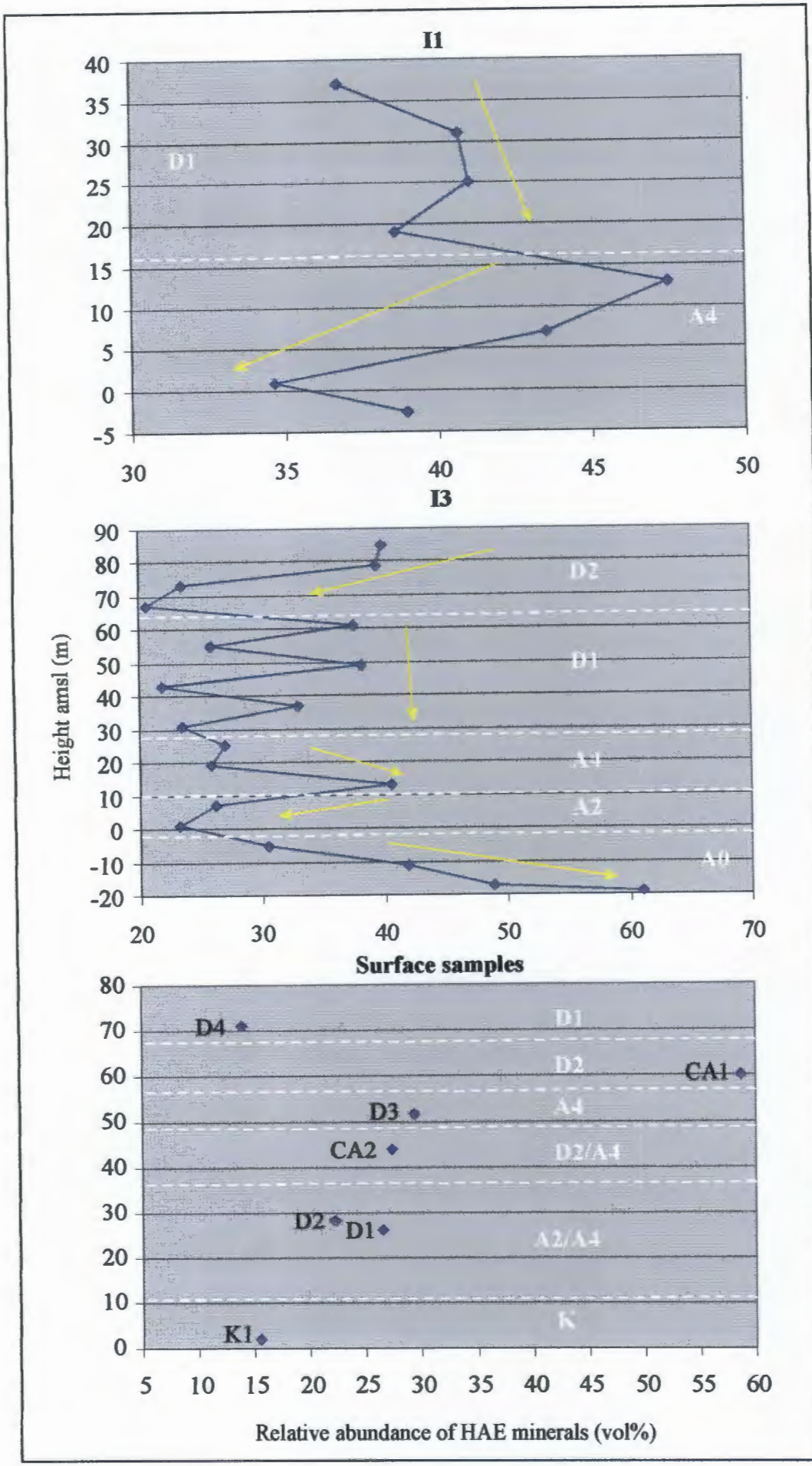

Figure 4.16 Down hole silt-fraction image analysis results showing the relative abundance of HAE minerals; boreholes I1 and I3 respectively as well as the surface samples. Yellow arrows indicate general trends. White dashed lines and corresponding letter and numerical value delineates dune units according to the silt-fraction.

(Unit D2), followed by a reset of the decreasing trend (*ca.* 34 %) at 39 m amsl upon which a further decrease to *ca.* 28 % at 15 m amsl occurs (Unit D1; Figure 4.16). A relative increase ensues to *ca.* 31 % at the bottom of the borehole (Unit A4).

Borehole I3

Borehole I3 contains *ca.* 40 % at the top of the borehole which decreases to *ca.* 21 % at 67 m amsl (Unit D2; Figure 4.14). Erratic relative increases and decrease follow (Unit D1) which stabilise at 31 m amsl (*ca.* 24 %). A relative increase follows to *ca.* 40 % at 13 m amsl, corresponding to Unit A4. This is followed by a decrease to *ca.* 23 % at 1 m amsl (Unit A2), after which a steady increase in abundance to the highest value observed at *ca.* 61 % at the base of the borehole. This steady increase in abundance has led to a further Unit A0 being defined.

Borehole C1

Borehole C1 contains *ca.* 27 % HAE minerals at the top of the borehole which increase to *ca.* 31 % at 13 m amsl, followed by a rapid decrease to 10 % at 1 m amsl (Unit F; Figure 4.15). A relative increase then observed to *ca.* 31 % at - 11 m amsl, followed by a slight decrease to *ca.* 27 % at - 17 m amsl. This overall increase defines Unit E. A slight increase in HAE minerals occurs to *ca.* 18 % at the bottom of the borehole, which can be attributed to Unit A4.

4.2.2.3 Stratigraphic units

Stratigraphic units have been preliminarily defined from the clay-fraction, however HAE mineral abundances allow further reinforcement as to the choice of units as follows:

- Unit K is confined to the base of the inland boreholes and is differentiated primarily by a very low HAE mineral abundance (*ca.* < 27 %). Sample K1 correlates well with Unit K, as in the clay-fraction, containing *ca.* 16 % HAE minerals (Figure 4.16).
- Unit A0 was not defined from the clay-fraction but is distinguished in the silt-fraction by a very rapid increase of HAE minerals from *ca.* 23 % to *ca.* 61 %. It forms the lowest most unit in borehole I3.
- Unit A2 overlies Unit A0 in borehole I3 and Unit K in boreholes L1 and L2. It is defined by a relatively high abundance of HAE minerals which show rapid decrease from *ca.* 40 % to *ca.* 20 % at its base. Samples D1, D2 and D4 show a fair correlation to this unit (Figure 4.16).

- Unit A4 overlies Unit A2 or Unit K. It is defined by a high to very high abundance of HAE minerals which generally show a steady decrease from *ca.* 45 % to *ca.* 25 % at the base of the unit. However borehole I3 shows a relative increase of HAE minerals towards the base of Unit A4. Units A2 and A4 are difficult to differentiate from one another using silt analyses. Samples D1 - D3 and CA2 show fair correlation to this unit (Figure 4.16).
- Unit D1 overlies Unit A4 and is restricted to the intermediate boreholes. It is defined by intermediate to high abundance of HAE minerals, showing variable down unit trends. Samples CA2, D3 and D4 correlate well with this unit, however samples D3 and D4 do not contain calcite in the clay-fraction and may correlate better with Unit A4 (Figure 4.16).
- Unit D2 overlies Unit D1 and is restricted to the intermediate boreholes I2 and I3 where it forms the uppermost unit. It is defined by a generally high to low abundance of HAE minerals which show a steady decrease from *ca.* 40 % to *ca.* 20 % at the base of the unit. Sample CA1 correlates well with this unit in the clay-fraction but is too enriched in HAE minerals to be confidently assigned to this unit on the basis of the silt-analysis (Figure 4.16).
- Unit E is restricted to the coastal borehole where it overlies Unit A4. It is defined by low to intermediate abundances of HAE minerals which show a steady increase from *ca.* 10 % to *ca.* 30 % at the base of the unit.
- Unit F is also restricted to the coastal borehole where it forms the uppermost unit. It is defined by the presence of intermediate to low abundances of HAE minerals. These show a relative decrease from *ca.* 30 % to *ca.* 10 % at the base of the unit.

4.3 DISCUSSION

As the surface area of silt is greater than the sand-sized counterparts, silt should be more sensitive to weathering. The weathering of minerals within the silt-fraction is characterised by the progressive increase of chemical grain weathering which ultimately masks all mechanical weathering features. The mechanical features provided useful information on the depositional environment of the silt. Upturned plates are typical of aeolian deposition whereas mechanical V's (base of Unit E) are associated with a littoral environment (Krinsley & Donahue, 1968; Nordstrom & Maragolis, 1972; Krinsley & Doornkamp, 1973; Lin *et al.*, 1974; Le Ribault, 1978; Kaldi *et al.*, 1978).

During chemical weathering by surface reactions, rather than by diffusion, feldspars and pyriboles dissolve and clays precipitate from solution (Berner & Holdren, 1979; Berner & Schott, 1982; Lee & Parsons, 1995). The rate of dissolution is consequently pH controlled (Nixon, 1979). Since the dunes are alkaline

(section 3.4) both aluminium and silica are slightly soluble (Allen, 1997) and together with a humid climate results in aluminium silicates weathering to form clays. Thus the older dune units contain greater abundances of clays and the silt grains show higher degrees of weathering.

The degree of weathering increases down hole and from the coastal to the inland boreholes. Silt-grains from Units F, E, D2 and D1 generally show slight to moderate degrees of weathering irrespective of which minerals are studied. Calcite grains were also only found within these units which correlates to calcite abundances within the clay-fraction.

Grains from Unit A4 showed a rapid increase in weathering with depth from moderate to high, indicating a relatively older age than the overlying units. The subsequent subdivision of Unit A4 within borehole L2, based on the image analysis results, into Unit A4 and Unit A2 is justified as Unit A2 grains show higher degrees of weathering than the overlying Unit A4. Similarly the separation of Unit A2 within borehole I3 into the basal Unit A0 was also justified as there was an increase in degrees of grain weathering from high to extreme. The presence of goethite "grains" also correlate well to high goethite abundances within the clay-fraction from these units, especially for Unit A0.

Mineral grains from Unit K showed extreme degrees of weathering independent of the mineral studied and is consequently expected to be the oldest unit present. "Ilmenite" was found only as altered ilmenite or leucoxene and quartz showed extreme dissolution. The absence of plagioclase and the presence of microcline also suggest a high degree of weathering.

A gradual down hole increase in weathering should result in an increase in the relative proportions of HAE minerals, if one assumes an initial dune containing homogenous units. Yet this was only observed in borehole I3. Borehole I2 shows a relative decrease in titanium and zirconium (XRF results, Appendix D2) which are generally considered immobile elements and thus should show a relative increase in abundance with weathering (assuming that there is significant mass loss due to dissolution and subsequent element translocation). These contrary results are perhaps due to either different source materials, depositional mineral sorting (climate related), and/or the result of reworking of the sediments. These factors could cause erratic abundances of these elements within the dunes. Also, these elements abundances are higher with respect to the bulk sample analyses (Section 5.1.3) which illustrates the natural abundance (preferential sorting) of zircon and Ti Fe oxides (magnetite, ilmenite etc.) in the silt-fraction. The abundance of silica is also diluted in the silt-fraction which indicates the preferential accumulation of minerals other than quartz.

The image analysis results proved useful in sedimentological unit identification whereas grain morphology provided greater constraint on the degree of weathering. Common minerals found in most samples such as quartz, feldspar, pyriboles and ilmenite were the most important minerals for determining weathering states and thus relative ages.

5 BULK SAMPLE

Comparison of the stratigraphy determined from the fine-fraction with that derived from bulk samples (Sudan, 1999) is not straightforward. Sudan (1999) used bulk samples subjected to aggressive RBM sample preparation techniques resulting in a loss of fines. As this would adversely effect bulk chemical compositions it was decided to run duplicate samples to determine more realistic bulk compositions and to investigate the magnitude of variation due to sample treatment.

The mineralogical composition of the bulk samples is dominated by quartz (60 - 90 %) with subordinate feldspar, amphibole (mainly hornblende), pyroxene (mainly augite), carbonate, ilmenite, leucoxene, rutile, magnetite, hematite, goethite, chromite, garnet (mainly pyrope, with some almandine), epidote, zircon, tourmaline, staurolite, kyanite, sphene, monazite, pyrite, apatite, glauconite, and various clays (Fockema, 1986; Hugo, 1990 & 1993; Singh & Dunlevey, 1997; Sudan, 1999). The total heavy minerals of these dunes are between 4 to 23 weight percent and contain fines between 4 to 25 weight percent (Fockema, 1986).

5.1 DOWN HOLE VARIATION

5.1.1 COLOUR

The most easily recognised variation within the coastal dune cordon is colour. Botha (1997b) recognised the problem of authors describing colours of the dunes differently and suggested standardising colour using the Munsell system. Colour is not only dependent on mineralogical composition of the dunes but also by the grain size. Clays are especially important in determining the overall colour due to their fine-nature and coatings they form around sand grains (Dunlevey, 1997; Singh & Dunlevey, 1997; Sudan, 1999). The colours, according to the Munsell system, are given in Appendix E1 and presented visually on the respective borehole logs (Appendix F).

In general, the top of the boreholes are dominated by browns (10 YR 3/2; 3/3; 3/4) which become more yellowish (10 YR 3/4; 4/4; 4/6; 5/6; 5/8) down hole, with olive browns and greys (2.5 YR 5/3; 6/6; 5 Y 6/2) found towards the bottom of the inland boreholes. Colours generally change value and chroma and occasionally hue when the abundance of fines is greater than 5 %. When the fine content is less than 5 %, dark browns (found at the top of many boreholes interpreted to be modern soil horizons rich in organics; section 3.4) and dark yellowish browns are normality. However, greater than 5 % fines result in variations

in colour according to goethite and kaolinite abundances within the clay-fraction as they coat the sand grains.

Yellow, red and strong brown hues are related to goethite (± hematite) abundances generally > 20 %. This corresponds to Schwertmann & Taylor's (1977) study where goethite was noted to be yellowish-brown (7.5 YR-10 YR), hematite being redder (5 R -2.5 YR) with the amorphous ferrihydrite being a reddish-brown (5 YR - 7.5 YR). The redness of hematite is independent of the water table (Walker, 1967). Olive and grey colours are attributed to kaolinite abundance > 40 %. Other clay minerals are not as important in determining the overall colour. Colour variation is thus dependent on the most abundant, strongly coloured fines/clay present (Figure 5.1).

5.1.1.1 Stratigraphic colour variation

Unit K is generally yellowish brown (10 YR 5/6) becoming light olive grey (5 Y 6/2) at the base. Unit A0 is characterised by a strong brown (7.5 YR 4/6) at the top of the unit becoming yellowish brown (10 YR 5/6), whereas Unit A2 is generally dark brown (10 YR 3/3) at the top becoming yellowish brown (10 YR 5/6) with depth. Unit A4 is generally a dark yellowish brown (10 YR 4/6) with borehole I1 showing reddening to the "Berea-type" red (Botha, 1997 b; 2.5 YR 4/6) towards the base. Unit D1 is generally dark brown (10 YR 3/3) at the top of the unit becoming dark yellowish brown (10 YR 3/4 or 4/4) with depth. Units D2, E and F are all a dark yellowish brown (10 YR 3/4 or 4/4).

Colour is not diagnostic in separating Units D, E and F whereas Units A (and subunits to a lesser extent) and K show distinct colours. Pye (1981) noted, from studying Holocene dunes from northeast Australia, that colour alone cannot be used as an adequate guide to age or morpho-stratigraphic correlation between different areas. Thus colour must be used with caution and may only be useful locally in differentiating dune units.

5.1.2 GRAIN SIZE PARAMETERS

Sedimentary environments (fluvial, beach and dunes) have been partially successfully differentiated by combinations of various grain textural parameters (Mason & Folk, 1958; Friedman, 1961 & 1979; Moiola & Weiser, 1968; Visser, 1969; Cooper, 1991; Wright, 1999; Sudan, 1999). However, Sudan (1999) noted that the presence of at least two distinct grain populations (light and heavy minerals, manifesting as bimodal grain distributions) and the mixture of different depositional beds in each sample (6 m sample intervals),

resulted in the reduction of environmental sensitivity. Textural parameters are consequently of limited use as a unit discrimination tool. The loss of fines by Sudan (1999) was greatly reduced in this study by less aggressive sample preparation techniques (Section 1.5.2). The removal of fines in Sudan's (1999) study may in fact provide more representative results when determining sedimentary environments from textural parameters, as 25 % of dune sand maybe fine material formed by post-depostional weathering (Chapters 3 & 4).

Previously defined stratigraphic units were subdivided not merely by the absolute textural parameters but by down hole compositional variations. Textural parameters were analysed using two methods. Samples were (1) wet-sieved to calculate the percentage of fines (< 63 μm) and (2) duplicate samples underwent particle size analysis for grain size distribution studies (Section 1.5.3.4).

5.1.2.1 Abundance of fines

All boreholes show an increase in the abundance of fines down hole (Figure 5.1), from *ca.* 2 % to *ca.* 20 %, except borehole C1 with a maximum of *ca.* 7 % fines occurs in the basal sample. Surface samples generally show < 1 % fines except samples K1 and Pond C which contain *ca.* 13 % and 99 % fines respectfully (Figure 5.1a). The extremely high fines of sample Pond C is due to the accumulation of clays settling from the wash over of mining Pond C (Figure 1.4). These high fines abundances are contrary to the study by Sudan (1999) in which greater than 1 % fines was rarely observed, even at the base of boreholes, indicating a significant loss of fines.

Units K, A0 and A2 generally contain > 5 % fines whereas Units D1, D2, E and F contain < 5 %. Unit A4 contains greater than > 5 % in boreholes C1, I1 and I2 whereas in boreholes L1, L2 and I3 it contains < 5 % fines. Stratigraphic dune units are thus not conclusively separated on the abundance of fines alone.

Experimental data revealed that wet sieving provided more accurate fines determination than light sourced diffraction methods (Section 5.1.2.2; Appendix E2). This is due to fines commonly being associated with grain coatings rather than discrete particles (Dunlevey, 1997; Singh & Dunlevey, 1997; Sudan, 1999).

5.1.2.2 Particle size analysis

Particle size analysis was studied using an incoherent light diffraction method (Section 1.5.3.4) with results presented in Appendix E2 with selected results presented graphically in Figures 5.2 to 5.4. Statistical

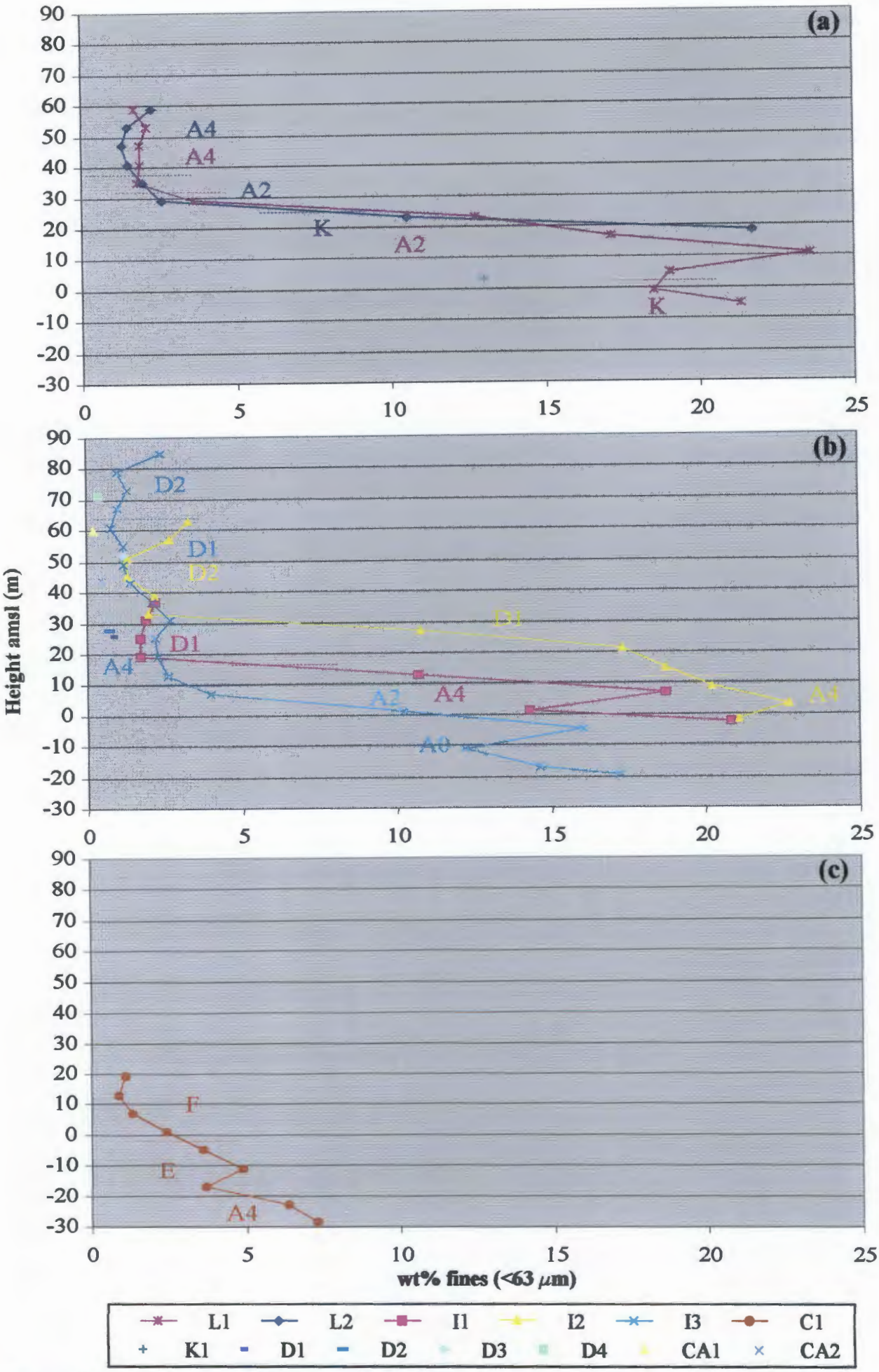

Figure 5.1 Down hole variation in percent fines obtained from wet-sieving for the; (a) Inland boreholes, (b) Intermediate boreholes, and (c) Coastal borehole. Stratigraphic units are shown with colours corresponding to boreholes.

textural parameters studied included mean grain size, sorting and skewness. These parameters provide numeric interpretations of the respective frequency distribution curves (Appendix H3).

Mean grain size

Variation in mean grain size depends on many factors, such as the transport medium and distance, the mean grain size of the source sediment, vegetation cover, heavy mineral abundances, and the degree of weathering. The majority of samples are well sorted medium-sands (200 - 375 μm) with an increase in fines down hole generally resulting in fine-sands (100 - 200 μm; Figure 5.2).

Borehole unit correlations

Borehole L1 can be divided into the upper Unit A4 which shows a fairly constant mean grain size of *ca.* 320 μm and Unit A2 which shows a steady decrease from 350 μm to 160 μm (average *ca.* 231 μm; Figure 5.2 a). The basal unit of borehole L1, Unit K is characterised by a mean grain size of *ca.* 225 μm.

Borehole L2 shows similar mean grain size trends with the upper Units A4 and A2 characterised by an average mean grain size of *ca.* 315 μm underlain by a comparatively finer Unit K (*ca.* 226 μm; Figure 5.2 a).

Borehole I1 can be subdivided by a relatively coarse upper Unit D1 (average *ca.* 338 μm) and a relatively finer lower Unit A4 which has an average mean grain size of *ca.* 170 μm (Figure 5.2 b).

Borehole I2 is characterised by the upper Unit D2 (average *ca.* 209 μm with a relatively coarse basal sample; 368 μm) underlain by the relatively coarser Unit D1 (average *ca.* 269 μm). The lower most Unit A4 shows a relatively finer average grain size (*ca.* 174 μm; Figure 5.2 b).

Borehole I3 is divided into the upper Units D2 and D1 which have average grain sizes of *ca.* 316 μm and *ca.* 313 μm respectively. Unit A4 shows a relatively coarse grained sediment (average *ca.* 353 μm) with underlying units becoming progressively finer grained with Unit A2 and basal Unit A0 containing an average grain size of *ca.* 330 μm and *ca.* 277 μm respectively (Figure 5.2 b).

Borehole C1 shows a relatively coarse upper Unit F (average *ca.* 369 μm) underlain by progressively finer Units E and A4 (average *ca.* 283 μm & 202 μm respectively; Figure 5.2 c). However, the basal sample of

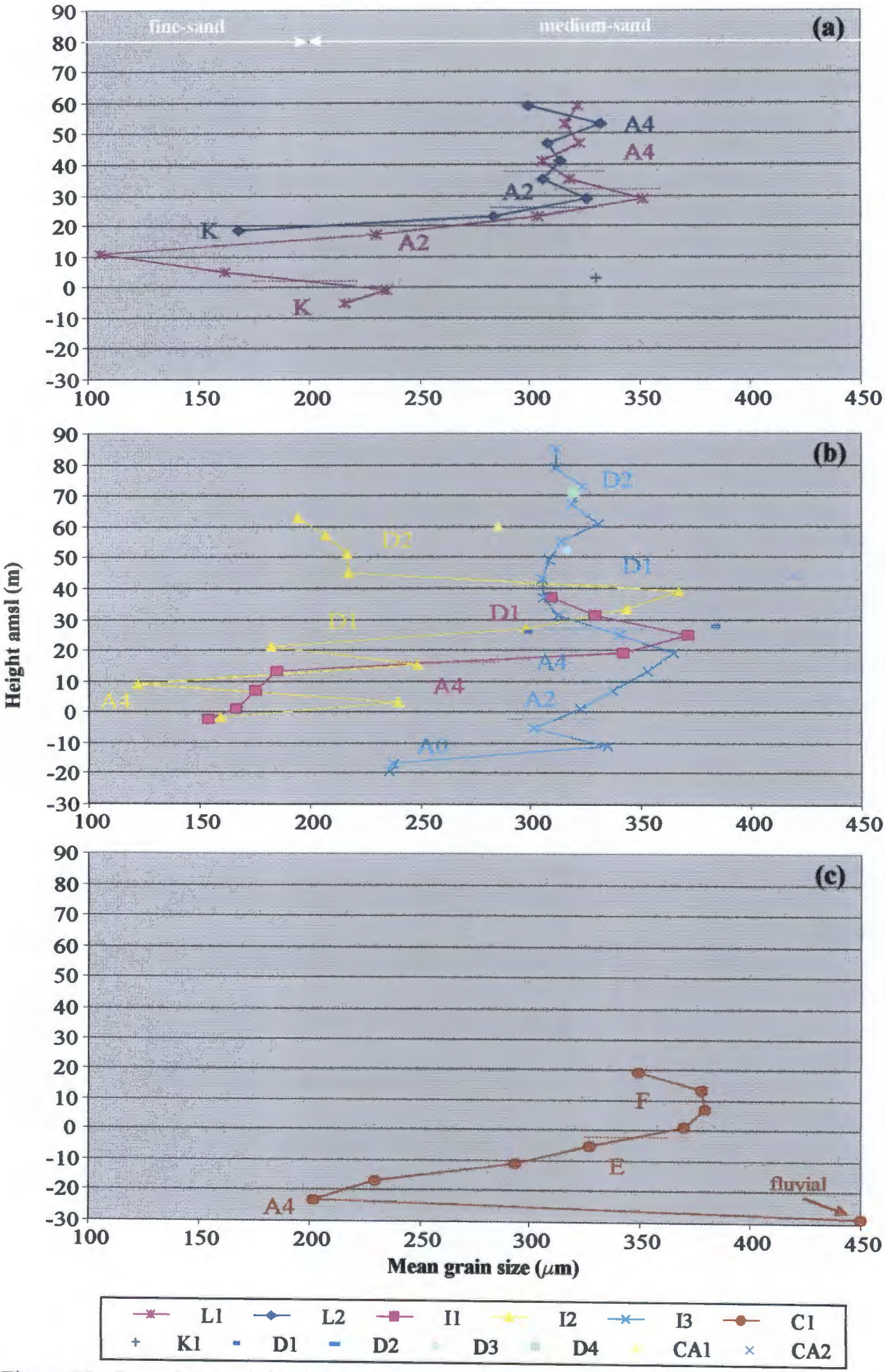

Figure 5.2 Down hole variation in mean grain size for the; (a) Inland boreholes, (b) Intermediate boreholes, and (c) Coastal borehole. Note the coarser nature of the basal sample of borehole C1, despite containing 7 % fines.

Unit A4, despite containing *ca.* 7 % fines, is relatively coarse with a mean grain size of 450 μm. Fine gravel (including lithic fragments; *ca.* 0.3 %) was also noted in this sample, suggesting a fluvial or beach origin.

Correlation of surface samples

Sample K1 has a mean grain size of 330 μm which is considerably coarser than the Unit K samples obtained from the inland boreholes (*ca.* 225 μm). This is probably the result of relatively fewer fines than similar samples from the inland boreholes. During excavation to sample K1 a white fines-rich fluid continuously drained from the cut face. This process is interpreted to be the cause of the relatively coarse nature of this sample. Samples D1 to D4 have similar grain sizes (*ca.* 320 μm) as Units A2, A4 or D1. CA1 has a similar mean grain size of the basal samples of Unit D2. CA2 has a relatively coarse mean grain size (420 μm), however carbonate concretions were observed during sample analysis. A finer mean grain size is consequently expected which can be correlated with previously defined Unit D2. Sample Pond C is a clay with an average grain size of 1 μm.

Sorting

Sorting is the sedimentological expression of the inclusive graphic standard deviation and provides information on the extent to which particle sizes are clustered about the mean (Folk & Ward, 1957). Most samples are described as well to moderately sorted. Samples with greater than *ca.* 15 % fines are poorly sorted and occasionally very poorly sorted (Folk & Ward, 1957; Figure 5.3).

Previously defined sedimentological units can be broadly separated by down hole variations in sorting. Unit K is characterised by moderately well sorted sands becoming poorly sorted towards the base of the unit. Unit A0 comprises moderately to poorly sorted sands. The overlying Unit A2 is moderately well sorted becoming moderately sorted with the sample at 11 m from borehole L1 being very poorly sorted. Unit A4 is characterised by the sands being well to moderately well sorted and occasionally moderately sorted (basal sample of borehole C1). Unit D1 is generally well sorted with borehole I2 showing moderately to poorly sorted sands towards the base of the unit. Unit D2 is characterised by well sorted and occasionally very well sorted sands. Borehole C1 is the only borehole to intersect Units E and F which contain moderately well sorted and well sorted sands respectively.

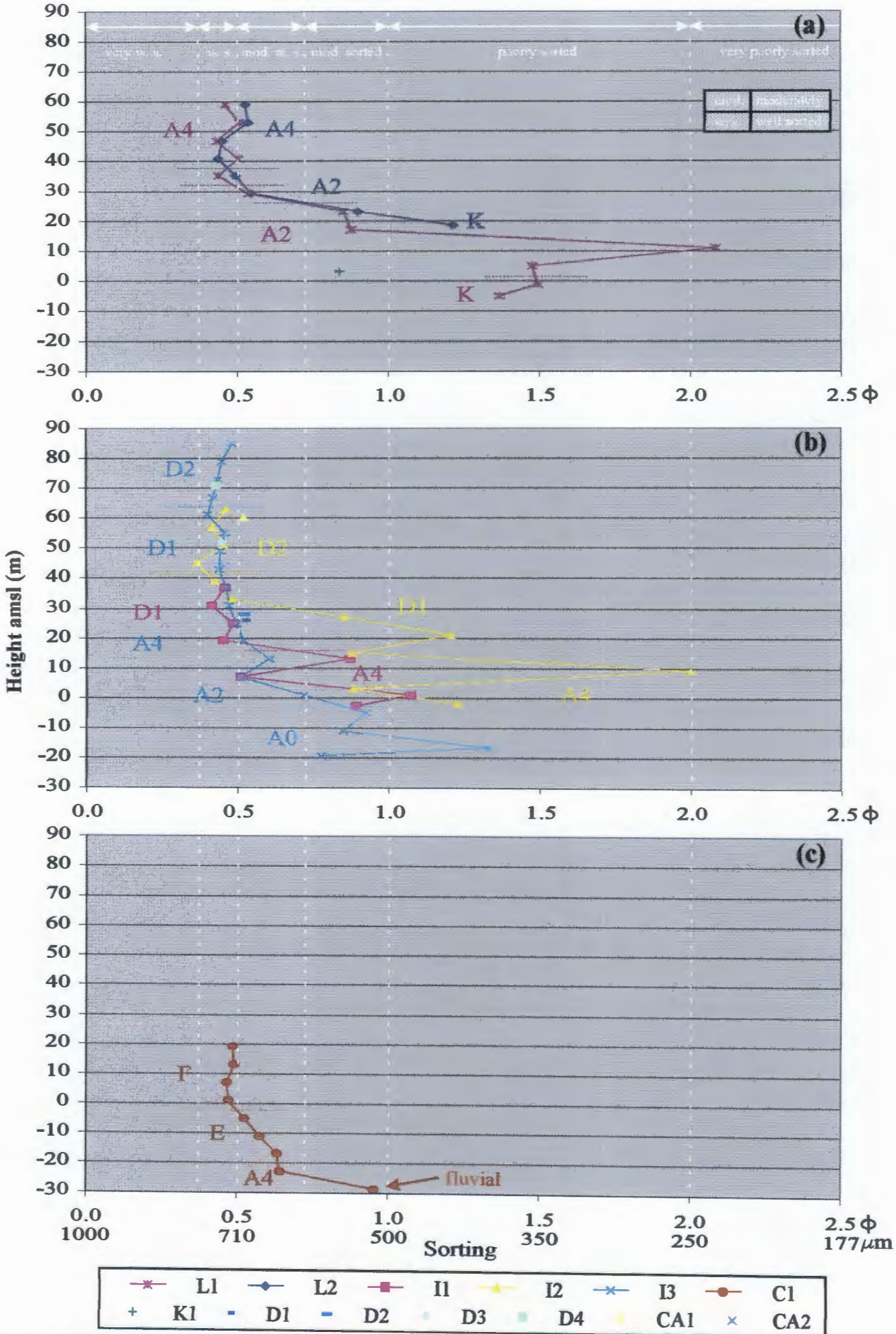

Figure 5.3 Down hole variation in grain sorting for the; (a) Inland boreholes, (b) Intermediate boreholes, and (c) Coastal borehole. Stratigraphic units are shown with colours corresponding to boreholes.

Skewness

Skewness is the measure of the coarse or fine bias of the grain-size distribution. Most samples have a positive value which indicate a "tail" of fines, typical of dune and fluvial sands (Friedman, 1961). Beach sands generally have a negative values of skewness because the fine grains are selectively winnowed by constant wave action (Friedman, 1961). Skewness increases down hole and can be described as near-symmetrical becoming strongly fine-skewed with increasing fines (Folk & Ward, 1957; Figure 5.4).

Unit K is characterised by fine-skewed to strongly fine-skewed sands, as are Units A0 and A2. Units A4 and D1 comprise near-symmetrical becoming fine-skewed and occasionally strongly fine-skewed towards the base of the unit. Unit D2 shows a near-symmetrical skewness in borehole I3 but is fine-skewed becoming near-symmetrical with depth in borehole I2, with the sample at 51 m having a negative skewness of - 0.02. Unit E is characterised by an increasing skewness becoming fine-skewed with depth, except the basal sample (- 17 m) which is near-symmetrical and has a negative skewness of - 0.01. The basal portions of this unit have been interpreted from the silt-fraction to be from a shallow marine to beach environment (Section 4.2.1.1). Unit F shows a progressive decrease in skewness from fine-skewed to being near-symmetrical towards the base of the unit.

According to all of the textural parameters the majority of sands are of typical aeolian origin. The relatively coarse basal sample of borehole C1 (Unit A4) is interpreted to be of fluvial origin. The base of Unit E (- 17 m) is interpreted to be a beach deposit which corresponds to Sudan's (1999) beach-foredune system. The sample at 51 m from borehole I3 is considered to be of aeolian origin and not a beach deposit (as the negative skewness suggests), as sea-levels have only been 5 m above the current level since the Mid-Pleistocene (Section 2.2.7) and consequently does not make stratigraphic sense.

5.1.3 GEOCHEMISTRY

Bulk geochemistry was used extensively by Sudan (1999) to characterise sedimentological units. Sudan (1999) showed that the element variations provided valuable information but were not diagnostic in subdividing units. More useful for dune stratigraphy was the use of chemical element ratios. Heavy mineral abundances also proved useful in separating more weathered units but these ratios are dependent on transport, grain density sorting and provenance. All samples (n = 75) were analysed for major element compositions (and zircon) of which boreholes I1, I2, L1, L2 and all surface samples (n = 47) were also analysed for trace element compositions (Appendix E3).

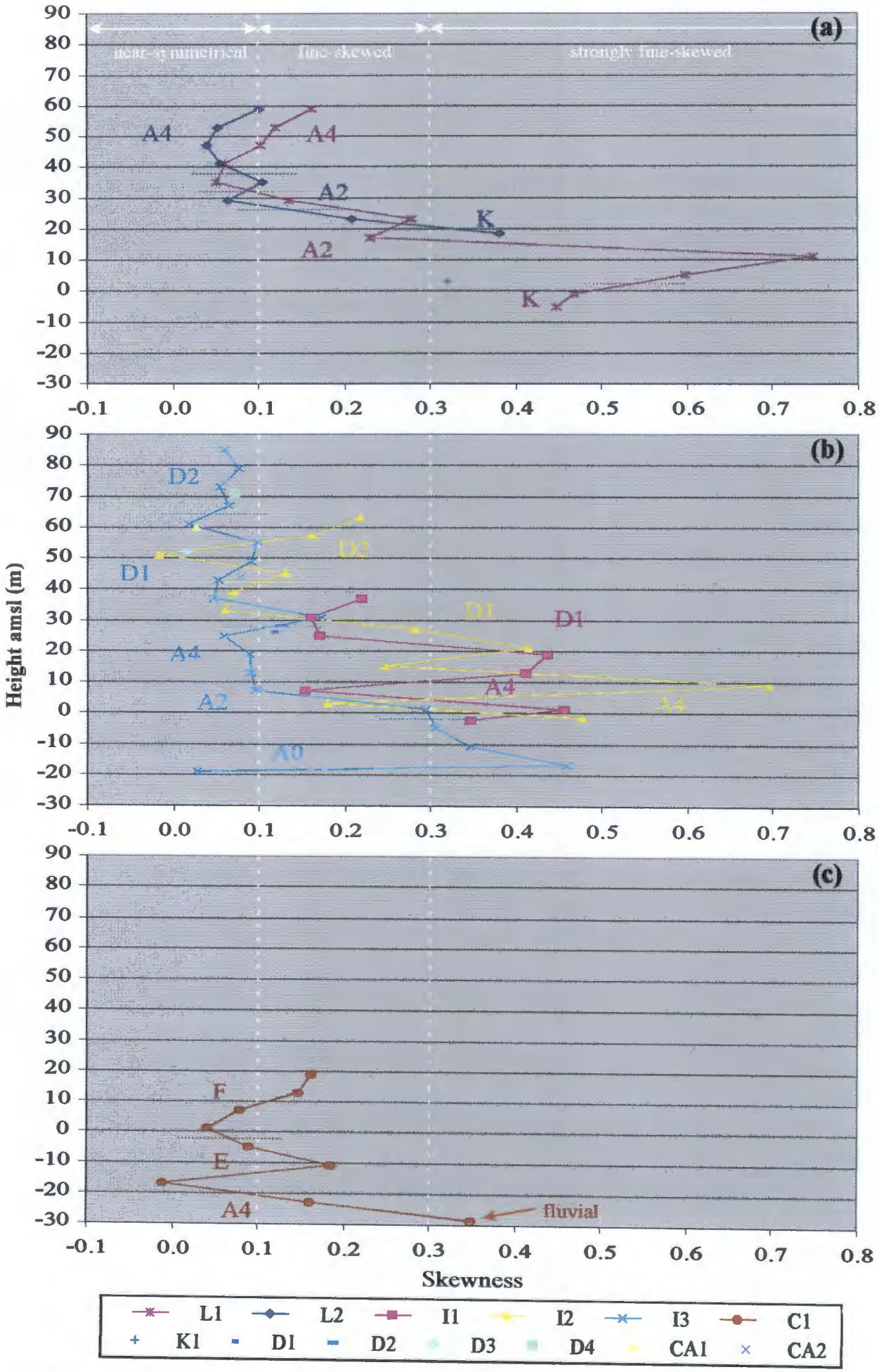

Figure 5.4 Down hole variation in grain skewness for the; (a) Inland boreholes, (b) Intermediate boreholes, and (c) Coastal borehole. Stratigraphic units are shown with colours corresponding to boreholes.

5.1.3.1 Major elements

Silica content varied between 64 to 95 weight percent, and shows an antipathetic variation with the other elements and has thus been excluded from the respective major element figures (Figures 5.5 & 5.6). There is a general increase in TiO_2, Fe_2O_3 and especially Al_2O_3 down hole which correlates to increasing fines and thus clay content. The abundance of Al_2O_3 is considerably higher (< 6.0 %) in the duplicate samples of Sudan (1999; Al_2O_3 rarely exceeding 3.0 %) which conforms to the loss of fines (and hence clays). This is especially true in those samples that are dominated by kaolinite in the clay-fraction. Only those elements that show distinctive trends will be discussed.

Borehole L1

Borehole L1 comprises the sequence of Units K, A2 and A4 respectively (Figure 5.5 a). Unit A4 is characterised by intermediate values (1.0 - 3.5 %) of Fe_2O_3, Al_2O_3, and TiO_2 which increase gradually down hole and significantly at the base of Unit A2. CaO values also increased gradually from 0.3 to 0.6 % towards the base of Unit A4. K_2O values remain relatively constant at *ca.* 0.5 % throughout Unit A4. The remaining major elements in Unit A4 have values generally less than 0.5 %.

Unit A2 is characterised by intermediate to high values of Fe_2O_3 and Al_2O_3 (1.5 - 5.8 %) which increase with depth. TiO_2 abundance varies erratically from 0.6 to 1.6 % with depth. CaO, Na_2O and MgO comprise less than 0.5 % and decrease towards the base of Unit A2. K_2O values are relatively high in the upper 12 m of this unit (0.8 % at 23 m amsl) but are subsequently lowered to 0.4 % at the base of the unit.

The basal Unit K is characterised by a relatively high abundance of Al_2O_3 (*ca.* 4.1 %) and intermediate values of Fe_2O_3 (*ca.* 2.0 %). TiO_2 shows a relative increase from 0.3 % to 2.0 % at the base of Unit K. K_2O also increases in abundance from 0.4 % to 0.7 % in the upper 6 m but is subsequently reduced to 0.6 % at the base of the unit. The remaining elements have relatively low abundances (< 0.2 %).

Borehole L2

Borehole L2 comprises a basal Unit K which is overlain by Units A2 and A4 respectively (Figure 5.5 b). Fe_2O_3 and TiO_2 show a strong positive correlation throughout the borehole. Unit A4 is characterised by a rapid decrease of Fe_2O_3 (4.2 to 2.3 %) and TiO_2 (3.1 to 1.5 %). Al_2O_3 shows a slight decrease from 2.0 to 1.7 %. The remaining elements exhibit relatively constant abundances within this unit and are generally less

than 0.5 %.

Unit A2 is characterised by an intermediate abundances of Fe_2O_3, TiO_2 and Al_2O_3 within the upper 6 m of this unit but shows a subsequent decrease at the base of the unit. The remaining elements (< 0.5 %) are slightly lower towards the base of the unit.

The basal Unit K is characterised by a rapid increase of Fe_2O_3 (2.0 to 3.9 %), TiO_2 (1.7 to 4.0 %) and Al_2O_3 (1.6 to 2.5 %) within the upper 6 m. Fe_2O_3 and TiO_2 are subsequently show a rapid decrease to less than 1 % at the base of the unit whereas Al_2O_3 shows a further increase to 6.1 %.

Borehole I1

Borehole I1 comprises Units A4 and D1 respectfully (Figure 5.5 c). Unit D1 is characterised by moderately high CaO abundances (*ca.* 3.4 %) at the top of the borehole, which is decreased to 0.3 % at the base of the unit. Fe_2O_3 and Al_2O_3 show very similar trends and abundances of *ca.* 2.0 %. They initially show a slight decrease in the upper 6 m of the borehole but subsequently increase towards the base of the unit. TiO_2 and K_2O show a progressive increase towards the base of the unit from 0.7 to 1.2 % and 0.5 to 0.6 % respectfully. MgO shows a rapid decrease from 0.8 to 0.1 % in the upper 6 m of the borehole, whereupon its abundance remains relatively constant throughout the remainder of the unit.

Unit A4 is characterised by a relative enrichment of Al_2O_3, Fe_2O_3 and TiO_2, except at the base of the unit where they are show a rapid decrease, except in the basal sample where a relative increase of Fe_2O_3 (2.6 %), TiO_2 (0.8 %) and Al_2O_3 (4.1 %) occurs. K_2O progressively increases towards the base of the unit from 0.6 to 1.2 % and consequently decreases to 0.9 %, whereas CaO progressively decreases from 0.3 to 0.1 %.

Borehole I2

Borehole I2 comprises a basal Unit A4, which is overlain by Units D1 and D2 respectfully (Figure 5.5 d). Unit D2 is characterised by very high CaO abundances which increases from 3.1 % at the top of the borehole to 6.6 % at 45 m amsl. It is subsequently rapidly decreased to 3.4 % at the base of the unit. Fe_2O_3, Al_2O_3, TiO_2, Na_2O and MgO are all progressively decreased in abundance towards the base of the unit and K_2O remains almost constant.

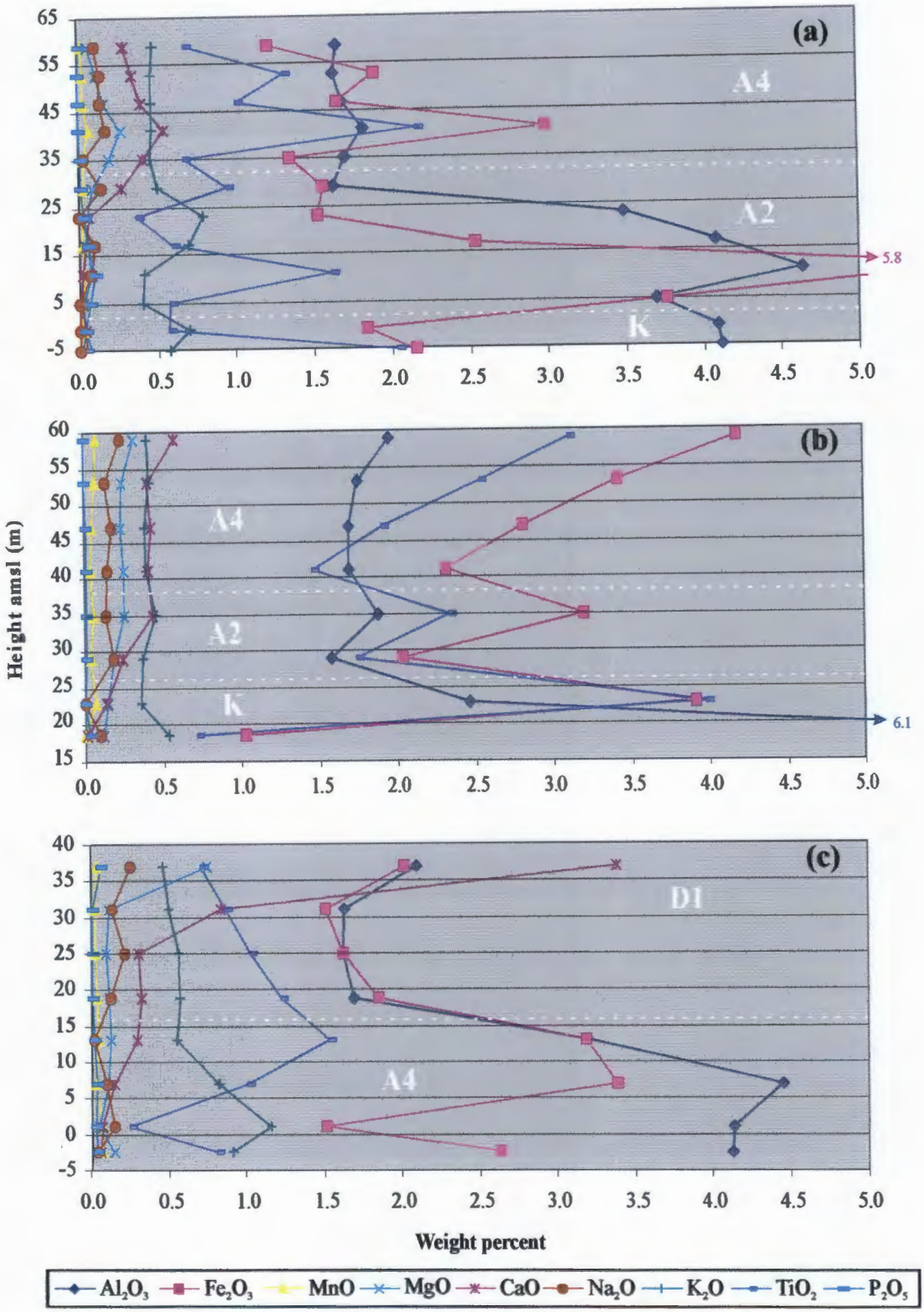

Figure 5.5 Major element abundances (excluding SiO_2) for; (a) Borehole L1, (b) Borehole L2 and (c) Borehole I1. White dashed lines and corresponding letter delineate units according to all analyses.

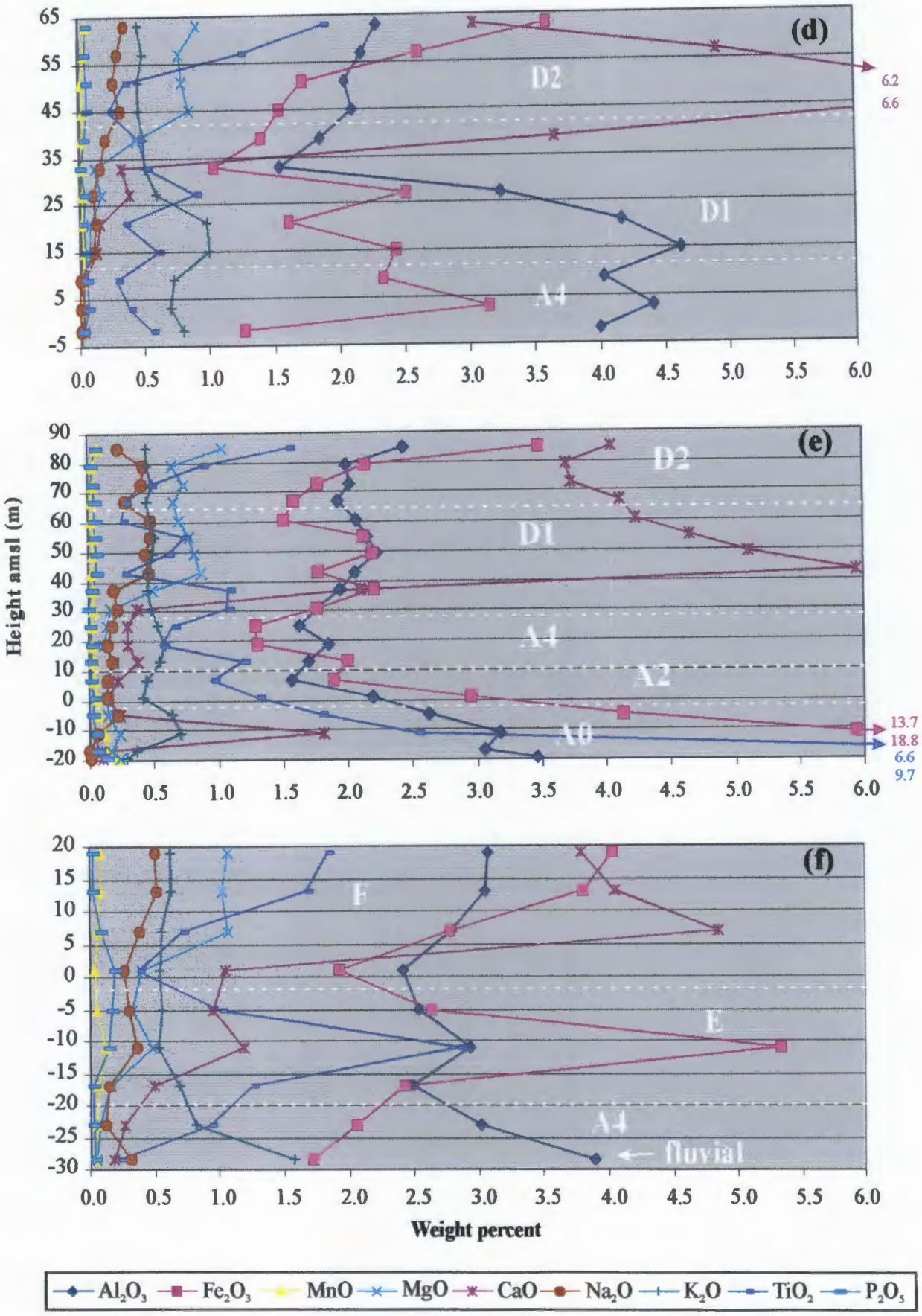

Figure 5.5 (continued) Major element abundances (excluding SiO_2) for; (d) Borehole I2, (e) Borehole I3 and (f) Borehole C1. White dashed lines and corresponding letter delineate units according to all analyses.

5.5 f). Unit F is characterised by a high CaO abundance which progressively increases from 3.8 % at the top of the borehole to 4.9 % at 7 m amsl. It is shows a rapid decrease to 1.0 % at the base of the Unit F. The other elements, except MgO and Na_2O, show an antipathetic relationship with CaO. MgO exhibits relatively high abundances and progressively decreases from 1.1 % at the top of the borehole to 0.4 % at the base of the unit. Similarly Na_2O decreases from 0.5 to 0.3 %. P_2O_5 shows a progressive increase in abundance from 0.03 to 0.19 % and corresponds to apatite within the clay-fraction.

Unit E is characterised by high abundances of Fe_2O_3 which shows a progressive increase from 1.9 % at the top of the unit to 5.3 % at -11 m amsl. It is subsequently shows a rapidly decrease to 2.4 % at the base of the unit. TiO_2 has a similar trend and increases from 0.4 to 2.8 % which is followed by a subsequent decrease to 1.2 % at the base of Unit E. Similarly the abundance of Al_2O_3 increases from 2.4 to 2.9 % and then decreases to 2.5 %. CaO and MgO show relative intermediate abundances of *ca.* 1 % and *ca.* 0.4 % respectively. The abundance of P_2O_5 shows a progressive decrease from 0.19 to 0.03 % towards the base of Unit E.

Unit A4 is characterised by intermediate abundances of Fe_2O_3, TiO_2 and Al_2O_3 with the latter showing a relative increases whereas the former two elements show a relative decrease down unit. K_2O shows a slight increase from 0.7 to 0.8 % whereas CaO shows a relative decrease from 0.5 to 0.3 % at the base of the unit. The basal fluvial sample (Unit A4) comprises a high abundance of Al_2O_3 (3.9 %) and an intermediate abundance of Fe_2O_3 (1.7 %). K_2O also shows a high abundance (1.6 %) whereas the other elements have a relatively low abundances (< 0.4 %).

Surface samples

Sample K1 contains a high abundance of Al_2O_3 (5.5 %) and a low Fe_2O_3 (0.6 %) abundance (Figure 5.6). This matches well with Unit K and supports their correlation. Sample D1 correlates well with Unit A2 due to its high Fe_2O_3 (5.6 %) and low CaO (0.9 %) abundance, whereas sample D2 correlates well with Unit A4 having intermediate abundances of Fe_2O_3 (3.4 %), Al_2O_3 (2.1 %) and TiO_2 (2.2 %) and a low abundance of CaO (0.6 %). Sample D3 shows a reasonable correlation to Unit A4, with intermediate values of Al_2O_3 (2.0 %), TiO_2 (1.5 %), Fe_2O_3 (2.3 %) however it is enriched with respect to CaO (1.9 %). Sample D4 correlates well with Unit D1 having an intermediate to high abundance of CaO (3.1 %) and intermediate abundances of Fe_2O_3 (3.0 %), Al_2O_3 (2.1 %) and MgO (0.6 %). Sample CA2 (Unit A4/D2?) contains intermediate abundances of CaO (4.7 %), Al_2O_3 (2.4 %), Fe_2O_3 (1.3 %) and K_2O (0.8 %) but a relatively low abundance of TiO_2 (0.2 %). Sample CA1 is relatively enriched with respect to CaO (4.8 %), Fe_2O_3 (8.3

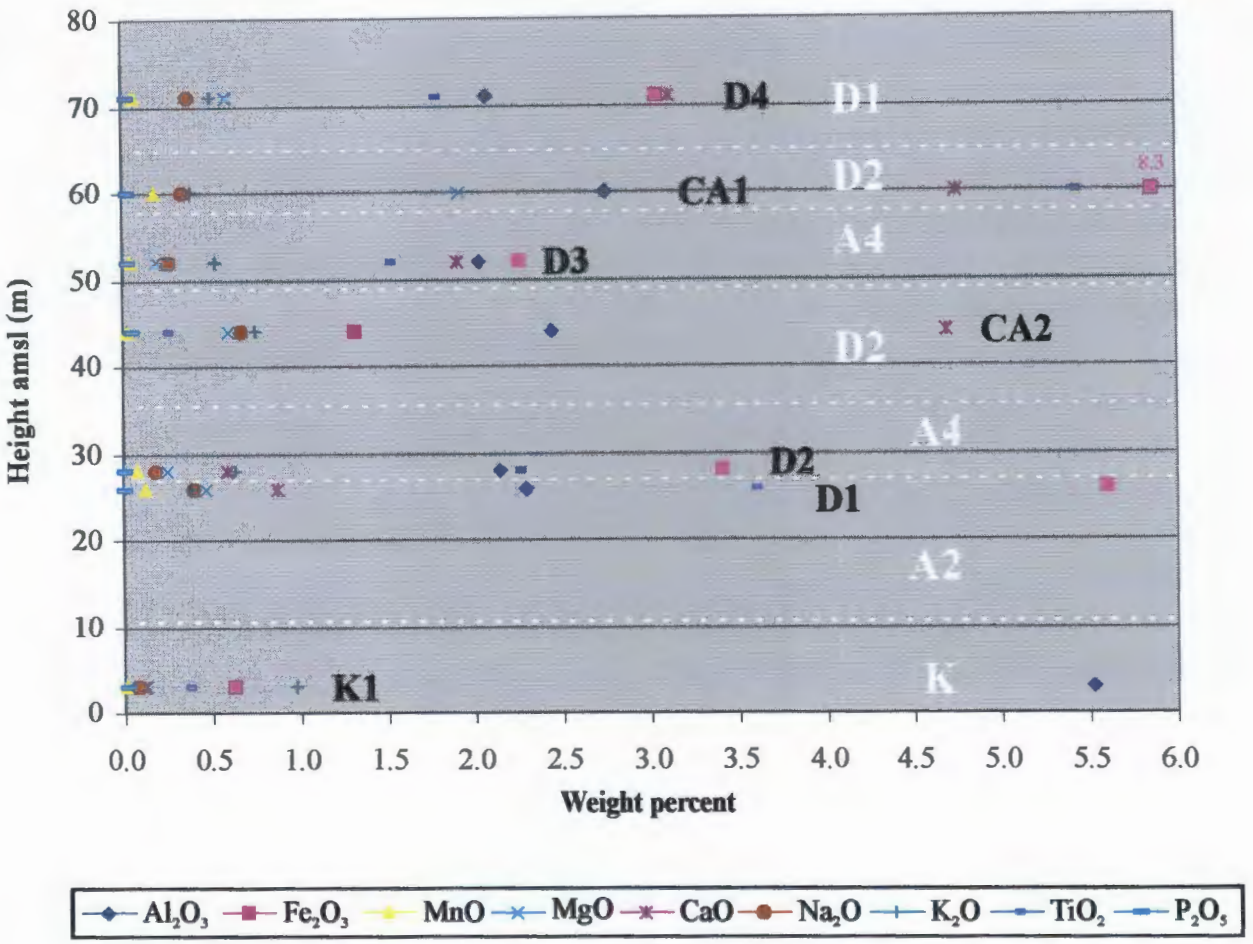

Figure 5.6 Major element abundances (excluding SiO_2) for the surface samples. White dashed lines and corresponding letter delineate units defined from grain size parameters and geochemistry. Black letters indicate sample number.

%), TiO_2 (5.4 %) and MgO (1.9 %) and correlates well with Unit D2.

5.1.3.2 Trace elements

Trace element abundances were not very useful in separating dune units with both immobile and mobile elements showing erratic distributions (Appendix E3). However, Zr is the most abundant trace element (155 to 11698 ppm) and down hole trends are useful in characterising (Figure 5.7). Zr abundances showed an almost linear relationship with TiO_2 suggesting hydraulic equivalence for zircon and ilmenite. Nb also has a similar linear relationship with TiO_2 as it is associated with ilmenite (Hugo, 1993). As Zr is the most useful stratigraphic indicator it is discussed below.

Unit K is characterised by a progressive decrease in Zr abundance towards the base of the unit. The top of Unit K has an intermediate Zr abundance of less than 3600 ppm. The base of the unit is generally lower in Zr (less than 650 ppm), except for borehole L1 in which one basal sample recorded 2048 ppm Zr.

Unit A0 is characterised by an intermediate Zr abundance which progressively increase from 1431 ppm to a very high abundance of 11698 ppm at base of the unit. The overlying Unit A2 is characterised in borehole I3 by a relatively constant intermediate abundance of *ca.* 1400 ppm. However in boreholes L1 and L2 by alternating intermediate (*ca.* 1200 ppm and 3053 ppm respectfully) and low abundances (*ca.* 500 and 450 ppm respectfully). Unit A4 is characterised by erratic Zr abundances which show decreasing trends towards the bottom of the unit in boreholes I1, L2, I3 and C1 but increasing abundace in boreholes L1 and I2. Zr abundances range from 177 ppm (borehole I2, sample at 9 m amsl) to 4656 ppm (borehole L2, sample at 59 m amsl). This erratic distribution is perhaps the result of reworking as suggested by the silt-fraction (Section 4)

Unit D1 is characterised by a progressive Zr abundance increase in borehole I1 from 598 to 1566 ppm at the base of the unit but a general low and erratic abundance in boreholes I2 (average 545 ppm) and I3 (average 457 ppm). The overlying Unit D2 is characterised by a progressive decrease of Zr with depth from intermediate abundances of *ca.* 2000 to low abundances of *ca.* 200 ppm. However sample CA1 has an anonymously very high Zr abundance of 7309 ppm.

Units E and F are only found in borehole C1 where they overly Unit A4. Unit E is characterised by progressive Zr abundance increase from 1360 ppm at the top of the unit to 3845 ppm towards the base. The overlying Unit F is characterised by progressive Zr abundance decrease from 2498 ppm at the top of the

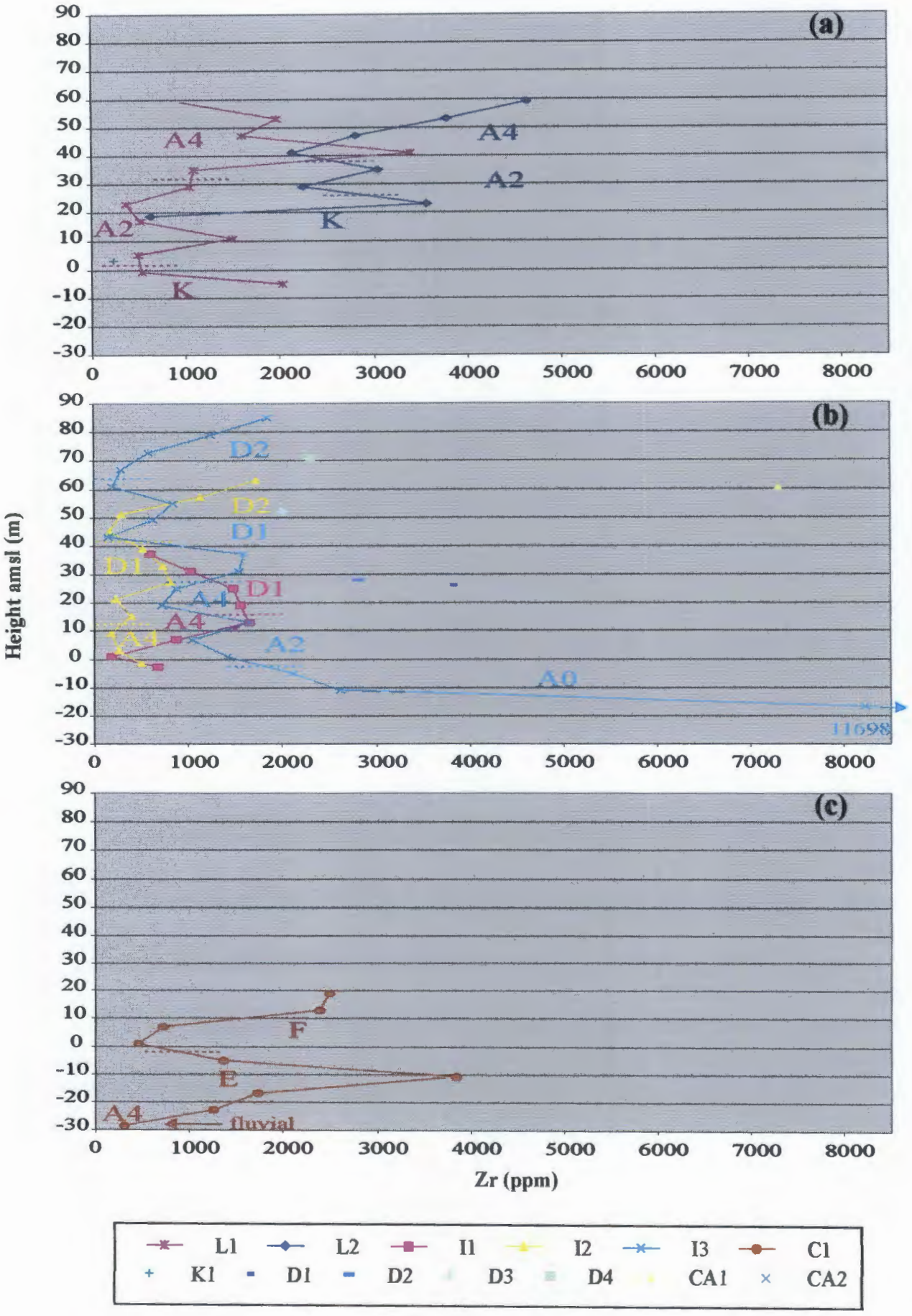

Figure 5.7 Down hole variations in Zr for; (a) Inland, (b) Intermediate, and (c) Coastal boreholes. The abundance of Zr in surface samples are shown as point data.

borehole to 460 ppm at the base of the unit.

5.1.3.3 $CaCO_3$

Acid digestion of $CaCO_3$ was used as a simple test to separate CaO abundances within silicates and more soluble carbonates (Figure 5.8; Appendix E3). Generally CaO abundances (determined by XRF) greater than 1 % corresponded to the presence of calcite within the sand- and clay-fraction. This test proved very successful in separating the less weathered calcified Units F, E, D2 and D1 from decalcified Units A4, A2, A0 and K.

Unit E contains very low carbonate abundances of *ca.* 0.5 % which has similar abundances as the basal portion of Unit D1. Unit D1 has a successive down unit decrease in carbonate from *ca.* 5.0 to 0.1 % however borehole I3 is enriched at 43 m amsl at 7.1 %. Units D2 and F have the highest $CaCO_3$ abundance of between 3.0 and 9.1 %.

5.1.3.4 Chemical element ratios

The samples analysed are from dune units which represents an open system due to high permeability and frequent precipitation. This results in both weathering of whole mineral grains and mobilization of select elements from minerals. The more mobile elements are either relocated within the dune profile or are removed from the dune system altogether.

TiO_2 / MgO

Titanium is generally contained within the minerals ilmenite, leucoxene, sphene and rutile within the ZNL and is considered to be immobile during weathering (Minarik *et al.*, 1983; Hugo, 1993). In contrast to this MgO is labile as its pryribole hosts are thus further susceptible to weathering (Henderson, 1982). The ratio of TiO_2 to MgO is thus a proxy for weathering with larger values indicating higher degrees of alteration or weathering. However the original concentrations of these two elements is dependent on sediment supply, climate, transport medium and transport distance. Using the TiO_2 / MgO ratio as a proxy of weathering must therefore be undertaken with caution as it assumes a homogeneous sediment supply.

There is a general increase in the TiO_2 / MgO ratio down hole and from the coastal to the inland boreholes (Figure 5.9). Units K, A0 and A2 have significantly higher TiO_2 / MgO ratio values than the other units

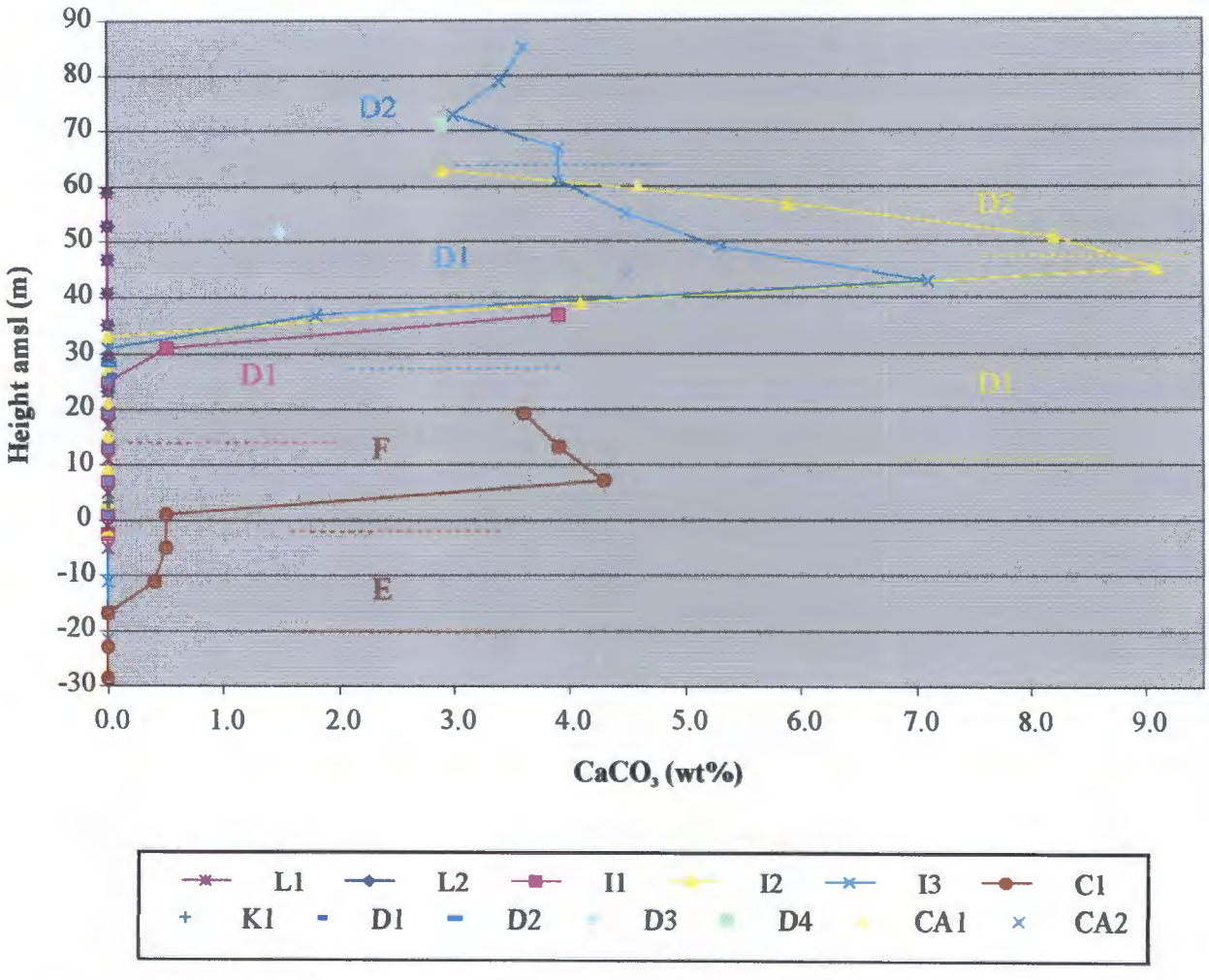

Figure 5.8 Down hole variation in the percent carbonate for all samples as determined by the carbonate bomb test.

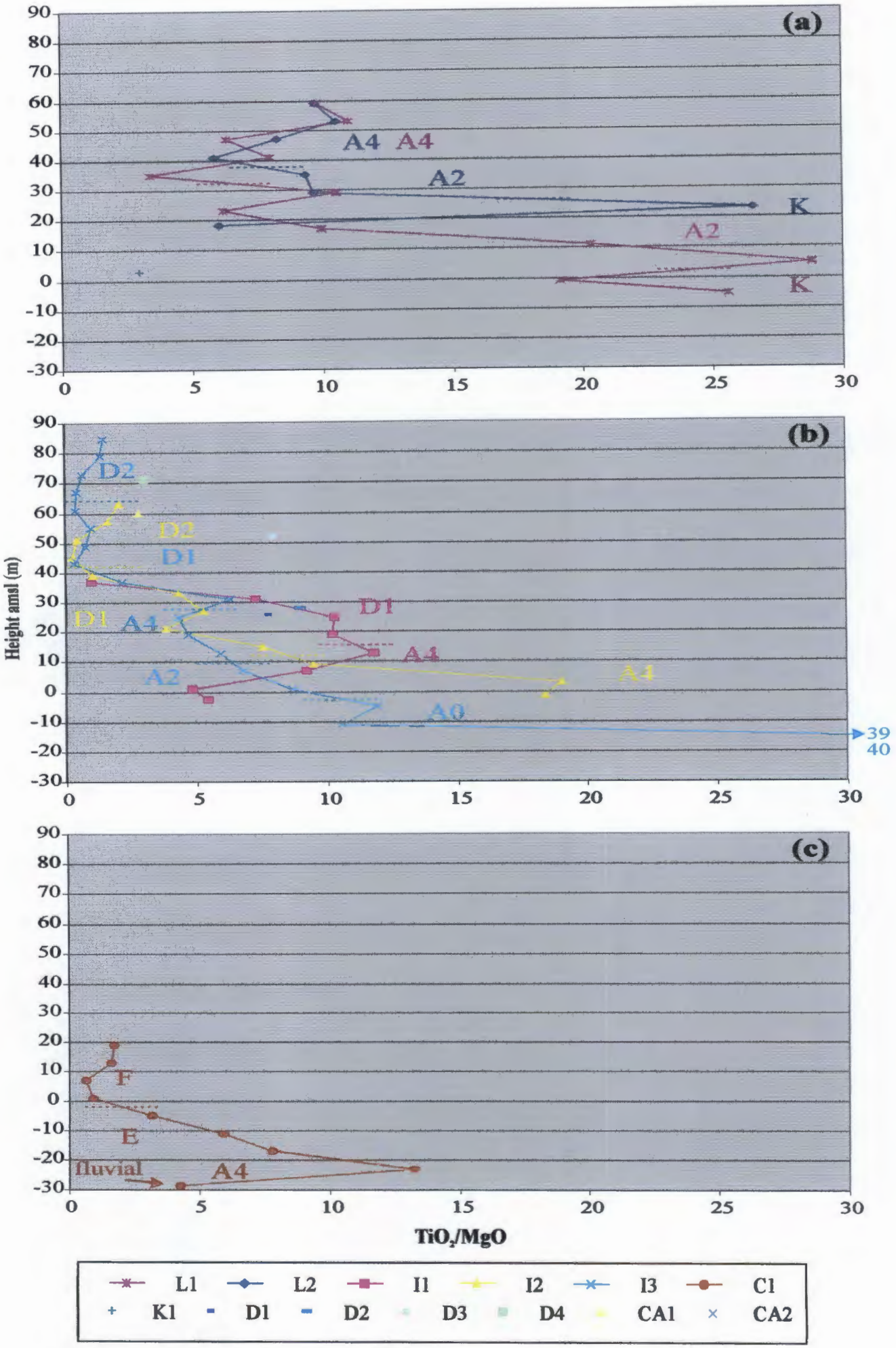

Figure 5.9 Down hole major element ratio plots of TiO_2/MgO (wt%/wt%) for the; (a) Inland, (b) Intermediate, and (c) Coastal boreholes.

implying more intense and/or prolonged weathering. The higher TiO_2 / MgO ratio values of Unit A0 compared to Unit K suggest that it is more weathered, however contrary evidence from the fine-fraction dispels this conclusion. Higher ratio values are probably the result of inherently greater abundances of heavy minerals.

Unit A4 has intermediate TiO_2/ MgO ratio values of between 5 and 12 which suggests it is younger than Units K, A0 and A2 but older than Units D1, D2, E and F. The latter units have ratio values generally less than 7.

Units F and D2 have the lowest TiO_2/ MgO ratio values of less than 3. These low ratio values corresponds well to high $CaCO_3$ abundances and suggests that a significant portion of MgO is contained within carbonates and not solely in pyriboles as suggested by Sudan (1999).

Chemical Index of Alteration

Chemical indices of alteration essentially measure the degree of depletion of mobile components relative to immobile components during weathering. Although many different weathering indices are cited throughout the literature, such as the Vogt ratio (V; Vogt, 1927; Roaldset, 1972), Weathering Index (WI; Parker, 1970), Modified Weathering Potential Index (MWPI; Reiche, 1943; Vogel, 1975) and the Chemical Index of Weathering (CIW; Harnois, 1988) perhaps the most simple and widely used is the Chemical Index of Alteration (CIA; Nesbitt & Young, 1982). The CIA is the ratio of immobile Al_2O_3 versus the sum of the relatively mobile elements CaO, Na_2O and K_2O. The larger the value of CIA, the greater the degree of weathering with a completely weathered sediment having an index value close to 100.

There is a general increase in CIA from the top of the coastal to base of the inland boreholes (Figure 5.10). Units K and A0 are the most weathered units with very high CIA values of between 65 and 90 corresponding to the high fines and consequently clays. Units A2, A4 and E show similar degrees of weathering with intermediate to high CIA values, between 50 and 85, at depth. Unit D1 has high CIA values in borehole I2 (60 - 80) but generally moderate values in borehole I3 (30 - 60), suggesting higher degrees of weathering within the former. This is to be expected as there is a lower CaO abundance. Units D2 and F have similar low becoming intermediate values of CIA (22 to 58) with depth. These low CIA values are attributed to a high labile CaO abundance.

For the weathering study of titanium bearing dune sands, the CIA is considered by the author to be more

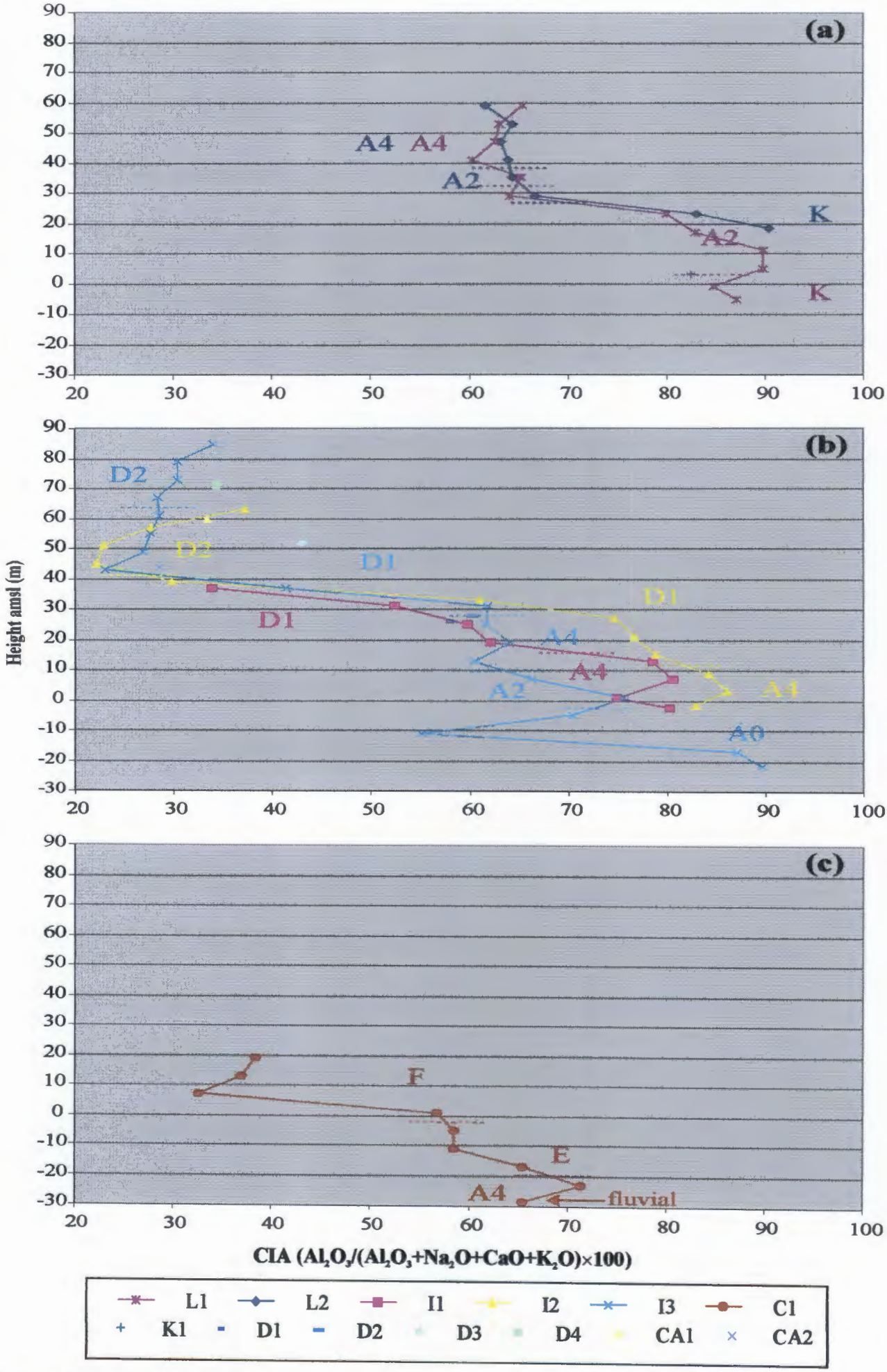

Figure 5.10 Down hole major element ratio plots of the Chemical Index of Alteration (CIA; Al_2O_3 / (Al_2O_3+Na_2O+CaO+K_2O)×100) for the; (a) Inland, (b) Intermediate, and (c) Coastal boreholes.

useful than the ratio of TiO_2 / MgO. Since titanium is absent from the calculation of CIA, any localised depositional concentrations (beach placers) will not be considered in determining the weathering state. Also, clays are products of weathering (essentially aluminium silicates) thus high CIA values indicate high clay abundances. The varying and increasing CIA values within units further suggests that units were deposited over a period of time.

5.1.3.5 Heavy mineral abundances

Heavy mineral abundance ratios are determined by RBM on the bulk samples as a continuous assessment of the ore reserves within ZNL. In the RBM laboratory, heavy minerals are separated using a combination of sieving (to remove fines), heavy liquid separation (tetrabromoethane; separates gangue quartz from heavy minerals) and finally by Carpco electro-magnetic separators with the aid of XRF (separates heavy minerals into their respective groups). For an exhaustive presentation of the RBM heavy mineral extraction procedure the reader is directed to Clarke (1998) with an explanation of the heavy mineral abbreviations used in this study presented in Table 5.1.

The most useful ratios for discriminating dune units based on their heavy mineral abundance has been shown by Clarke (1998), Sudan (1999) and Whitmore *et al.* (1999) to be EHM / THM and Magn / Ilm. Both of these ratios are consequently proxies for weathering as they represent the proportions of more resistant versus less resistant minerals. These ratios values were obtained from boreholes drilled every 50 m (6 m down hole sample intervals) along the two cross-sections studied (n = 631); Figures 1.8 & 1.9) to allow stratigraphic units to be correlated between previously defined boreholes units. This was achieved by creating colour contour (Kriging statistical method) maps of the respective ratios along the two cross-sections studied using Surfer 7.0 (1999) software. All heavy mineral ratios are presented in Appendix E4.

Table 5.1 Abbreviation explanations used in heavy mineral abundance ratios.

Abbreviation	Explanation
EHM	Economic Heavy Minerals; includes ilmenite, rutile, zircon and minor monazite and leucoxene
THM	Total Heavy Minerals; includes ilmenite, leucoxene, rutile, zircon, monazite, pyriboles, garnet and epidote
Magn	Magnetite; includes ilmenite (*ca.* 12-14 %), magnetite (*ca.* 50 %), titano-magnetite (*ca.* 15-20 %) and some minor phosphates
Ilm	Ilmenite and altered ilmenite

EHM / THM

High EHM / THM values are interpreted to represent mature sediment (older) which is depleted in the comparatively less resistant alumina-silicates comparted to more stable ilmenite, rutile and zircon. This ratio was successful in separating Units D and A and to a lesser extent K (Figures 5.11 & 5.12). Consequently there is a general increase in the ratio EHM / THM down hole and from the coastal to the inland boreholes. The subunits however were not as clearly separated. Units F and E were indistinguishable from Unit D based on the EHM / THM ratio.

Units D, E, F generally have low ratio values < 0.47 indicating a relatively non-weathered sediment. Unit D1 generally shows slightly higher ratio values (0.25 - 0.47) than Units D2, E and F indicating a relatively older sediment. Unit A exhibits comparatively higher EHM / THM values which generally increase down hole and are between 0.47 and 0.70. Subunit subdivision is ambiguous however there is a progressive increase in the EHM / THM ratio from Units A4, A2 and A0. Unit K is indistinguishable from Unit A0 based on EHM / THM ratios and has values > 0.65.

Magn / Ilm

The ratio Magn / Ilm is essentially the abundance of magnetite and titanomagnetite within the sample as ilmenite is common. Higher values of this ratio indicates higher abundances of magnetite and titanomagnetite and thus, due to their relative instability, a younger age. Sudan (1999) showed that while this ratio was not a reliable discriminate of relatively younger sediments it was useful in distinguishing older

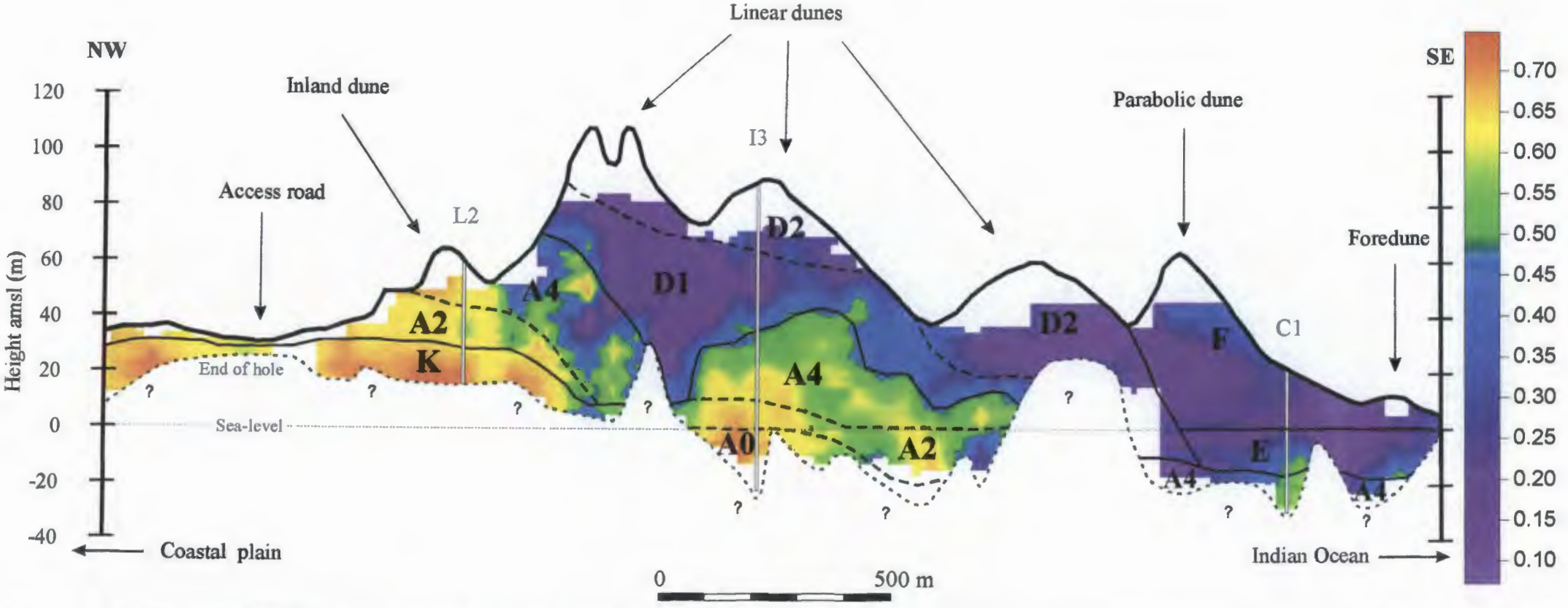

Figure 5.11 Coast normal (NW/SE) cross-section through the central part of the Zulti North lease area. A colour contour map of Economic heavy minerals / Total heavy minerals (EHM / THM) has been overlayed showing correlation of units between previously defined boreholes (L2, I3 and C1). Higher values represent higher proportions of more stable ilmenite, rutile and zircon and thus higher degrees of alteration. Unit boundaries are solid whereas subunit boundaries are separated with dashed lines. EHM / THM ratio values were successful in separating Units D, E and F (< 0.47), Unit A (0.47 to 0.70) and Unit K (> 0.65).

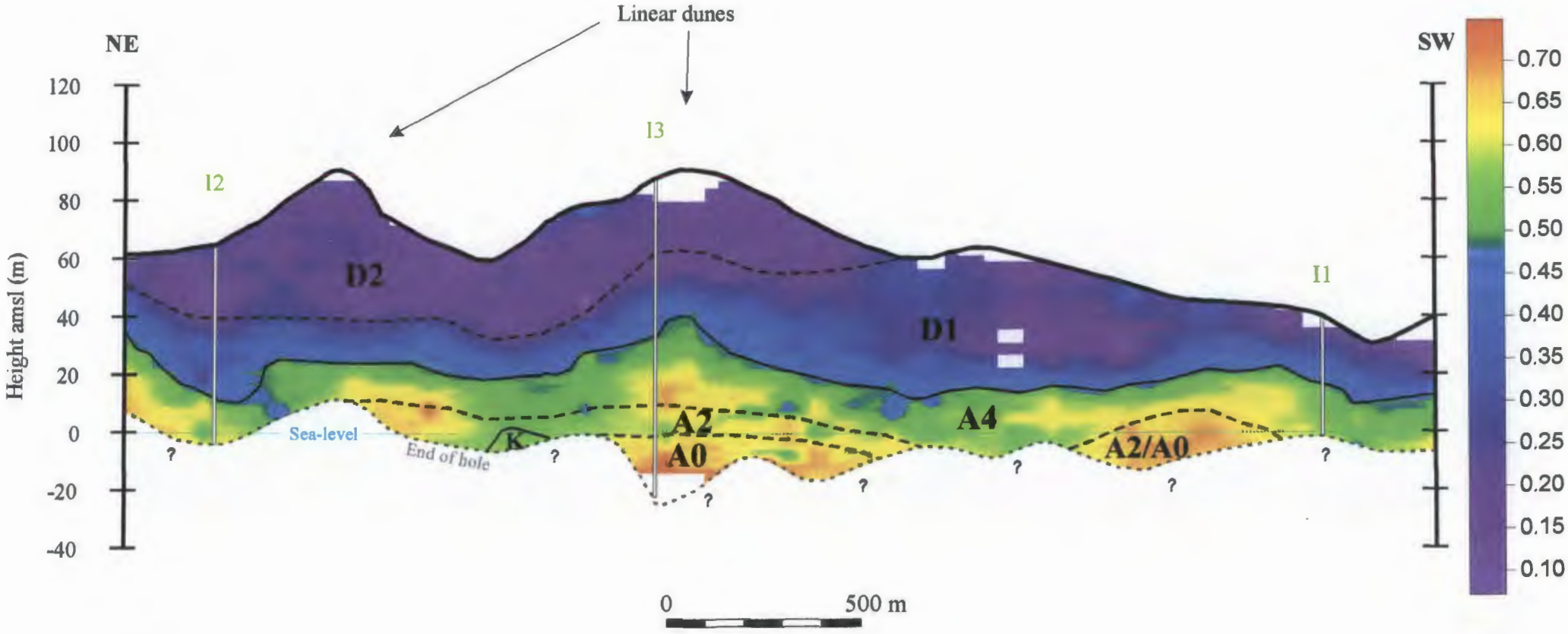

Figure 5.12 Coast parallel (NE/SW) cross-section through the central part of the Zulti North lease area. A colour contour map of Economic heavy minerals / Total heavy minerals (EHM / THM) has been overlayed showing correlation of units between previously defined boreholes (I1, I2 and I3). Higher values represent higher proportions of more stable ilmenite, rutile and zircon and thus higher degrees of alteration. Unit boundaries are solid whereas subunit boundaries are separated with dashed lines. EHM / THM ratio values were successful in separating Units D, E and F (< 0.47), Unit A (0.47 to 0.70) and Unit K (> 0.65).

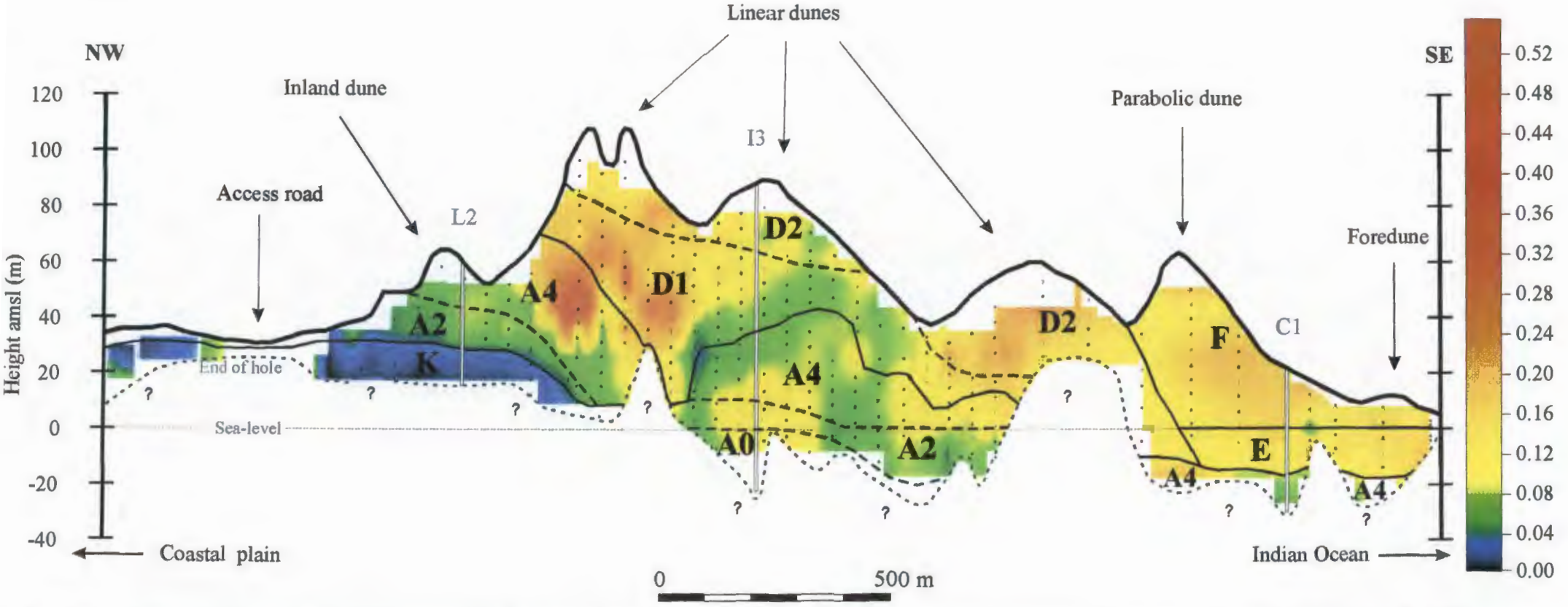

Figure 5.13 Coast normal (NW/SE) cross-section through the central part of the Zulti North lease area. A colour contour map of Magnetite / Ilmenite (Magn / Ilm) has been overlayed showing correlation of units between previously defined boreholes (L2, I3 and C1). Lower values represent low abundances of unstable magnetite and thus higher degrees of alteration. Unit boundaries are solid whereas subunit boundaries are separated with dashed lines. Magn / Ilm ratio values were successful in separating Units D, E and F (0.05 to 0.54), Unit K (< 0.03) and to a lesser extent Unit A (0.04 to 0.20).

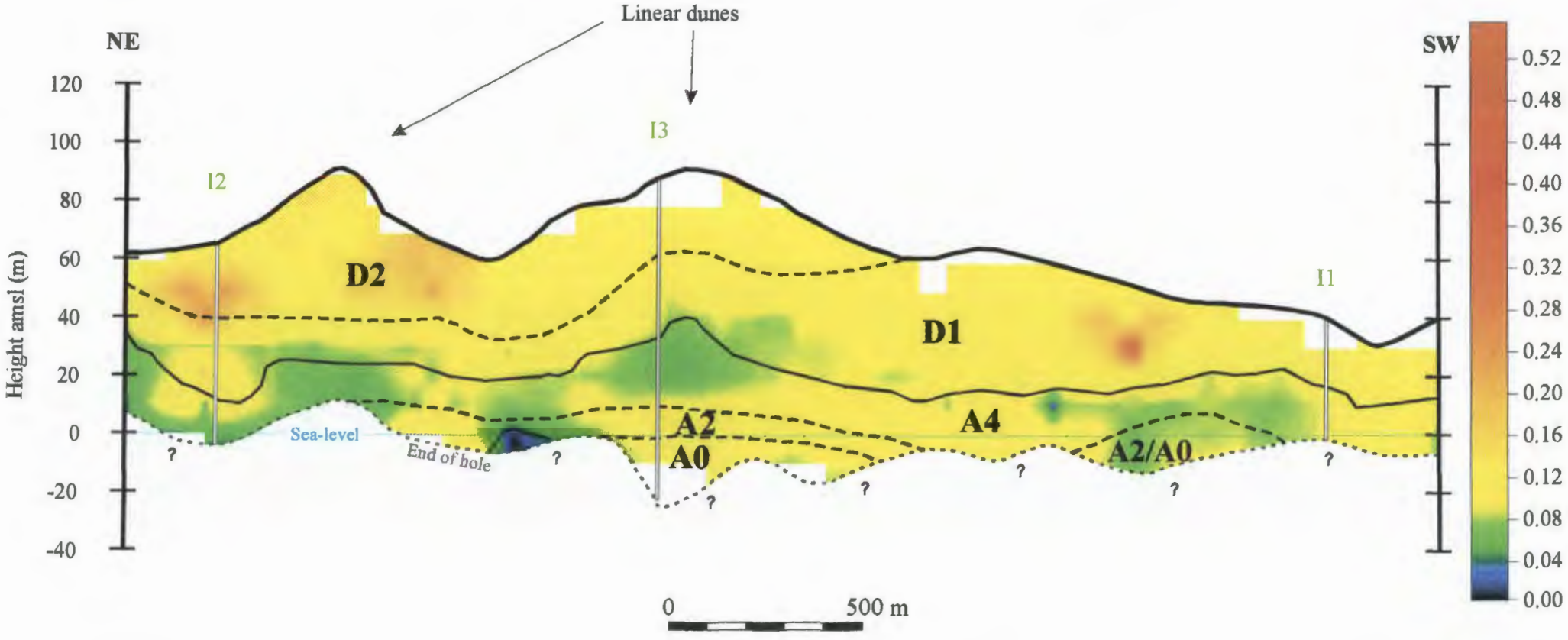

Figure 5.14 Coast parallel (NE/SW) cross-section through the central part of the Zulti North lease area. A colour contour map of Magnetite / Ilmenite (Magn / Ilm) has been overlayed showing correlation of units between previously defined boreholes (I1, I2 and I3). Lower values represent low abundances of unstable magnetite and thus higher degrees of alteration. Unit boundaries are solid whereas subunit boundaries are separated with dashed lines.Magn / Ilm ratio values were successful in separating Units D, E and F (0.05 to 0.54), Unit K (< 0.03) and to a lesser extent Unit A (0.04 to 0.20).

units. This ratio is consequently successful in separating Unit K and to a lesser extent Unit A from Units D, E and F (Figures 5.13 & 5.14).

Unit K is typified by a decrease of magnetite having extremely low ratio values (< 0.03) whereas Unit A has Magn / Ilm values generally between 0.04 and 0.20. However, Unit A4 in the inland dune has relatively high ratio values < 0.50. The relatively younger Units D, E and F are indistinguishable by Magn / Ilm values which range from 0.05 to 0.54.

5.2 DISCUSSION

There is a general increase in weathering down hole and from the coastal to the inland boreholes resulting in the more weathered dune units containing higher abundances of fines and consequently clays. Weathering is first manifested by the leaching of free-draining dune sands, in an open system, of unstable calcite suggesting dune Units A and K are older as they are decalcified. Also, the weathering of relatively unstable ferro-magnesium minerals such as pyriboles and magnetite results in a depletion of these minerals. Over time, the relatively mobile iron (Fe^{2+}) and magnesium are leached and the more immobile Al_2O_3 remains and is concentrated (Nesbitt & Young, 1982; Chamley, 1989; Pye, 1993). Thus Unit K having the highest abundances of Al_2O_3 (*ca.* 3 - 6 %), is considerably more weathered (older) than the other identified units.

The colour of the dunes is controlled by the amount of fines and more importantly by their composition (Section 3). Goethite (± hematite ± ferrihydrite) occurs as grain coatings and is formed as iron is liberated from the weathering of pyriboles, magnetite and ilmenite and is responsible for yellowish-brown to reddish-brown colours (Schwertmann & Taylor, 1977). This reddening process is relatively rapid taking only a few thousand years (Pye, 1993). Humic colloids have been identified in dunes of northeastern Australia as being responsible for the dark brown colours (Pye, 1993). Abundant kaolinite gives the dunes an olive brown and grey appearance and has only been identified in northeastern Australia in dunes that are older than *ca.* 160 ka (Lees *et al.*, 1990).

This tentatively separates three broad dune packages of similar weathering states and thus ages; olive brown and grey Unit K (fines 10 - 22 %; CIA = 65 - 90), dark brown to yellowish brown and occasionally red Unit A (fines 3 - 24 %; CIA = 50 - 90), and dark yellowish brown calcified Units D, E and F (fines < 5 %, CIA = 22 - 60). Unit A is further subdivided into progressively more weathered subunits A4 (fines 4 - 22 %; CIA = 50 - 85), A2 (fines 5 - 24 %; CIA = 60 - 90) and A0 (fines 10 - 17 %; CIA = 55 - 90) respectively. These broad dune packages of similar weathering are reinforced by the heavy mineral ratios

of EHM / THM and Magn / Ilm. Units D, E and F are comparatively less weathered with ratio values < 0.47 and 0.05 to 0.54 respectfully. Unit A has ratio values between 0.47 and 0.70 and between 0.04 and 0.20 respectfully. Unit K has ratio values > 0.65 and < 0.03 respectfully.

In-situ weathering of the dunes has produced abundant fine-grained sediment which hampers interpretation of textural parameters when determining depositional environments. The work by Sudan (1999) may therefore be more applicable to depositional environment studies using textural parameters as much of the fines were lost from his samples during preparation. Nevertheless, grain size analysis revealed that most samples were of probable aeolian origin being well sorted to moderately sorted, fine- to medium-sands. However, the base of borehole C1 is relatively coarse (Unit A4; 450 μm) containing gravel and is interpreted to be of fluvial origin. Also the base of Unit E has been interpreted from the silt-fraction to be from a littoral environment (Section 4.2.1.1) which is further confirmed by having a negative skewness (-0.01; fines *ca.* 4 %) and being near-symmetrical (Friedman, 1961). Detailed studies of the depositional environment would necessitate careful sample preparation and should be combined with grain morphology studies.

6 LUMINESCENCE DATING

Luminescence dating is a dating method initially developed in the 1960's for dating pottery. However, since 1979 the method has been successfully applied to dating Quaternary dune sands between *ca.* 800 000 to 30 BP (Nanson *et al.*, 1992; Stokes, 1992; Stokes *et al.*, 1998; Vogel *et al.*, 1999). The method is based upon the fact that many naturally occurring minerals, including quartz and feldspars, are able to act as dose meters, recording the amount of ionizing radiation (alpha, beta, gamma and cosmic rays) that they are exposed to. The energy absorbed from ionising radiation frees electrons to move through the crystal lattice and some are trapped at imperfections in the lattice. Subsequent heating of the crystal or stimulation by absorption of infrared light can release some of these trapped electrons with an associated emission of light - thermoluminescence (TL) or infrared stimulated luminescence (IRSL) respectively. By combining measurements of the luminescence of a sample and the natural radioactivity of the surrounding sediment, the age of the sample when it was last exposed to cosmic radiation (light) can be determined.

IRSL targets a specific population of trapped electrons in K-feldspars grains which are extremely light sensitive, and upon exposure to sunlight for minutes will cause all electrons to be ejected effectively zeroing (bleaching) the traps (Mejdahl, 1985). The TL technique targets two different electron traps in quartz grains which respond differently to zeroing and require days of exposure to sunlight in order to effectively zero them. Thus long exposure to sunlight will reset specific electron traps and provide a burial date of the sands (TL) as well as an age of any subsequent brief reworking of the sediment (IRSL). The uncertainty on luminescence dates is typically in the range of approximately 5 to 12 % of the sample age.

6.1 PAST WORK

Botha (pers. comm, 2001) is presently dating a variety of dunes along the northern KZN coastal plain as part of an ongoing study of the stratigraphy of the Maputaland Group. To date, these ages have not been compiled, except for the white kaolinite-rich sands near 5-Mile beach north of Richards Bay. These sands were deposited between *ca.* 350 to 250 ka BP (Dr N. Porat, Geological Survey of Israel, pers. comm, 1999 *In:* Maud & Botha, 2000). Two combined TL and IRSL dates from the current study area have been analysed by Sudan (1999; Figure 1.4). Luminescence dating of sample RBM 1 gave a depositional age of 12 800 ± 2 100 BP and a brief reworking event at 6 500 ± 450 BP. Sample RBM 2 was deposited 7 400 ± 2 600 BP with a reworking event at 2 100 ± 142 BP.

6.2 RESULTS

To gain further clarity on dune ages within the study area, six samples (D1 - D4, CA1 and CA2) were dated by S. Woodborne & G. Collett at the CSIR Quaternary Dating Research Unit using both TL and IRSL techniques (Figure 6.1). For a detailed account of the luminescence dating technique and results refer to Appendix G and Table 6.1.

Table. 6.1 Luminescence dating results for selected surface samples.

Sample	D1	D2	D3	D4	CA1	CA2
TL (ka BP)	173 ± 40	21.6 ± 2.0	26.4 ± 2.9	17.1 ± 1.9	1.1 ± 0.1	22.7 ± 1.4
IRSL (ka BP)	188 ± 10	1.6 ± 0.4	9.4 ± 0.6	0.4 ± 0.03	0.154 ± 0.009	5.3 ± 0.4

There are three basic age groups which the samples fall into; the oldest being sample D1 which is dated at *ca.* 180 ka BP, followed by samples D2, D3, D4 and CA2 which are all *ca.* 20 ka BP and the youngest sample (CA1) is *ca.* 1 ka BP. All samples, except D1, have been subsequently reworked during Holocene times.

Only sample D1 is well bleached as both the TL and IRSL dates are statistically the same at *ca.* 180 ka BP. This sample was therefore likely to have been deposited during sea-level lowering (end of oxygen isotope stage 7) leading to the penultimate glacial event (Figure 2.4).

The remaining samples show a large disparity between their TL and IRSL dates making literal interpretation of the results difficult. This is most likely due to very rapid remobilisation and deposition (or slumping) of the sand without significant time to zero the luminescence signal.

None of the samples dated between 150 and 75 ka BP. This is tentatively due to these samples being extensively reworked leading up to and during the last glacial maximum (*ca.* 19 ka BP). It is apparent that samples D2, D3, D4, CA2 and by inference the bulk of the coastal dune cordon were probably deposited during the last glacial maximum in response to lower sea-levels (- 130 m). At this time a large flat exposed shelf, as well as a drier climate and a higher wind regime is expected to have reworked voluminous amounts of sediments (Section 2.2.7). Subsequent rapid reworking or possible multiple reworking of these sediments occurred during the Late Pleistocene and Holocene. Sample CA1 represents the youngest sands deposited

Figure 6.1 (over leaf) Photographs showing the locality of surface samples. (a) Mining Pond D showing the floating concentration plant. Also shown are sample localities D3 and D4; photograph taken towards east-north-east. Sample positions D1 and D2 are just to the south (right) of the photograph. (b) Sample positions of D1 and D2; white dashed line separates two distinct dune units. (c) Close up photograph showing an upper thinly bedded dune unit underlain by a massive dune unit. (d) Photograph taken just south of sample position CA2 showing the positions of samples CA1 and PondC; photograph taken looking south with mining pond C to the west. White dashed line separates brown unconsolidated sands (left) and orange unconsolidated sands (right). (e) Close up photograph of sample CA1. Note the black colour of the sands caused by abundant heavy minerals. (f) Close up photograph of sample CA2, showing numerous shell fragments and palaeosols. Note the plastic tube used to contain the sample for luminescence dating (g) Sample K1, 2 mile beach; photograph taken towards the west. Note the mudrock forming the base of the semi-consolidated white clayey sands which are overlain by orange semi-consolidated clayey sands.


a
D4
D3
To D1 & D2
Mining pond D

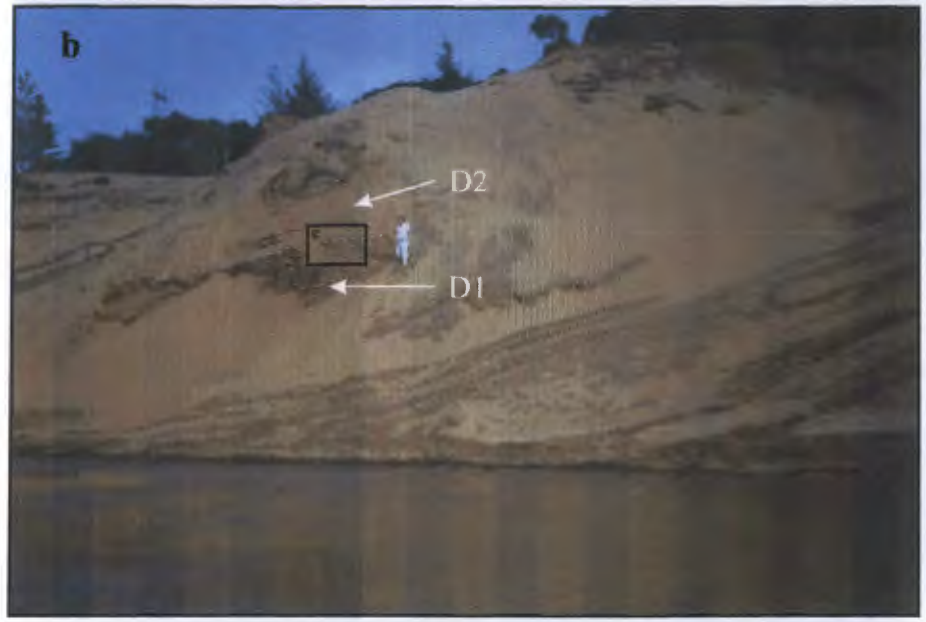
b
D2
D1

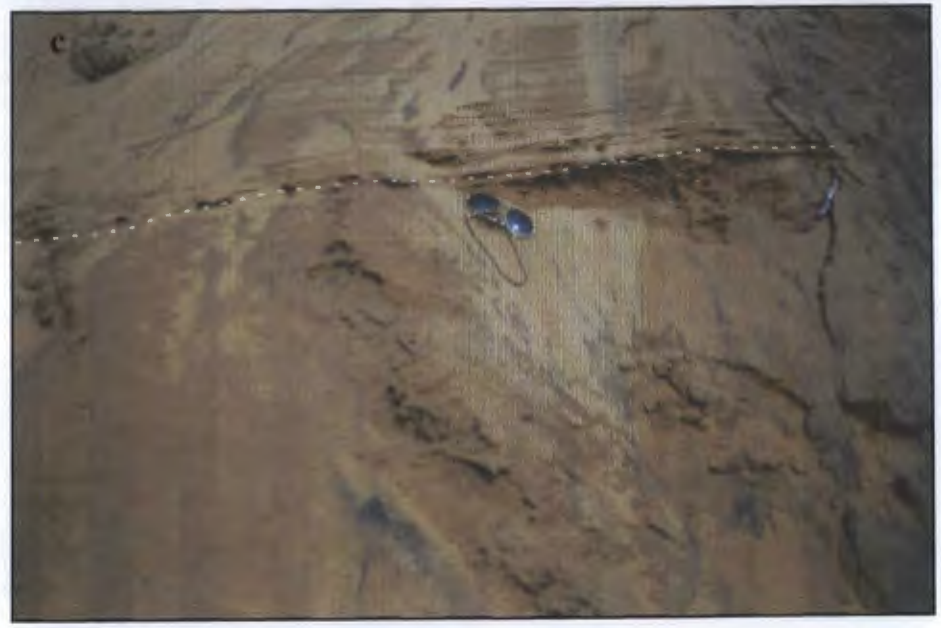
c

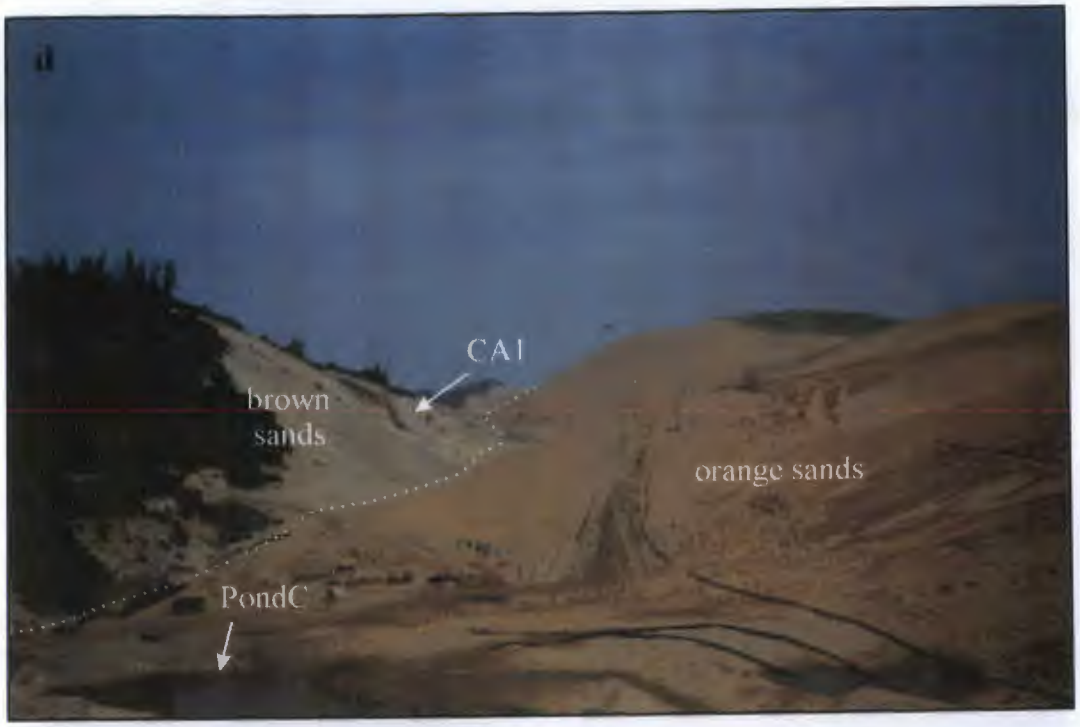
d
CA1
brown
sands
orange sands
PondC


e


f

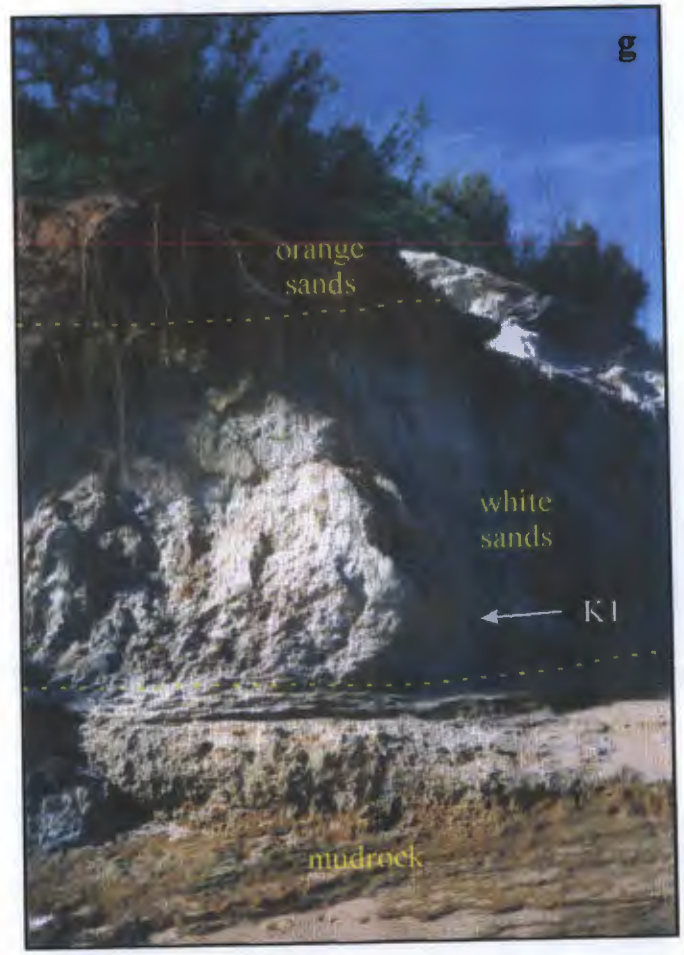
g
orange
sands
white
sands
K1
mudrock

during the late Holocene (*ca.* 1100 BP) and reworked very recently (*ca.* 154 BP).

6.3 LUMINESCENCE AGES

6.3.1 UNIT K

The kaolinite-rich Unit K has been dated as part of a regional study by Drs G. Botha and N. Porat. Their work indicates ages between *ca.* 250 to 350 ka BP (Dr N. Porat, Geological Survey of Israel, pers. comm, 1999 *In:* Maud & Botha, 2000) which corresponds to oxygen isotope Stages 8 -10. Unit K was suspected as being the oldest unit studied as it showed the highest degree of weathering in terms of its CIA and almost completely weathered silt-grains. The clay-fraction is also dominated by kaolinite which is considered the ultimate weathering product within the current climatic regime (Chamley, 1989; Section 3).

6.3.2 UNITS A0 AND A2

Unit A0 has not been directly dated. Given its stratigraphic position, its high degree of weathering and abundant fines it is expected to be in the order of 130 to 250 ka BP. Sample D1 correlates well with Unit A2 and is interpreted to have been deposited *ca.* 180 ka BP in response to the marine regression during the onset of the penultimate glacial event.

6.3.3 UNIT A4

Unit A4 is represented by samples D2 and D3 and is dated between 19 600 and 23 600 BP and 23 500 and 29300 BP respectively (*ca.* last glacial maxima). These samples also show reworking during the Holocene. It is suspected that these samples represent material that has been successively reworked from older dunes of *ca.* 75 and 150 ka. Also, their low fines content, low CIA and variable degrees of silt weathering confirms reworking with younger sand. Sample CA2, although containing abundant carbonate (*ca.* 5 %), reveals similar ages (21 300 to 24 100 BP) and Holocene reworking. However it is suspected that it obtained its high carbonate abundance during reworking with younger sands as did sample D3 (*ca.* 1 % carbonate). Whereas sample D2 was decalcified perhaps due to recent leaching. Sample CA2 therefore correlates with Unit A4 rather than Unit D2, as suggested by its high carbonate content. Unit A4 represents an extensive dune building time caused by sea-level lowering entering the last glacial maxima and has subsequently been reworked during the Holocene.

6.3.4 UNIT D1

Sample D4 (17.1 ± 1.9 ka BP) correlates well with Unit D1 and is enriched in carbonate (*ca.* 3 %). This unit probably represents dune building during the subsequent rise in sea-level after the last glacial maxima and has also been subsequently reworked within the latter part of the Holocene. Any addition of carbonate has thus not had sufficient time to be leached. Sudan (1999) obtained an age of 12.8 ± 2.1 BP for the inland section of Unit D1 (Sudan's Unit D2; redefined in section 7) corresponding to sea-level stillstands during the sea-level transgression (Ramsay, 1999). It was subsequently reworked during the Holocene at 6 500 ± 450 BP. A similar older dune sequence, as in Unit A4, is suspected to have been the source of sand for this unit.

6.3.5 UNIT D2, E AND F

Calcified Units D2, E and F represent the most recent accretion of sand within the ZNL. They are all Holocene in age and show recent reworking. Sudan (1999) indicated that his Unit E formed at 7 400 ± 2 600 BP with a reworking event at 2 100 ± 142 BP, however no bulk sample analyses was done on the sample as a control. Based on results from this study this sample is correlated to Unit D2 due to its stratigraphic position and age. Sample CA1 (1 000 to 1 200 BP; reworked at 154 BP) correlates well with Unit D2. It is suspected that sample CA1 represents material that has been reworked from Unit D2 giving it its similar properties but is in fact a superficial, recently remobilised dune.

Unit E is suspected to have formed during the Mid-Holocene at *ca.* 3 000 BP during a minor sea-level low (Figure 2.5; Ramsay, 1995). The overlying smectite-rich Unit F is the youngest and least weathered and, although not dated, is probably less than 1 000 BP.

7 GEOLOGICAL EVOLUTION AND REVISED CHRONOSTRATIGRAPHY

Eight Quaternary sedimentological units (K, A0, A2, A4, D1, D2, E and F) were identified in the central ZNL from diverse data gained from six boreholes up to 111 m long (L1, L2, I1, I2, I3 and C1; Figures 7.1 & 7.2). Analysis of fines proved successful in separating all units with depositional interpretation being aided by bulk sample analysis. Lateral extensions of these units were interpreted from heavy mineral abundance ratios obtained from boreholes drilled on a 50 m grid.

There is a general increase in fines down hole and from the coastal to the inland dunes. This correlates to measurements of dune weathering and consequently the formation and depletion of various clays. The alteration state (CIA), silt morphology and clay mineralogy of the samples were used to infer a relative age for dune units which was then correlated with absolute ages from luminescence dating. Local relative sea-level curves further aided in depositional and chronological interpretations (Figure 2.4).

This section interprets the geological evolution of the central ZNL (Figure 7.3 and summarised in Table 7.1) and correlates the units with the informal stratigraphy of the Maputaland Group as proposed by Botha (1997a).

The base of the Zulti-North deposit is irregular (Figures 7.1 & 7.2) and is interpreted, based on regional studies (Botha, 1997 a), to be mudrocks of the Port Durnford Formation. The evolution of this basal topography, within the inland portion of the ZNL, pre-dates Units K and could have formed from either fluvial and/or marine erosional events. The basal topography of the coastal regions is interpreted to have formed in response to sea-level fluctuations in response to glaciation (Figures 7.3 a to j).

Unit K forms the core of the dune cordon and most likely overlies the Port Durnford Formation. It is a yellowish brown to light olive grey, poorly sorted, semi-consolidated upper fine sand (Figure 7.1 & 7.2). It is characterised by a high kaolinite (< 74 %) abundance within the clay-fraction, low HAEM (*ca.* 23 %) within the silt-fraction, very high fines (10 - 20 %), negligible carbonate content and extreme degrees of grain weathering (CIA = 65 - 90; Magn / Ilm < 0.03; EHM / THM > 0.65). Unit K is consequently correlated to the Kosi Bay Formation and has been dated between 250 - 350 ka (Dr N. Porat, Geological Survey of Israel, pers. comm, 1999 *In:* Maud & Botha, 2000). This is in agreement with the extreme degrees of grain weathering and the occurrence of kaolinite which is derived from the leaching of aluminium-silicates, especially during sub-tropical interglacial climates. The age of 70 000 ± 5 000 BP (Oschadleus & Vogel, 1996) obtained for the basal lignite which forms the base of the Kosi Bay Formation,

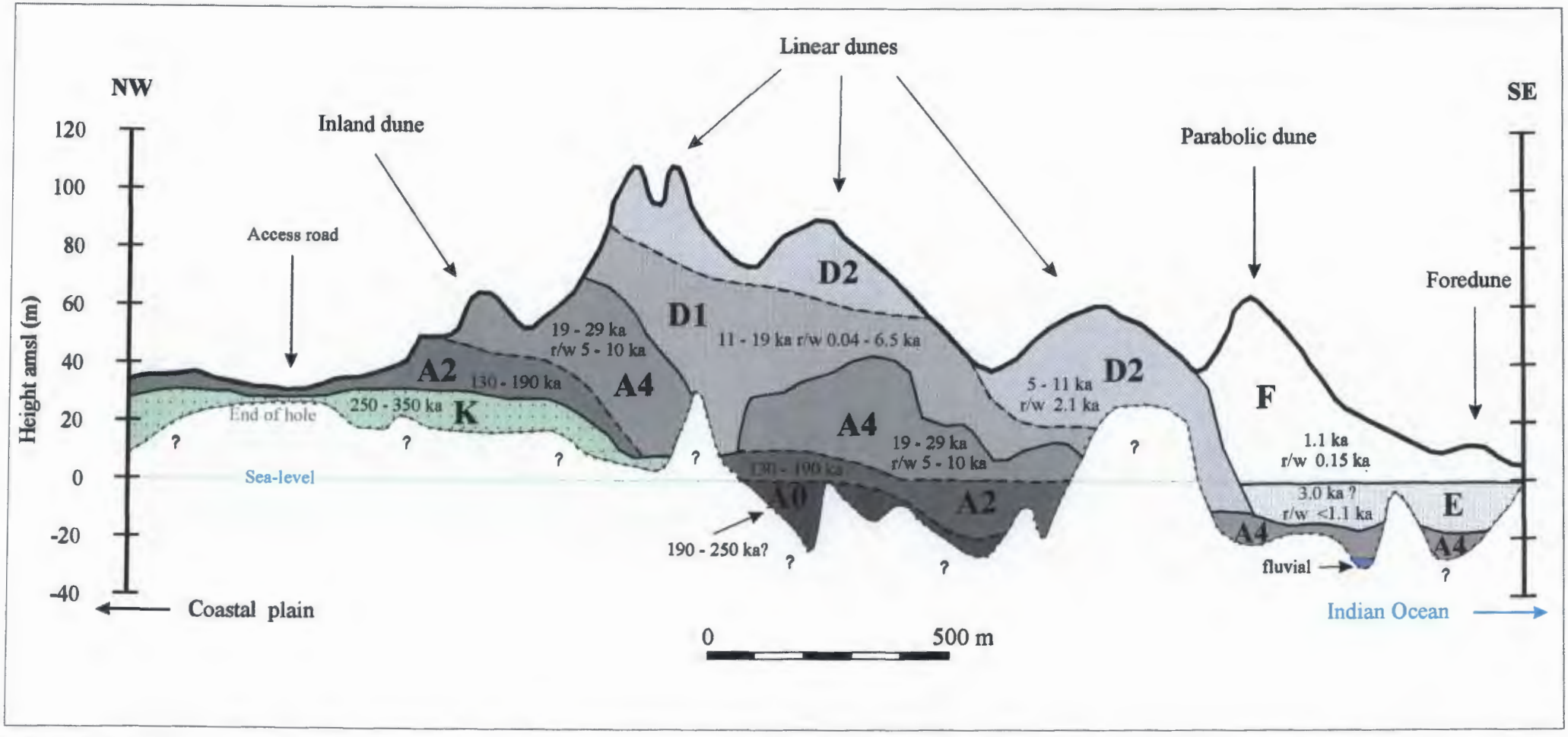

Figure 7.1 Coast normal (NW/SE) cross-section through the central part of the Zulti North lease area. Refer to Table 7.1 for unit characteristics. Ages are from luminescence dating with the abbreviation "r/w" used to denote periods of reworking.

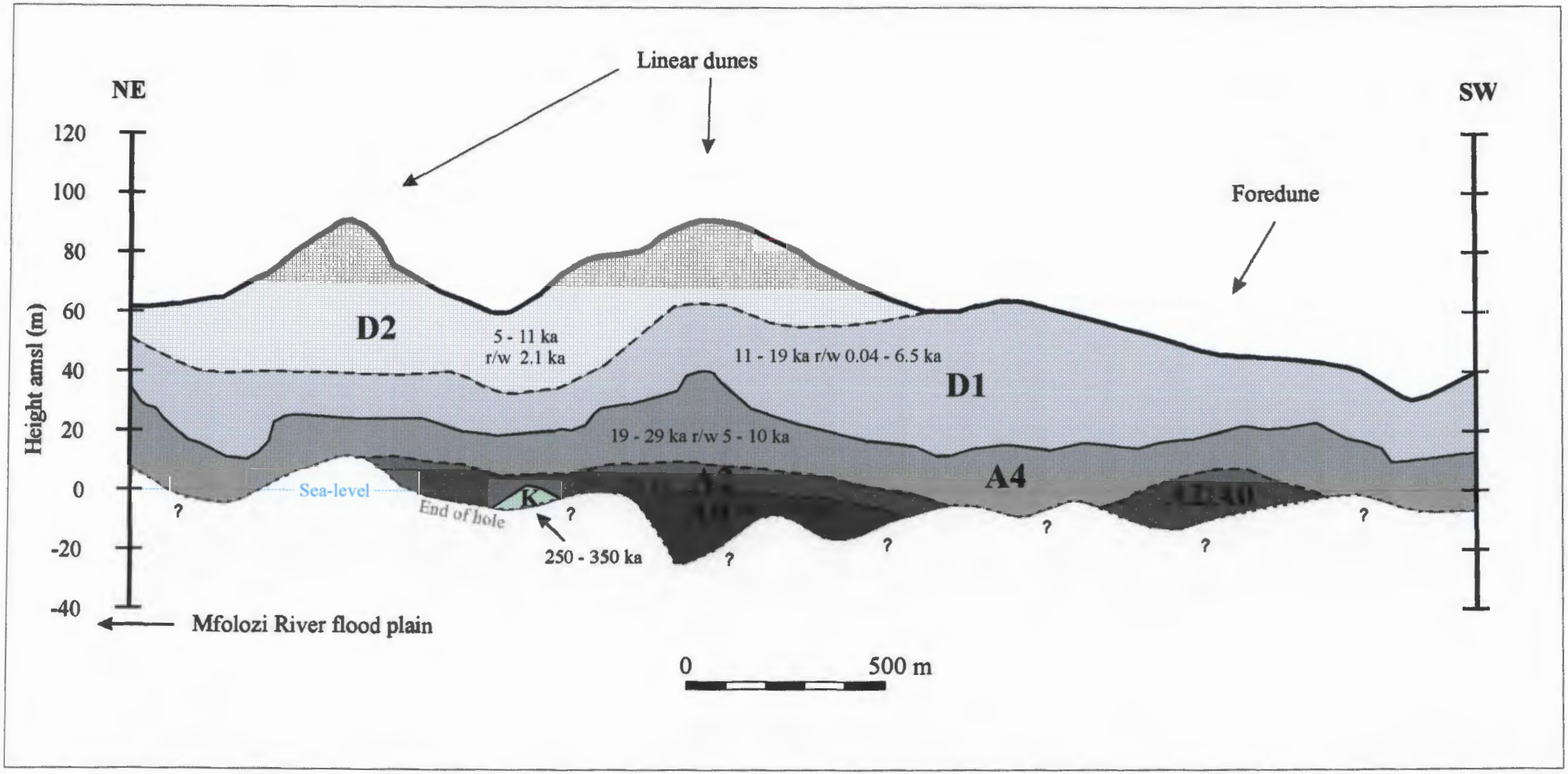

Figure 7.2 Coast parallel (NE/SW) cross-section through the central part of the Zulti North lease area. Refer to Table 7.1 for unit characteristics. Ages are from luminescence dating with the abbreviation "r/w" used to denote periods of reworking.

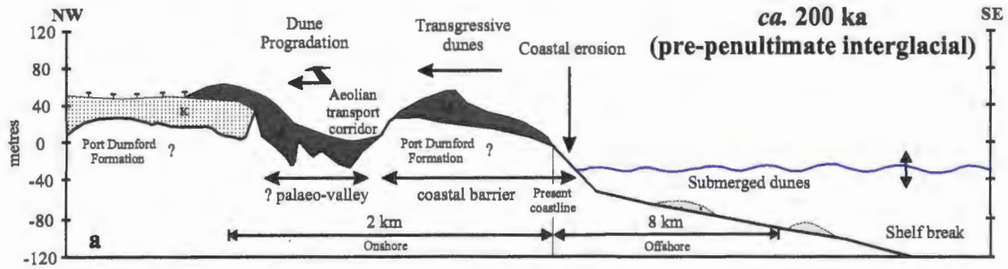

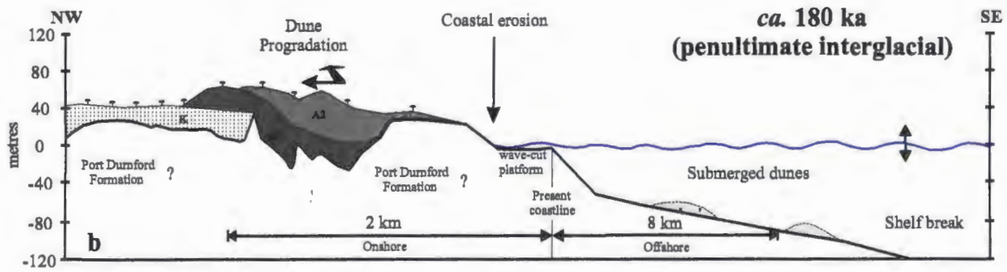

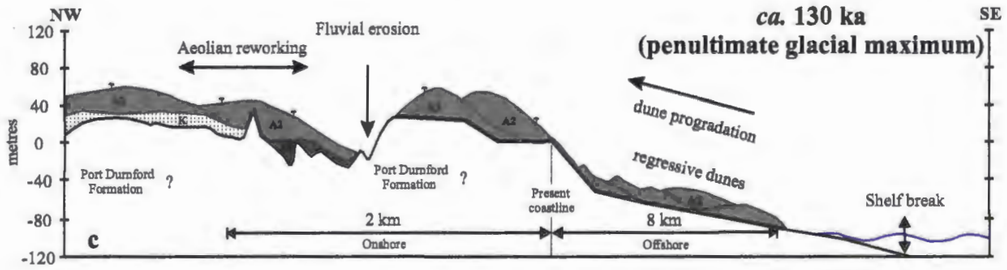

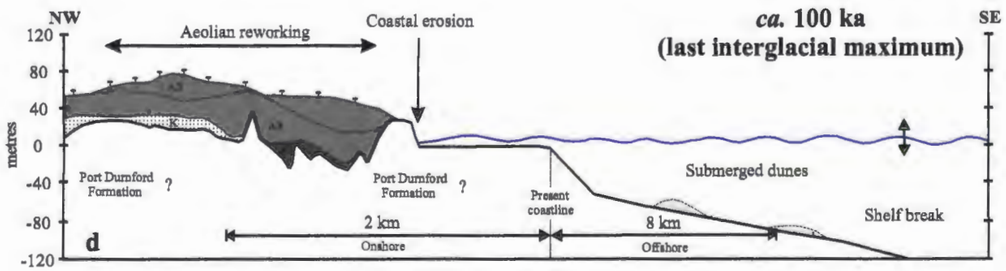

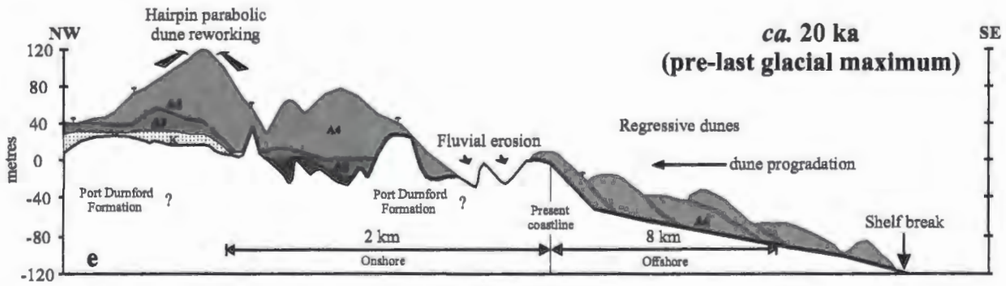

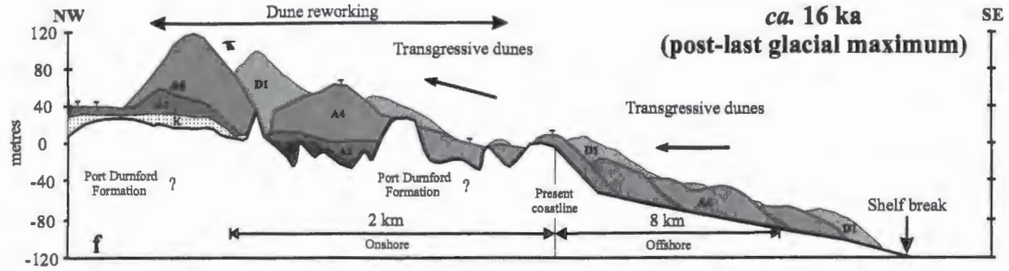

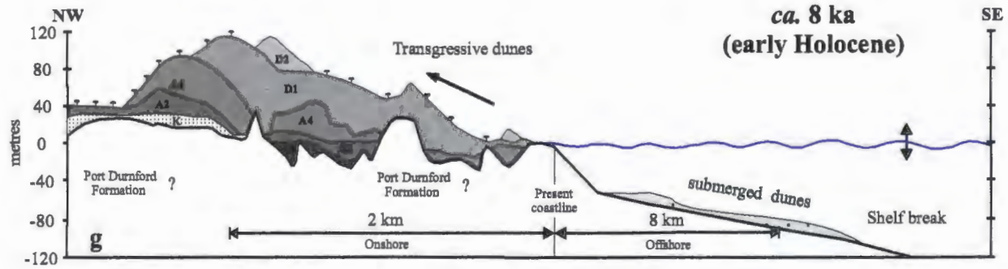

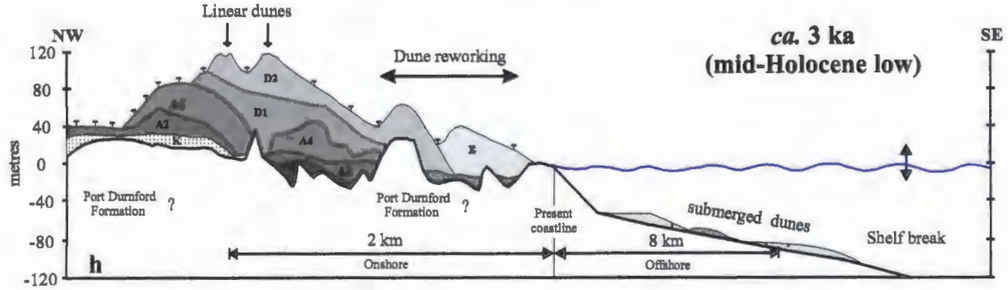

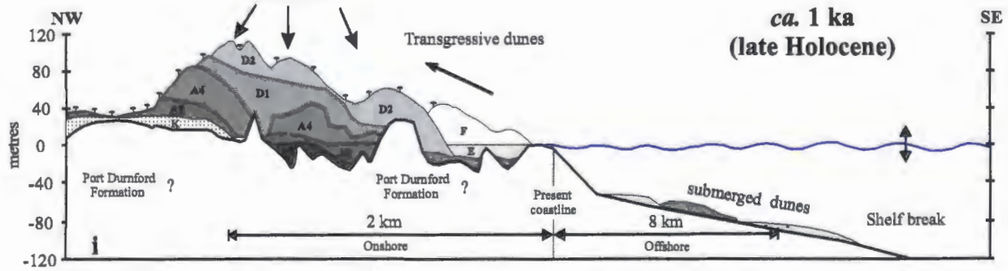

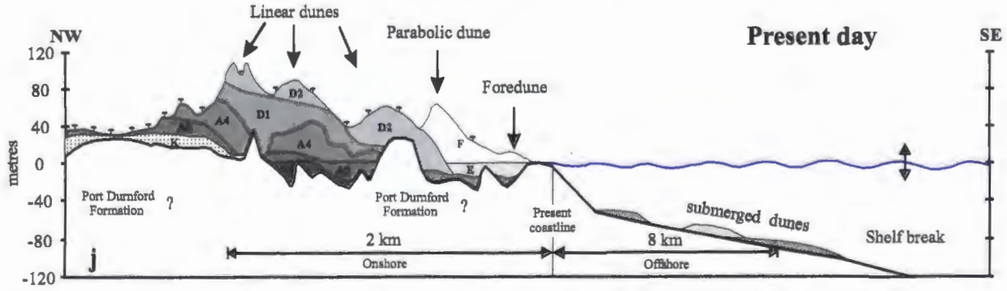

Figure 7.3 Series of cartoons (a - j) showing a model for the geological evolution of the central Zulti North lease in response to Quaternary sea-level fluctuations. The sections are taken coast normal and correspond to Figure 7.1. Refer to text for details.

therefore seems unlikely (section 2.1.5). Occurrence of the lignite, although not found in the central ZNL, further suggests a lagoonal / shallow low energy fluvial environment for the base of this unit. However, there is no evidence for this in the study area and the author thus suggests that the sands are tentatively (dominated) of aeolian origin.

Unit A0 is a strong brown to yellowish brown, moderately sorted, semi-consolidated lower medium sand. It is characterised by goethite (20 - 67 %), interstratifications (*ca.* 20 %) and kaolinite (9 - 22 %) which dominate the clay-fraction, abundant HAEM (30 - 61 %) within the silt-fraction, abundant fines (10 - 17 %), negligible bulk carbonate content and high to extreme degrees of grain weathering (CIA = 55 - 90; Magn / Ilm 0.05 - 0.15; EHM / THM 0.52 - 0.75). Although Unit A0 has not be dated, it is expected from the high degree of grain weathering, the accumulation of goethite rather than kaolinite (Nahon, 1986) and its stratigraphic position to be in the order of *ca.* 190 - 250 ka. This would place its deposition with the marine transgression prior to the penultimate interglacial highstand at *ca.* 180 ka (Figure 7.3 a). The coastal barrier comprising Port Durnford rocks resulted in dunes staked up against it due to the prevailing winds, as well as being transported up a north/south alined palaeo-valley which acted as an aeolian transport corridor (Figure 7.3 a). This corridor must have been cut-off from the ocean as there is no evidence for marine or lagoonal deposits and the sands are consequently of probable distal aeolian origin. These aeolian sands are correlated to the base of the KwaMbonambi Formation.

Unit A2 is a dark brown to yellowish brown, moderately well sorted, unconsolidated becoming semi-consolidated upper fine to lower medium sand. It is characterised by goethite (20 - 60 %), quartz (10 - 50 %), interstratifications (10 - 30 %) and kaolinite (10 - 33 %) dominating the clay-fraction, abundant HAEM (22 - 47 %) within the silt-fraction, intermediate to abundant fines (5 - 24 %), negligible bulk carbonate content and high to extreme degrees of grain weathering (CIA = 60 - 90; Magn / Ilm 0.05 - 0.13; EHM / THM 0.52 - 0.70). This unit was initially deposited during the highstand (- 5 m) of the warm penultimate interglacial event (*ca.* 180 ka) resulting in further infilling of the aeolian transport corridor. The high sea-level resulted in extensive coastal erosion to form a well developed wave-cut platform (Figure 7.3 b). The dunes were subsequently reworked during the regression brought on by cooler, windier, less vegetated glacial conditions of the penultimate glacial maximum at *ca.* 130 ka (Figure 7.3 c). At this time minor fluvial erosion shaped the eastern side of the palaeo-valley as rejuvenated rivers flowed coast parallel between the inland dunes and the coastal barrier of Port Durnford rock. The sands of Unit A2 are consequently of probable distal aeolian origin with very minor fluvial inputs and can be correlated to the KwaMbonambi Formation.

Unit A4 (19 - 29 ka) was derived from repetitive reworking of the older units during the late Pleistocene sea-level and climatic oscillations (Figure 7.3 d & e). The last interglacial highstands (126 ka, + 5 m and 100 ka, + 4 m respectfully) resulted in further coastal erosion and development of an extensive wave-cut platform. The high sea-levels also resulted in the existing dunes established on the shelf to be drowned and reworked (Figure 7.3 d). The last glacial maximum resulted in a cooler climate, lowered sea-level, higher wind regimes and sparse vegetation resulting in extensive reworking of the shelf sediments and further dune stacking (Tinley, 1986; Nicholson & Flohn, 1980; Butzer *et al.*, 1978; Tyson, 1986). Also, the lower sea-levels promoted the rejuvenation of rivers which cut into the exposed wave-cut platform (Figure 7.3 e). Unit A4 is a dark yellowish brown to red, poorly to well sorted, unconsolidated lower fine to lower medium sand. It is characterised by quartz (10 - 90 %), goethite (5 - 44 %), interstratifications (12 - 34 %) and kaolinite (3 - 38 %) dominating the clay-fraction, intermediate to high HAEM (15 - 47 %) within the silt-fraction, low to intermediate fines (4 - 22 %), negligible carbonate content and moderate to high degrees of grain weathering (CIA = 50 - 85; Magn / Ilm 0.05 - 0.56; EHM / THM 0.40 - 0.69). The sands of Unit A4 are of probable distal aeolian and local fluvial origin and was subsequently reworked during the Holocene. It is consequently correlated to the base of the Sibayi Formation which gives this formation a slightly older Late Pleistocene depositional age rather than the Holocene age of Botha (1997 a).

After the last glacial maximum sea-level rose rapidly with the ameliorating climate, inundating the shelf while eroding, reworking and submerging dunes on the shelf. Extensive reworking of the coastal sediments during the transgression produced Unit D1 (11 - 19 ka; Figure 7.3 f). Unit D1 is a dark brown to dark yellowish brown, well sorted, calcareous unconsolidated lower medium sand. It is characterised by quartz (10 - 58 %), calcite (1 - 25 %) and interstratifications (14 - 34 %) dominating the clay-fraction, intermediate to high HAEM (20 - 42 %) within the silt-fraction, low to intermediate fines (1 - 19 %), low to high carbonate content (0.5 - 9 %) and moderate degrees of grain weathering (CIA = 23 - 78; Magn / Ilm 0.05 - 0.48; EHM / THM 0.13 - 0.47). This unit is most likely of distal aeolian origin and is correlated to the Sibayi Formation.

The onset of the Holocene was dominated by a transgressive moist lacustrine period (Scholtz, 1986; Deacon & Lancaster, 1988) as sea-level stabilised to today's level resulting in the deposition (at *ca.* 11 - 5 ka) and later reworking (at *ca.* 2.1 ka) of Unit D2. Unit D2 is a dark yellowish brown, well sorted, unconsolidated calcareous upper fine to lower medium sand. It is characterised by quartz (20 - 56 %) and calcite (10 - 61 %) dominating the clay-fraction, intermediate to high HAEM (15 - 50 %) within the silt-fraction, low fines (1 - 4 %), intermediate to high carbonate content (3 - 8 %) and slight degrees of grain weathering (CIA = 23 - 35; Magn / Ilm 0.07 - 0.44; EHM / THM 0.05 - 0.37). This transgressive unit is

Table 7.1 Summary of discriminative characteristics and interpretation of the eight sedimentological units defined in the central Zulti North lease. Note: Colours are given in the moist state in accordance to the Munsell Colour (2001) System. Average grain size is presented as Upper Medium (U.M. = 350 - 500 μm), Lower Medium (L.M. = 250 - 350 μm), Upper Fine (U.F. = 177 - 250 μm) & Lower Fine (L.F. = 125 - 177 μm). Weath. = Weathering, Int. = Intermediate, Mod. = Moderate. HAEM = High Atomic Element Minerals. CIA = Chemical Index of Alteration. EHM = Economic Heavy Minerals, THM = Total Heavy Minerals, Magn = Magnetite + ilmenite, Ilm = Ilmenite & Zr = Zirconium. * Not recognised by South Africa Committee for Stratigraphy.

Units	Clay-fraction	Silt-fraction		Bulk sample										Facies interpretation	Approx. Age (ka)		Litho-strati-graphy*
	Composition	HAEM	Grain weath.	Colour	% Fines	Grain size	Grain sorting	CO_3^{2-}	TiO_2/ MgO	CIA	EHM/ THM	Magn / Ilm	Zr		deposition	reworking	
F	Quartz, interstrat., smectite, calcite & collophane	Low - Int.	Slight	Dark yellowish brown	Low	U. M. Sand	Well	Low - Int.	Low	Low	Low	High	Int. - Low	Aeolian dune proximal	1.1	0.15	Silbayi Formation
E	Smectite, calcite, collophane & goethite	Low - Int.	Slight	Dark yellowish brown	Low	L. M. Sand	Well - Mod. well	Low	Int.	Int.	Low	High	Int. - High	Aeolian dune transgressive & proximal shallow marine	3.0 ?	< 1.1	
D2	Calcite & quartz	Low - High	Slight	Dark yellowish brown	Low	U. F. - L. M. Sand	Well	Int. - High	Low	Low	Low	High	Low - Int.	Aeolian dune transgressive proximal/distal	5 - 11	2.1	
D1	Quartz, calcite & interstratification	Int. - High	Moderate	Dark brown - Dark yellowish brown	Low - Int.	L. M. Sand	Well	Low - High	Int. - High	Low - Int.	Low	High	Low - Int.	Aeolian dune transgressive distal	11 - 19	0.04 - 6.5	
A4	Quartz, goethite, interstratification & kaolinite	Int. - High	Moderate - High	Dark yellowish brown - Red	Low - Int.	L. F. - L. M. Sand	Well - Poor	—	Int. - High	Int.	Int.	Int. - High	Low - High	Aeolian dune regressive / transgressive distal. Local fluvial inputs	19 - 29	5 - 10	
A2	Goethite, quartz interstratification & kaolinite	High	High - Extreme	Dark brown - Yellowish brown	Int. - High	U. F. - L. M. Sand	Mod. well	—	Int.	Int.	Int.	Int.	Int.	Aeolian dune regressive distal. Local fluvial inputs ?	130 - 190		KwaMbonambi Formation
A0	Goethite, interstratification & kaolinite	High - Extreme	High - Extreme	Strong brown - Yellowish brown	High - Very High	L. M. Sand	Mod.	—	High - Extreme	Int. - High	Int. - High	Int.	Extreme	Aeolian dune transgressive distal	190 - 250 ?		
K	Kaolinite	Low	Extreme	Yellowish brown - Light olive grey	Very High	U. F. Sand	Poor	—	High	High	High	Low	Low - High	Aeolian dune regressive / transgressive distal, lagoonal, fluvial ?	250 - 350		Kosi Bay Formation

of probable distal/proximal aeolian origin and is correlated to the Sibayi Formation.

The mid-Holocene highstand resulted in only minor reworking as the higher temperatures experienced promoted proliferation of vegetation and thus dune stability. Sea-level briefly fell to - 2 m at *ca.* 3 ka whereupon Unit E was deposited initially as shallow marine sediments and consequently as transgressive dune sediments. Unit E is a dark yellowish brown, well to moderately well sorted, unconsolidated calcareous lower medium sand. It is characterised by smectite (10 - 60 %), calcite (1 - 18 %), collophane (1 - 20 %) and goethite (13 - 20 %) dominating the clay-fraction, low to intermediate HAEM (16 - 31 %) within the silt-fraction, low fines (*ca.* 4 %), low carbonate content (*ca.* 0.5 %) and slight degrees of grain weathering (CIA = 58 - 65; Magn / Ilm 0.09 - 0.18; EHM / THM 0.07 - 0.45). The presence of smectite and carbonates are in agreement with its Holocene age as the moderate alkalinity, caused by calcite, favours the formation of smectite and encourages flocculation and thus retards clay migration (Chamley, 1989; Birkeland, 1984; Tinley, 1986). Smectite is a typical Holocene clay mineral formed under a humid sub-tropical climate, which with time, would be leached to form kaolinite as found in the older units (Chamley, 1989; Birkeland, 1984). This unit was consequently reworked less than 1.1 ka and is correlated to the Sibayi Formation.

Unit F represents the most coastal and recent proximal dune accretion within the study area being deposited at *ca.* 1.1 ka and reworked in modern times (150 BP). Unit F is a dark brown to dark yellowish brown, well sorted, unconsolidated calcareous lower medium sand. It is characterised by quartz (20 - 44 %), interstratifications (8 - 23 %), smectite (0 - 14 %), calcite (5 - 12 %) and collophane (0 - 28 %) dominating the clay-fraction, low to intermediate HAEM (10 - 30 %) within the silt-fraction, low fines (*ca.* 2 %), low to intermediate bulk carbonate content (0.8 - 4.4 %) and slight degrees of grain weathering (CIA = 32 - 57; Magn / Ilm 0.10 - 0.24; EHM / THM 0.05 - 0.40). The source of collophane is debatable (Section 3.4), nevertheless its presence, together with calcite and smectite, indicates a relatively young age as these minerals would be leached rapidly under prevailing climatic conditions. This unit is correlated to the Sibayi Formation.

7.1 CONCLUSIONS

The composition/mineralogy and abundance of clay and silt within the ZNL positively identifies eight sedimentological units previously identified from the sand-fraction (Sudan, 1999). Depositional environments were difficult to determine from the fines especially in the more weathered units as *in situ* clay formation alters the grain size and surface morphology characteristics. Variations within the fines

provides greater discrimination to the Holocene units and resulted in the youngest Unit F being differentiated from the underlying Unit E. The early-Pleistocene Unit K is the oldest unit in the study area (250 - 350 ka) and is correlated to the Kosi Bay Formation, consisting of a semi-consolidated clayey sand. The semi-consolidated mid-Pleistocene KwaMbonambi Formation is represented by Units A0 and A2 respectfully and is overlain by the unconsolidated late-Pleistocene to Holocene Sibayi Formation; which is older than previous considered.

The northern KwaZulu-Natal coastal dune cordon has undergone numerous phases of dune accretions and destructions during the Quaternary, generally in response to climatic changes brought on by glacial events. Glacial periods represents dune building phases as sea-level was lower causing the shelf to be exposed, the climate was drier resulting in less vegetation, and the wind regime was higher, which together with sparser vegetation, allowed greater sand mobility. Conversely interglacial periods resulted in dune stability and *in situ* clay formation due to weathering.

This study has shown that weathering resulting in clay mineral formation is fundamental to resolving the complex stratigraphy of the dune cordon. Although this study only represents some dunes, the results are encouraging and should be applicable throughout the northern KwaZulu-Natal coastal dune cordon and perhaps in similar aeolian environments abroad.

REFERENCES CITED

Allen, P.A. (1997). *Earth Surface Processes.* Blackwell Science, Oxford, 404 pp.

Allsopp, H.L., Manton, W.I., Bristow, J.W. & Erlank, A.J. (1984). Rb-Sr Geochronology of Karoo Felsic Volcanics. *Spec. Publ. geol. Soc. S. Afr.*, **13**, 273-280.

Assallay, A.M., Rogers, C.D.F., Smalley, I.J. & Jefferson, I.F. (1998). Silt: 2 - 62 μm, 9 - 4 ϕ. *Earth-Science Reviews*, **45**, 61-88.

Avery, D.M. (1982 a). Micromammals as palaeoenvironmental indicators and an interpretation of the late Quaternary in the southern Cape Province, South Africa. *Annals of the South African Museum*, **85**, 183-374.

Avery, D.M. (1982 b). The micromammalian fauna from Border Cave, KwaZulu, South Africa. *Journal of Archaeological Science*, **9**, 187-204.

Bailey, S.W. (1980 a). Structures of layer silicates. *In*: Brindley, G.W., Brown, G., Eds.,*Crystal structures of clay minerals and their X-ray identification.* Mineral. Soc. Monograph No. 5, London, 495 pp.

Bailey, S.W. (1980 b). Summary of recommendations of AIPEA nomenclature committee on clay minerals. *Am. Mineral*, **65**, 1-7.

Bailey, S.W. (1988). Introduction. *Reviews of Mineralogy*, Mineralogical Society of America, Washington, **19**, 1-8.

Battey, M.H. (1981). *Mineralogy for students, 2nd edition.* Longman Scientific & Technical, UK, 355 pp.

Begg, G.W. (1978). The estuaries of Natal. *Natal Town and Regional Planning Project*, **41**, 657 pp.

Berner, R.A. & Holdren, G.R. Jr (1979). Mechanism of feldspar weathering - II. Observations of feldspars from soils. *Geochimica et Cosmochimica Acta*, **43**, 1173-1186.

Berner, R.A. & Schott, J. (1982). Mechanisms of pyroxene and amphibole weathering II. Observations of soil grains. *Am. J. Sci.*, **282**, 1214-1231.

Birkeland, P.W. (1984). *Soils and Geomorphology.* Oxford University Press, New York, 372 pp.

Blatt, H. (1987). Oxygen isotopes and the origin of quartz. *J. Sed. Petrol.*, **57**, 373-377.

Botha, G.A. (1997 a). The Maputaland Group: a provisional lithostratigraphy for coastal KwaZulu-Natal. *In: Maputaland focus on the Quaternary evolution of the south-east African costal plain* (Ed.). International Union for Quaternary Research Workshop Abstracts, Council for Geoscience, Private Bag X112, Pretoria, South Africa, 21-26.

Botha, G.A. (1997 b). Do all people "see" the same colours? *In: Maputaland focus on the Quaternary evolution of the south-east African costal plain* (Ed.). International Union for Quaternary Research Workshop Abstracts, Council for Geoscience, Private Bag X112, Pretoria, South Africa, pg 87.

Brindley, G.W. & Brown, G. (1980). Crystal structures of clay minerals and their X-ray identification. *Mineral. Soc. Monograph No. 5*, London, 495 pp.

Butzer, K.W., Stuckenrath, R., Bruzewicz, A.J. & Helgren, D.M. (1978). Late Cenozoic paleoclimates of the Gaap Escarpment, Kalahari margin, South Africa. *Quaternary Research*, **10**, 310-339.

Byström-Brusewitz, A.M. (1975). Studies of the Li test to distinguish beidellite from montmorillonite. *Proceedings International Clay Conf., 1972, Mexico City.* Applied Publishing, Wilmette, Ill., 419-428.

Chamley, H. (1989). *Clay Sedimentology.* Springer-Verlag, Berlin, 623 pp.

Chappell, J. & Shackleton, N.J. (1986). Oxygen isotopes and sea level. *Nature*, **324**, 137-140.

Charlesworth, E.G. (1981). *Tectonics and metamorphism of the northern margin of the Namaqua-Natal Mobile Belt, near Eshowe, Natal.* PhD. thesis (unpubl.), University of Natal, 433 pp.

Clark, R.J. (1998). The geological structure of the Zulti North ore body from heavy mineral abundance ratios. Hons. thesis (unpubl.), University of Natal, 140 pp.

Cooper, M.R. (1988). A new species of trigoniid bivalve from the Lower Cretaceous (Albian) of Zululand. *S. Afr. J. Geol.*, **91**, 326-328.

Cooper, J.A.G. (1991). *Sedimentary Models and Geomorhological Classification of River-Mouths on a Subtropical, Wave-Dominated Coast, Natal, South Africa.* PhD. thesis (unpubl.), University of Natal, Durban, 401 pp.

Davies, J.L. (1964). A morphogenic approach to world shorelines. *Zeitschr. für Geomorphol.*, **8**, 27-42.

Davies, O. (1975). The older coastal dunes in Natal and Zululand and their relation to former shorelines. Proc. S. Afr. Soc. Quat. Res. 1976, *Ann. S. Afr. Mus.*, **71**, 19-32.

Deacon, J & Lancaster, N. (1988). *Late Quaternary Palaeoenvironments of Southern Africa.* Clarendon Press, Oxford, 225 pp.

Deer, W.A., Howie, R.A. & Zussman, J. (1992). *An introduction to the rock-forming minerals, 2nd edition.* Longman Scientific & Technical, UK, 549 pp.

Dingle, R.V. (1981). The Campanian and Maastrichtian ostracods of south east Africa. *Ann. S. Afr. Mus.*, **85**, 1-181.

Dunlevey, J.N. (1997). The Berea Red Sands. *Heavy Minerals 1997.* S.A. Inst. of Mining & Metallurgy, JHB., 237-240.

Du Toit, A.L. (1921). The Karoo Dolerites of South Africa: A Study in Hypabyssal Injection. *Trans. geol. Soc. S. Afr.*, **23** (1920), 1-42.

Du Toit, A.L. (1954). *Geology of South Africa., 3rd Edn.* Oliver and Boyd, Edinburgh, 611 pp.

Eales, H.V., Marsh, J.S. & Cox, K.G. (1984). The Karoo Igneous Province: An Introduction. *Spec. Publ. geol. Soc. S. Afr.*, **13**, 1-26.

Eglington, B.M., Harmer, R.E. & Kerr, A. (1989). Isotope and Geochemical Constraints on Proterozoic Crustal Evolution in South-Eastern Africa. *Precambrian Research*, **45**, 159-174.

Encarnación, J., Flemming, T.H., Elliot, D.H. & Eales, H.V. (1996). Synchronous emplacement of Ferrar and Karoo dolerites and the early breakup of Gondwana. *Geology*, **24(6)**, 535-538.

Flemming, B.W. (1981). Factors Controlling Shelf Sediment Dispersal Along the Southeast African Continental Margin. *Marine Geology*, **42**, 259-277.

Flemming, B.W. & Hay, R. (1988). Sediment distribution and dynamics of the Natal continental shelf. *In:*

Schumann, E.H. (Ed). *Coastal Ocean studies off Natal.* Lecture Notes on Coastal and Estuarine Studies, 26. Spinger-Verlag, Berlin, 47-49.

Fockema, P.D. (1986). The heavy mineral deposits north of Richards Bay. *In:* Anhaeusser, C.R & Maske, S. (Eds). *Mineral Deposits of South Africa.* Geol. Soc. S. Afr., Johannesburg, 2301-2307.

Folk, R.L. & Ward, W.C. (1957). Brazos River Bar: A study in the significance of grain size parameters. *J. Sed. Petrol.*, **27**, 3-26.

Friedman, G.M. (1961). Distinction between dune, beach and river sands from their textural characteristics. *J. Sed. Petrol.*, **31**, 514-529.

Friedman, G.M. (1979). Address of the retiring president of the International Association of Sedimentologists: differences in size distributions of populations of particles among sands of various origins. *Sedimentology*, **26**, 3-32.

Gibbs, R.J. (1965). Error due to segregation in quantitative clay mineral X-ray diffraction mounting techniques. *Amer. Mineral*, **50**, 741-751.

Goodlad, S.W. (1986). Tectonic and sedimentary history of the mid-Natal Valley (S.W. Indian Ocean). *Joint Geological Survey/UCT Mar. Geol. Bull.*, **15**, 415 pp.

Goodman, P.S. (1990). *Soil, vegetation and large herbivore relations in Mkuzi Game Reserve, Natal.* PhD. thesis (unpubl.), University of Witwatersrand, JHB, 324 pp.

Grab, S. (2000). Periglacial Features. *In:* Partridge, T.C. & Maud, R.R. (Eds.) *The Cenozoic of southern Africa.* Oxford University Press, 207-217 pp.

Griffiths, J.C. (1967). *Scientific Method in Analysis of Sediments.* McGraw-Hall, New York, 508 pp.

Grim, R.E. (1968). *Clay Mineralogy.* McGraw-Hill, New York, 596 pp.

Hammerbeck, E.C.I. (1976). Titanium. *In:* Coetzee, C.B. (Ed.) *Mineral resources of the Republic of South Africa. Geol. Surv. S. Afr. Handbook 7, 5th ed.*, 221-226.

Harnois, L. (1988). The CIW Index: A new chemical index of weathering. *Sed. Geol.*, **55**, 319-322.

Hayes, M.O. (1979). Barrier island morphology as a function of tidal and wave regime. *In:* Leatherman, S.P. (Ed.) *Barrier islands from the Gulf of Mexico.* Academic Press, New York, 3-22.

Henderson, P. (1982). *Inorganic geochemistry.* Pergamon Press, Oxford, 353 pp.

Hegner, E., Kröner, A. & Hofman, A.W. (1993). Trace elements and isotopic constraints of the origin of Archaean Pongola and Usushwana Igneous Suites in Swaziland. *Abstracts Africa Geocongress, Swaziland.*

Howard, W.R. (1985). Late Quaternary Southern Indian Ocean circulation. *S. Afr. J. Sci.*, **81**, 253-254.

Hugo, V.E. (1990). The relative abundance and alteration of iron-titanium oxides along the South African coastline. *Abstracts Geocongress '90, Geol. Soc. S. Afr., Cape Town*, 261-264.

Hugo, V.E. (1993). *A study of titanium-bearing oxides in heavy mineral deposits along the east coast of South Africa.* PhD. thesis (unpubl.), University of Natal, 357 pp.

Hunter, I.T. (1988). Climate and Weather off Natal. *In:* Schumann, E.H. (Ed). *Coastal Ocean studies off Natal.* Lecture Notes on Coastal and Estuarine Studies, 26. Spinger-Verlag, Berlin, 81-100.

Jackson, M.L. (1959). Frequency distribution of clay minerals in major soil groups as related to factors of soil formation. *Clays Clay Mineral.*, **6**, 133-143.

Johnson, C.H. (1986). The geology of the Zululand titanium deposits. *Abstracts Geocongress '86. Geol. Soc. S. Afr.*, JHB., 417-420.

Johnson, M.R. (1976). *Stratigraphy and sedimentology of the Cape and Karoo Sequences in the eastern Cape Province*: PhD. thesis (unpubl.), Rhodes University, 336 pp.

Johnson, M.R. (1984). The Geology of the Queenstown Area: Expl. Sheet 3126 (Queenstown). *Geol. Surv. S. Afr.*, 21 pp.

Joussaume, S. & Taylor, K.E. (1995). Status of the Palaeoclimate Modelling Intercomparison Project (PMIP). WCRP report, proc. *First Int. AMIP. Sci. Conf.*, **92**, 425-430.

Kaldi, J., Krinsley, D.H. & Lawson, D. (1978). Experimentally produced aeolian surface textures on quartz sand grains from various environments. *In:* Whalley, W.B. (Ed.) *Scanning electron microscopy in the study of sediments*. Geo Abstracts, Norwich, England, 261-274.

Kennedy, W.J. & Klinger, H.C. (1975). Cretaceous faunas from Zululand and Natal, South Africa. Introduction, Stratigraphy. *Bull. Brit. Mus. Nat. Hist.*, **25(4)**, 265-315.

King, L.C. & Maud, R.R. (1964). *The geology of Durban and Environs. Geological Survey Bulletin Number 42.* Government Printer, Pretoria, South Africa, 55 pp.

Klinger, H.C. & Kennedy, W.J. (1990). Metaplacenticeras subtilstriatum (Jimbo, 1894), (Cephalopoda: Ammonoidea) from the St. Lucia Formation (Cretaceous), Zululand. *S. Afr. J. Geol.*, **93**, 443-445.

Krinsley, D.H. & Donahue, J. (1968). Environmental interpretation of sand grain surface textures by electron microscopy. *Bulletin of the Geological Society of America*, **79**, 743-748.

Krinsley, D.H. & Doornkamp, J.C. (1973). *Atlas of quartz sand surface textures.* Cambridge University Press, 91 pp.

Krinsley, D.H. & Smalley, I.J. (1973). The shape and nature of small sedimentary quartz particles. *Science*, **180**, 1227-1279.

Krinsley, D.H. & McCoy, F. (1978). Aeolian quartz and silt. *In:* Whalley, W.B. (Ed.) *Scanning electron microscopy in the study of sediments*. Geo Abstracts, Norwich, England, 249-260.

Kuenen, P. H. (1969). Origin of quartz silt. *J. Sed. Petrol.*, **39**, 1631-1633.

Lee, M.R., Hodson, M.E. & Parsons, I. (1998). The role of intragranular microtextures and microstructures in chemical and mechanical weathering: Direct comparisons of experimentally and naturally weathered alkali feldspar. *Geochimica et Cosmochimica Acta*, **62**, 2771-2788.

Lee, M.R. & Parsons, I. (1995). Microtextural controls of weathering of perthitic alkali feldspars. *Geochimica et Cosmochimica Acta*, **59**, 4465-4488.

Lees, B.G., Lu, Y & Head, J. (1990). Reconnaissance thermoluminescence dating of northern Australian coastal dune systems. *Quat. Res.*, **34**, 169-185.

Le Ribault, L. (1978). Exoscopy of quartz sand grains. *In:* Whalley, W.B. (Ed.) *Scanning electron microscopy in the study of sediments*. Geo Abstracts, Norwich, England, 319-328.

Le Roux, J.S. (1990). Spatial variations in the rate of fluvial erosion (sediment production) over South Africa. *Water South Africa*, **16**, 185-194.

Lin, I.J., Rohrlich, V. & Slatkine, A. (1974). Surface microtextures of heavy minerals from the Mediterranean coast of Israel. *Society of Economic Paleontologists and Mineralogists,* 1282-1295.

Linström, W. (1987). The Geology of the Dundee Area. Expl. Sheet 2830 (Dundee). *Geol. Surv. S. Afr.*, 52 pp.

Linström, W & Marshall, C.G.A. (1982). The geology of areas 2731A&C. *Geol. Surv. S. Afr.* (unpubl.).

Liu, K.W. (1995). Diagenesis of the Neogene Uloa Formation of Zululand, South Africa. *S. Afr. J. Geol.,* **98(1)**, 25-34.

Marshall, C.G.A & von Brunn, V. (1999). The Stratigraphy and Origin of the Natal Group. *S. Afr. J. Geol.,* **102(1)**, 15-25.

Martyn, D. (1992). Climates of the World. *Developments in Atmospheric Science*, **18**, 251-256.

Mason, C.C. & Folk, R.L. (1958). Differentiating of beach, dune, and aeolian flat environments by size analysis, Mustang Island, Texas. *J. Sed. Petrol.*, **28/2**, 211-226.

Matthews, P.E. (1959). The Metamorphism and Tectonics of the Pre-Cape Formation in the Post-Ntingwe Thrust-Belt, S.W. Zululand, Natal. *Trans. geol. Soc. S. Afr.*, **62**, 257-322.

Matthews, P.E. (1981). Eastern or Natal Sector of the Namaqua-Natal Mobile Belt in Southern Africa. *In:* Hunter, D.R. (Ed.) *Precambrian of the Southern Hemisphere.* Elsevier, Amsterdam, 705-715.

Maud, R.R. (1968). Quaternary geomorphology and soil formation in coastal Natal. *Zeitschrift für Geomorphologie N.F.,* 7, 155-199.

Maud, R.R. (1980). The climate and geology of Maputaland. *In:* Bruton, M.N. & Cooper, K.H. (Eds.) *Studies on the Ecology of Maputaland.* Rhodes University and the Natal branch of the Wildlife Society of Southern Africa, 1-7.

Maud, R.R. (1993). Port Durnford Formation. *In: Quaternary Geology of the Natal and Zululand Coast, South Africa.* IUCS, UNESCO, Council for Geoscience, Private Bag X112, Pretoria, South Africa, pg 12.

Maud, R.R. & Orr, W.N. (1975). Aspects of post-Karoo geology in the Richards Bay area. *Trans. geol. Soc. of S. Afr.*, **78**, 101-109.

Maud, R.R.& Botha, G.A. (2000). Macro-scale geomorphic evolution of southern Africa. *In:* Partridge, T.C. & Maud, R.R. (Eds.) *The Cenozoic of southern Africa.* Oxford University Press, 3-32 pp.

McCormick, S., Cooper, J.A.G., & Mason, T.R. (1992). Fluvial sediment yield to the Natal coast: a review. *S. Afr. J. aquat. Sci.*, **18(½)**, 74-88.

McMillan, I.K. (1997). Quaternary sub-surface stratigraphy of the Maputaland coastal plain. *In:* Botha, G.A. (Ed.) *Maputaland focus on the Quaternary evolution of the south-east African costal plain.* International Union for Quaternary Research Workshop Abstracts, Council for Geoscience, Private Bag X112, Pretoria, South Africa, 21-26.

Mejdahl, V. (1985). Thermoluminescence dating based on feldspars. *Nuclear Tracks and Radiation Measurements*, **10**, 133-136.

Méring, J. (1949). L'Intérference des Rayons X dans les systems á stratification désordonnée. Acta Crystallogr.,

2, 371-377.

Meth, D.L. (1996). *The geology and geochemistry of the Rooi Rand dyke swarm.* MSc. thesis (unpubl.), University of Natal, 190 pp.

Milliman, J.D. & Emery, K.O. (1968). Sea-levels during the past 35 000 years. *Science*, **162**, 1121-1123.

Milliman, J.D. & Meade, R.H. (1983). World-wide delivery of river sediments to the oceans. *Journal of Geology*, **91**, 1-21.

Minarik, L., Absolon, D., Kollnerova, K & Klecka, A. (1983). Chemical changes of granite during its weathering. *In:* Augustithis, S.S. (Ed.) *Leaching and diffusion in rocks and their weathering products.* Theophrastus Publishing & Proprietary Co., S.A., Athens, Greece, 562 pp.

Moiola, R.J. & Weiser, D. (1968). Textural parameters: an evaluation. *J. Sed. Petrol.*, **38**, 45-53.

Moore, D.M. & Reynolds, R.C. Jr. (1989). *X-ray diffraction and the identification and analysis of clay minerals.* Oxford University Press, New York, 378 pp.

Munsell (2000). *Munsell soil colour charts, year 2000 revised washable edition.* GretagMacbeth, New York.

Nahon, D. (1986). Evolution of iron crusts in tropical landscapes. *In:* Colman, S.M. & Dethier, D.P. (Eds.) *Rates of chemical weathering of rocks and minerals.* Academic Press, New York, London, 169-191.

Nanson, G.C., Chen, X.Y., Price, D.M. (1992). Lateral migration thermoluminescence chronology and colour variation of longitudinal dunes near Birdsville in the Simpson Desert central Australia. *Earth Surface Processes and Landforms*, **17**, 807-819.

Nealson, K. H. (1983). The microbial iron cycle. *In:* Krumbein, W.E. (Ed.) *Microbial Geochemistry.* Blackwell Scientific Publications, 159-190.

Nemecz, E. (1981). *Clay Minerals.* Akadémiai Kiadó, Budapest, 547 pp.

Nesbitt, H.W. & Young, G.M. (1982). Early Proterozoic climates and plate motion inferred from major element chemistry of lutites. *Nature*, **299**, 715-717.

Nicholson, J. (1983). Sedimentary aspects of the Mvumase Project. *In:* McLachlan, A. & Erasmus, T. (Eds.) *Sandy beaches as ecosystems.* Dr. W. Junk, The Hague, 191-197.

Nicholson, S.E. & Flohn, H. (1980). African environmental and climatic changes and the general atmospheric circulation in the Late Pleistocene and Holocene. *Climatic Change*, **2**, 313-348.

Nixon, R.A. (1979). Differences in incongruent weathering of plagioclase and microcline - cation leaching versus precipitates. *Geology*, 7, 221-224.

Nordstrom, C.E. & Margolis, S.V. (1972). Sedimentary history of central California shelf sands as revealed by scanning electron microscopy. *J. Sed. Petrol.*, **42/3**, 527-536.

Novich, B.E. & Martin, R.T. (1983). Solvation methods for expandable clays. *Clays Clay Mineral*, **31**, 235-238.

Oschadleus, H.D., Vogel, J.C., & Scott, L. (1996). Radiometric date of the Port Durnford peat and development of yellow-wood forest along the South African east coast. *S. Afr. J. Sci.*, **92**, 43-45.

Parker, A. (1970). An index of weathering for silicate rocks. *Geol. Mag.*, **107**, 501-504.

Partridge, T.C. & Maud, R.R. (1987). Geomorphic evolution of southern Africa since the Mesozoic. *S.Afr. J. Geol.*, **90(2)**, 179-208.

Pietersen, K. J. (1992). *Richards Bay Zircon*. MSc. thesis (unpubl.), University of Natal, 158 pp.

Pooley, E. (1994). *The complete field guide to trees of Natal, Zululand and Transkei.* Natal Flora Publications Trust, 512 pp.

Pooley, E. (1998). *A field guide to wild flowers KwaZulu-Natal and the Eastern Region.* Natal Flora Publications Trust, 630 pp.

Pye, K. (1981). Rate of dune reddening in a humid tropical climate. *Nature*, **290**, 582-584.

Pye, K. (1983). Formation of quartz silt during humid tropical weathering of dune sands. *Sediment. Geol.*, **34**, 267-282.

Pye, K. (1993). Late Quaternary development of coastal parabolic megadune complexes in northeastern Australia. *Spec. Publs. Int. Ass. Sediment*, **16**, 23-44.

Ramsay, P.J., Cooper, J.A.G., Wright, C.I. & Mason, T.R. (1989). The occurrence and formation of ladderback ripples in subtidal, shallow marine sands, Zululand, South Africa. *Mar. Geol.*, **86**, 229-235.

Ramsay, P.J. (1994). Marine geology of the Sodwana Bay shelf, southeast Africa. *Marine Geology*, **120(3/4)**, 225-247.

Ramsay, P.J. (1995). 9000 Years of Sea-level change along the southern African coastline. *Quaternary International*, **31**, 71-75.

Ramsay, P.J. (1996). *Quaternary Marine Geology of the Sodwana Bay Continental Shelf, Northern KwaZulu-Natal. Bulletin 117*, Council for Geoscience, Pretoria, 85 pp.

Ramsay, P.J. (1997). Quaternary Marine Geology and Sea-level Changes: Sodwana Bay Shelf. *In:* Botha, G.A. (Ed). *Maputaland focus on the Quaternary evolution of the south-east African coastal plain*. International Union for Quaternary Research Workshop Abstracts, Council for Geoscience, Private Bag X112, Pretoria, South Africa, 53-56.

Ramsay, P.J. (1999). Sea-level changes in the Quaternary and the potential for offshore heavy mineral placer deposits on the southeast African shelf. *In:* Stimson, R.G. (Ed). *Heavy Minerals 1999*. The South African institute of mining and metallurgy, symposium series S23, Johannesburg, 11-13.

Rasband, W. (2000). ImageJ1.16f software. National Institutes for Health, USA (wayne@codon.nih.gov or http://rsb.info.nih.gov/ij).

Reiche, P. (1943). Graphic representation of chemical weathering. *J. Sed. Petrol.*, **13**, 58-68.

Retsch Technology. (2000). Crystalsizer particle sizer. www.retsch.de.

Reynolds, R.C. (1980). Interstratified clay minerals. In: Brindley, G.W., Brown, G. (Eds.)*Crystal structures of clay minerals and their X-ray identification*. Mineral. Soc. Monograph No. 5, London, 249-303.

Roaldset, E. (1972). Mineralogy and geochemistry of Quaternary clays in the Numedal area, southern Norway. *Norsk Geol. Tidsskr.*, **52**, 335-369.

Roberts, D.L. (1981). *The Stratigraphy and Sedimentology of the Natal Group in the Durban Area*. MSc. thesis (unpubl.), University of Natal, 118 pp.

Rossouw, J. (1984). *Review of existing wave data, wave climate and design waves for South African and South West African (Namibian) coastal waters.* CSIR Report T/SEA 8 401, Stellenbosch, 61 pp.

Saggerson, E.P., Bristow & J.W. Armstrong, R.A. (1983). The Rooi Rand dyke swarm. *S. Afr. J. Sci.*, **79**, 365-369.

Scholtz, A. (1986). *Palynological and palaeobotanical studies in the southern Cape.* MA. thesis (unpubl.), University of Stellenbosch, 280 pp.

Schink, J.C., Stockwell, J.H. & Ellis, R.A. (1979). An improved device for gasometric determination of carbonate in sediment. *Jour. Sed. Petr.*, **49**, 651-653.

Schumann, E.H. & Orren, M.J. (1980). The physio-chemical characteristics of the south-west Indian Ocean in relation to Maputaland. *In:* Bruton, M.N. & Cooper K.H. (Eds.). *Studies on the Ecology of Maputaland.* Wildlife Society of South Africa, Durban, 8-11.

Schumann, E.H. (1988). Physical Oceanography off Natal. *In:* Schumann, E.H. (Ed). *Coastal Ocean studies off Natal. Lecture Notes on Coastal and Estuarine Studies, 26.* Spinger-Verlag, Berlin, 101-130.

Schwertmann, U. & Taylor, R.M. (1977). Iron oxides. *In:* Dixon, J.B. & Weed, S.B. (Eds.). *Minerals in soil environments.* Soil Science Society of America, Madison, Wisc., 145-180.

Scott, L., Cooremans, B., & Maud, R.R. (1992). Preliminary palynological evaluation of the Port Durnford Formation at Port Durnford, Natal, South Africa. *S. Afr. J. Sci.*, **88**, 470-474.

Setlow, L.W. (1978). Age determination of reddened coastal dunes in northwest Florida, USA, by the use of scanning electron microscopy. *In:* Whalley, W.B. (Ed.) *Scanning electron microscopy in the study of sediments.* Geo Abstracts, Norwich, England, 283-305.

Singh, V. (1995). *Mineral stratigraphy of the Kosi Bay Formation.* MSc. thesis (unpubl.), University of Durban-Westville, 171 pp.

Singh, V. & Dunlevey, J.N. (1997). Mineral stratigraphy of the Kosi Bay Formation, northern KwaZulu-Natal. *Heavy Minerals 1997.* S.A. Inst. of Mining & Metallurgy, JHB., 251-254.

Smart, P & Tovey, N.K. (1981). *Electron microscopy of soils and sediments: examples.* Clarendon Press, Oxford, 177 pp.

Smalley, I.J. & Krinsley, D.H. (1974). Quartz cleavage and quick clays. *Science*, **184**, 183-184.

Schwertmann, U. & Taylor, R.M. (1977). Iron oxides. *In:* Dixon, J.B. & Weed, S.B. (Eds.) *Minerals in soil environments: Soil Science Society of America, Madison, Wisc.*, 145-180.

South African Committee for Stratigraphy (SACS) (1980). Stratigraphy of South Africa. Part 1 (Comp. L. E. Kent). Lithostratigraphy of the Republic of South Africa, South West Africa/Namibia, and the Republics of Bophuthatswana, Transkei and Venda. *Handb. geol. Surv. S. Afr.*, **8**, 690 pp.

South African Tide Tables (1997). *The Hydrographer.* South African Navy, Private Bag X1, Tokai, 7966, 259 pp.

South African Weather Bureau. (1986). *Climate of South Africa, Climate Statistics up to 1984.* Government Printer, Pretotia.

Stewart, J. (1998). *The Geology of the Uloa Formation, Richards Bay.* Hons. thesis (unpubl.), University of Natal, Durban, 73 pp.

Stokes, S. (1992). Optical dating of young (modern) sediments using quartz: results from a selection of

depositional environments. *Quaternary Science Reviews*, **11**, 153-159.

Stokes, S., Haynes, G., Thomas, D.S.G., Horrocks, J.L., Higginson, M., Malifa, M. (1998). Punctuated aridity in southern Africa during the last glacial cycle: the chronology of linear dune construction in the northeastern Kalahari. *Palaeogeography, Palaeoclimatology, Palaeoecology*, **137**, 305-322.

Sudan, P. (1999). *Sedimentology, stratigraphy and geological history of part of the northern KwaZulu-Natal coastal dune cordon, South Africa.* MSc. thesis (unpubl.), University of Natal, 181 pp.

Surfer (1999). Surfer Version 7.0, surface mapping system, *Golden Software Inc.*, 809 14th Street Golden, Colorado, USA, 80401-1866 (http://www.goldensoftware.com).

Swart, D.H. (1980). *Effect of Richards Bay Harbour development on the adjacent coastline.* CSIR Research Report T/SEA 8015, Stellenbosch, 40 pp.

Swart, D.H. (1987). *Erosion of a Manmade Dune, Beachwood Mangrove Nature Reserve.* CSIR Research Report T/SEA 8713, Stellenbosch, 28 pp.

Swart, D.H. & Serdyn, J. de V. (1981). *Statistical Analysis of Visually Observed Wave data from Voluntary Observing Ships for South African East Coast.* Volume 9. Unpublished CSIR Report, 141 pp.

Tankard, A.J. (1976). Cenozoic sea-level changes, a discussion. *Annals of the South African Museum*, **71**, 1-17.

Tankard, A.J., Jackson, M.P.A., Eriksson, K.A., Hobday, D.K., Hunter, D.R. & Minter, W.E.L. (1982). *Crustal evolution of Southern Africa (3,8 billion years of earth history).* Springer-Verlag, New York, 523 pp.

The Air Survey Co. (1986). Air photography number 16-3-3, SUR 100/86, taken on the 12/5/1986, scale 1:150 000.

Thomas, R.J., Bullen, W.D., de Klerk, I., Scogings, A.J. (1990). The distribution and genesis of precious and base metal mineralization in the Natal Metamorphic Province, South Africa. *S. Afr. J. Geol.*, **93**, 683-695.

Thomas, R.J. & Eglington, B. M. (1990). A Rb-Sr, Sm-Nd and U-Pb zircon isotopic study of the Mzumbe Suite, the oldest intrusive granitoid in southern Natal, South Africa. *S. Afr. J. Geol.*, **93**, 761-765.

Thomas, R.J., Marshall, C.G.A., Watkeys, M.K., Fitch, F.J. & Miller, J.A. (1992). K-Ar and $^{40}Ar/^{39}Ar$ dating of the Natal Group, southeast Africa-a post Pan-African molasse? *J. Afr. Earth Sci.*, **15**, 453-471.

Tinley, K.L. (1986). Coastal Dunes of South Africa. *South African National Scientific Programmes Report*, **109**, 300 pp.

Tyson, P.D. (1986). *Climatic Change and Variability in Southern Africa.* Oxford University Press, Cape Town, 220 pp.

Van Heerden, I.L. & Swart, D.H. (1986). *An assessment of past and present geomorphological and sedimentary processes operative in the St. Lucia estuary and environs.* Marine Geoscience and Sediment Dynamics Division, National Research Institute for Oceanology, CSIR Research Report No. 569.

Velde, B. (1985). *Clay minerals. A physical-chemical explanation of their occurrence.* Developments in Sedimentology, **40**, Elsevier, Amsterdam, 427 pp.

Visser, G.S. (1969). Grain size distributions and depositional processes. *J. Sed. Petrol.*, **39**, 1074-1106.

Visser, J.N.J. (1974). The Table Mountain Group: a Study in the Deposition of Quartz Arenites on a Stable Shelf. *Trans. geol. Soc. S. Afr.*, **73(3)**, 229-237.

Visser, D.J.L. (1989). *Explanation of the 1: 1 000 000 Geological Map, Fourth Edition, 1984: The Geology of the Republic of South Africa, Transkei, Bophuthatswana, Venda and Ciskei and the Kingdoms of Lesotho and Swaziland* (Ed). Geol. Surv. S. Afr., 491 pp.

Vogel, D.E. (1975). Precambrian weathering in acid metavolcanic rocks from the Superior Province, Villebon Township, southcentral Quebec, Canada. *Can. J. Earth Sci.*, **12**, 2080-2085.

Vogel, J.C., Wintle, A.G. & Woodborne, S.M. (1999). Focus: Luminescence dating of coastal sands: Overcoming changes in environmental dose rate. *J. of Archaeological Science*, **26**, 729-733.

Vogt, T. (1927). Sulitjelmafeltets geologi og petrografi. *Nor. Geol. Unders*, **121**, 1-560.

Walker, T.R. (1967). Formation of Red Beds in Modern and Ancient Deserts. *Geol. Soc. America Bulletin*, **78**, 353-368.

Ware, C.I. (1997). *Geotechnical and Geochemical Properties of "Hippo Mud" in the Durban Area.* Hons. thesis (unpubl.), University of Natal, 84 pp.

Watkeys, M.K., Mason, T.R., & Goodman, P.S. (1993). The rôle of geology in the development of Maputaland, South Africa. *J. Afr. Earth Sci.*, **16**, 205-221.

Weaver, C.E. (1989). Clays, Muds, and Shales. *Developments in Sedimentology*, **44**, Elsevier, Amsterdam, 819 pp.

Weaver, C.E. & Pollard, L.D. (1973). *The chemistry of clay minerals.* Elsevier Scientific Publishing company, 213 pp.

Whitmore, G., Uken, R., Meth, D. *et al.* (1999). *KwaZulu-Natal 3500 million years of geological history.* Education geology museum pamphlet, School of Geological and Computer Sciences, University of Natal, 2 pp.

Williams, D.F., Moore, W.S. & Fillion, R.S. (1981). Role of glacial Arctic Ocean ice sheets in Pleistocene oxygen isotope and sea-level records. *Earth and Planetary Science Letters*, **56**, 157-166.

Wilson, M.J. (1987). *A handbook of determinative methods in clay mineralogy.* Blackie, Glasgow, 308 pp.

Wolmarans, L.G. & Du Preez, J.W. (1986).The Geology of the St Lucia Area.. Expl. Sheet 27½32 (St Lucia). *Geol. Surv. S. Afr.*, 42 pp.

Wright, C.I. (1999). *The Cenozoic Evolution of the Northern KwaZulu-Natal Coastal Plain, South Africa.* PhD. thesis (unpubl.), University of Natal, 255 pp.

Wright, C.I., McMillan, I.K. & Mason, T.R., (1990). Foraminifera and sedimentation patterns in the St. Lucia Estuary mouth, Zululand, South Africa. *S. Afr. J. Geol.*, **93**, 592-601.

Wright, C.I. & Mason, T.R. (1993). Management and sediment dynamics of St. Lucia Estuary mouth, Zululand, South Africa. *Environmental Geology*, **22**, 227-241.

5. The measuring cylinder is placed in a controlled environment set at 20 °C, and left until the sample-water mixture is at this temperature.
6. When the test is to be commenced, the sample in the cylinder is redispersed using a several firm up and down movements of the plunger stirrer.
7. The stop watch is started as soon as step (6) is complete.
8. Clay-sized particles (<2 μm) concentrate in the top 30 cm of the column are siphoned off after 23 hours, 17 minutes (assuming a specific gravity of 2.65) and discarded.
9. Repeat stages 3 to 8 until the water siphoned off is nearly clear (usually 21-25 repeats).
10. The remaining silt concentrate is oven dried at 60 °C.

APPENDIX A2

Clay extraction

Apparatus. The following apparatus are required.

(1) As is Appendix A.1. Silt extraction.
(2) A centrifuge capable of taking four one litre containers (cation saturation).

Procedure. The procedure is as follows.

(1) As is Appendix A.1. Silt extraction procedure (1) to (7).
(8) The clay-sized particles (<2 μm) which concentrate in the top 30 cm of the slurry column are then siphoned off after 23 hours, 17 minutes (assuming a specific gravity of 2.65) and retained in a 5 litre bucket.
(9) Repeat stages 3 to 8 for eight repeats to get a representative clay sample.
(10) The retained sample representing the clay sized fraction is split into two sub-samples.
(11) One sub-sample is oven dried at 40 °C and the other is saturated with Mg^{2+}.
(12) Saturation with Mg^{2+} is achieved by the procedure outlined by Moore & Reynolds (1989).

APPENDIX B

Method for the determination of relative percentage of air-dried, back-packed XRD traces

Quantitative analysis requires that the integrated intensity (I) is used as clay minerals give intrinsically broad lines because of small scattering domains, structural disorder, mixed layering, or some combination of these factors.

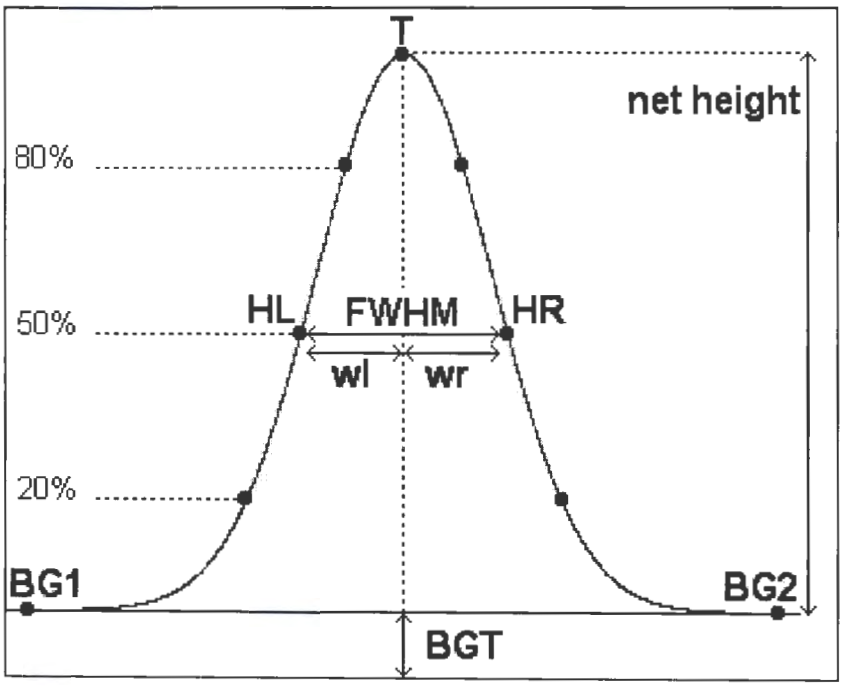

I = net height of the strongest peak of a given mineral × FWHM.

Where	**T**	Top of peak.
	HL	Half maximum at the left (low angle) side of the peak.
	HR	Half maximum at the right (high angle) side of the peak.
	BG1	First point used to fit the background.
	BG2	Second point used to fit the background.
	BGT	Background intensity at the top position.
	FWHM	Full width at half maximum.
	wl	Half width at half maximum (HWHM) of the left (low angle) side of the peak.
	wr	Half width at half maximum of the right (high angle) side of the peak.

Background: Calculated as a straight line from points BG1 to BG2.

Position: Determined by fitting a parabola to the maximum of the peak.

Height: Maximum of the parabola used to find the position of the peak. The net height is calculated by subtracting the background intensity at the peak position from the total height.

FWHM: Determined by fitting parabolas or straight lines from 20 % to 80 % of the maximum at both sides of the peak and then taking the horizontal distance between the lines at 50 % of the net height of the fitted peak.

APPENDIX C

APPENDIX C1

XRD clay abundances (relative modal percentage)

Borehole	D/H Interval	Height amsl (m)	Quartz	Calcite	Goeth+Hem	Plagioclase	Microcline	Ilmenite	Kaolinite	Illite	Smectite	I/S	Collophane
	0-6	37	36	17	16	4	0	0	9	0	1	17	0
	6-12	31	40	12	13	0	6	0	12	0	0	17	0
	12-18	25	57	1	10	0	5	0	8	0	0	20	0
I1	18-24	19	48	0	14	0	7	0	13	0	0	17	0
	24-30	13	20	0	23	0	2	0	34	0	0	22	0
	30-36	7	14	0	23	0	4	0	29	0	0	30	0
	36-42	1	18	0	22	0	5	0	31	0	0	23	0
	42-43	-3	16	0	22	0	3	0	25	0	4	29	0
	0-6	59	47	0	9	2	5	0	16	0	0	20	0
	6-12	53	61	0	2	1	6	0	4	0	0	27	0
	12-18	47	60	0	2	2	7	0	6	0	0	23	0
	18-24	41	53	0	8	4	5	1	9	0	0	21	0
	24-30	35	51	0	10	4	7	0	5	0	0	22	0
	30-36	29	30	0	18	0	7	0	32	0	0	12	0
L1	36-42	23	18	0	25	0	4	0	31	0	0	21	0
	42-48	17	17	0	31	0	3	0	30	0	0	19	0
	48-54	11	13	0	42	0	1	0	33	0	0	10	0
	54-60	5	8	0	62	0	1	0	18	0	0	11	0
	60-66	-1	19	0	28	0	3	0	39	0	0	10	0
	66-68.5	-5	22	0	10	0	0	0	60	0	0	9	0
	0-6	63	27	40	10	4	6	0	0	0	2	11	0
	6-12	57	23	62	3	4	0	0	0	0	1	6	0
	12-18	51	37	43	6	3	0	0	0	0	2	9	0
	18-24	45	40	29	3	5	8	0	0	0	1	13	0
	24-30	39	57	9	11	4	0	0	0	0	0	19	0
	30-36	33	52	4	5	5	7	0	2	0	0	25	0
I2	36-42	27	20	0	28	0	3	0	26	0	0	25	0
	42-48	21	25	0	17	0	5	0	19	0	0	34	0
	48-54	15	11	0	39	0	2	0	29	1	0	19	0
	54-60	9	16	0	30	0	3	0	23	0	0	28	0
	60-66	3	19	0	41	0	2	0	26	0	0	12	0
	66-69.4	-2	24	0	20	0	4	0	38	1	0	14	0
	0-6	59	47	0	16	0	4	1	9	0	0	22	0
	6-12	53	56	0	7	0	6	1	5	0	0	25	0
	12-18	47	46	0	18	0	9	2	6	0	0	20	0
	18-24	41	52	0	14	0	6	1	9	0	0	17	0
L2	24-30	35	48	0	16	3	6	0	4	0	0	23	0
	30-36	29	42	0	17	6	9	2	1	0	0	23	0
	36-42	23	31	0	1	0	6	1	39	0	0	22	0
	42-45	19	22	0	0	0	0	0	74	0	0	4	0
	0-6	85	43	48	3	0	0	0	0	0	1	5	0
	6-12	79	38	36	10	3	0	0	0	0	0	12	0
	12-18	73	46	26	10	5	0	0	0	0	0	14	0
	18-24	67	41	15	11	7	12	0	0	0	0	14	0
	24-30	61	42	23	13	7	0	0	0	0	0	16	0
	30-36	55	50	21	9	3	0	0	0	0	0	16	0
	36-42	49	50	17	13	4	0	0	0	0	0	15	0
	42-48	43	41	20	9	7	9	0	0	0	0	14	0
	48-54	37	45	6	8	7	9	2	2	0	0	21	0
	54-60	31	47	0	16	4	9	0	3	0	0	20	0
I3	60-66	25	44	0	22	4	7	0	4	0	0	19	0
	66-72	19	44	0	22	3	7	0	3	0	0	21	0
	72-78	13	43	0	19	3	7	0	12	1	0	16	0
	78-84	7	45	0	20	0	5	0	10	0	0	20	0
	84-90	1	26	0	26	0	4	1	13	0	0	30	0
	90-96	-5	45	0	20	2	6	1	11	0	0	16	0
	96-102	-11	22	0	29	0	3	0	22	0	0	24	0
	102-108	-17	5	0	63	0	0	0	14	0	0	18	0
	108-111.4	-19	6	0	67	0	0	0	8	0	0	18	0
	0-6	19	43	7	12	8	8	0	12	0	0	10	0
	6-12	13	45	11	15	10	0	0	12	0	0	7	0
	12-18	7	27	10	15	4	0	0	6	0	11	18	9
	18-24	1	17	4	12	2	0	0	0	0	14	24	27
C1	24-30	-5	13	18	17	2	0	0	0	0	32	6	13
	30-36	-11	10	5	15	2	0	0	0	0	60	0	9
	36-42	-17	22	0	19	7	0	0	21	0	10	18	2
	42-48	-23	22	0	26	4	0	0	15	0	0	33	0
	48-53	-29	13	0	39	3	0	0	22	0	0	23	0
D1		26	27	0	26	0	0	0	18	0	0	29	0
D2		28	31	0	20	0	4	0	19	0	0	25	0
D3		52	36	0	20	0	5	0	17	0	0	22	0
D4		71	45	0	18	4	0	0	8	0	0	25	0
CA1		60	28	35	7	5	8	3	0	0	0	14	0
CA2		44	19	63	3	2	0	1	0	0	0	12	0
K1		3	26	0	0	0	0	0	67	1	0	6	0
PondC		Various	35	13	12	5	0	0	5	0	2	28	0

APPENDIX C2

Clay geochemistry & calcium carbonate calculation

	Drilling	Height					Weight (%)								Put CO_2 back in =		Equivalent
Borehole	Interval	amsl (m)	SiO_2	Al_2O_3	Fe_2O_3	MnO	MgO	CaO	Na_2O	K_2O	TiO_2	P_2O_5	Cr_2O_3	NiO	Total	LOI	$CaCO_3$
I1	0-6m	37.0	44.07	17.18	18.60	0.3508	2.50	11.84	0.40	1.49	1.6463	1.68	0.0613	0.0120	100.01	25.44	15
I1	6-12m	31.0	50.15	21.03	16.58	0.3000	1.25	5.85	0.29	1.29	2.6103	0.57	0.0710	0.0171	100.01	19.48	8
I1	12-18m	25.0	51.39	21.60	18.38	0.3287	0.98	2.10	0.43	1.37	2.9362	0.43	0.0716	0.0163	100.03	18.29	3
I1	18-24m	19.0	51.15	22.37	18.52	0.3348	0.95	1.63	0.49	1.35	2.8350	0.44	0.0773	0.0146	100.16	18.26	2
I1	24-30m	13.0	48.14	30.06	17.13	0.1219	0.84	0.91	0.15	0.92	1.3351	0.26	0.1174	0.0150	100.00	18.00	1
I1	30-36m	7.0	48.63	29.35	17.20	0.0889	1.03	0.95	0.07	0.98	0.9814	0.24	0.0870	0.0122	99.62	17.81	1
I1	36-42m	1.0	51.09	30.20	14.12	0.4042	1.14	0.66	0.29	1.35	0.6039	0.22	0.0406	0.0082	100.13	17.81	1
I1	42-43m	-2.5	49.55	28.36	16.99	0.2768	1.51	0.48	0.05	1.10	0.8853	0.34	0.0699	0.0124	99.62	18.56	1
L1	12-18m	47.0	53.08	22.67	16.79	0.2627	1.35	0.70	0.34	1.46	2.7460	0.43	0.0802	0.0168	99.93	17.19	1
L1	60-66m	-1.0	47.33	32.04	17.17	0.0344	0.53	0.13	0.12	1.20	0.8900	0.37	0.1039	0.0104	99.93	14.83	0
I2	18-24m	45.0	48.89	13.79	14.84	0.2552	2.73	15.12	0.71	1.55	1.5576	0.50	0.0477	0.0111	100.00	19.46	20
I2	42-48m	21.0	44.78	30.06	20.57	0.1560	0.68	0.27	0.22	1.25	0.9303	0.48	0.0869	0.0153	99.50	15.48	0
I2	48-54m	15.0	48.83	30.02	16.65	0.2125	1.01	0.84	0.08	1.17	0.7665	0.31	0.0433	0.0134	99.95	15.58	1
I2	66-69.4m	-1.7	51.82	33.45	10.88	0.0274	0.66	0.24	0.19	1.33	0.9932	0.22	0.1367	0.0112	99.96	14.45	0
PondC	Sample 1	various	48.36	20.90	17.59	0.3723	1.84	6.01	0.60	1.22	2.4964	0.44	0.0862	0.0144	99.92	22.74	8
PondC	Sample 2	various	48.45	21.10	17.59	0.3654	1.83	5.77	0.57	1.20	2.6439	0.45	0.0879	0.0131	100.08	14.35	8

Step 1	CaO * (100-LOI)/100	Recalculate the relative wt % of major elements + LOI (volatiles) to sum to 100 %
Step 2	(1)*44/100	Calculate the molecular wt % of CO_2 given the wt % CaO assuming all CaO in $CaCO_3$
Step 3	(2) + CaO*(100-LOI)/100	Calculate wt % $CaCO_3$
Step 4	LOI-(CaO*(100-LOI))/100*(44/100)	Subtract the wt % CO_2 liberated from $CaCO_3$ from the total LOI
Step 5	(3) + ((3)*(4)/100)	Recalculate the relative wt % of major elements to 100 % (volatile free)

APPENDIX D

APPENDIX D1

Silt scanning electron microscope backscattered image analysis results (Percentages are in volume %)

Surface samples					Borehole	I1		
Sample	Height amsl(m)	% Light	% Dark	Grain Count	Height amsl(m)	% Light	% Dark	Grain Count
D1	26	27	73	12126	37	37	63	7037
D2	28	22	78	8094	31	41	59	7647
D3	52	29	71	8709	25	41	59	6447
D4	71	14	86	7276	19	39	61	4126
CA1	60	59	41	8889	13	47	53	12667
CA2	44	27	73	5864	7	44	56	3424
K1	2	16	84	38863	1	35	65	5748
					-2.5	39	61	7725
Borehole	L1				Borehole	I2		
Height amsl(m)	% Light	% Dark	Grain Count		Height amsl(m)	% Light	% Dark	Grain Count
59	34	66	11097		63	51	49	11761
53	35	65	11735		57	36	64	12088
47	33	67	8759		51	34	66	11938
41	38	62	7348		45	21	79	14112
35	33	67	10644		39	34	66	11331
29	48	52	8442		33	32	68	15996
23	45	55	11626		27	27	73	21514
17	30	70	10977		21	22	78	10897
11	24	76	19104		15	28	72	10079
5	21	79	18527		9	17	83	14815
-1	27	73	7205		3	21	79	25120
-5.25	22	78	10627		-2	31	69	9350
Borehole	L2				Borehole	I3		
Height amsl(m)	% Light	% Dark	Grain Count		Height amsl(m)	% Light	% Dark	Grain Count
59	35	65	8882		85	40	60	11501
53	33	67	10997		79	39	61	15209
47	30	70	13303		73	23	77	15413
41	27	73	13960		67	21	79	15906
35	30	70	11262		61	38	62	10878
29	22	78	15902		55	26	74	15205
23	24	76	9194		49	38	62	13054
18.5	23	77	11617		43	22	78	20131
Borehole	C1				37	33	67	12146
Height amsl(m)	% Light	% Dark	Grain Count		31	24	76	18404
19	27	73	7847		25	27	73	14766
13	31	69	8623		19	26	74	11803
7	18	82	17353		13	40	60	16587
1	10	90	18889		7	26	74	13479
-5	19	81	13222		1	23	77	15271
-11	31	69	9093		-5	30	70	11833
-17	27	73	11434		-11	42	58	16128
-23	17	83	23841		-17	49	51	16335
-28.5	18	82	14292		-19	61	39	22580

APPENDIX D2

Silt geochemistry

High	Fe_2O_3+MnO+TiO_2+Cr_2O_3+NiO+Zr (%)
Low	P_2O_5+K_2O+Na_2O+CaO+Al_2O_3+SiO_2 (%)

23-Jun-2000

MAJOR ELEMENT COMPOSITIONS - WEIGIIT %

Borehole	Interval	Height amsl (m)	SiO_2	Al_2O_3	Fe_2O_3	MnO	MgO	CaO	Na_2O	K_2O	TiO_2	P_2O_5	Cr_2O_3	NiO	Total	L.O.I.	Zr (ppm)	Zr (%)	High	Low
I2	0-6m	63	57.35	5.29	13.13	0.2639	3.42	8.29	0.93	0.66	8.505	0.13	0.0911	0.0043	98.07	3.87	79057	0.7906	22.78	72.65
I2	6-12m	57	61.22	4.93	10.85	0.2198	2.33	9.57	0.89	0.77	7.194	0.12	0.0774	0.0045	98.18	5.65	55692	0.5569	18.90	77.50
I2	12-18m	51	72.92	4.95	7.17	0.1356	1.95	7.14	0.76	0.86	3.485	0.07	0.0509	0.0048	99.48	3.90	3672.3	0.3672	11.21	86.67
I2	18-24m	45	74.30	5.13	6.74	0.1139	2.16	7.18	0.93	0.82	1.909	0.10	0.0371	0.0037	99.42	3.96	1622.2	0.1622	8.97	88.46
I2	24-30m	39	71.59	5.39	9.20	0.1785	1.98	3.79	0.88	0.96	4.962	0.07	0.0521	0.0041	99.06	1.39	4318.2	0.4318	14.83	82.68
I2	30-36m	33	75.16	5.65	8.62	0.1481	1.34	2.35	0.94	1.12	3.810	0.06	0.0502	0.0035	99.25	0.79	3416.0	0.3416	12.97	85.28
I2	36-42m	27	76.32	7.29	6.34	0.1196	0.86	1.66	0.71	2.28	3.738	0.07	0.0247	0.0011	99.43	1.80	3342.0	0.3342	10.56	88.33
I2	42-48m	21	83.81	7.39	3.31	0.0477	0.19	0.33	0.70	2.58	1.221	0.05	0.0158	0.0027	99.65	2.15	1080.1	0.1080	4.71	94.86
I2	48-54m	15	79.87	8.29	5.43	0.0729	0.22	0.25	0.73	2.76	2.110	0.07	0.0000	0.0002	99.81	2.77	2476.4	0.2476	7.86	91.97
I2	54-60m	9	84.83	8.09	2.83	0.0258	0.08	0.04	0.26	3.16	0.697	0.07	0.0161	0.0003	100.10	2.56	363.5	0.0364	3.61	96.45
I2	60-66m	3	83.73	7.40	3.67	0.0285	0.09	0.02	0.00	3.06	1.410	0.06	0.0134	0.0015	99.47	2.35	1523.9	0.1524	5.28	94.27
I2	66-69.4m	-2	84.32	6.23	2.69	0.0469	0.10	0.02	0.20	3.17	2.574	0.01	0.0235	0.0000	99.38	1.60	3319.3	0.3319	5.67	93.95

APPENDIX E

APPENDIX E1

Colour index

Borehole	Interval (m)	Height amsl (m)	Hue		Value/Chroma	Name	Relative *in situ* w (%)	KEY	
	0-6	37	10	YR	4/4	Dark yellowish brown	SM	D	dry
	6-12	31	10	YR	4/4	Dark yellowish brown	SM / D	SM	slightly moist
	12-18	25	10	YR	4/4	Dark yellowish brown	SM / D	M	moist
I1	18-24	19	10	YR	4/3	Brown	SM / D	S	saturated
	24-30	13	5	YR	4/6	Yellowish red	S		
	30-36	7	2.5	YR	4/6	Red	S		
	36-42	1	10	YR	4/4	Dark yellowish brown	S		
	42-43	-2.5	2.5	Y	6/6	Olive brown	S		
	0-6	59	10	YR	4/6	Dark yellowish brown	SM		
	6-12	53	10	YR	4/6	Dark yellowish brown	SM		
	12-18	47	10	YR	4/4	Dark yellowish brown	SM / D		
	18-24	41	10	YR	4/4	Dark yellowish brown	SM / D		
	24-30	35	10	YR	4/4	Dark yellowish brown	SM / D		
L1	30-36	29	10	YR	4/4	Dark yellowish brown	SM		
	36-42	23	7.5	YR	4/4	Strong brown	M		
	42-48	17	10	YR	5/6	Yellowish brown	S		
	48-54	11	10	YR	5/6	Yellowish brown	S		
	54-60	5	10	YR	5/6	Yellowish brown	S		
	60-66	-1	10	YR	5/8	Yellowish brown (mottled)	S		
	66-68.5	-5.25	2.5	Y	5/3	Light olive brown	S		
	0-6	63	10	YR	3/2	Very dark greyish brown	M		
	6-12	57	10	YR	4/3	Brown	SM		
	12-18	51	10	YR	4/3	Brown	SM /D		
	18-24	45	10	YR	4/4	Dark yellowish brown	SM / D		
	24-30	39	10	YR	4/4	Dark yellowish brown	SM / D		
	30-36	33	10	YR	4/4	Dark yellowish brown	SM / D		
I2	36-42	27	10	YR	4/4	Dark yellowish brown	S		
	42-48	21	10	YR	4/6	Dark yellowish brown	S		
	48-54	15	10	YR	4/6	Dark yellowish brown	S		
	54-60	9	10	YR	5/6	Yellowish Brown	S		
	60-66	3	10	YR	5/8	Yellowish Brown	S		
	66-69.4	-1.7	2.5	Y	6/6	Olive brown	S		
	0-6	59	10	YR	3/3	Dark brown	M		
	6-12	53	10	YR	3/4	Dark yellowish brown	SM / M		
	12-18	47	10	YR	3/4	Dark yellowish brown	SM		
L2	18-24	41	10	YR	3/4	Dark yellowish brown	SM		
	24-30	35	10	YR	3/4	Dark yellowish brown	SM		
	30-36	29	10	YR	3/4	Dark yellowish brown	SM		
	36-42	23	10	YR	4/2	Dark greyish brown	S		
	42-45	18.5	5	Y	6/2	Light olive grey (mottled)	S		
	0-6	85	10	YR	3/4	Dark yellowish brown	SM / D		
	6-12	79	10	YR	3/4	Dark yellowish brown	SM / D		
	12-18	73	10	YR	3/4	Dark yellowish brown	SM / M		
	18-24	67	10	YR	3/4	Dark yellowish brown (mottled)	SM / M		
	24-30	61	10	YR	3/3	Dark brown	SM / M		
	30-36	55	10	YR	3/3	Dark brown	SM / M		
	36-42	49	10	YR	3/4	Dark yellowish brown	SM / M		
	42-48	43	10	YR	3/4	Dark yellowish brown	SM / M		
	48-54	37	10	YR	3/4	Dark yellowish brown	SM / M		
I3	54-60	31	10	YR	4/4	Dark yellowish brown	SM / M		
	60-66	25	10	YR	4/4	Dark yellowish brown	SM / M		
	66-72	19	10	YR	4/4	Dark yellowish brown	SM / M		
	72-78	13	10	YR	3/3	Dark brown	M		
	78-84	7	10	YR	4/4	Dark yellowish brown	M		
	84-90	1	7.5	YR	4/6	Strong brown (mottled)	M		
	90-96	-5	10	YR	4/3	Brown	M / S		
	96-102	-11	10	YR	4/4	Dark yellowish brown	M / S		
	102-108	-17	10	YR	5/6	Yellowish brown	S		
	108-111.4	-19.2	10	YR	5/6	Yellowish brown	S		
	0-6	19	10	YR	3/2	Very dark greyish brown	SM / M		
	6-12	13	10	YR	3/2	Very dark greyish brown	SM		
	12-18	7	10	YR	3/4	Dark yellowish brown	SM		
	18-24	1	10	YR	4/4	Dark yellowish brown	SM / M		
C1	24-30	-5	10	YR	4/4	Dark yellowish brown	M		
	30-36	-11	10	YR	3/4	Dark yellowish brown	M		
	36-42	-17	10	YR	3/4	Dark yellowish brown	M		
	42-48	-23	10	YR	4/6	Dark yellowish brown	M		
	48-53	-28.5	10	YR	4/6	Dark yellowish brown	M / S		
D1		26	10	YR	3/3	Dark brown	M / SM		
D2		28	10	YR	3/4	Dark yellowish brown	SM / M		
D3		52	10	YR	3/4	Dark yellowish brown	M / SM		
D4		71	10	YR	4/4	Dark yellowish brown	M		
CA1		60	10	YR	3/2	Very dark greyish brown	M		
CA2		44	10	YR	4/4	Dark yellowish brown	M		
K1		2	5	Y	6/2	Light olive grey	S		
PondC		Various	10	YR	3/4	Dark yellowish brown	S		

APPENDIX E2

Grain size parameters

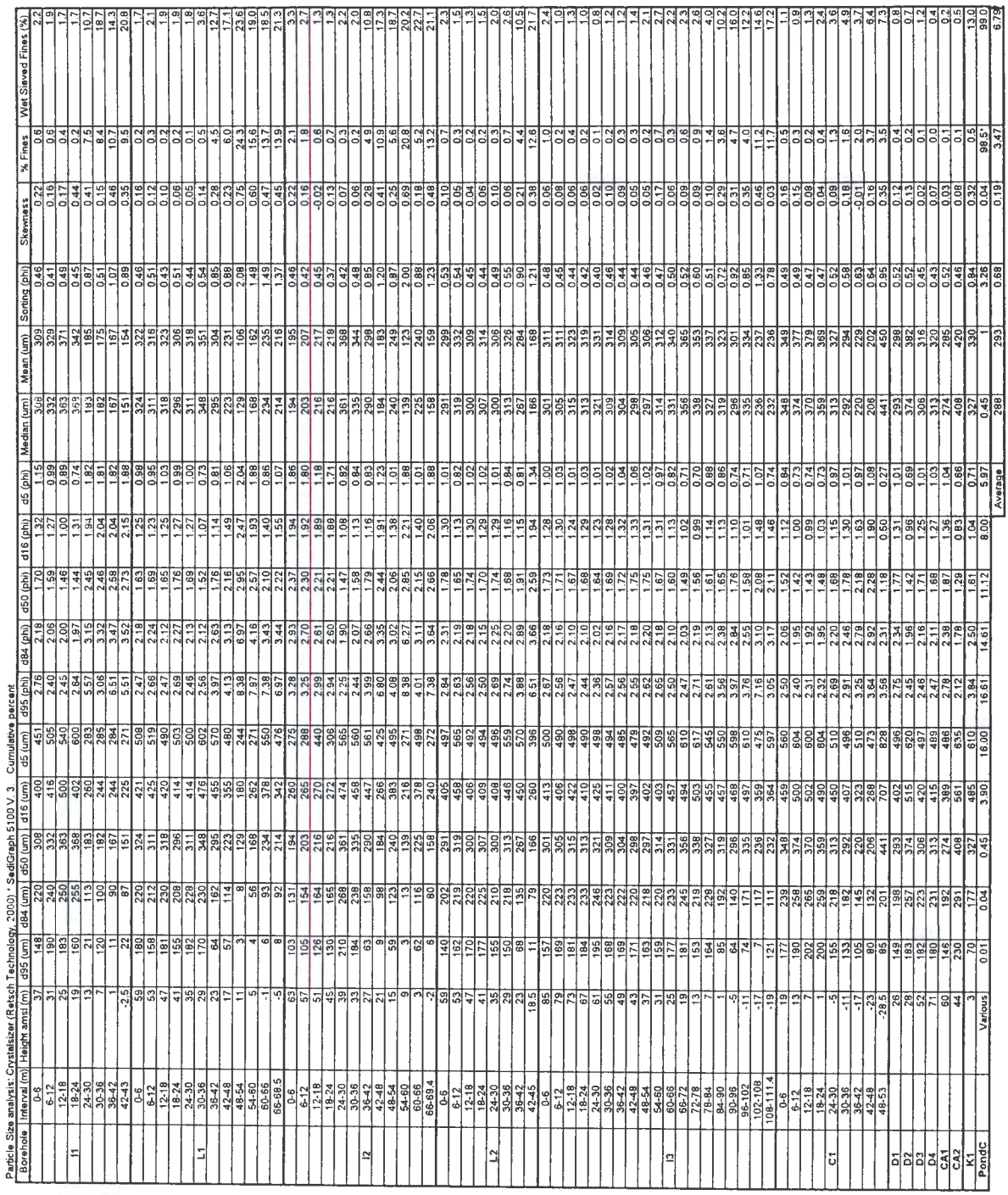

Particle Size analysis: Crystalsizer (Retsch Technology, 2000) + SediGraph 5100 V.3 Cumulative percent

Borehole	Interval (m)	Height amsl (m)	d95 (um)	d84 (um)	d50 (um)	d16 (um)	d5 (um)	d95 (phi)	d84 (phi)	d50 (phi)	d16 (phi)	d5 (phi)	Median (um)	Mean (um)	Sorting (phi)	Skewness	% Fines	Wet Sieved Fines (%)
	0-6	37	148	220	308	400	451	2.76	2.19	1.70	1.32	1.15	308	309	0.46	0.22	0.6	2.2
	6-12	31	190	240	332	416	505	2.40	2.06	1.59	1.27	0.99	332	329	0.41	0.16	0.6	1.9
	12-18	25	183	250	363	500	540	2.45	2.00	1.46	1.00	0.89	363	371	0.49	0.17	0.4	1.7
I1	18-24	19	160	255	368	402	600	2.64	1.97	1.44	1.31	0.74	369	342	0.45	0.44	0.2	1.7
	24-30	13	21	113	183	260	283	5.57	3.15	2.45	1.94	1.82	183	185	0.87	0.41	7.5	10.7
	30-36	7	120	100	182	244	285	3.06	3.32	2.46	2.04	1.81	182	175	0.51	0.15	8.4	18.7
	36-42	1	11	90	167	244	284	6.51	3.47	2.58	2.04	1.82	167	167	1.07	0.46	10.7	14.3
	42-43	-2.5	22	87	151	225	271	5.51	3.52	2.73	2.15	1.88	151	154	0.89	0.35	9.5	20.8
	0-6	59	180	220	324	421	508	2.47	2.18	1.83	1.25	0.98	324	322	0.48	0.16	0.2	1.7
	6-12	53	158	212	311	425	519	2.66	2.24	1.69	1.23	0.95	311	316	0.51	0.12	0.3	2.1
	12-18	47	181	230	318	420	490	2.47	2.12	1.65	1.25	1.03	318	323	0.43	0.10	0.2	1.9
	18-24	41	155	208	296	414	503	2.69	2.27	1.76	1.27	0.99	296	306	0.51	0.06	0.2	1.9
	24-30	35	182	228	311	414	500	2.46	2.13	1.69	1.27	1.00	311	318	0.44	0.05	0.1	1.8
L1	30-36	29	170	230	348	476	602	2.56	2.12	1.52	1.07	0.73	348	351	0.54	0.14	0.5	3.6
	36-42	23	64	162	295	455	570	3.97	2.63	1.76	1.14	0.81	295	304	0.85	0.28	4.5	12.7
	42-48	17	57	114	223	355	480	4.13	3.13	2.16	1.49	1.06	223	231	0.88	0.23	6.0	17.1
	48-54	11	3	8	129	180	244	8.38	6.97	2.95	2.47	2.04	129	106	2.09	0.75	24.3	23.6
	54-60	5	4	56	168	262	271	7.87	4.16	2.57	1.93	1.88	168	162	1.48	0.60	15.6	19.0
	60-66	-1	6	93	234	378	550	7.38	3.43	2.10	1.40	0.86	234	235	1.49	0.47	13.7	18.5
	66-68.5	-5	8	92	214	342	476	6.97	3.44	2.22	1.55	1.07	214	216	1.37	0.45	13.9	21.3
	0-6	63	103	131	194	260	275	3.28	2.93	2.37	1.94	1.86	194	195	0.46	0.22	2.1	3.3
	6-12	57	105	154	203	265	288	3.25	2.70	2.30	1.92	1.80	203	207	0.42	0.16	1.8	2.7
	12-18	51	126	164	216	270	440	2.99	2.61	2.21	1.89	1.18	216	217	0.45	-0.02	0.6	1.3
	18-24	45	130	165	216	272	308	2.94	2.60	2.21	1.88	1.71	216	218	0.37	0.13	0.7	1.3
	24-30	39	210	268	361	474	565	2.25	1.90	1.47	1.08	0.92	361	368	0.42	0.07	0.3	2.2
	30-36	33	184	238	335	458	560	2.44	2.07	1.58	1.13	0.84	335	344	0.48	0.06	0.2	2.0
I2	36-42	27	63	158	290	447	561	3.99	2.66	1.79	1.16	0.83	290	298	0.85	0.28	4.9	10.8
	42-48	21	9	98	184	266	425	6.80	3.35	2.44	1.91	1.23	184	183	1.20	0.41	10.9	17.3
	48-54	15	59	123	240	383	495	4.08	3.02	2.06	1.38	1.01	240	249	0.87	0.25	5.6	18.7
	54-60	9	3	13	139	216	271	8.38	6.27	2.85	2.21	1.88	139	123	2.00	0.69	20.8	20.2
	60-66	3	62	116	225	378	498	4.01	3.11	2.15	1.40	1.01	225	240	0.88	0.18	5.2	22.7
	66-69.4	-2	6	80	158	240	272	7.38	3.64	2.66	2.06	1.88	158	159	1.23	0.48	13.2	21.1
	0-6	59	140	202	291	405	497	2.84	2.31	1.78	1.30	1.01	291	299	0.53	0.10	0.7	2.3
	6-12	53	162	219	319	458	565	2.63	2.19	1.65	1.13	0.82	319	332	0.54	0.05	0.3	1.5
	12-18	47	170	220	300	406	492	2.56	2.18	1.74	1.30	1.02	300	308	0.45	0.04	0.2	1.3
	18-24	41	177	225	307	409	494	2.50	2.15	1.70	1.29	1.02	307	314	0.44	0.06	0.2	1.5
L2	24-30	35	155	210	300	408	496	2.69	2.25	1.74	1.29	1.01	300	306	0.49	0.10	0.3	2.0
	30-36	29	150	218	313	446	559	2.74	2.20	1.88	1.16	0.84	313	326	0.55	0.06	0.7	2.6
	36-42	23	88	135	267	450	570	3.88	2.89	1.91	1.15	0.81	267	284	0.90	0.21	4.4	10.5
	42-45	18.5	11	79	166	260	396	6.51	3.66	2.59	1.94	1.34	166	168	1.21	0.38	12.6	21.7
	0-6	85	157	220	301	413	500	2.67	2.18	1.73	1.28	1.00	301	311	0.48	0.06	1.0	2.4
	6-12	79	169	223	305	406	490	2.56	2.16	1.71	1.30	1.03	305	311	0.45	0.08	0.2	1.0
	12-18	73	181	233	315	422	498	2.47	2.10	1.67	1.24	1.01	315	323	0.44	0.06	0.4	1.3
	18-24	67	184	233	313	410	490	2.44	2.10	1.68	1.29	1.03	313	319	0.42	0.06	0.2	1.0
	24-30	61	195	246	321	425	498	2.36	2.02	1.64	1.23	1.01	321	331	0.40	0.02	0.1	0.8
	30-36	55	168	223	309	411	494	2.57	2.16	1.69	1.28	1.02	309	314	0.46	0.10	0.2	1.2
	36-42	49	169	222	304	400	485	2.56	2.17	1.72	1.32	1.04	304	309	0.44	0.09	0.3	1.2
	42-48	43	171	220	298	397	479	2.55	2.18	1.75	1.33	1.06	298	305	0.44	0.05	0.3	1.4
	48-54	37	163	218	297	402	492	2.62	2.20	1.75	1.31	1.02	297	306	0.46	0.05	0.2	2.1
	54-60	31	159	220	314	403	509	2.65	2.18	1.67	1.31	0.97	314	312	0.47	0.17	0.7	2.7
I3	60-66	25	177	233	331	457	565	2.50	2.10	1.60	1.13	0.82	331	340	0.50	0.06	0.3	2.2
	66-72	19	181	245	356	494	610	2.47	2.03	1.49	1.02	0.71	356	365	0.52	0.09	0.6	2.3
	72-78	13	153	219	338	503	617	2.71	2.19	1.56	0.99	0.70	338	353	0.60	0.09	0.9	2.8
	78-84	7	194	228	327	455	545	2.81	2.13	1.61	1.14	0.89	327	337	0.51	0.10	1.4	4.0
	84-90	1	85	192	319	457	590	3.56	2.38	1.65	1.13	0.86	319	323	0.72	0.29	3.6	10.2
	90-96	-5	64	140	296	468	598	3.97	2.84	1.78	1.10	0.74	296	301	0.92	0.31	4.7	16.0
	96-102	-11	74	171	335	497	610	3.76	2.55	1.58	1.01	0.71	335	334	0.85	0.35	4.0	12.2
	102-108	-17	7	117	236	359	475	7.16	3.10	2.08	1.48	1.07	236	237	1.33	0.46	11.2	14.6
	108-111.4	-19	121	111	232	364	597	3.05	3.17	2.11	1.46	0.74	232	236	0.78	0.03	11.7	17.2
	0-6	19	177	239	348	459	560	2.50	2.06	1.52	1.12	0.84	348	349	0.49	0.16	0.5	1.1
	6-12	13	190	258	374	500	604	2.40	1.95	1.42	1.00	0.73	374	377	0.49	0.15	0.3	0.9
	12-18	7	202	265	370	502	600	2.31	1.92	1.43	0.99	0.74	370	379	0.47	0.08	0.2	1.3
	18-24	1	200	259	359	490	604	2.32	1.95	1.48	1.03	0.73	359	369	0.47	0.04	0.4	2.4
C1	24-30	-5	155	218	313	450	510	2.69	2.20	1.68	1.15	0.97	313	327	0.52	0.09	1.3	3.6
	30-36	-11	133	182	292	407	496	2.91	2.46	1.78	1.30	1.01	292	294	0.58	0.18	1.6	4.9
	36-42	-17	105	145	220	323	510	3.25	2.79	2.18	1.63	0.97	220	229	0.63	-0.01	2.0	3.7
	42-48	-23	80	132	206	288	473	3.64	2.92	2.28	1.90	1.08	206	202	0.64	0.18	3.7	6.4
	48-53	-28.5	85	201	441	707	828	3.56	2.31	1.18	0.50	0.27	441	450	0.95	0.35	3.5	7.3
D1		26	149	198	293	402	496	2.75	2.34	1.77	1.31	1.01	293	298	0.52	0.12	0.4	0.8
D2		28	183	257	374	515	620	2.45	2.96	1.42	0.96	0.69	374	382	0.52	0.13	0.2	0.7
D3		52	192	223	306	420	497	2.46	2.16	1.71	1.25	1.01	306	316	0.45	0.02	0.1	1.2
D4		71	190	231	313	415	489	2.47	2.11	1.68	1.27	1.03	313	320	0.43	0.07	0.0	0.4
CA1		60	146	192	274	389	496	2.79	2.38	1.97	1.36	1.04	274	285	0.52	0.03	0.1	0.2
CA2		44	230	291	409	561	835	2.12	1.78	1.29	0.83	0.66	408	420	0.46	0.08	0.1	0.5
K1		3	70	177	327	485	610	3.84	2.50	1.61	1.04	0.71	327	330	0.84	0.32	0.5	13.0
Pondc		Various	0.01	0.04	0.45	3.90	16.00	16.61	14.61	11.12	8.00	5.97	0.45	1	3.26	0.04	98.5*	99.0
													Average	288	293	0.68	0.19	3.47	6.79

APPENDIX E3

Bulk XRF geochemistry (weight %), wet sieving and carbonate bomb results

Processed October 1999			MAJOR ELEMENT COMPOSITIONS Weight %										*Carbonate Bomb		
IGNITED	Interval	Height amsl (m)	SiO_2	Al_2O_3	Fe_2O_3	MnO	MgO	CaO	Na_2O	K_2O	TiO_2	P_2O_5	Total	L.O.I.	*$CaCO_3$
	0-6M	37	89.42	2.10	2.02	0.0382	0.75	3.38	0.26	0.46	0.7082	0.07	99.20	2.61	3.9
	6-12M	31	93.60	1.63	1.51	0.0267	0.12	0.84	0.14	0.50	0.8720	0.01	99.24	1.03	0.5
	12-18M	25	93.87	1.62	1.62	0.0295	0.10	0.31	0.22	0.56	1.0313	0.01	99.36	0.59	0.0
I1	18-24M	19	93.40	1.69	1.85	0.0373	0.12	0.33	0.13	0.57	1.2279	0.01	99.37	0.69	0.0
	24-30M	13	90.13	3.19	3.18	0.0461	0.13	0.30	0.02	0.55	1.5337	0.02	99.11	1.66	0.0
	30-36M	7	89.09	4.45	3.38	0.0310	0.11	0.15	0.10	0.82	1.0129	0.04	99.19	2.57	0.0
	36-42M	1	91.74	4.13	1.51	0.0738	0.05	0.07	0.15	1.16	0.2428	0.03	99.15	1.94	0.0
	42-43M	-2.5	90.32	4.12	2.63	0.0686	0.15	0.06	0.04	0.91	0.8148	0.04	99.16	2.42	0.0
	0-6M	59	94.67	1.66	1.22	0.0241	0.07	0.29	0.11	0.48	0.6868	0.01	99.23	0.66	0.0
	6-12M	53	93.25	1.64	1.90	0.0344	0.12	0.35	0.14	0.47	1.3246	0.00	99.23	0.55	0.0
	12-18M	47	93.83	1.70	1.66	0.0331	0.16	0.40	0.14	0.47	1.0144	0.00	99.40	0.65	0.0
	18-24M	41	90.54	1.83	3.00	0.0604	0.27	0.55	0.18	0.47	2.1717	0.00	99.07	0.62	0.0
	24-30M	35	94.33	1.71	1.36	0.0279	0.20	0.42	0.03	0.46	0.6833	0.01	99.23	0.60	0.0
L1	30-36M	29	94.34	1.63	1.57	0.0281	0.09	0.27	0.14	0.50	0.9509	0.01	99.54	0.77	0.0
	36-42M	23	92.81	3.49	1.53	0.0201	0.06	0.07	0.00	0.80	0.3724	0.03	99.19	1.72	0.0
	42-48M	17	90.97	4.08	2.54	0.0226	0.06	0.04	0.10	0.70	0.5964	0.05	99.16	2.22	0.0
	48-54M	11	86.28	4.64	5.80	0.0317	0.08	0.02	0.08	0.42	1.6242	0.10	99.07	2.93	0.0
	54-60M	5	90.55	3.70	3.76	0.0169	0.02	0.01	0.00	0.41	0.5758	0.07	99.11	2.38	0.0
	60-66M	-1	91.98	4.09	1.84	0.0095	0.03	0.03	0.00	0.70	0.5740	0.03	99.28	2.12	0.0
	66-68.5M	-5.25	90.06	4.11	2.14	0.0278	0.08	0.04	0.00	0.57	2.0485	0.01	99.09	2.21	0.0
	0-6M	63	86.43	2.30	3.61	0.0668	0.92	3.05	0.36	0.46	1.8954	0.06	99.15	1.95	2.9
	6-12M	57	86.76	2.19	2.62	0.0444	0.78	4.92	0.30	0.50	1.2595	0.05	99.44	3.53	5.9
	12-18M	51	87.48	2.06	1.73	0.0264	0.80	6.19	0.27	0.46	0.3620	0.07	99.45	4.50	8.2
	18-24M	45	87.40	2.11	1.55	0.0326	0.86	6.60	0.33	0.47	0.2383	0.07	99.65	4.90	9.1
	24-30M	39	90.49	1.86	1.41	0.0210	0.44	3.67	0.21	0.50	0.4601	0.04	99.10	3.07	4.1
I2	30-36M	33	95.66	1.55	1.04	0.0168	0.12	0.32	0.16	0.51	0.5190	0.01	99.90	0.35	0.0
	36-42M	27	91.16	3.25	2.52	0.0258	0.17	0.39	0.11	0.60	0.9002	0.04	99.15	2.00	0.0
	42-48M	21	92.49	4.18	1.61	0.0225	0.09	0.16	0.13	0.98	0.3451	0.03	100.05	2.40	0.0
	48-54M	15	91.05	4.63	2.44	0.0294	0.08	0.13	0.11	1.00	0.6030	0.04	100.11	2.65	0.0
	54-60M	9	92.15	4.04	2.34	0.0168	0.03	0.03	0.00	0.73	0.2837	0.05	99.68	2.14	0.0
	60-66M	3	91.10	4.42	3.15	0.0105	0.02	0.02	0.00	0.69	0.3798	0.07	99.86	2.59	0.0
	66-69.4M	-1.7	92.70	4.00	1.27	0.0045	0.03	0.03	0.00	0.79	0.5509	0.02	99.40	2.13	0.0
	0-6M	59	88.23	1.96	4.19	0.0798	0.32	0.58	0.23	0.41	3.1179	0.00	99.12	0.97	0.0
	6-12M	53	90.37	1.76	3.42	0.0663	0.24	0.41	0.14	0.42	2.5363	0.00	99.36	0.70	0.0
	12-18M	47	92.00	1.70	2.81	0.0461	0.23	0.43	0.17	0.39	1.9123	0.01	99.70	0.85	0.0
L2	18-24M	41	93.01	1.70	2.32	0.0367	0.25	0.41	0.15	0.40	1.4625	0.01	99.74	0.87	0.0
	24-30M	35	90.27	1.88	3.20	0.0615	0.25	0.44	0.14	0.46	2.3404	0.01	99.04	0.65	0.0
	30-36M	29	92.72	1.58	2.04	0.0378	0.18	0.24	0.18	0.37	1.7460	0.01	99.10	0.75	0.0
	36-42M	23	88.03	2.46	3.92	0.0713	0.15	0.14	0.00	0.36	3.9865	0.00	99.13	1.51	0.0
	42-45M	18.5	91.42	6.08	1.03	0.0012	0.12	0.01	0.10	0.53	0.7216	0.03	100.05	3.07	0.0

TRACE ELEMENT (PPM)

S	Cl	F	Nb	Y	Rb	Zr	Sr	U	Th	Ba	Sc	Cr	V	La	Zn	Cu
187	105	600	8.0	12.5	13.6	598.2	125.1	0.8	2.6	115.2	5.8	95.3	47.2	45.6	15.2	0.0
113	86	400	11.0	13.8	15.5	1029.0	50.5	0.9	6.7	137.3	4.8	100.0	36.9	20.0	11.2	0.0
165	60	200	13.2	15.5	16.3	1482.1	37.4	0.8	8.9	161.7	4.4	127.0	45.9	7.6	13.5	0.0
36	60	400	14.5	17.6	16.4	1565.7	38.0	0.9	7.5	141.4	4.4	133.4	47.8	0.0	11.9	0.0
51	34	600	17.2	19.9	17.2	1655.3	30.8	2.1	10.7	163.7	12.0	182.5	82.7	34.4	18.5	2.1
270	44	700	10.8	16.9	26.7	876.0	27.5	2.7	10.3	210.5	17.1	141.3	77.6	22.8	18.2	0.4
91	82	500	2.3	15.0	34.1	183.4	33.6	0.0	2.4	406.9	6.4	37.0	22.6	10.3	10.9	0.4
41	42	500	10.0	34.4	30.1	681.2	26.6	2.1	6.6	296.4	13.3	102.1	46.2	24.1	16.8	0.0
84	41	400	8.7	12.1	13.7	957.5	34.3	0.0	1.7	127.7	3.4	85.0	34.9	7.3	8.7	0.0
35	45	200	16.1	17.5	12.7	1976.3	37.4	1.8	4.3	127.9	5.3	136.2	53.0	0.0	14.2	0.0
28	36	200	13.5	15.6	13.3	1612.8	38.1	0.0	5.3	106.2	4.6	122.0	44.3	21.4	13.3	0.0
328	34	300	29.1	29.0	13.4	3400.7	46.0	1.8	8.5	139.8	8.1	224.1	77.5	6.9	19.9	0.0
45	39	300	10.4	13.1	13.6	1083.0	39.1	0.8	2.8	119.5	3.8	114.4	36.6	0.0	11.6	0.0
45	69	100	10.9	12.6	13.8	1040.5	29.5	0.0	5.5	148.3	4.7	88.2	43.7	8.7	12.5	0.7
63	118	300	4.2	12.5	24.2	374.1	23.7	0.0	2.5	245.8	6.3	57.7	35.9	11.8	17.9	8.2
80	106	600	6.9	19.1	22.6	517.4	17.9	0.8	5.4	206.2	10.3	105.3	66.7	28.1	19.6	7.3
86	51	1100	18.7	25.3	14.7	1504.3	9.4	1.9	9.6	106.6	25.1	290.2	140.6	15.0	23.8	0.0
123	179	900	6.1	16.2	12.9	483.5	9.6	0.0	6.0	113.8	10.7	167.0	75.4	13.0	19.1	2.3
39	222	500	5.5	34.7	21.6	535.0	17.9	0.3	4.2	214.3	12.0	117.1	49.7	7.8	14.2	5.7
148	473	300	21.9	44.8	19.5	2048.2	15.6	3.0	19.7	166.1	26.7	258.0	135.0	40.6	37.6	27.3
208	88	1000	18.8	22.9	13.1	1735.6	108.9	1.2	7.9	127.0	10.4	183.8	89.2	10.1	22.4	0.0
273	73	900	13.0	17.8	13.4	1142.0	168.0	0.0	4.9	129.2	6.9	127.5	63.0	0.0	18.3	0.0
302	50	1000	3.3	10.9	12.0	285.5	208.0	0.3	1.5	119.5	5.7	81.4	35.2	0.0	13.0	0.0
386	58	900	2.8	8.8	12.4	164.4	222.1	0.9	0.0	134.6	5.5	76.8	33.2	0.0	13.1	0.0
236	65	500	5.5	11.1	14.4	515.2	144.8	0.4	2.0	136.7	4.5	73.3	32.4	0.0	11.2	0.0
24	48	200	6.3	9.3	13.5	739.3	34.0	1.3	5.7	135.8	2.2	72.1	29.5	10.9	8.9	0.7
84	76	900	9.6	15.4	19.3	817.1	32.6	0.4	7.5	176.9	9.0	118.0	62.3	48.1	15.7	0.4
49	110	500	2.8	14.4	28.9	229.5	34.6	0.2	2.5	304.7	8.9	41.7	43.2	16.1	16.9	6.7
56	93	800	7.0	18.1	31.1	394.5	31.2	1.4	4.2	282.3	14.3	61.3	54.3	3.9	20.2	3.1
42	184	500	3.3	11.7	23.1	177.0	18.5	0.1	2.8	195.8	7.3	114.2	49.8	38.1	19.5	9.6
72	194	900	4.0	19.3	20.5	253.4	16.0	0.0	3.1	194.2	9.6	138.6	82.0	19.9	22.0	8.8
36	203	400	6.7	24.6	25.0	506.1	20.1	0.9	5.6	211.7	11.1	125.8	79.5	1.5	23.2	18.2
66.9	75	445	39.3	34.7	13.5	4656.1	46.9	4.4	17.4	106.9	8.9	259.3	118.5	11.3	24.0	2.0
45.1	51	292	32.9	29.4	11.9	3795.8	40.9	4.5	13.0	119.6	7.1	230.9	91.9	20.2	24.1	2.6
28.5	22	353	26.3	22.9	10.8	2819.4	38.7	2.5	12.4	106.2	6.6	203.7	68.1	10.8	15.5	4.9
28.6	44	215	21.7	20.0	11.0	2152.3	37.8	2.4	5.6	125.6	4.8	170.9	57.4	13.1	11.8	3.5
36.3	86	461	30.2	25.7	12.6	3052.6	41.4	4.2	11.8	132.6	7.0	192.6	90.4	81.7	17.8	3.1
38.5	124	15	22.6	17.7	10.0	2251.6	28.6	0.5	8.7	108.5	5.4	124.8	68.0	0.0	11.4	3.1
111.6	320	292	45.1	35.3	11.7	3582.0	23.4	4.3	26.4	113.4	22.8	253.5	169.1	34.4	21.6	7.1
141.8	169	123	9.4	15.9	19.4	629.6	14.0	1.1	4.9	171.0	18.5	182.7	62.0	48.7	11.3	7.3

Ni	Pb	Ga	**Mill Contamination Co**	Ce	Nd	As	Sn	Ta	Mo	**Mill Contamination W**	Cd	TiO_2/MgO	Zr/(P_2O_5*100)	CIA	% fines
8.6	0.0	10.5	134.0	8.7	4.3	2.8	7	12	6	640	0	0.94	85.46	33.87	2.2
5.3	0.0	10.8	191.3	17.1	9.1	1.4	3	18	11	933	0	7.27	1029.00	52.41	1.9
3.9	1.0	12.0	312.8	27.7	8.2	1.5	1	20	13	1498	0	10.31	1482.10	59.78	1.7
5.6	4.3	10.4	242.1	22.3	5.3	0.6	2	17	14	1192	0	10.23	1565.70	62.13	1.7
10.8	8.9	11.7	109.0	34.7	12.8	8.3	6	15	17	540	0	11.80	827.65	78.57	10.7
9.6	2.3	13.4	131.4	37.3	24.5	8.7	2	12	8	609	0	9.21	219.00	80.62	18.7
6.6	8.2	12.7	168.5	11.5	8.7	3.3	1	5	2	724	0	4.86	61.13	74.95	14.3
9.6	11.1	12.7	136.1	28.4	21.8	4.1	2	16	8	572	0	5.43	170.30	80.31	20.8
4.0	0.0	12.0	302.9	19.0	7.5	0.8	2	10	8	1298	1	9.81	957.50	65.35	1.7
4.8	0.0	12.0	305.9	19.0	1.8	1.3	3	10	17	1367	0	11.04	#DIV/0!	63.08	2.1
5.7	0.0	12.6	313.8	28.6	20.7	0.4	3	9	14	1428	0	6.34	#DIV/0!	62.73	1.9
8.3	0.0	13.1	234.1	29.1	6.3	4.3	0	23	28	1169	0	8.04	#DIV/0!	60.40	1.9
5.3	4.3	12.0	246.0	12.9	0.0	0.9	4	8	7	1127	1	3.42	1083.00	65.27	1.8
4.3	0.0	12.5	234.9	21.8	9.1	0.5	2	0	10	1076	0	10.57	1040.50	64.17	3.6
9.3	0.0	13.0	162.5	14.1	7.2	4.4	1	11	4	735	0	6.21	124.70	80.05	12.7
10.5	1.1	12.2	148.8	22.3	12.6	6.9	2	10	5	667	0	9.94	103.48	82.93	17.1
14.7	0.0	14.6	126.4	66.4	35.1	12.1	8	0	14	598	1	20.30	150.43	89.92	23.6
13.7	0.8	10.2	126.1	16.4	4.1	6.1	0	7	6	532	2	28.79	69.07	89.81	19.0
5.8	0.2	12.9	134.2	22.5	16.0	0.8	0	14	4	568	0	19.13	178.33	84.85	18.5
8.7	3.4	12.7	150.3	109.3	53.1	2.8	1	16	18	657	0	25.61	2048.20	87.08	21.3
11.5	2.4	12.3	140.9	38.9	15.4	3.1	4	0	16	684	0	2.06	289.27	37.28	3.3
8.6	2.4	11.1	108.4	32.8	15.6	3.3	4	8	10	529	0	1.61	228.40	27.69	2.7
7.9	0.0	10.7	109.2	5.4	2.4	1.9	0	1	3	534	0	0.45	40.79	22.94	1.3
7.7	0.0	11.7	129.3	20.4	8.7	0.7	3	8	3	620	0	0.28	23.49	22.19	1.3
5.0	0.0	11.5	202.9	11.0	1.6	3.0	0	11	4	936	0	1.05	128.80	29.81	2.2
4.1	1.4	11.7	270.2	11.3	0.0	0.0	0	16	9	1198	0	4.33	739.30	61.02	2.0
7.9	2.7	12.0	108.3	27.2	12.5	4.4	4	15	7	451	1	5.30	204.28	74.71	10.8
7.0	0.0	11.8	98.4	22.8	12.8	6.8	0	16	2	376	1	3.83	76.50	76.70	17.3
9.8	8.5	12.3	129.9	16.2	11.5	10.3	1	16	0	514	0	7.54	98.63	78.88	18.7
11.0	0.0	13.1	154.6	16.2	7.6	10.2	5	4	4	656	2	9.46	35.40	84.17	20.2
9.0	0.0	13.3	119.6	18.1	4.9	3.4	2	3	1	506	1	18.99	36.20	86.16	22.7
7.0	0.0	12.9	188.9	25.3	11.6	0.0	0	12	3	806	0	18.36	253.05	82.99	21.1
8.5	0.7	0.0	225.0	59.2	20.6	7.3	15	15	29	1122	0	9.74	#DIV/0!	61.64	2.3
7.7	0.0	1.2	182.9	55.3	28.2	3.3	24	2	22	930	1	10.57	#DIV/0!	64.47	1.5
6.6	0.4	1.7	198.3	27.7	10.5	0.0	23	0	17	1024	1	8.31	2819.40	63.20	1.3
6.7	0.0	0.3	179.9	22.1	6.6	1.3	26	19	17	960	2	5.85	2152.30	63.91	1.5
7.4	0.0	2.2	181.5	44.3	13.9	1.4	25	9	19	952	1	9.36	3052.60	64.38	2.0
6.2	0.0	0.0	216.9	62.3	14.8	1.0	26	0	18	1177	0	9.70	2251.60	66.67	2.6
15.5	2.7	0.8	99.8	98.4	35.1	1.6	27	7	27	509	0	26.58	#DIV/0!	83.11	10.5
15.6	6.5	5.3	76.5	72.2	27.8	0.0	34	11	4	413	3	6.01	209.87	90.48	21.7

Gen	Interval	Height amsl (m)	SiO_2	Al_2O_3	Fe_2O_3	MnO	MgO	CaO	Na_2O	K_2O	TiO_2	P_2O_5	Cr_2O_3	NiO	Total	*Carbonate Bomb L.O.I.	*$CaCO_3$
	0-6M	85	86.33	2.45	3.49	0.0729	1.05	4.05	0.23	0.46	1.5516	0.06	0.0424	0.0025	99.78	3.12	3.6
	6-12M	79	89.28	2.00	2.14	0.0424	0.66	3.70	0.43	0.46	0.8831	0.03	0.0300	0.0010	99.67	3.00	3.4
	12-18M	73	90.01	2.03	1.78	0.0333	0.74	3.74	0.42	0.50	0.4810	0.04	0.0222	0.0013	99.81	2.84	3.0
	18-24M	67	90.28	1.93	1.59	0.0269	0.67	4.12	0.29	0.46	0.2878	0.05	0.0195	0.0009	99.72	3.35	3.9
	24-30M	61	90.16	2.08	1.52	0.0277	0.70	4.23	0.49	0.49	0.2559	0.05	0.0207	0.0006	100.02	3.39	3.9
	30-36M	55	88.30	2.16	2.13	0.0388	0.78	4.66	0.49	0.51	0.7399	0.05	0.0271	0.0014	99.89	3.61	4.5
	36-42M	49	87.86	2.23	2.19	0.0392	0.82	5.11	0.45	0.50	0.6116	0.06	0.0274	0.0013	99.90	3.92	5.3
	42-48M	43	87.90	2.07	1.78	0.0297	0.87	5.95	0.47	0.47	0.2729	0.07	0.0190	0.0012	99.90	4.58	7.1
	48-54M	37	91.03	1.95	2.21	0.0418	0.50	2.11	0.19	0.46	1.0867	0.02	0.0328	0.0010	99.63	1.90	1.8
I3	54-60M	31	93.80	1.76	1.77	0.0354	0.17	0.38	0.22	0.49	1.0676	0.00	0.0272	0.0011	99.72	0.69	0.0
	60-66M	25	94.70	1.64	1.29	0.0234	0.15	0.30	0.18	0.54	0.6484	0.01	0.0213	0.0001	99.50	0.75	0.0
	66-72M	19	94.78	1.86	1.31	0.0227	0.12	0.30	0.15	0.59	0.5619	0.02	0.0236	0.0002	99.74	0.76	0.0
	72-78M	13	93.35	1.70	2.00	0.0418	0.20	0.38	0.18	0.55	1.1900	0.01	0.0326	0.0009	99.65	0.52	0.0
	78-84M	7	94.19	1.57	1.89	0.0328	0.14	0.22	0.14	0.44	0.9495	0.01	0.0246	0.0020	99.62	0.64	0.0
	84-90M	1	92.06	2.19	2.96	0.0589	0.15	0.15	0.14	0.42	1.3025	0.04	0.0303	0.0020	99.50	1.24	0.0
	90-96M	-5	89.55	2.63	4.13	0.0818	0.15	0.24	0.22	0.64	1.7881	0.03	0.0368	0.0016	99.50	1.29	0.0
	96-102M	-11	85.01	3.17	5.94	0.1139	0.24	1.82	0.06	0.70	2.5306	0.05	0.0436	0.0026	99.68	1.62	0.0
	102-108M	-17	73.45	3.06	13.74	0.1501	0.17	0.09	0.00	0.36	6.6411	0.06	0.0892	0.0035	97.82	2.07	0.0
	108-111.4M	-19.2	63.71	3.47	18.75	0.2226	0.24	0.10	0.01	0.29	9.6910	0.13	0.1281	0.0049	96.73	2.24	0.0
	0-6M	19	84.43	3.07	4.04	0.0886	1.07	3.80	0.50	0.63	1.8336	0.03	0.0565	0.0033	99.56	2.46	3.6
	6-12M	13	84.59	3.05	3.81	0.0893	1.02	4.05	0.52	0.63	1.6644	0.03	0.0540	0.0020	99.49	2.50	3.9
	12-18M	7	86.56	2.79	2.78	0.0585	1.07	4.85	0.38	0.55	0.7099	0.09	0.0296	0.0023	99.85	3.47	4.3
	18-24M	1	92.63	2.41	1.92	0.0339	0.40	1.04	0.26	0.54	0.3743	0.19	0.0246	0.0009	99.82	1.06	0.5
C1	24-30M	-5	91.09	2.53	2.63	0.0525	0.32	0.95	0.30	0.55	1.0085	0.17	0.0198	0.0023	99.62	1.02	0.5
	30-36M	-11	85.29	2.93	5.33	0.1205	0.48	1.19	0.36	0.53	2.8447	0.14	0.0560	0.0056	99.27	1.28	0.4
	36-42M	-17	92.03	2.49	2.42	0.0595	0.16	0.49	0.15	0.68	1.2498	0.03	0.0143	0.0004	99.78	1.96	0.0
	42-48M	-23	92.25	3.01	2.05	0.0422	0.07	0.27	0.12	0.82	0.9262	0.03	0.0165	0.0000	99.60	1.13	0.0
	48-53M	-28.5	91.48	3.89	1.72	0.0605	0.05	0.18	0.31	1.57	0.2136	0.04	0.0185	0.0011	99.53	1.24	0.0

Zr (ppm)	TiO_2/MgO	Zr/(P_2O_5*100)	CIA	% fines
1854.6	1.48	309.10	34.08	2.4
1246.2	1.34	415.41	30.35	1.0
580.3	0.65	145.09	30.34	1.3
291.1	0.43	58.21	28.38	1.0
198.0	0.37	39.60	28.53	0.8
851.5	0.95	170.30	27.62	1.2
623.4	0.75	103.90	26.90	1.2
155.9	0.31	22.27	23.10	1.4
1601.8	2.17	800.89	41.40	2.1
1546.4	6.28	#DIV/0!	61.75	2.7
870.6	4.32	870.57	61.65	2.2
725.9	4.68	362.94	64.14	2.3
1663.6	5.95	1663.64	60.50	2.6
1043.3	6.78	1043.28	66.24	4.0
1431.4	8.68	357.86	75.52	10.2
2117.5	11.92	705.82	70.51	16.0
2628.3	10.54	525.65	55.13	12.2
8218.3	39.07	1369.72	87.18	14.6
11697.9	40.38	899.84	89.66	17.2
2498.4	1.71	832.80	38.38	1.1
2394.6	1.63	798.21	36.97	0.9
722.8	0.66	80.31	32.56	1.3
460.4	0.94	24.23	56.71	2.4
1359.8	3.15	79.99	58.43	3.6
3844.6	5.93	274.62	58.48	4.9
1731.6	7.81	577.22	65.35	3.7
1260.2	13.23	420.07	71.33	6.4
301.1	4.27	75.27	65.38	7.3

urface samples — Major Element Compositions (Weight %) — Carbonate Bomb

	Height amsl (m)	SiO_2	Al_2O_3	Fe_2O_3	MnO	MgO	CaO	Na_2O	K_2O	TiO_2	P_2O_5	Total	L.O.I.	$CaCO_3$	TiO_2/MgO	Zr/(P_2O_5*100)	CIA	% fines
D1	26	85.04	2.29	5.60	0.1293	0.47	0.88	0.40	0.39	3.5866	0.00	98.78	0.66	0.0	7.63	#DIV/0!	57.83	0.8
D2	28	89.58	2.14	3.41	0.0762	0.25	0.59	0.18	0.64	2.2325	0.00	99.11	0.58	0.0	8.93	#DIV/0!	60.28	0.7
D3	52	90.92	2.03	2.26	0.0484	0.19	1.90	0.26	0.53	1.5060	0.02	99.66	0.68	1.5	7.93	1002.85	43.01	1.2
D4	71	88.03	2.08	3.04	0.0652	0.59	3.11	0.38	0.50	1.7704	0.02	99.60	1.20	2.9	3.00	1155.40	34.27	0.4
CA1	60	74.03	2.75	8.26	0.1820	1.92	4.74	0.34	0.39	5.4086	0.02	98.03	2.35	4.6	2.82	3654.45	33.45	0.2
CA2	44	89.25	2.44	1.32	0.0285	0.60	4.69	0.67	0.75	0.2371	0.05	100.04	3.72	4.5	0.40	33.16	28.54	0.5
K1	3	92.14	5.52	0.63	0.0062	0.12	0.11	0.08	0.98	0.3586	0.01	99.95	2.53	0.0	2.99	235.70	82.51	13.0
Pond C	Various	48.45	21.10	17.59	0.3654	1.83	5.77	0.57	1.20	2.6439	0.45	99.98	14.35	5.6	1.44	12.60	73.67	98.5

ace (ppm)	S	Cl	F	Nb	Y	Rb	Zr	Sr	U	Th	Ba	Sc	Cr	V	La	Zn	Cu
D1	21	642	364	47.5	42.7	10.9	3804.0	56.0	3.1	17.1	115.6	17.7	336.4	185.5	13.8	36.3	1.7
D2	25	561	321	30.0	29.8	16.3	2808.2	50.7	0.0	13.5	169.7	8.3	263.9	114.2	7.1	20.1	0.0
D3	31	108	133	20.4	20.0	14.7	2005.7	42.7	2.7	8.8	135.6	7.2	157.4	77.1	27.2	15.5	1.6
D4	87	318	224	23.5	25.3	13.3	2310.8	80.9	2.3	9.8	130.6	8.6	220.4	95.1	6.1	19.9	1.1
CA1	269	772	420	69.8	63.0	10.5	7308.9	175.6	5.8	30.0	91.2	21.3	566.4	281.9	61.5	46.9	0.0
CA2	287	78	77	2.7	9.3	18.5	165.8	179.1	1.3	0.0	196.7	4.5	65.6	27.9	27.7	12.1	2.8
K1	106	62	70	6.0	10.0	26.3	235.7	27.8	1.2	0.8	273.7	14.3	111.1	83.7	0.0	10.0	7.4
Pond C	351	-	-	28.0	86.0	55.0	567.0	185.0	4.0	48.0	268.0	96.0	862.0	390.0	116.0	104.0	17.0

**Mill Contam * No contamination — **Mill Contamination

ice (ppm)	Ni	Pb	Ga	Co**	Ce	Nd	As	Sn	Ta	Mo	W**	Cd
D1	19.6	11.5	3.0	198.2	63.7	28.3	4.6	0	17	22	992	0
D2	13.6	4.0	3.2	317.9	56.8	21.5	2.3	20	27	20	1671	0
D3	11.6	10.0	4.3	335.8	29.0	7.1	2.4	27	24	14	1808	1
D4	13.5	4.1	2.6	278.4	47.9	13.0	3.1	21	8	14	1492	0
CA1	28.9	1.2	2.7	239.1	120.0	47.0	8.3	12	19	36	1086	0
CA2	11.5	0.0	4.7	225.6	10.8	0.0	0.2	33	12	0	1296	1
K1	7.1	0.8	7.4	196.0	30.9	13.3	0.0	30	5	0	1078	2
PondC	131.0	16.0	22.0	50*	283.0	126.0	48.0	-	-	-	-	-

APPENDIX E4

Heavy mineral ratios (coast parallel)

X	Y	Z	LocalX	LetterY	LocalY	EHM/TH	Magn/Ilm
10041.88	1045.639	38.94	1000	K/1	1050	0.12	0.09
10041.88	1045.639	32.94	1000	K/1	1050	0.12	0.12
10041.88	1045.639	26.94	1000	K/1	1050	0.09	0.27
10041.88	1045.639	20.94	1000	K/1	1050	0.48	0.10
10041.88	1045.639	14.94	1000	K/1	1050	0.53	0.13
10041.88	1045.639	8.94	1000	K/1	1050	0.45	0.06
10041.88	1045.639	2.94	1000	K/1	1050	0.65	0.11
10041.88	1045.639	-3.06	1000	K/1	1050	0.69	0.06
10041.88	1045.639	-9.06	1000	K/1	1050	0.61	0.11
10227.39	998.98	30.11	1020	K	1000	0.23	0.15
10227.39	998.98	24.11	1020	K	1000	0.44	0.11
10227.39	998.98	18.11	1020	K	1000	0.38	0.11
10227.39	998.98	12.11	1020	K	1000	0.61	0.10
10227.39	998.98	6.11	1020	K	1000	0.55	0.13
10227.39	998.98	0.11	1020	K	1000	0.41	0.11
10227.39	998.98	-5.89	1020	K	1000	0.69	0.06
10329.85	944.204	40.41	1030	J/1	950	0.19	0.14
10329.85	944.204	34.41	1030	J/1	950	0.27	0.13
10329.85	944.204	28.41	1030	J/1	950	0.53	0.09
10329.85	944.204	22.41	1030	J/1	950	0.57	0.08
10329.85	944.204	16.41	1030	J/1	950	0.68	0.07
10329.85	944.204	10.41	1030	J/1	950	0.57	0.07
10329.85	944.204	4.41	1030	J/1	950	0.58	0.10
10329.85	944.204	-1.59	1030	J/1	950	0.73	0.06
10485.13	904.766	43.5	1050	J	900	0.40	0.08
10485.13	904.766	37.5	1050	J	900	0.42	0.07
10485.13	904.766	31.5	1050	J	900	0.55	0.07
10485.13	904.766	25.5	1050	J	900	0.60	0.06
10485.13	904.766	19.5	1050	J	900	0.57	0.09
10485.13	904.766	13.5	1050	J	900	0.69	0.06
10485.13	904.766	7.5	1050	J	900	0.70	0.08
10485.13	904.766	1.5	1050	J	900	0.69	0.07
10485.13	904.766	-4.5	1050	J	900	0.66	0.05
10780.56	886.748	48.26	1080	J	900	0.31	0.12
10780.56	886.748	42.26	1080	J	900	0.16	0.20
10780.56	886.748	36.26	1080	J	900	0.18	0.20
10780.56	886.748	30.26	1080	J	900	0.35	0.09
10780.56	886.748	24.26	1080	J	900	0.52	0.08
10780.56	886.748	18.26	1080	J	900	0.59	0.10
10780.56	886.748	12.26	1080	J	900	0.64	0.09
10780.56	886.748	6.26	1080	J	900	0.76	0.06
10780.56	886.748	0.26	1080	J	900	0.62	0.12
10780.56	886.748	-5.74	1080	J	900	0.73	0.15
10926.98	834.255	54.75	1090	H/1	850	0.50	0.11
10926.98	834.255	48.75	1090	H/1	850	0.42	0.18
10926.98	834.255	42.75	1090	H/1	850	0.20	0.14
10926.98	834.255	36.75	1090	H/1	850	0.06	1.00
10926.98	834.255	30.75	1090	H/1	850	0.24	0.08
10926.98	834.255	24.75	1090	H/1	850	0.48	0.06
10926.98	834.255	18.75	1090	H/1	850	0.56	0.07
10926.98	834.255	12.75	1090	H/1	850	0.55	0.06
10926.98	834.255	6.75	1090	H/1	850	0.70	0.07
10926.98	834.255	0.75	1090	H/1	850	0.60	0.06
10926.98	834.255	-5.25	1090	H/1	850	0.70	0.04
11026.11	830.436	56.45	1100	H/1	850	0.19	0.13
11026.11	830.436	50.45	1100	H/1	850	0.23	0.07
11026.11	830.436	44.45	1100	H/1	850	0.18	0.11
11026.11	830.436	38.45	1100	H/1	850	0.08	0.28
11026.11	830.436	32.45	1100	H/1	850	0.05	0.38
11026.11	830.436	26.45	1100	H/1	850	0.29	0.08
11026.11	830.436	20.45	1100	H/1	850	0.53	0.09
11026.11	830.436	14.45	1100	H/1	850	0.60	0.10
11026.11	830.436	8.45	1100	H/1	850	0.73	0.04
11026.11	830.436	2.45	1100	H/1	850	0.71	0.12
11026.11	830.436	-3.55	1100	H/1	850	0.70	0.04
11026.11	830.436	-9.55	1100	H/1	850	0.61	0.08
11227.61	762.532	65.27	1120	H	800	0.15	0.20
11227.61	762.532	59.27	1120	H	800	0.24	0.14
11227.61	762.532	53.27	1120	H	800	0.22	0.14
11227.61	762.532	47.27	1120	H	800	0.23	0.14
11227.61	762.532	41.27	1120	H	800	0.14	0.17
11227.61	762.532	29.27	1120	H	800	0.21	0.13
11227.61	762.532	23.27	1120	H	800	0.47	0.11
11227.61	762.532	17.27	1120	H	800	0.63	0.02
11227.61	762.532	11.27	1120	H	800	0.63	0.11
11227.61	762.532	5.27	1120	H	800	0.60	0.12
11227.61	762.532	-0.73	1120	H	800	0.44	0.19
11227.61	762.532	-6.73	1120	H	800	0.54	0.10
11417.29	695.795	60.59	1140	G	700	0.30	0.10
11417.29	695.795	54.59	1140	G	700	0.32	0.09
11417.29	695.795	48.59	1140	G	700	0.27	0.10
11417.29	695.795	42.59	1140	G	700	0.28	0.09
11417.29	695.795	36.59	1140	G	700	0.25	0.13
11417.29	695.795	30.59	1140	G	700	0.25	0.09
11417.29	695.795	24.59	1140	G	700	0.52	0.07
11417.29	695.795	18.59	1140	G	700	0.48	0.09
11417.29	695.795	12.59	1140	G	700	0.39	0.14
11417.29	695.795	6.59	1140	G	700	0.64	0.11
11417.29	695.795	0.59	1140	G	700	0.63	0.12
11619.81	637.21	73.07	1160	F/1	650	0.22	0.11
11619.81	637.21	67.07	1160	F/1	650	0.22	0.11
11619.81	637.21	61.07	1160	F/1	650	0.05	0.29
11619.81	637.21	55.07	1160	F/1	650	0.13	0.14
11619.81	637.21	49.07	1160	F/1	650	0.21	0.15
11619.81	637.21	43.07	1160	F/1	650	0.22	0.09
11619.81	637.21	37.07	1160	F/1	650	0.41	0.07
11619.81	637.21	31.07	1160	F/1	650	0.41	0.09
11619.81	637.21	25.07	1160	F/1	650	0.47	0.08
11619.81	637.21	19.07	1160	F/1	650	0.63	0.09
11619.81	637.21	13.07	1160	F/1	650	0.71	0.12
11619.81	637.21	7.07	1160	F/1	650	0.30	0.08
11619.81	637.21	1.07	1160	F/1	650	0.74	0.11
11619.81	637.21	-4.93	1160	F/1	650	0.72	0.09
11619.81	637.21	-10.93	1160	F/1	650	0.69	0.06
11840.7	611.249	87.39	1180	F/1	650	0.16	0.18
11840.7	611.249	81.39	1180	F/1	650	0.14	0.17
11840.7	611.249	75.39	1180	F/1	650	0.17	0.16
11840.7	611.249	69.39	1180	F/1	650	0.15	0.19
11840.7	611.249	63.39	1180	F/1	650	0.13	0.16
11840.7	611.249	57.39	1180	F/1	650	0.19	0.12
11840.7	611.249	51.39	1180	F/1	650	0.42	0.07
11840.7	611.249	45.39	1180	F/1	650	0.43	0.07
11840.7	611.249	39.39	1180	F/1	650	0.40	0.09
11840.7	611.249	33.39	1180	F/1	650	0.44	0.09
11840.7	611.249	27.39	1180	F/1	650	0.38	0.09
11840.7	611.249	21.39	1180	F/1	650	0.46	0.08
11840.7	611.249	15.39	1180	F/1	650	0.67	0.09
11840.7	611.249	9.39	1180	F/1	650	0.57	0.14
11840.7	611.249	3.39	1180	F/1	650	0.66	0.11
11840.7	611.249	-2.61	1180	F/1	650	0.73	0.10
11840.7	611.249	-8.61	1180	F/1	650	0.55	0.06

X	Y	Z	LocalX	LetterY	LocalY	EHM/TH	Magn/Ilm
12123.04	530.332	80.58	1210	E	500	0.40	0.08
12123.04	530.332	74.58	1210	E	500	0.16	0.15
12123.04	530.332	68.58	1210	E	500	0.12	0.16
12123.04	530.332	62.58	1210	E	500	0.26	0.06
12123.04	530.332	56.58	1210	E	500	0.19	0.09
12123.04	530.332	50.58	1210	E	500	0.05	0.33
12123.04	530.332	44.58	1210	E	500	0.31	0.09
12123.04	530.332	38.58	1210	E	500	0.21	0.29
12123.04	530.332	32.58	1210	E	500	0.59	0.06
12123.04	530.332	26.58	1210	E	500	0.52	0.08
12123.04	530.332	20.58	1210	E	500	0.58	0.12
12123.04	530.332	14.58	1210	E	500	0.44	0.15
12123.04	530.332	8.58	1210	E	500	0.61	0.05
12123.04	530.332	2.58	1210	E	500	0.68	0.01
12213.12	479.157	78.38	1220	E	500	0.10	0.13
12213.12	479.157	72.38	1220	E	500	0.09	0.13
12213.12	479.157	66.38	1220	E	500	0.16	0.13
12213.12	479.157	60.38	1220	E	500	0.14	0.16
12213.12	479.157	54.38	1220	E	500	0.11	0.16
12213.12	479.157	48.38	1220	E	500	0.10	0.21
12213.12	479.157	42.38	1220	E	500	0.39	0.07
12213.12	479.157	36.38	1220	E	500	0.44	0.10
12213.12	479.157	30.38	1220	E	500	0.53	0.04
12213.12	479.157	24.38	1220	E	500	0.50	0.06
12213.12	479.157	18.38	1220	E	500	0.52	0.11
12213.12	479.157	12.38	1220	E	500	0.50	0.11
12213.12	479.157	6.38	1220	E	500	0.51	0.08
12431.03	453.219	59.72	1240	D/1	450	0.24	0.08
12431.03	453.219	53.72	1240	D/1	450	0.22	0.11
12431.03	453.219	47.72	1240	D/1	450	0.12	0.19
12431.03	453.219	41.72	1240	D/1	450	0.10	0.21
12431.03	453.219	35.72	1240	D/1	450	0.25	0.07
12431.03	453.219	29.72	1240	D/1	450	0.40	0.07
12431.03	453.219	23.72	1240	D/1	450	0.52	0.11
12431.03	453.219	17.72	1240	D/1	450	0.55	0.07
12431.03	453.219	11.72	1240	D/1	450	0.49	0.05
12431.03	453.219	5.72	1240	D/1	450	0.53	0.02
12431.03	453.219	-0.28	1240	D/1	450	0.58	0.01
12572.97	395.863	68.83	1255	D	400	0.10	0.34
12572.97	395.863	62.83	1255	D	400	0.22	0.16
12572.97	395.863	56.83	1255	D	400	0.12	0.44
12572.97	395.863	50.83	1255	D	400	0.12	0.28
12572.97	395.863	44.83	1255	D	400	0.22	0.10
12572.97	395.863	38.83	1255	D	400	0.48	0.08
12572.97	395.863	32.83	1255	D	400	0.44	0.10
12572.97	395.863	26.83	1255	D	400	0.49	0.05
12572.97	395.863	20.83	1255	D	400	0.54	0.15
12572.97	395.863	14.83	1255	D	400	0.80	0.08
12572.97	395.863	8.83	1255	D	400	0.62	0.03
12572.97	395.863	2.83	1255	D	400	0.57	0.30
12718.27	353.707	75.13	1270	C/1	350	0.21	0.17
12718.27	353.707	69.13	1270	C/1	350	0.26	0.13
12718.27	353.707	63.13	1270	C/1	350	0.27	0.13
12718.27	353.707	57.13	1270	C/1	350	0.05	0.35
12718.27	353.707	51.13	1270	C/1	350	0.09	0.18
12718.27	353.707	45.13	1270	C/1	350	0.23	0.13
12718.27	353.707	39.13	1270	C/1	350	0.31	0.09
12718.27	353.707	33.13	1270	C/1	350	0.38	0.09
12718.27	353.707	27.13	1270	C/1	350	0.59	0.04
12718.27	353.707	21.13	1270	C/1	350	0.69	0.04
12718.27	353.707	15.13	1270	C/1	350	0.55	0.06
12718.27	353.707	9.13	1270	C/1	350	0.71	0.02
12829.61	350.743	92.01	1280	C	300	0.17	0.20
12829.61	350.743	86.01	1280	C	300	0.18	0.22
12829.61	350.743	80.01	1280	C	300	0.12	0.29
12829.61	350.743	74.01	1280	C	300	0.19	0.24
12829.61	350.743	68.01	1280	C	300	0.19	0.23
12829.61	350.743	62.01	1280	C	300	0.23	0.14
12829.61	350.743	56.01	1280	C	300	0.50	0.07
12829.61	350.743	50.01	1280	C	300	0.34	0.14
12829.61	350.743	44.01	1280	C	300	0.49	0.08
12829.61	350.743	38.01	1280	C	300	0.49	0.07
12829.61	350.743	32.01	1280	C	300	0.55	0.05
12829.61	350.743	26.01	1280	C	300	0.51	0.08
12829.61	350.743	20.01	1280	C	300	0.62	0.07
12829.61	350.743	14.01	1280	C	300	0.40	0.05
12829.61	350.743	8.01	1280	C	300	0.63	0.03
12829.61	350.743	2.01	1280	C	300	0.65	0.04
12927.23	295.33	81.8	1290	C	300	0.29	0.11
12927.23	295.33	75.8	1290	C	300	0.25	0.12
12927.23	295.33	69.8	1290	C	300	0.23	0.13
12927.23	295.33	63.8	1290	C	300	0.14	0.18
12927.23	295.33	57.8	1290	C	300	0.13	0.17
12927.23	295.33	51.8	1290	C	300	0.10	0.22
12927.23	295.33	45.8	1290	C	300	0.09	0.19
12927.23	295.33	39.8	1290	C	300	0.25	0.12
12927.23	295.33	33.8	1290	C	300	0.39	0.08
12927.23	295.33	27.8	1290	C	300	0.54	0.05
12927.23	295.33	21.8	1290	C	300	0.44	0.09
12927.23	295.33	15.8	1290	C	300	0.44	0.08
12927.23	295.33	9.8	1290	C	300	0.37	0.09
13116.97	249.04	66.32	1310	B/1	250	0.27	0.11
13116.97	249.04	60.32	1310	B/1	250	0.11	0.25
13116.97	249.04	54.32	1310	B/1	250	0.12	0.22
13116.97	249.04	48.32	1310	B/1	250	0.04	0.77
13116.97	249.04	42.32	1310	B/1	250	0.25	0.11
13116.97	249.04	36.32	1310	B/1	250	0.40	0.07
13116.97	249.04	30.32	1310	B/1	250	0.43	0.08
13116.97	249.04	24.32	1310	B/1	250	0.14	0.33
13116.97	249.04	18.32	1310	B/1	250	0.64	0.06
13116.97	249.04	12.32	1310	B/1	250	0.64	0.06
13116.97	249.04	6.32	1310	B/1	250	0.47	0.07
13116.97	249.04	0.32	1310	B/1	250	0.70	0.02
13216.49	185.631	61.3	1320	B	200	0.21	0.13
13216.49	185.631	55.3	1320	B	200	0.27	0.10
13216.49	185.631	49.3	1320	B	200	0.38	0.07
13216.49	185.631	43.3	1320	B	200	0.39	0.09
13216.49	185.631	37.3	1320	B	200	0.53	0.06
13216.49	185.631	31.3	1320	B	200	0.55	0.06
13216.49	185.631	25.3	1320	B	200	0.69	0.06
13216.49	185.631	19.3	1320	B	200	0.67	0.04
13216.49	185.631	13.3	1320	B	200	0.69	0.04
12037.27	605.307	87.75	1200	E1	550	0.171	0.19
12037.27	605.307	81.75	1200	E1	550	0.244	0.11
12037.27	605.307	75.75	1200	E1	550	0.212	0.12
12037.27	605.307	69.75	1200	E1	550	0.156	0.16
12037.27	605.307	63.75	1200	E1	550	0.101	0.17
12037.27	605.307	57.75	1200	E1	550	0.236	0.09
12037.27	605.307	51.75	1200	E1	550	0.47	0.09
12037.27	605.307	45.75	1200	E1	550	0.463	0.08
12037.27	605.307	39.75	1200	E1	550	0.489	0.07
12037.27	605.307	33.75	1200	E1	550	0.534	0.05
12037.27	605.307	27.75	1200	E1	550	0.586	0.05
12037.27	605.307	21.75	1200	E1	550	0.706	0.06
12037.27	605.307	15.75	1200	E1	550	0.703	0.11
12037.27	605.307	9.75	1200	E1	550	0.55	0.13
12037.27	605.307	3.75	1200	E1	550	0.545	0.11
12037.27	605.307	-2.25	1200	E1	550	0.797	0.10
12037.27	605.307	-8.25	1200	E1	550	0.589	0.10

Heavy mineral ratios (coast normal)

X	Y	Z	Hole	LocalY	Magn/Ilm	EHM/THM
12033.88	163.794	69.38	1200A	100	0.18	0.292
12033.88	163.794	63.38	1200A	100	0.22	0.410
12033.88	163.794	57.38	1200A	100	0.07	0.547
12033.88	163.794	51.38	1200A	100	0.05	0.615
12033.88	163.794	45.38	1200A	100	0.07	0.429
12033.88	163.794	39.38	1200A	100	0.09	0.796
12033.88	163.794	33.38	1200A	100	0.05	0.838
12033.88	163.794	27.38	1200A	100	0.01	0.895
12033.88	163.794	21.38	1200A	100	0.01	0.770
12033.88	163.794	15.38	1200A	100	0.02	0.760
12033.01	60.086	55.47	1200AA	0	0.07	0.672
12033.01	60.086	49.47	1200AA	0	0.08	0.554
12033.01	60.086	43.47	1200AA	0	0.09	0.655
12033.01	60.086	37.47	1200AA	0	0.05	0.665
12033.01	60.086	31.47	1200AA	0	0.02	0.533
12033.01	60.086	25.47	1200AA	0	0.01	0.661
12037.72	112.527	59.1	1200AA1	50	0.08	0.358
12037.72	112.527	53.1	1200AA1	50	0.06	0.511
12037.72	112.527	47.1	1200AA1	50	0.07	0.515
12037.72	112.527	41.1	1200AA1	50	0.10	0.420
12037.72	112.527	35.1	1200AA1	50	0.06	0.546
12037.72	112.527	29.1	1200AA1	50	0.01	0.796
12037.72	112.527	23.1	1200AA1	50	0.01	0.817
12031.57	260.764	108.67	1200B	200	0.18	0.254
12031.57	260.764	102.67	1200B	200	0.11	0.274
12031.57	260.764	96.67	1200B	200	0.14	0.219
12031.57	260.784	90.67	1200B	200	0.17	0.367
12031.57	260.764	84.67	1200B	200	0.22	0.568
12031.57	260.764	78.67	1200B	200	0.10	0.299
12031.57	260.764	72.67	1200B	200	0.14	0.590
12031.57	260.764	66.67	1200B	200	0.33	0.712
12031.57	260.764	60.67	1200B	200	0.35	0.786
12031.57	260.764	54.67	1200B	200	0.38	0.044
12031.57	260.764	48.67	1200B	200	0.67	0.019
12031.57	260.764	42.67	1200B	200	0.08	0.334
12031.57	260.764	36.67	1200B	200	0.09	0.329
12031.57	260.764	30.67	1200B	200	0.06	0.494
12031.57	260.764	24.67	1200B	200	0.07	0.398
12031.57	260.764	18.67	1200B	200	0.03	0.566
12031.57	260.764	12.67	1200B	200	0.04	0.402
12034.94	306.629	96.61	1200B/1	250	0.14	0.153
12034.94	306.629	90.61	1200B/1	250	0.13	0.167
12034.94	306.629	84.61	1200B/1	250	0.21	0.108
12034.94	306.629	78.61	1200B/1	250	0.24	0.093
12034.94	306.629	72.61	1200B/1	250	0.30	0.066
12034.94	306.629	66.61	1200B/1	250	0.20	0.104
12034.94	306.629	60.61	1200B/1	250	0.14	0.164
12034.94	306.629	54.61	1200B/1	250	0.14	0.156
12034.94	306.629	48.61	1200B/1	250	0.11	0.276
12034.94	306.629	42.61	1200B/1	250	0.06	0.593
12034.94	306.629	36.61	1200B/1	250	0.05	0.602
12034.94	306.629	30.61	1200B/1	250	0.06	0.606
12034.94	306.629	24.61	1200B/1	250	0.07	0.457
12034.94	306.629	18.61	1200B/1	250	0.06	0.632
12034.94	306.629	12.61	1200B/1	250	0.05	0.525
12034.94	306.629	6.61	1200B/1	250	0.07	0.500
12036.99	-37.236	65.98	1200BB	-100	0.07	0.860
12036.99	-37.236	59.98	1200BB	-100	0.06	0.645
12036.99	-37.236	53.98	1200BB	-100	0.06	0.633
12036.99	-37.236	47.98	1200BB	-100	0.04	0.665
12036.99	-37.236	41.98	1200BB	-100	0.04	0.669
12036.99	-37.236	35.98	1200BB	-100	0.06	0.597
12036.99	-37.236	29.98	1200BB	-100	0.01	0.834
12036.99	-37.236	23.98	1200BB	-100	0.01	0.892
12030.9	15.255	61.61	1200BB1	-50	0.07	0.624
12030.9	15.255	55.61	1200BB1	-50	0.07	0.639
12030.9	15.255	49.61	1200BB1	-50	0.08	0.573
12030.9	15.255	43.61	1200BB1	-50	0.10	0.485
12030.9	15.255	37.61	1200BB1	-50	0.05	0.622
12030.9	15.255	31.61	1200BB1	-50	0.01	0.769
12030.9	15.255	25.61	1200BB1	-50	0.01	0.854
12030.9	15.255	19.61	1200BB1	-50	0.01	0.794
12036.98	353.868	107.99	1200C	300	0.14	0.239
12036.98	353.868	101.99	1200C	300	0.13	0.239
12036.98	353.868	95.99	1200C	300	0.14	0.190
12036.98	353.868	89.99	1200C	300	0.13	0.252
12036.98	353.868	83.99	1200C	300	0.15	0.152
12036.98	353.868	77.99	1200C	300	0.17	0.263
12036.98	353.868	71.99	1200C	300	0.30	0.135
12036.98	353.868	65.99	1200C	300	0.20	0.317
12036.98	353.868	59.99	1200C	300	0.44	0.164
12036.98	353.868	53.99	1200C	300	0.08	0.208
12036.98	353.868	47.99	1200C	300	0.19	0.491
12036.98	353.868	41.99	1200C	300	0.27	0.553
12036.98	353.868	35.99	1200C	300	0.09	0.300
12036.98	353.868	29.99	1200C	300	0.12	0.557
12036.98	353.868	23.99	1200C	300	0.09	0.393
12045.77	397.012	89.12	1200C/1	350	0.24	0.145
12045.77	397.012	83.12	1200C/1	350	0.21	0.147
12045.77	397.012	77.12	1200C/1	350	0.20	0.121
12045.77	397.012	71.12	1200C/1	350	0.19	0.112
12045.77	397.012	65.12	1200C/1	350	0.13	0.198
12045.77	397.012	59.12	1200C/1	350	0.09	0.369
12045.77	397.012	53.12	1200C/1	350	0.41	0.133
12045.77	397.012	47.12	1200C/1	350	0.16	0.201
12045.77	397.012	41.12	1200C/1	350	0.23	0.163
12045.77	397.012	35.12	1200C/1	350	0.21	0.132
12031.39	-142.848	45.4	1200CC	-200	0.04	0.660
12031.39	-142.848	39.4	1200CC	-200	0.06	0.655
12031.39	-142.848	33.4	1200CC	-200	0.02	0.747
12031.39	-142.848	27.4	1200CC	-200	0.01	0.794
12031.39	-142.848	21.4	1200CC	-200	0.01	0.736
12029.12	-86.12	49.56	1200CC1	-150	0.05	0.606
12029.12	-86.12	43.56	1200CC1	-150	0.05	0.602
12029.12	-86.12	37.56	1200CC1	-150	0.04	0.664
12029.12	-86.12	31.56	1200CC1	-150	0.01	0.786
12029.12	-86.12	25.56	1200CC1	-150	0.00	0.909
12029.12	-86.12	19.56	1200CC1	-150	0.01	0.869
12031.27	455.652	76.22	1200D	400	0.14	0.271
12031.27	455.652	70.22	1200D	400	0.13	0.198
12031.27	455.652	64.22	1200D	400	0.18	0.171
12031.27	455.652	58.22	1200D	400	0.16	0.119
12031.27	455.652	52.22	1200D	400	0.29	0.235
12031.27	455.652	46.22	1200D	400	0.39	0.203
12031.27	455.652	40.22	1200D	400	0.17	0.186
12031.27	455.652	34.22	1200D	400	0.09	0.402
12031.27	455.652	28.22	1200D	400	0.10	0.455
12031.27	455.652	22.22	1200D	400	0.14	0.214
12031.27	455.652	16.22	1200D	400	0.18	0.409
12031.27	455.652	10.22	1200D	400	0.08	0.525
12040.55	502.956	76.65	1200D/1	450	0.18	0.134
12040.55	502.956	70.65	1200D/1	450	0.10	0.202
12040.55	502.956	64.65	1200D/1	450	0.14	0.166
12040.55	502.956	58.65	1200D/1	450	0.09	0.182
12040.55	502.956	52.65	1200D/1	450	0.27	0.057
12040.55	502.956	46.65	1200D/1	450	0.07	0.275
12040.55	502.956	40.65	1200D/1	450	0.04	0.500
12040.55	502.956	34.85	1200D/1	450	0.03	0.502
12040.55	502.956	28.65	1200D/1	450	0.03	0.599
12040.55	502.956	22.65	1200D/1	450	0.04	0.611
12040.55	502.956	16.65	1200D/1	450	0.05	0.691
12040.55	502.958	10.65	1200D/1	450	0.05	0.625
12040.55	502.956	4.65	1200D/1	450	0.04	0.646

X	Y	Z	Hole	LocalY	Magn/Ilm	EHM/THM
12029.445	-183.903	40.2	1200DD	-300	0.05	0.730
12029.445	-183.903	34.2	1200DD	-300	0.05	0.862
12029.445	-183.903	28.2	1200DD	-300	0.01	0.713
12029.445	-183.903	22.2	1200DD	-300	0.01	0.836
12029.445	-183.903	40.2	1200DD1	-250	0.04	0.593
12029.445	-183.903	34.2	1200DD1	-250	0.02	0.700
12029.445	-183.903	28.2	1200DD1	-250	0.01	0.832
12037.681	552.746	83.94	1200E	500	0.11	0.422
12037.681	552.746	77.94	1200E	500	0.17	0.245
12037.681	552.746	71.94	1200E	500	0.12	0.271
12037.681	552.746	65.94	1200E	500	0.12	0.226
12037.681	552.746	59.94	1200E	500	0.22	0.122
12037.681	552.746	53.94	1200E	500	0.08	0.615
12037.681	552.746	47.94	1200E	500	0.07	0.355
12037.681	552.746	41.94	1200E	500	0.07	0.533
12037.681	552.746	35.94	1200E	500	0.05	0.383
12037.681	552.746	29.94	1200E	500	0.04	0.581
12037.681	552.746	23.94	1200E	500	0.05	0.533
12037.681	552.746	17.94	1200E	500	0.09	0.577
12037.681	552.746	11.94	1200E	500	0.10	0.676
12037.681	552.746	5.94	1200E	500	0.11	0.734
12037.681	552.746	-0.06	1200E	500	0.06	0.815
12037.681	552.746	-6.06	1200E	500	0.06	0.837
12037.27	605.307	87.75	1200E/1	550	0.19	0.171
12037.27	605.307	81.75	1200E/1	550	0.11	0.244
12037.27	605.307	75.75	1200E/1	550	0.12	0.212
12037.27	605.307	69.75	1200E/1	550	0.16	0.156
12037.27	605.307	63.75	1200E/1	550	0.17	0.101
12037.27	605.307	57.75	1200E/1	550	0.09	0.236
12037.27	605.307	51.75	1200E/1	550	0.09	0.470
12037.27	605.307	45.75	1200E/1	550	0.08	0.463
12037.27	605.307	39.75	1200E/1	550	0.07	0.489
12037.27	605.307	33.75	1200E/1	550	0.05	0.534
12037.27	605.307	27.75	1200E/1	550	0.05	0.586
12037.27	605.307	21.75	1200E/1	550	0.06	0.706
12037.27	605.307	15.75	1200E/1	550	0.11	0.703
12037.27	605.307	9.75	1200E/1	550	0.13	0.550
12037.27	605.307	3.75	1200E/1	550	0.11	0.545
12037.27	605.307	-2.25	1200E/1	550	0.10	0.797
12037.27	605.307	-8.25	1200E/1	550	0.10	0.689
12026.386	-342.032	33.66	1200EE	-400	0.11	0.587
12026.386	-342.032	27.66	1200EE	-400	0.11	0.566
12026.718	-293.097	35.53	1200EE/1	-350	0.01	
12026.718	-293.097	29.53	1200EE/1	-350	0.00	
12026.718	-293.097	23.53	1200EE/1	-350	0.00	
12045.439	650.669	89.72	1200F	600	0.10	0.246
12045.439	650.669	83.72	1200F	600	0.07	0.378
12045.439	650.669	77.72	1200F	600	0.06	0.424
12045.439	650.669	71.72	1200F	600	0.11	0.227
12045.439	650.669	65.72	1200F	600	0.11	0.260
12045.439	650.669	59.72	1200F	600	0.07	0.425
12045.439	650.669	53.72	1200F	600	0.06	0.518
12045.439	650.669	47.72	1200F	600	0.07	0.462
12045.439	650.669	41.72	1200F	600	0.05	0.470
12045.439	650.669	35.72	1200F	600	0.06	0.506
12045.439	650.669	29.72	1200F	600	0.06	0.499
12045.439	650.669	23.72	1200F	600	0.06	0.592
12045.439	650.669	17.72	1200F	600	0.18	0.719
12045.439	650.669	11.72	1200F	600	0.14	0.734
12045.439	650.669	5.72	1200F	600	0.12	0.654
12046.076	702.611	82.81	1200F/1	650	0.10	0.302
12046.076	702.611	76.81	1200F/1	650	0.12	0.265
12046.076	702.611	70.81	1200F/1	650	0.10	0.315
12046.076	702.611	64.81	1200F/1	650	0.09	0.379
12046.076	702.611	58.81	1200F/1	650	0.06	0.397
12046.076	702.611	52.81	1200F/1	650	0.06	0.556
12046.076	702.611	46.81	1200F/1	650	0.07	0.553
12046.076	702.611	40.81	1200F/1	650	0.06	0.460
12046.076	702.611	34.81	1200F/1	650	0.05	0.645
12046.076	702.611	28.81	1200F/1	650	0.09	0.551
12046.076	702.611	22.81	1200F/1	650	0.08	0.547
12046.076	702.611	16.81	1200F/1	650	0.08	0.505
12046.076	702.611	10.81	1200F/1	650	0.12	0.554
12046.076	702.611	4.81	1200F/1	650	0.16	0.504
12046.076	702.611	-1.19	1200F/1	650	0.11	0.668
12046.076	702.611	-7.19	1200F/1	650	0.16	0.576
12020.681	-517.783	33.5	1200FF	-500	0.03	0.582
12020.681	-517.783	27.5	1200FF	-500	0.04	0.657
12049.481	739.961	76.48	1200G	700	0.07	0.172
12049.481	739.961	70.48	1200G	700	0.10	0.295
12049.481	739.961	64.48	1200G	700	0.06	0.245
12049.481	739.961	58.48	1200G	700	0.07	0.308
12049.481	739.961	52.48	1200G	700	0.06	0.494
12049.481	739.961	46.48	1200G	700	0.06	0.612
12049.481	739.961	40.48	1200G	700	0.08	0.512
12049.481	739.961	34.48	1200G	700	0.11	0.545
12049.481	739.961	28.48	1200G	700	0.07	0.583
12049.481	739.961	22.48	1200G	700	0.09	0.605
12049.481	739.961	16.48	1200G	700	0.11	0.609
12049.481	739.961	10.48	1200G	700	0.10	0.281
12049.481	739.961	4.48	1200G	700	0.13	0.644
12049.481	739.961	-1.52	1200G	700	0.10	0.673
12049.481	739.961	-7.52	1200G	700	0.12	0.512
12049.82	787.193	70.9	1200G/1	750	0.14	0.176
12049.82	787.193	64.9	1200G/1	750	0.07	0.450
12049.82	787.193	58.9	1200G/1	750	0.06	0.598
12049.82	787.193	52.9	1200G/1	750	0.06	0.507
12049.82	787.193	46.9	1200G/1	750	0.08	0.465
12049.82	787.193	40.9	1200G/1	750	0.10	0.320
12049.82	787.193	34.9	1200G/1	750	0.07	0.558
12049.82	787.193	28.9	1200G/1	750	0.07	0.384
12049.82	787.193	22.9	1200G/1	750	0.09	0.525
12049.82	787.193	16.9	1200G/1	750	0.06	0.676
12049.82	787.193	10.9	1200G/1	750	0.07	0.608
12049.82	787.193	4.9	1200G/1	750	0.05	0.481
12049.82	787.193	-1.1	1200G/1	750	0.04	0.518
12020.182	-611.876	36.9	1200GG	-600	0.00	0.631
12020.182	-611.876	30.9	1200GG	-600	0.00	0.849
12020.182	-611.876	24.9	1200GG	-600	0.00	0.835
12052.847	856.451	58.41	1200H	800	0.09	0.313
12052.847	856.451	52.41	1200H	800	0.09	0.379
12052.847	856.451	46.41	1200H	800	0.07	0.408
12052.847	856.451	40.41	1200H	800	0.06	0.479
12052.847	856.451	34.41	1200H	800	0.10	0.271
12052.847	856.451	28.41	1200H	800	0.12	0.401
12052.847	856.451	22.41	1200H	800	0.08	0.467
12052.847	856.451	16.41	1200H	800	0.06	0.569
12052.847	856.451	10.41	1200H	800	0.04	0.557
12052.847	856.451	4.41	1200H	800	0.04	0.612
12052.847	856.451	-1.59	1200H	800	0.06	0.561
12052.847	856.451	-7.59	1200H	800	0.05	0.447
12053.802	896.639	48.82	1200H/1	850	0.06	0.442
12053.802	896.639	42.82	1200H/1	850	0.07	0.390
12053.802	896.639	36.82	1200H/1	850	0.07	0.365
12053.802	896.639	30.82	1200H/1	850	0.07	0.419
12053.802	896.639	24.82	1200H/1	850	0.06	0.474
12053.802	896.639	18.82	1200H/1	850	0.07	0.570
12053.802	896.639	12.82	1200H/1	850	0.09	0.592
12053.802	896.639	6.82	1200H/1	850	0.07	0.551
12053.802	896.639	0.82	1200H/1	850	0.07	0.504
12053.802	896.639	-5.18	1200H/1	850	0.06	0.705
12053.802	896.639	-11.18	1200H/1	850	0.05	0.557

X	Y	Z	Hole	LocalY	Magn/Ilm	EHM/THM
12019.56	-719.963	34.7	1200HH	-700	0.01	0.718
12019.56	-719.963	28.7	1200HH	-700	0.00	0.757
12019.56	-719.963	22.7	1200HH	-700	0.05	0.609
12019.56	-719.963	16.7	1200HH	-700	0.08	0.645
12019.56	-719.963	10.7	1200HH	-700	0.03	0.780
12025.35	904.584	47.94	1200J	900	0.10	0.337
12025.35	904.584	41.94	1200J	900	0.08	0.420
12025.35	904.584	35.94	1200J	900	0.07	0.368
12025.35	904.584	29.94	1200J	900	0.08	0.383
12025.35	904.584	23.94	1200J	900	0.11	0.345
12025.35	904.584	17.94	1200J	900	0.12	0.253
12025.35	904.584	11.94	1200J	900	0.08	0.322
12025.35	904.584	5.94	1200J	900	0.09	0.643
12025.35	904.584	-0.06	1200J	900	0.10	0.525
12025.35	904.584	-6.06	1200J	900	0.08	0.545
12025.35	904.584	-12.06	1200J	900	0.08	0.746
12024.51	958.03	38.2	1200J/1	950	0.09	
12024.51	958.03	32.2	1200J/1	950	0.13	
12024.51	958.03	26.2	1200J/1	950	0.08	
12024.51	958.03	20.2	1200J/1	950	0.09	
12024.51	958.03	14.2	1200J/1	950	0.09	
12024.51	958.03	8.2	1200J/1	950	0.13	
12024.51	958.03	2.2	1200J/1	950	0.09	
12024.51	958.03	-3.8	1200J/1	950	0.07	
12024.51	958.03	-9.8	1200J/1	950	0.07	
12024.51	958.03	-15.8	1200J/1	950	0.07	
12024.35	1007.773	35.86	1200K	1000	0.13	0.225
12024.35	1007.773	29.86	1200K	1000	0.28	0.145
12024.35	1007.773	23.86	1200K	1000	0.16	0.437
12024.35	1007.773	17.86	1200K	1000	0.11	0.394
12024.35	1007.773	11.86	1200K	1000	0.08	0.569
12024.35	1007.773	5.86	1200K	1000	0.09	0.653
12024.35	1007.773	-0.14	1200K	1000	0.09	0.553
12024.35	1007.773	-6.14	1200K	1000	0.03	0.284
12024.35	1007.773	-12.14	1200K	1000	0.04	0.245
12022.45	1044.872	39.67	1200K/1	1050	0.14	
12022.45	1044.872	33.67	1200K/1	1050	0.14	
12022.45	1044.872	27.67	1200K/1	1050	0.19	
12022.45	1044.872	21.67	1200K/1	1050	0.17	
12022.45	1044.872	15.67	1200K/1	1050	0.11	
12022.45	1044.872	9.67	1200K/1	1050	0.09	
12022.45	1044.872	3.67	1200K/1	1050	0.08	
12022.45	1044.872	-2.33	1200K/1	1050	0.07	
12022.45	1044.872	-8.33	1200K/1	1050	0.08	
12025.99	1105.87	50.44	1200L	1100	0.21	0.302
12025.99	1105.87	44.44	1200L	1100	0.19	0.323
12025.99	1105.87	38.44	1200L	1100	0.23	0.184
12025.99	1105.87	32.44	1200L	1100	0.19	0.151
12025.99	1105.87	26.44	1200L	1100	0.28	0.172
12025.99	1105.87	20.44	1200L	1100	0.13	0.289
12025.99	1105.87	14.44	1200L	1100	0.10	0.626
12025.99	1105.87	8.44	1200L	1100	0.23	0.494
12025.99	1105.87	2.44	1200L	1100	0.08	0.473
12025.99	1105.87	-3.56	1200L	1100	0.07	0.384
12025.99	1105.87	-9.56	1200L	1100	0.06	0.744
12025.99	1105.87	-15.56	1200L	1100	0.07	0.619
12050.23	1180.818	60.24	1200M	1200	0.18	0.186
12050.23	1180.818	54.24	1200M	1200	0.33	0.066
12050.23	1180.818	48.24	1200M	1200	0.21	0.133
12050.23	1180.818	42.24	1200M	1200	0.23	0.126
12050.23	1180.818	36.24	1200M	1200	0.15	0.258
12050.23	1180.818	30.24	1200M	1200	0.14	0.291
12050.23	1180.818	24.24	1200M	1200	0.11	0.420
12050.23	1180.818	18.24	1200M	1200	0.12	0.278
12053.25	1272.15	53.08	1200N	1300	0.19	0.168
12053.25	1272.15	47.08	1200N	1300	0.17	0.170
12053.25	1272.15	41.08	1200N	1300	0.17	0.212
12053.25	1272.15	35.08	1200N	1300	0.13	0.306
12053.25	1272.15	29.08	1200N	1300	0.14	0.259
12057.6	1370.839	38.6	1200P	1400	0.12	0.203
12057.6	1370.839	32.6	1200P	1400	0.14	0.138
12057.6	1370.839	26.6	1200P	1400	0.11	0.276
12066.09	1475.071	64.52	1200R	1500	0.15	0.369
12066.09	1475.071	58.52	1200R	1500	0.22	0.250
12066.09	1475.071	52.52	1200R	1500	0.09	0.439
12066.09	1475.071	46.52	1200R	1500	0.09	0.372
12066.09	1475.071	40.52	1200R	1500	0.17	0.124
12066.09	1475.071	34.52	1200R	1500	0.16	0.137
12066.09	1475.071	28.52	1200R	1500	0.19	0.068
12066.09	1475.071	22.52	1200R	1500	0.21	0.057
12066.09	1475.071	16.52	1200R	1500	0.11	0.225
12066.09	1475.071	10.52	1200R	1500	0.11	0.323
12066.09	1475.071	4.52	1200R	1500	0.14	0.217
12066.09	1475.071	-1.48	1200R	1500	0.10	0.337
12066.09	1475.071	-7.48	1200R	1500	0.13	0.137
12066.09	1475.071	-13.48	1200R	1500	0.13	0.351
12066.09	1475.071	-19.48	1200R	1500	0.27	0.244
12069.25	1563.791	45.58	1200S	1600	0.15	0.413
12069.25	1563.791	39.58	1200S	1600	0.17	0.386
12069.25	1563.791	33.58	1200S	1600	0.19	0.254
12069.25	1563.791	27.58	1200S	1600	0.23	0.230
12069.25	1563.791	21.58	1200S	1600	0.12	0.333
12069.25	1563.791	15.58	1200S	1600	0.18	0.315
12069.25	1563.791	9.58	1200S	1600	0.13	0.230
12069.25	1563.791	3.58	1200S	1600	0.14	0.214
12069.25	1563.791	-2.42	1200S	1600	0.14	0.251
12069.25	1563.791	-8.42	1200S	1600	0.08	0.329
12069.25	1563.791	-14.42	1200S	1600	0.07	0.374
12074.88	1661.81	27.26	1200T	1700	0.17	0.286
12074.88	1661.81	21.26	1200T	1700	0.21	0.255
12074.88	1661.81	15.26	1200T	1700	0.17	0.268
12074.88	1661.81	9.26	1200T	1700	0.17	0.209
12074.88	1661.81	3.26	1200T	1700	0.17	0.139
12074.88	1661.81	-2.74	1200T	1700	0.16	0.361
12074.88	1661.81	-8.74	1200T	1700	0.12	0.499
12074.88	1661.81	-14.74	1200T	1700	0.08	0.582
12080.05	1761.836	17.8	1200V	1800	0.16	
12080.05	1761.636	11.8	1200V	1800	0.17	
12080.05	1761.636	5.8	1200V	1800	0.11	
12080.05	1761.636	-0.2	1200V	1800	0.13	
12086.38	1862.982	10.94	1200W	1900	0.15	0.265
12086.38	1862.982	4.94	1200W	1900	0.16	0.281
12086.38	1862.982	-1.06	1200W	1900	0.14	0.239
12086.38	1862.982	-7.06	1200W	1900	0.18	0.244
12086.38	1862.982	-13.06	1200W	1900	0.10	0.400
12086.38	1862.982	-19.06	1200W	1900	0.10	0.565
12090.95	1964.884	10.05	1200X	2000	0.15	0.323
12090.95	1964.884	4.05	1200X	2000	0.17	0.250
12090.95	1964.884	-1.95	1200X	2000	0.12	0.454
12090.95	1964.884	-7.95	1200X	2000	0.22	0.207
12090.95	1964.884	-13.95	1200X	2000	0.21	0.243
12090.95	1964.884	-19.95	1200X	2000	0.20	0.239
12097.41	2046.013	5.83	1200Y	2000	0.14	0.307
12097.41	2046.013	-0.17	1200Y	2000	0.16	0.279
12080.1	1761.56	22.0	1200R/B	1750	0.23	0.046
12080.1	1761.56	16.0	1200R/B	1750	0.25	0.049
12080.1	1761.56	10.0	1200R/B	1750	0.05	0.047
12080.1	1761.56	4.0	1200R/B	1750	0.02	0.093
12080.1	1761.56	-2.0	1200R/B	1750	0.08	0.092
12080.1	1761.56	-8.0	1200R/B	1750	0.30	0.094
12080.1	1761.56	-14.0	1200R/B	1750	0.06	0.096
12080.1	1761.56	-20.0	1200R/B	1750	0.04	0.170
12080.1	1761.56	-26.0	1200R/B	1750	0.01	0.231

APPENDIX F

Borehole logs with selected bulk sample, silt-fraction and clay-fraction analyses

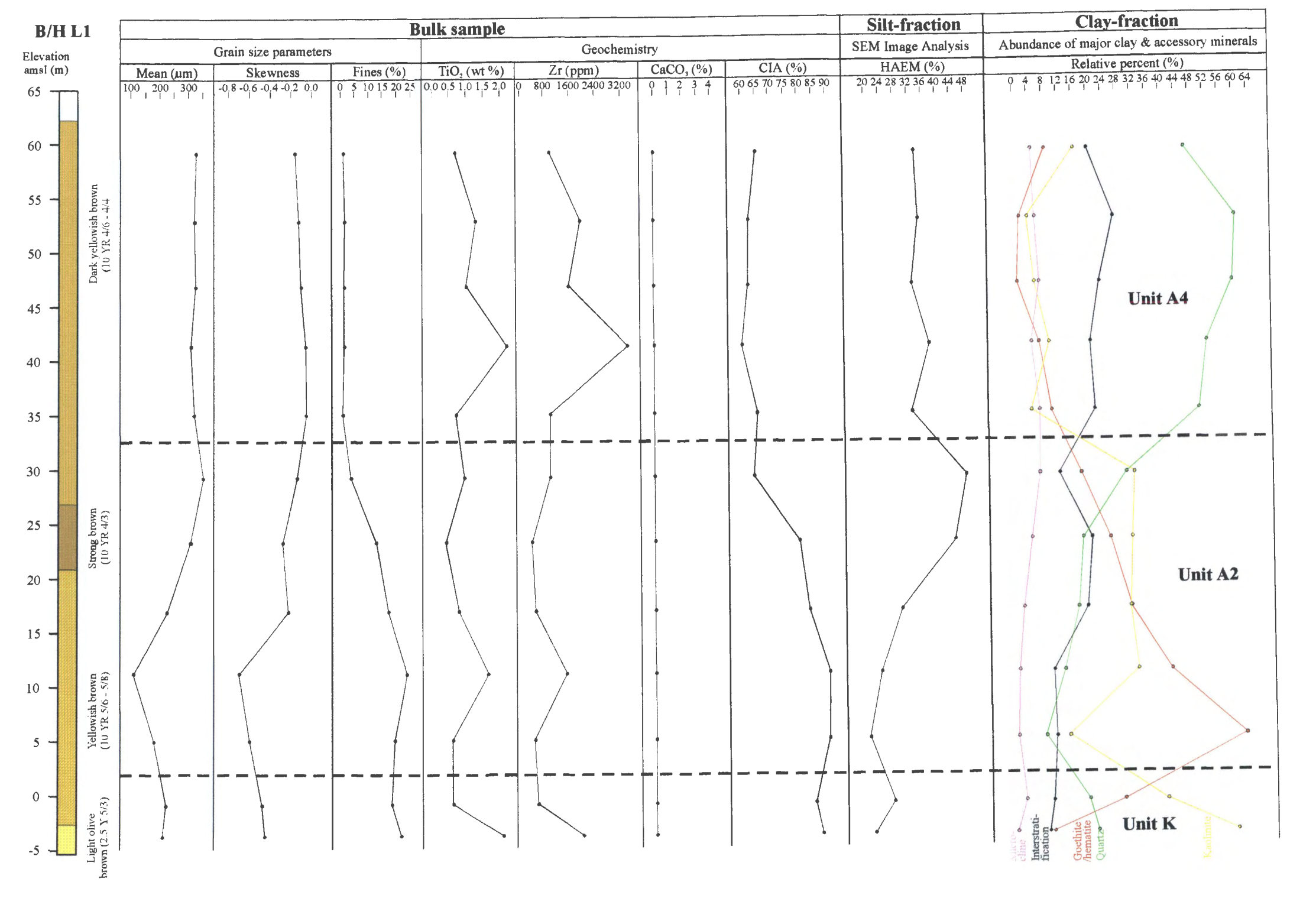
B/H L1
Elevation amsl (m)
Bulk sample
Grain size parameters
Mean (µm)
Skewness
Fines (%)
Geochemistry
TiO2 (wt %)
Zr (ppm)
CaCO3 (%)
CIA (%)
Silt-fraction
SEM Image Analysis
HAEM (%)
Clay-fraction
Abundance of major clay & accessory minerals
Relative percent (%)
Dark yellowish brown (10 YR 4/6 - 4/4
Strong brown (10 YR 4/3)
Yellowish brown (10 YR 5/6 - 5/8)
Light olive brown (2.5 Y 5/3)
Unit A4
Unit A2
Unit K
Interstratification
Goethite /hematite
Quartz
Kaolinite

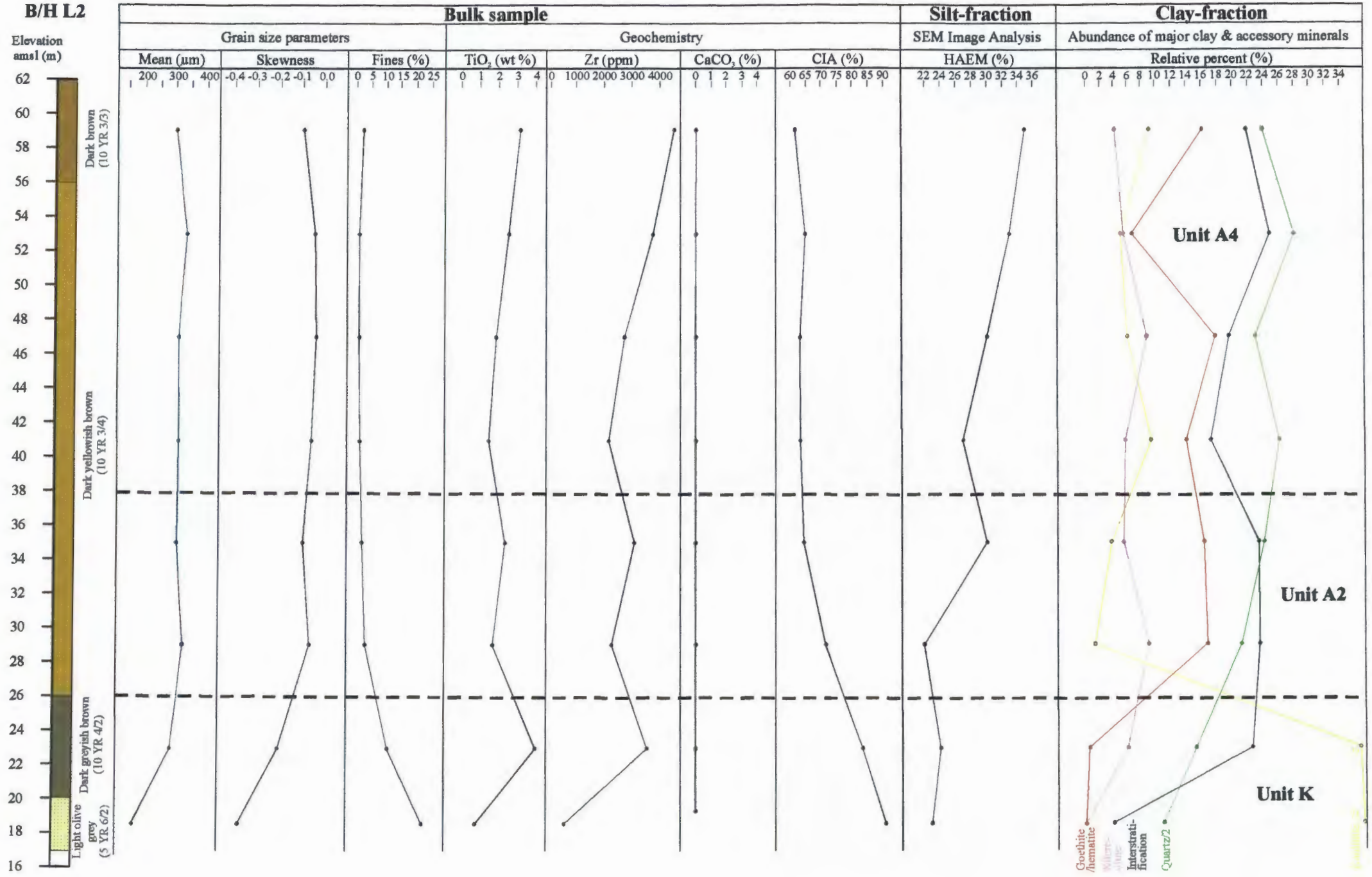
B/H L2
Elevation amsl (m)
62
60
58
56
54
52
50
48
46
44
42
40
38
36
34
32
30
28
26
24
22
20
18
16
Dark brown (10 YR 3/3)
Dark yellowish brown (10 YR 3/4)
Dark greyish brown (10 YR 4/2)
Light olive grey (5 YR 6/2)
Bulk sample
Grain size parameters
Mean (µm)
200 300 400
Skewness
-0.4 -0.3 -0.2 -0.1 0.0
Fines (%)
0 5 10 15 20 25
Geochemistry
TiO2 (wt %)
0 1 2 3 4
Zr (ppm)
0 1000 2000 3000 4000
CaCO3 (%)
0 1 2 3 4
CIA (%)
60 65 70 75 80 85 90
Silt-fraction
SEM Image Analysis
HAEM (%)
22 24 26 28 30 32 34 36
Clay-fraction
Abundance of major clay & accessory minerals
Relative percent (%)
0 2 4 6 8 10 12 14 16 18 20 22 24 26 28 30 32 34
Unit A4
Unit A2
Unit K
Goethite /hematite
Interstrati-fication
Quartz/2

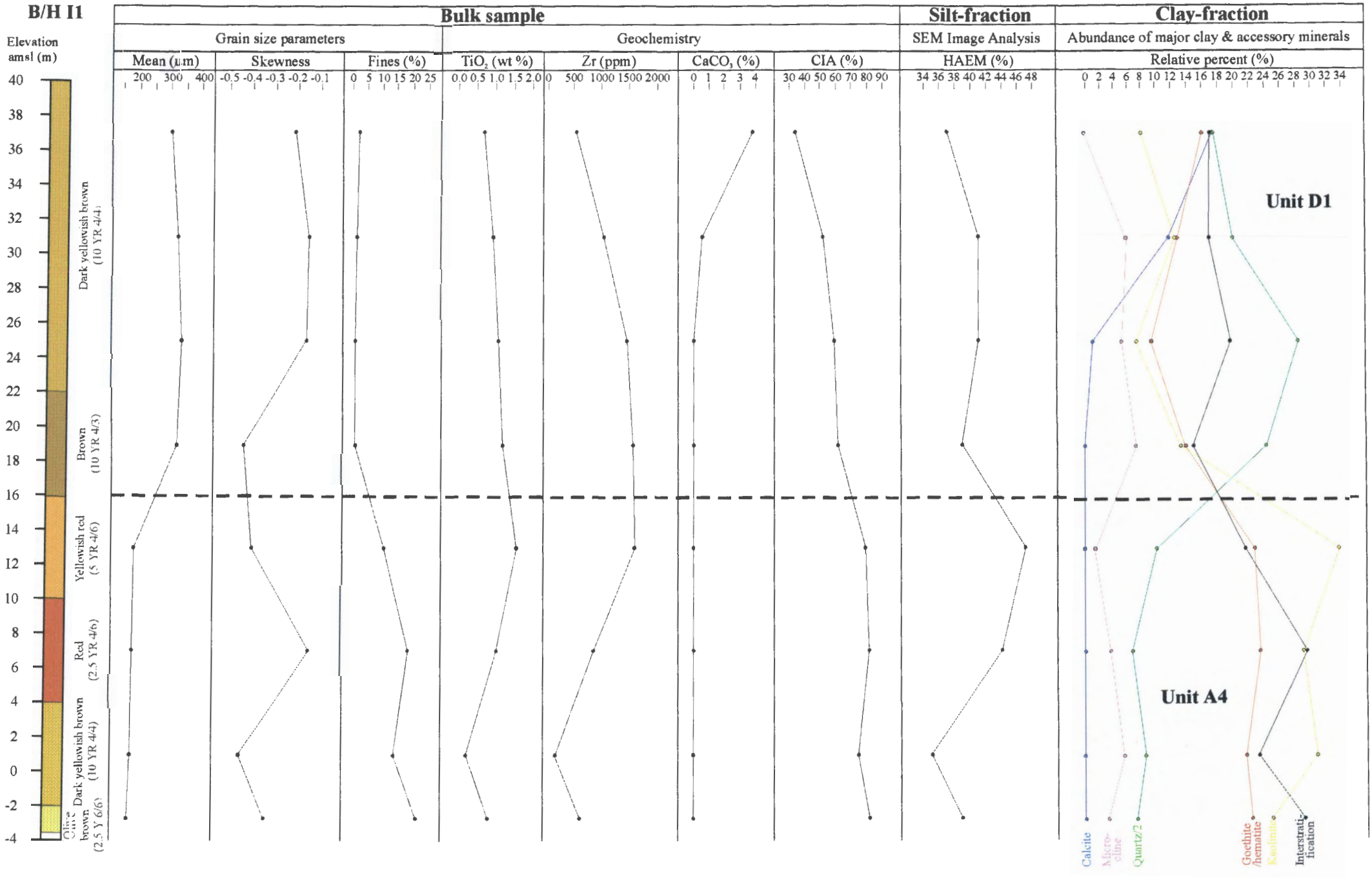
B/H I1
Bulk sample
Silt-fraction
Clay-fraction
Grain size parameters
Geochemistry
SEM Image Analysis
Abundance of major clay & accessory minerals
Elevation amsl (m)
Mean (µm)
Skewness
Fines (%)
TiO2 (wt %)
Zr (ppm)
CaCO3 (%)
CIA (%)
HAEM (%)
Relative percent (%)
Dark yellowish brown (10 YR 4/4)
Brown (10 YR 4/3)
Yellowish red (5 YR 4/6)
Red (2.5 YR 4/6)
Dark yellowish brown (10 YR 4/4)
Olive brown (2.5 Y 6/6)
Unit D1
Unit A4
Calcite
Micro-cline
Quartz/2
Goethite /hematite
Kaolinite
Interstrati-fication

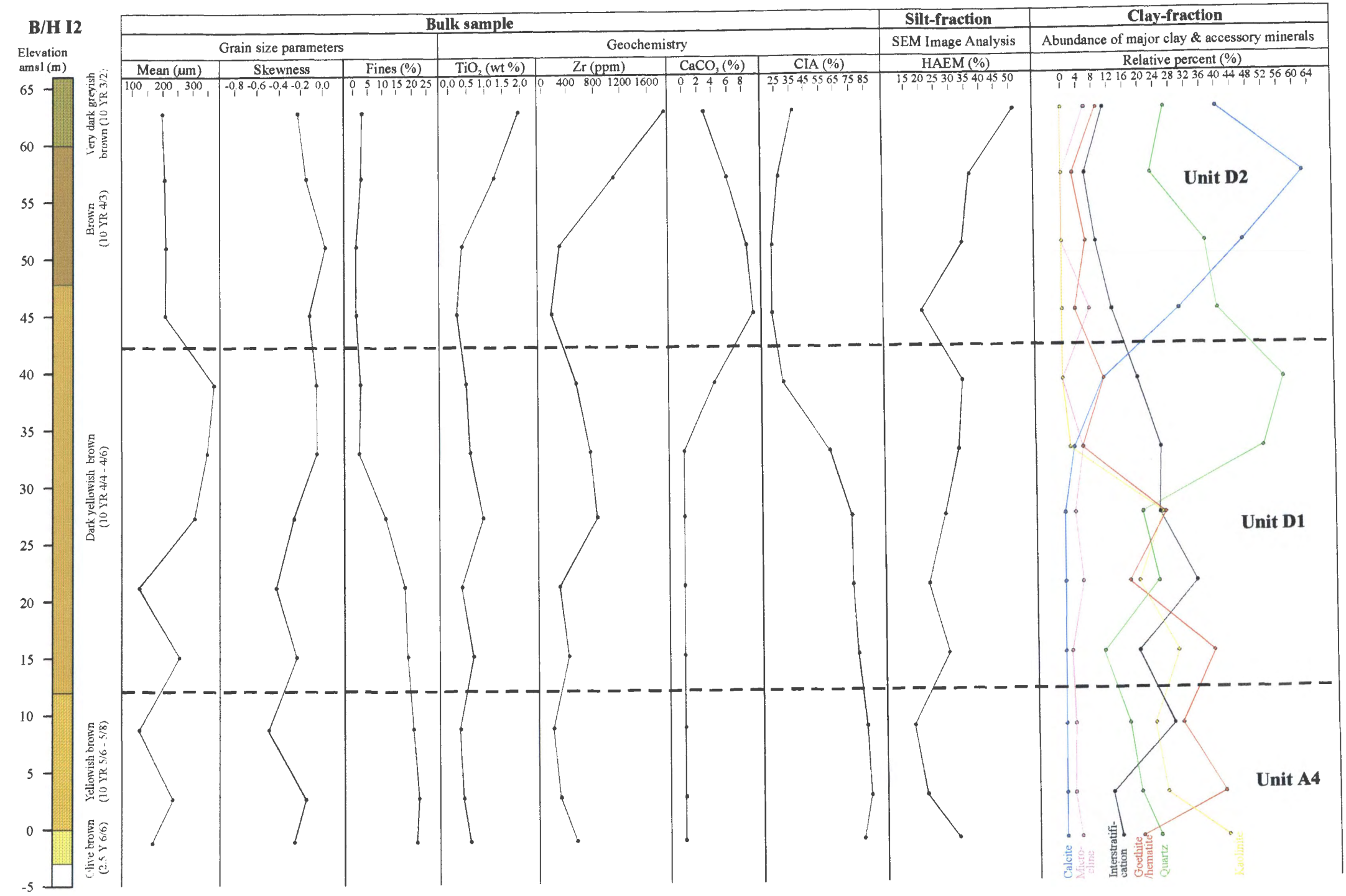
B/H I2
Elevation amsl (m)
Very dark greyish brown (10 YR 3/2)
Brown (10 YR 4/3)
Dark yellowish brown (10 YR 4/4 - 4/6)
Yellowish brown (10 YR 5/6 - 5/8)
Olive brown (2.5 Y 6/6)
Bulk sample
Grain size parameters
Mean (µm)
Skewness
Fines (%)
Geochemistry
TiO2 (wt %)
Zr (ppm)
CaCO3 (%)
CIA (%)
Silt-fraction
SEM Image Analysis
HAEM (%)
Clay-fraction
Abundance of major clay & accessory minerals
Relative percent (%)
Unit D2
Unit D1
Unit A4
Calcite
Micro-cline
Interstratifi-cation
Goethite /hematite
Quartz
Kaolinite

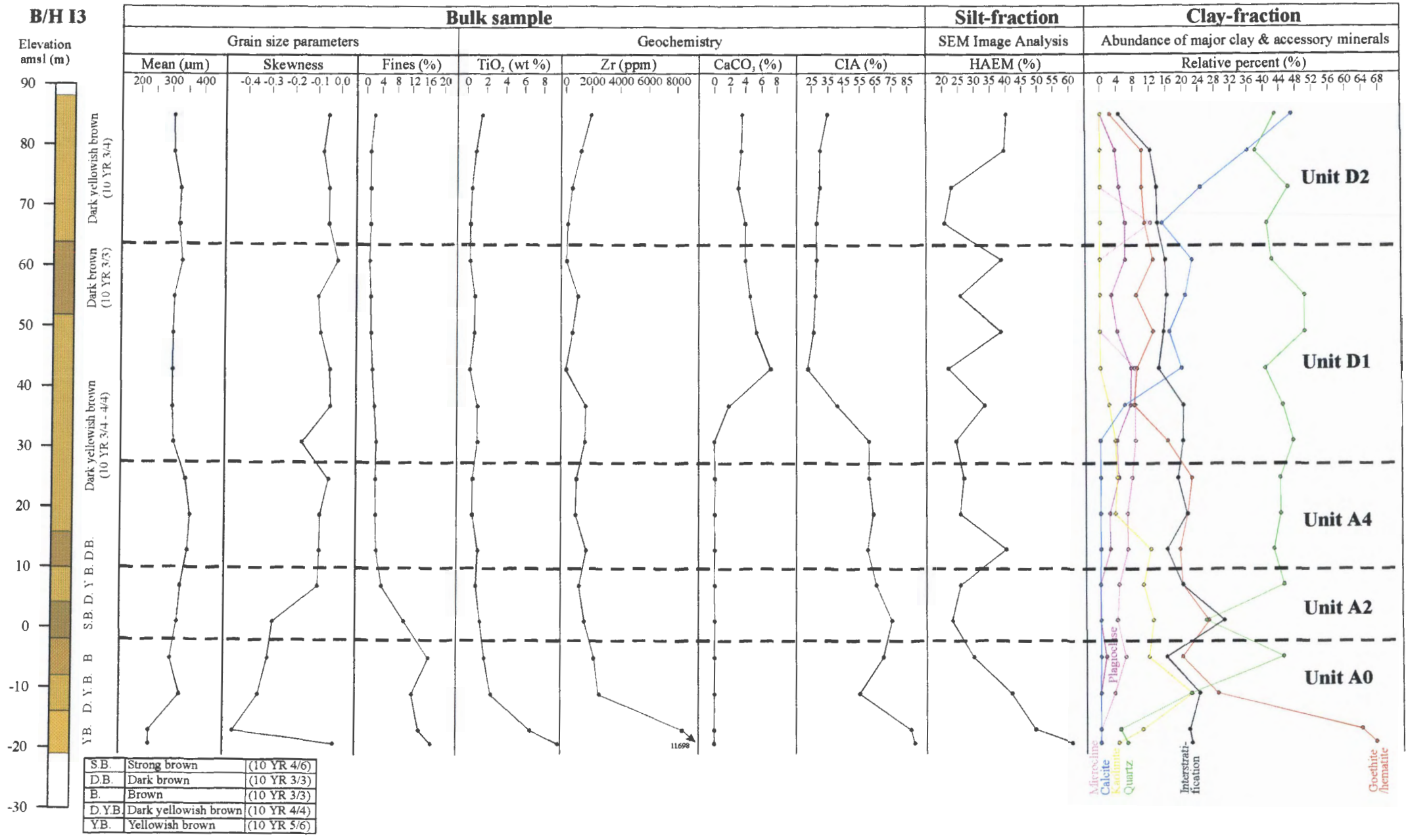
B/H I3
Elevation amsl (m)
Bulk sample
Grain size parameters
Geochemistry
Silt-fraction
SEM Image Analysis
Clay-fraction
Abundance of major clay & accessory minerals
Mean (µm)
Skewness
Fines (%)
TiO2 (wt %)
Zr (ppm)
CaCO3 (%)
CIA (%)
HAEM (%)
Relative percent (%)
Dark yellowish brown (10 YR 3/4)
Dark brown (10 YR 3/3)
Dark yellowish brown (10 YR 3/4 - 4/4)
S.B.
D.Y.B.
D.B.
B
D.Y.B.
Y.B.
Unit D2
Unit D1
Unit A4
Unit A2
Unit A0
11698
Minnesline
Calcite
Kaolinite
Quartz
Plagioclase
Interstrati-fication
Goethite /hematite
S.B. Strong brown (10 YR 4/6)
D.B. Dark brown (10 YR 3/3)
B. Brown (10 YR 3/3)
D.Y.B. Dark yellowish brown (10 YR 4/4)
Y.B. Yellowish brown (10 YR 5/6)

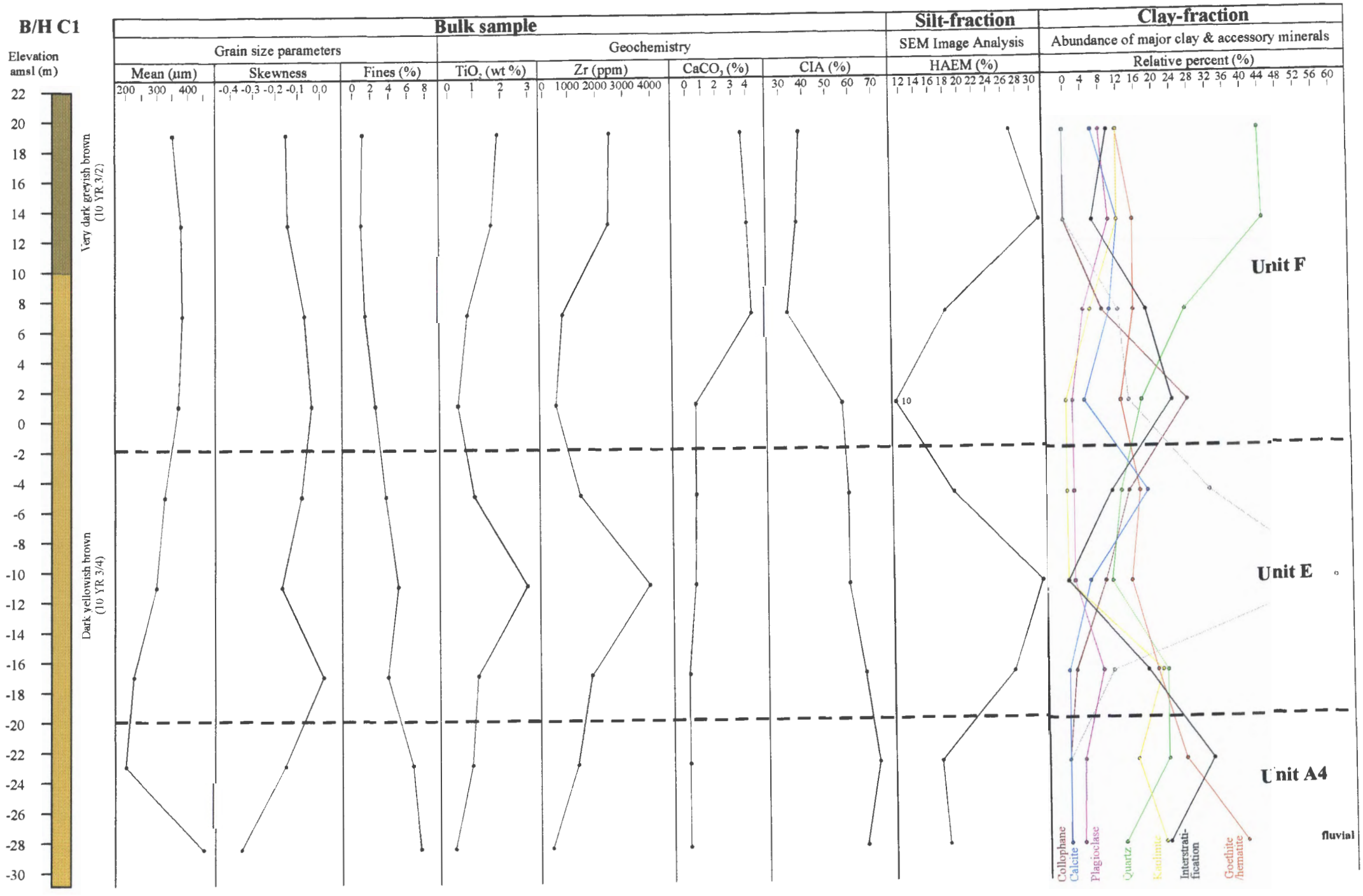
B/H C1
Elevation amsl (m)
Very dark greyish brown (10 YR 3/2)
Dark yellowish brown (10 YR 3/4)
Bulk sample
Grain size parameters
Mean (µm)
Skewness
Fines (%)
Geochemistry
TiO2 (wt %)
Zr (ppm)
CaCO3 (%)
CIA (%)
Silt-fraction
SEM Image Analysis
HAEM (%)
Clay-fraction
Abundance of major clay & accessory minerals
Relative percent (%)
Unit F
Unit E
Unit A4
fluvial
Collophane
Calcite
Plagioclase
Quartz
Kaolinite
Interstrati-fication
Goethite /hematite

APPENDIX G

FURTHER LUMINESCENCE DATES FOR THE ZULULAND DUNE CORDON, RICHARDS BAY, KWAZULU-NATAL, SOUTH AFRICA.

STEPHAN WOODBORNE & GILL COLLETT

QUATERNARY DATING RESEARCH UNIT,
ENVIRONMENTEK
CSIR

January 2001

Terms of reference

The coastal foreland between Richards Bay and St. Lucia on the Zululand coast of Kwazulu-Natal is part of a mining concession held by TISAND (PTY) LIMITED and RICHARDS BAY IRON & TITANIUM (PTY) LIMITED. Geological research on these dunes is being conducted by Mr. Chris Ware on behalf of TISAND (PTY) LIMITED and RICHARDS BAY IRON & TITANIUM (PTY) LIMITED. The dating results that are presented in this report were commissioned by Dr. Greg Whitmore of the University of Natal on behalf of Mr. Ware. The results are subject to a confidentiality agreement between the CSIR and Tisand, and will not be made available by the CSIR to any parties other than Mr. Ware and Dr. Whitmore at the University of Natal. The CSIR is not obliged to share the results with TISAND (PTY) LIMITED and RICHARDS BAY IRON & TITANIUM (PTY) LIMITED, and any disclosure will be made by Mr. Ware and Dr. Whitmore in terms of the contractual relation ship between TISAND (PTY) LIMITED and RICHARDS BAY IRON & TITANIUM (PTY) LIMITED and the University of Natal and its representatives.

Introduction

Luminescence dating techniques are acknowledged as the appropriate approach to determining the age of sand deposition in coastal dunes. The technique is based on the accumulation of radiation damage in the mineral crystal that makes up the sand grains. At the time of deposition the sand grains are presumed to be wind transported over a reasonable distance ensuring that the grains are individually exposure to sufficient sunlight to anneal all previous radiation damage. The source of radiation is uranium, thorium, rubidium and potassium that are ubiquitous in sand bodies, as well as cosmic radiation. Hence at the time of deposition it is assumed that there was no radiation damage in the grains, and that any radiation damage that is detected in the present is the result of the ambient radiation flux and the duration of the burial. Based on the zeroing assumption, the age of deposition can then be calculated from the radiation dose rate that is a measure of the *in situ* radiation flux that the grains experienced (D), and the radiation dose equivalent that the grains have absorbed (equivalent dose D_E). The age is given by the equation:

$$AGE = \frac{D_E}{D}$$

The radiation damage comprises electrons that are displaced from their normal position in the crystal lattice by the energy input from the radiation. The electrons are lodged in "traps" and can be ejected by heating or exposure to light. This is the reason why sunlight exposure zeroes the radiation damage. Different luminescence dating techniques target very specific traps. Using Infrared Stimulated Luminescence (IRSL) the grains are exposed to infrared light with a wavelength of 880 nm, which ejects the electrons from a specific energy trap. The population of electrons that is affected by IRSL is extremely light sensitive, and exposure to sunlight for minutes rather than hours will effectively zero the traps. The thermoluminescence (TL) technique uses heat to eject the electrons from the traps. The grains are carefully heated to a temperature of 425°C, and in the process electron traps of progressively higher energy are affected. Two traps are of particular significance in the TL techniques. The first is stimulated at 325°C, and the second at 375°C. The former is called the "rapidly bleaching peak" and the latter is called the "slow bleaching peak" (RBP and SBP respectively). As the name implies the two traps respond differently with respect to zeroing. While the difference between the RBP and SBP is to be noted, the zeroing of the traps associated with the TL technique requires sunlight exposure in the order of days and so the difference between the IRSL technique and the TL technique is of particular significance.

Just as the zeroing of the luminescence signal is a critical assumption in the dating of dunes, so too is the assumption that the dose rate has remained constant through time. This can present a problem as the carbonate in coastal dunes is subject to diagenetic changes that may significantly impact on the dose rate. Luminescence dating techniques can be used to assess if the dose rate that is measured in the present is the same as the dose rate that has applied through the entire deposition history of the dune, provided certain conditions have been met (Vogel et al. 1999). The essential assumption is common to the standard dating approach, and that is that the luminescence signal was zeroed at the time of deposition.

Following the work of Sudan, six additional samples were selected from the dune sequence in the vicinity of Richards Bay for the purposes of luminescence dating. All samples were collected in PVC pipes that were forced into the exposed sections of the dunes. The sample sites were carefully selected to ensure that the samples came from *in situ* material and not slumped sections. The core that was removed in the tube remained intact ensuring negligible sunlight exposure except for the material at each end. This was subsequently excluded from the analytical samples. The analytical protocols used in this study are the same as those used

in the previous analyses, and the results of the Sudan study are included for ease of comparison.

Sample pretreatment

The exposed sand at each end of the sample tubes was discarded in dark condition. An aliquot of the remaining material was used for thick source alpha counting (Daybreak system) to determine the uranium and thorium content, as well as XRF analysis to determine the potassium content of the sediment (results presented in table 1). The remaining unexposed material was acidified (conc. HCl) to dissolve the carbonates that were present, and washed in sodium hydroxide to exclude organic contaminants. The samples were dried and sieved to the size fractions indicated in table 1. The selected grain size fraction was subject to magnetic separation to exclude metallic and magnetic grains, and finally density separation in sodium polytungstate solution at S.G. 2.58 and 2.62 to isolate the desired mineral fraction. The grains that floated in the S.G. 2.58 solution are presumed to be high potassium feldspars, which were used in the IRSL analysis, and the grains that sank in the S.G. 2.62 solution are presumed to be quartz, which was used in the TL analysis (Mejdahl 1985). This protocol allows for two different luminescence dating techniques to be applied to the same sample.

Equivalent Dose measurements

In the case of both IRSL and TL techniques a regeneration approach was used to determine the D_E value for the sediment. The IRSL analysis was done on 5 aliquots of grains that were mounted on aluminium disks. Each disk was measured in the IRSL machine using four short infrared exposures of 0.1s. This yielded the natural IRSL signal of each aliquot. The samples were then zeroed by exposure to bright sunlight for 5 days and then re-measured to give a bleached signal. The IRSL signal was then regenerated by successive exposure of each aliquot to a calibrated radiation dose. After each irradiation the aliquot was measured and then re-irradiated until the regenerated IRSL signal was in excess of the natural signal. Regression analysis of the data, presented graphically in figure 1, yielded the required D_E values. The values for each aliquot were normalised to the average natural IRSL signal.

A multiple aliquot approach was used to determine the D_E value using the TL technique. A minimum of 5 aliquots of quartz was placed on stainless steel planchettes for the purpose of the measurement. Each aliquot was carefully weighed for subsequent mass normalisation between aliquots. The TL measurement used a heating rate of 1.5 °C/s up to a maximum of 425 °C. A further 5 aliquots was prepared for the bleached measurement and thereafter each regeneration curve represents the average of 5 aliquots. The results of the TL analysis are presented in figure 2. In order to determine the relationship between the RBP and the SBP the ratio between the natural measurement and the regeneration measurements is presented in figure 2. Differences between the ratio at 325 °C and 375 °C are indicative of poor bleaching. Where bleaching is inadequate it is more appropriate to use the data from the 325 °C peak as it is the more likely component of the TL signal to have been zeroed, although there is still the possibility that the signal was not entirely zeroed and a residual signal at the time of deposition would render dates that are too old. Reliance on the 375 °C peak exacerbates this problem. The integration of the relevant TL data yielded the growth curves in figure 2 that are the basis of the regressions that yield the required D_E values.

In both the IRSL and TL analyses the samples were subject to a preheat before each measurement. This involved heating the aliquots to 160 °C for 16 hours. A 24 hour relaxation period was allowed between irradiations and preheats, and between preheats and

measurement. A correction was made for the impact of successive preheats on the IRSL samples (Duller 1991).

Results

The results of the dosimetry and the D_E evaluations are presented in table 1. Initial scrutiny of the plateau data for the TL analyses suggests that on sample D1 was well zeroed, while samples D2, D3, D4, CA1 and CA2 show a distinct difference between the RBP and SBP. This suggests poor zeroing and possibly age over-estimations in the latter samples. In the case of sample CA1 the extremely young age means that the discrepancy is negligible. The inter-aliquot variability in the IRSL analyses is often a reflection of poor zeroing. Slight variations in the proportion of well-zeroed and poorly zeroed grains within each aliquot produce different D_E values that, when normalised, results in different growth curves. Figure 3 presents the natural IRSL values for each aliquot in the entire analysis plotted against the associated D_E values. Linear trends towards the origin are indicative of poor zeroing. This suggests that samples RBM2 (Sudan study), CA2 and D1 are well zeroed while the rest are not. The sensitiviy data presented in figure 3 also suggests the possibility that samples D2, D4 and CA1 derive from a common origin.

Combining the evidence for zeroing from both the IRSL and TL analyses it is clear that only one sample, D1, is well zeroed. This is supported by the fact that the TL and IRSL dates are statistically the same date at about 180 ka. It is likely that this dune was formed as sea levels dropped at the end of oxygen isotope stage 7.

With the exception of sample D1 the evidence for poor zeroing clouds the literal interpretation of the results. In particular a comparison of the IRSL and TL dates yields significant differences. When such discrepant results occur there is a tendency to attribute the reason to the instability of the dating signal in the feldspars, and hence to discard the IRSL results. However, the mechanisms that are involved such as anomalous fading and sensitivity changes, are likely to yeld progressively bigger IRSL/TL disparities for progressively older samples. No such trend exists in this set of sample (figure 4), and indeed the smallest error is associated with the oldest sample. This supports the conclusion that was previously suggested in the study by Sudan that inadequate zeroing has occurred at the time of deposition. If this position is adopted then the IRSL dates must be interpreted as the likely date of deposition, although it must be considered that the IRSL signal itself may not have been zeroed and the desired date is possibly even younger. The TL dates associated with the SBP, particularly where there is a large difference between the date derived from the RBP and SBP, provide some indication of the original date of deposition prior to the reworking of the dune. In the same way that the IRSL is an overestimation of the date of reworking, the TL date is an underestimation of the original date of sand generation. The evidence suggests that most of the original dune formation took place prior to the last ice age, and the current landscape represents the same sand that has been shifted around during the Holocene. Only sample CA1 yields a young IRSL and a young TL date. This may represent recent inputs of sand into the landscape.

This proposal that dune sands are poorly zeroed is counter-intuitive as the mechanism for deposition is presumed to zero the signal adequately. It must be concluded that the standard mode of formation for the dunes in question does not apply, and that the mode of transport involves very rapid mobilisation and re-deposition of the sand without sufficient time to zero the luminescence signal. The exact mechanism is not clear, but possibilities include large scale slumping of steep dunes that may become deforested as a result of environmental factors, or possibly the role of major environmental events.

Conclusions

On the basis of the available data there appears to have been at least two, but possibly three periods of sand generation in the Richards Bay area. The first occurred at the end of oxygen isotope stage 7 at 180 ka (sample D1). The second occurred prior to the last ice age (c.16 ka). It is likely that this sand was generated on the landscape at an earlier stage, possibly oxygen isotope stage 5, and has been reworked on numerous occasions. Since non of the anticipated evidence for dune formation between 100ka and 75 ka has been found, it is possible that the these dunes have been reworked entirely, which also introduces the possibility that part of the 180 ka dune was also reworked. This would be largely dependent on which dunes were exposed and the dynamic interaction between environmental conditions such as rainfall and wind and vegetation cover. The third possible input of sand is represented by sample CA1 which may be sand that was generated during the Holocene.

References

Duller, G.A.T. 1991. Equivalent dose determination using single aliquots. Nuclear tracks and radiation measurements 18:371-78.

Mejdahl, V. 1985. Thermoluminescence dating based on feldspars. Nuclear Tracks and Radiation Measurements 10:133-36.

Vogel, J.C.; Wintle, A.G. & Woodborne, S.M. 1999. Focus: Luminescence dating of coastal sands: Overcoming changes in environmental dose rate. Journal of Archaeological Science 26:729-33.

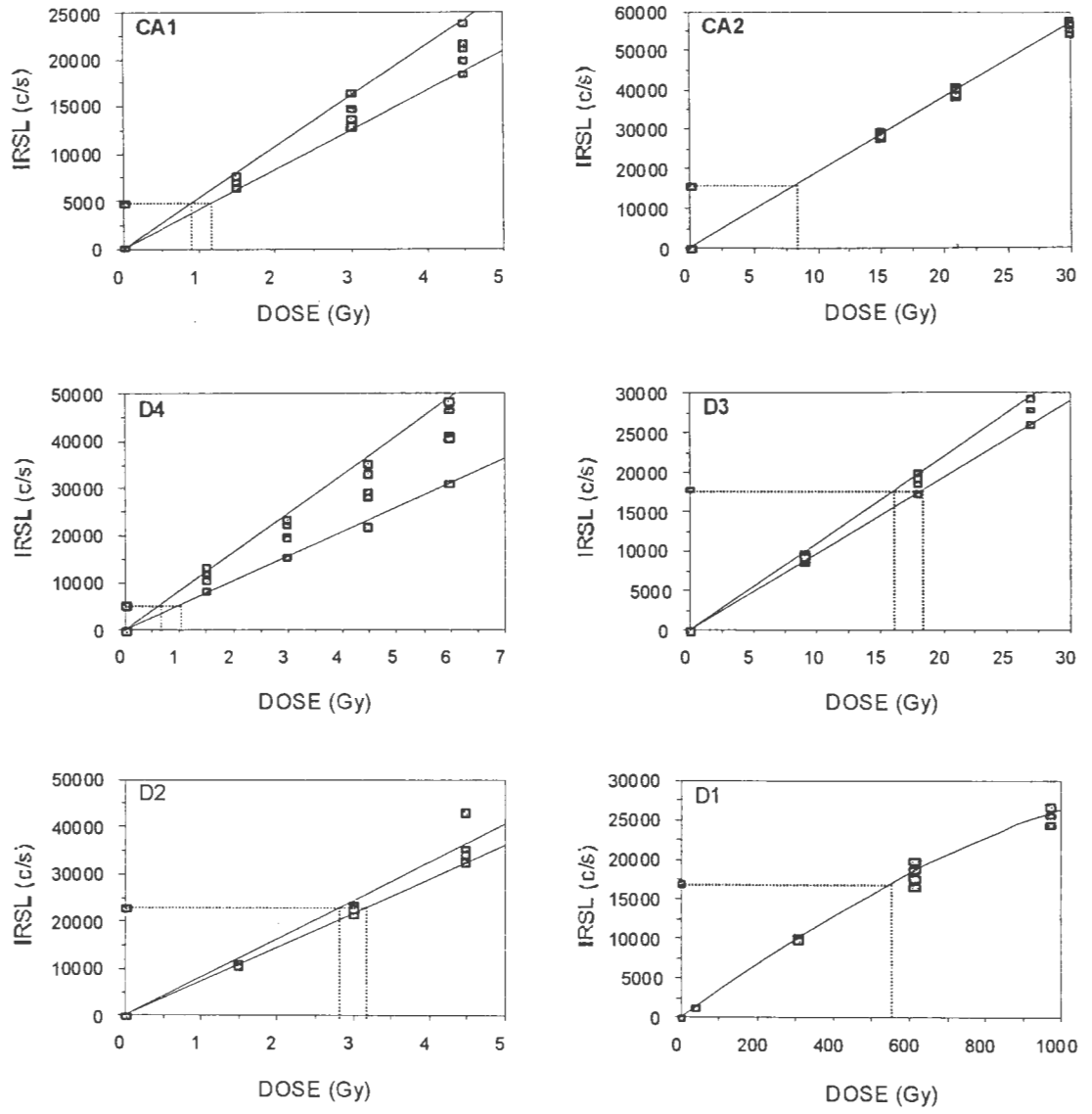

Figure 1. Infrared stimulated luminescence (IRSL) growth curves. The growth curves for each sample are normalised to the average natural IRSL. The variability in the growth curve between aliquots in samples CA1, D4, D3, and D2 results in poor precision on the D_E values that are obtained. This is an indication of poor bleaching. In contrast samples CA2 and D1 appear to be adequately bleached.

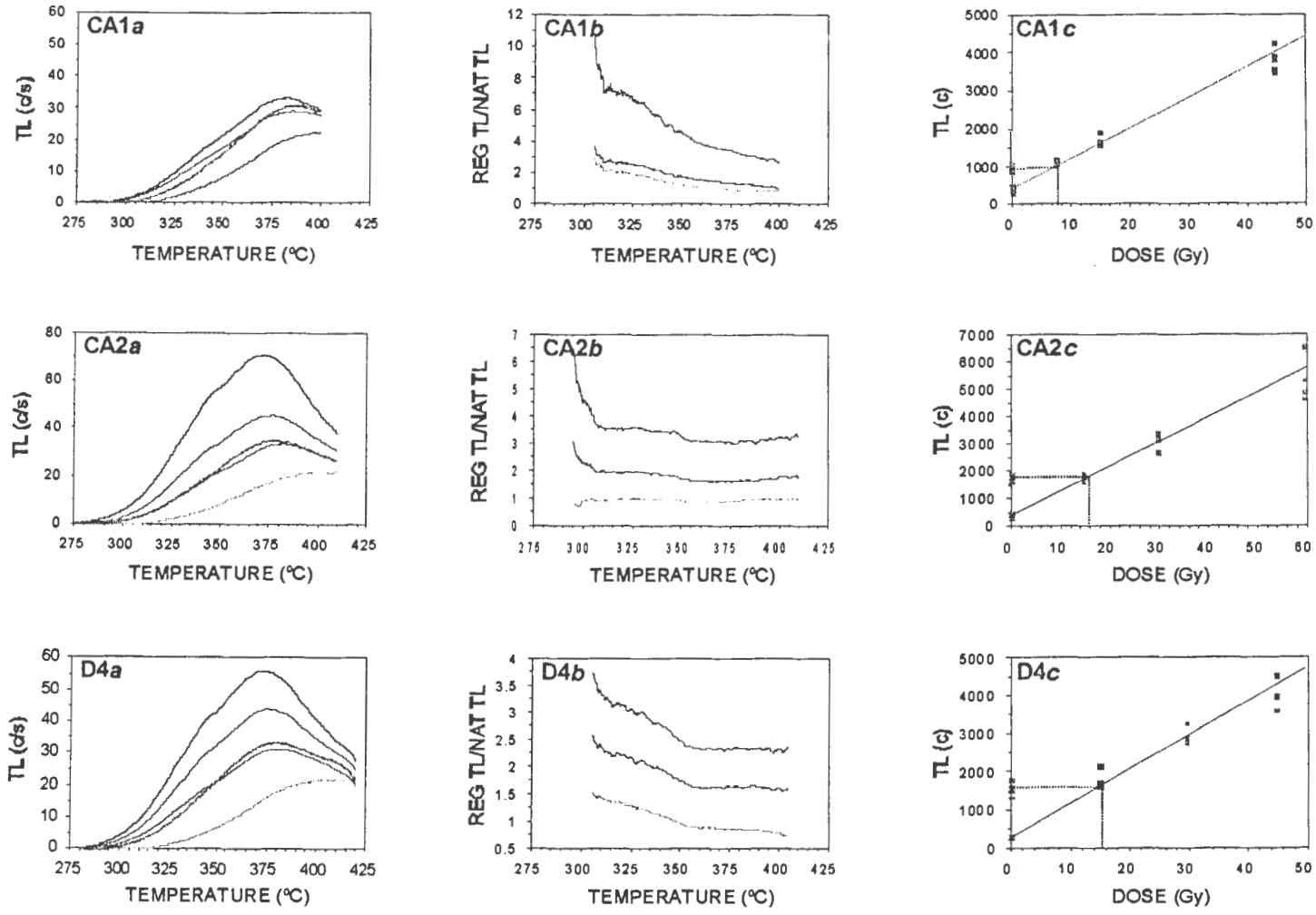

Figure 2. Graphic presentation of luminescence data. For each sample the italicised *a* represents the glow curves, *b* represents the plateau and is an indication of the degree of bleaching, and *c* represents the growth curve derived from integration of the glow curves.

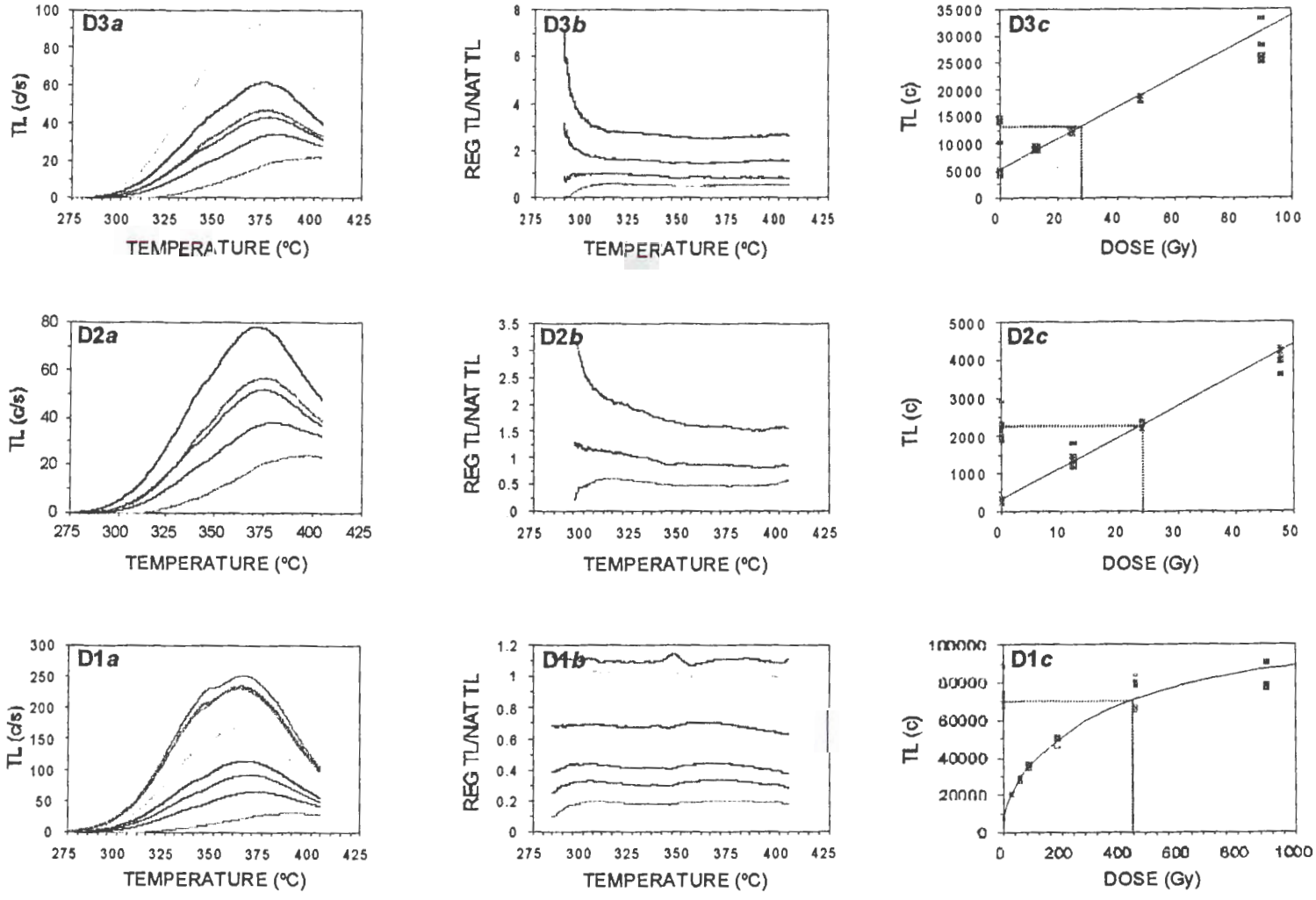

Figure 2 continue

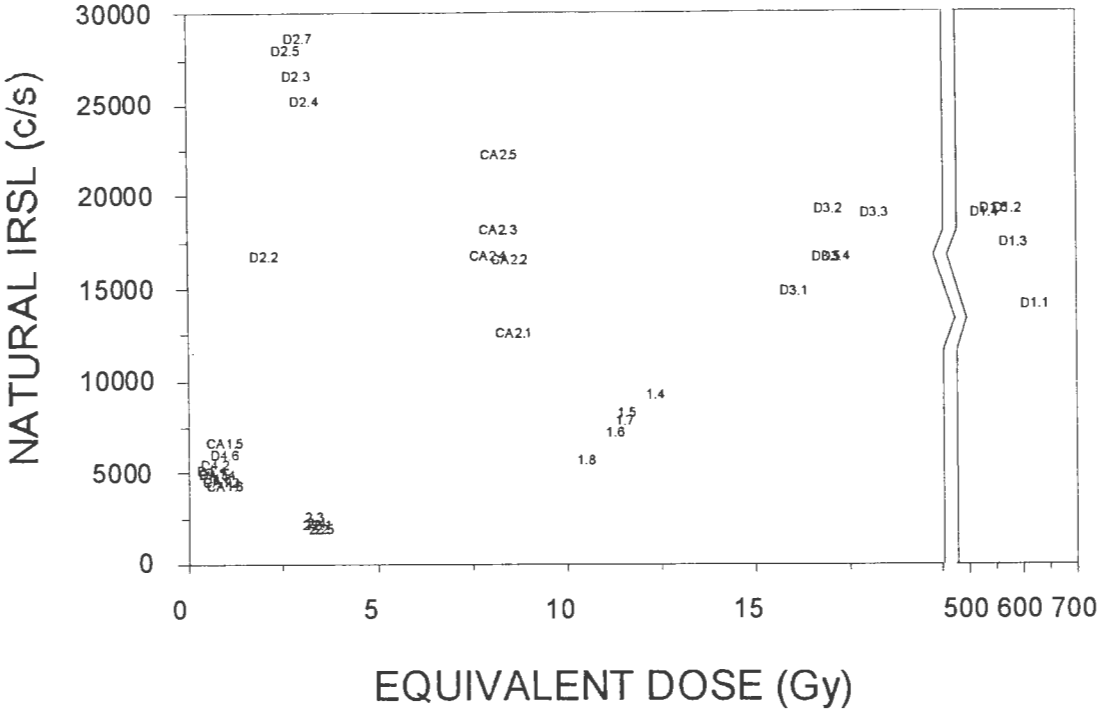

Figure 3. The sensitivity of the IRSL signal is portrayed in a plot of natural IRSL signal vs. DE for each sample aliquot. Linear trends towards the origin imply similar sensity between aliquots. Large spreads of points with the same sensitivity indicates poor bleaching.

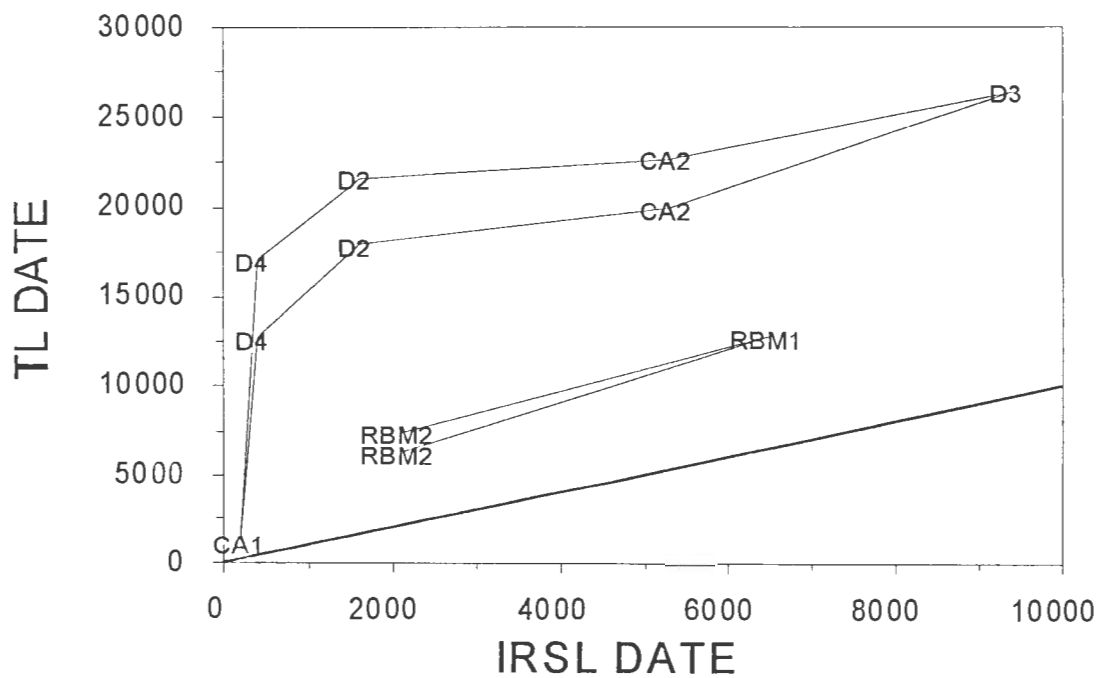

Figure 4. A plot of IRSL date vs. TL date shows no particular trend that might suggest that sensitivity changes or fading might account for the differences between the two techniques

Table 1. Summary of dosimetry and age calculation data.

SAMPLE	RBM1	RBM2	RBM D1	RBM D2	RBM D3	RBM D4	RBM CA1	RBM CA2
BULK SAND:								
%K	0.23±0.01	0.20±0.01	0.06±0.01	0.20±0.01	0.13±0.01	0.12±0.01	0.06±0.01	0.43±0.01
ppm Th	4.24±0.66	2.47±0.05	14.79±0.20	7.09±0.12	5.92±0.11	5.72±0.09	40.65±0.40	2.73±0.06
ppm U	1.09±0.17	1.25±0.03	4.84±0.07	2.09±0.04	2.07±0.04	2.25±0.04	11.12±0.11	0.48±0.01
% Water (estimated)	8±4	8±4	8±4	8±4	8±4	8±4	8±4	8±4
GRAINS:								
Grain size (μm)	250-300	250-300	150-212	150-212	212-300	212-300	212-300	212-300
Density	<2.58	<2.58	<2.58	<2.58	<2.58	<2.58	<2.58	<2.58
Magnetic separation	Yes	Yes	Yes	Yes	Yes	Yes	Yes	Yes
Etch	0μm	0μm	0μm	0μm	0μm	0μm	0μm	0μm
DOSE RATE (μGy/a):								
Gamma + Cosmic	534±43	460±21	1305±61	688±32	543±28	556±28	3115±153	377±17
Alpha (IRSL)	49±12	41±9	294±71	134±32	86±20	89±20	512±117	29±7
Alpha (TL)	47±12	39±9	282±68	128±31	83±19	85±19	503±114	28±6
Beta (IRSL)	1186±81	1146±109	1451±91	6066±91	1198±106	1207±106	2870±155	1159±106
Beta (TL)	356±30	317±19	907±51	526±30	434±25	443±25	2083±114	396±22
Total (IRSL)	1769±108	1648±109	3050±151	1888±100	1827±111	1851±112	6497±321	1566±106
Total (TL)	937±76	816±38	2494±147	1345±75	1060±60	1084±61	5701±319	803±40
EQUIVALENT DOSE - D_E (Gy):								
IRSL Regeneration	11.5±0.3	3.5±0.1	572±16.5	2.95±0.78	17.11±0.34	0.78±0.07	1.00±0.04	8.31±0.11
TL (325 °C)	12.0±1.7	5.1±1.0	431.2±96.7	24.04±1.65	27.98±2.68	13.78±0.82	6.08±0.38	16.04±0.56
TL (375 °C)		6.1±2.1		29.06±2.20		18.50±1.82		18.18±0.69
AGE (ka)								
IRSL Regeneration	6.5±0.5	2.1±0.1	188±10	1.6±0.4	9.4±0.6	0.4±0.03	0.154±0.009	5.3±0.4
TL (325 °C)	12.8±2.1	6.3±1.3	173±40	17.9±1.6	26.4±2.9	12.7±1.0	1.1±0.1	20.0±1.2
TL (375 °C)		7.4±2.6		21.6±2.0		17.1±1.9		22.7±1.4